O2 Reduction in Enzymatic Biofuel Cells

Nicolas Mano, Anne de Poulpiquet

O_2 Reduction in Enzymatic Biofuel cells

Nicolas Mano[a,b,⊥*] and Anne de Poulpiquet[c,⊥]

[a] CNRS, CRPP, UPR 8641, 33600 Pessac, France

[b]Univ. Bordeaux, CRPP, UPR 8641, 33600 Pessac, France

*mano@crpp-bordeaux.cnrs.fr

[c] Bioénergétique et Ingénierie des Protéines, CNRS-AMU, 31, chemin Aiguier, 13009 Marseille, France

[⊥] both authors contibuted equally to this work

Abstract

Catalytic four-electron reduction of O_2 to water is one of the most extensively studied electrochemical reactions due to O_2 exceptional availability and high O_2/H_2O redox potential, which may in particular allow highly energetic reactions in fuel cells. To circumvent the use of expensive and inEfficient Pt catalysts, multicopper oxidases (MCOs) have been envisioned because they provide Efficient O_2 reduction with almost no overpotential. MCOs have been used to elaborate enzymatic biofuel cells (EBFCs), a sub-class of fuel cells in which enzymes replace the conventional catalysts. A glucose/O_2 EBFC, with a glucose oxidizing anode and a O_2 reducing MCO cathode, could become the *in vivo* source of electricity that would power sometimes in the future integrated medical devices. This review covers the challenges and advances in the electrochemistry of MCOs and their use in EBFCs with a particular emphasis in the last 6 years. First basic features of MCOs and EBFCs are presented. Clues provided by electrochemistry to understand these enzymes, and how they behave once connected at electrodes, are described. Progresses realized in the development of Efficient biocathodes for O_2 reduction relying both on direct and mediated electron transfer mechanism are then discussed. Some implementations in EBFCs are finally presented.

CONTENTS

Symbols

ABTS: 2,2'-azinobis(3-ethylbenzothiazolin-6-sulfonate)

AFM: Atomic force microscopy

AMT: 4-aminothiophenol

AR: Alternative resting

AuNPs: Gold nanoparticles

BDD: Boron doped diamond

BET: Specific surface area determined by the method of Brunauer, Emmett and Teller

BOD: Bilirubin oxidase

BP: Buckypaper

***Bp*-BOD:** Bilirubin oxidase from *Bacillus pumilus*

***Bs*-BOD**: Bilirubin oxidase from *Bacillus subtilis*

CA: Chronoamperometry

CFCs: Conventional fuel cells

***Cf*-laccase**: Laccase from *Cerrena fulvocinerea*

***Cm*-laccase**: Laccase from *Cerrena maxima*

CNFs: Carbon nanofibers

CNPs: Carbon nanoparticles

CNTs: Carbon nanotubes

CueO: Copper efflux oxidase

***Cu*-laccase**: Laccase from *Cerrena unicolor*

COx: Cytochrome oxidase

CV: Cyclic voltammetry

CVD: Chemical vapor deposition

CMF: Carbon microfiber

Cyt *c*: Cytochrome *c*

DET: Direct electron transfer

DFT: Density functional theory

DMP: 2,6-dimethoxyphenol

DNA: Desoxyribo nucleic acid

DPI: Dual polarization interferometry

EBFCs: Enzymatic biofuel cells

EC: Enzyme class

ECR: Electron cyclotron resonance

EDX: Energy dispersive X-ray analysis

EPR: Electron paramagnetic resonance

ESSA: Electroactive specific surface area

ET: Electron transfer

FAD: Flavin adenine dinucleotide

FDH: Fructose Dehydrogenase

***Fp*-laccase**: Laccase from *Fusarium proliferatum*

GA: Glutaraldehyde

GC: Glassy Carbon

GDH: Glucose dehydrogenase

GDL: Gas diffusion layer

GO: Graphene oxide

GOx: Glucose oxidase

Hase: Hydrogenase

HET: Heterogeneous electron transfer

HOPG: Highly oriented pyrolytic graphite

HRP: Horseradish peroxidase

IET: Internal electron transfer

KB: Ketjen black

LDG: Low density graphite

LED: Light emitting diode

LMCOs: Laccase-like Multicopper Oxidases

LSV: Linear sweep voltammetry

***Ma*-Laccase:** Laccase from *Melanocarpus albomyces*

MCOs: Multicopper oxidases

MET: Mediated electron transfer

MgOC: Magnesium oxide template mesoporous carbon

MHA: Mercapto-hexanoic acid

***Mo*-BOD:** Bilirubin oxidase from *Magnaporthae orizae*

MPA: Mercapto-propionic acid

***Mv*-BOD**: Bilirubin oxidase from *Myrothecium verrucaria*

MW-CNTs: Multi-wall carbon nanotubes

NAD^+: Nicotinamide adenine dinucleotide

NHE: Normal hydrogen electrode

NHS: N-Hydroxysuccinimide

NI: Native intermediate

OCP: Open circuit potential

OCV: Open circuit voltage

PAA: Polyacrylamide

PAMAM: Polyamidoamine

PBS: Phosphate buffered saline

PBSE: Pyrene butyric succinimidyl ester

***Pc*-laccase:** Laccase from *Pycnoporus cinnabarinus*

PDB: Protein data bank

PDMS: Polydimethylsiloxane

PFC: Plastic formed carbon

PG: Pyrolytic graphite

PI: Peroxide intermediate

PLA: Polylactic acid

PLL: Poly-L-lysine

PM-IRRAS: Polarization modulated infra-red spectroscopy

PPO: Polyphenol oxidase

PPY: Polypyrrole

PQQ: Pyrroloquinoline quinone

PSS : Polystyrene sulfonate

PVDF: Polyvinylidene fluoride

PVI: Poly(N-vinylimidazole)

QCM: Quartz crystal microbalance

QCM-D: Quartz crystal microbalance with dissipation monitoring

QM/MM: Quantum mechanical and molecular mechanics

RO: Resting oxidized

RRDE: Rotating ring disc electrode

RVC: Reticulated vitreous carbon

Rv*-laccase:* Laccase from *Rhus vernicifera*

SAMs: Self-assembled monolayer

Sc*-laccase:* Small laccase from *Steptomyces coelicolor*

SECM: Scanning electrochemical microscopy

SERS: Surface enhanced Raman spectroscopy

SGZ: Syringaldazine

SPG: Spectroscopic graphite

SPR: Surface plasmon resonance

STM: Scanning tunneling microscopy

SW-CNTs: Single-wall carbon nanotubes

SWV: Square wave voltammetry

***Ta*-laccase:** Laccase from *Trichaptum abietinum*

TBAB: Tetrabutylammonium ions

TNC: Tri-nuclear copper cluster

***To*-laccase:** Laccase from *Trametes ochracea*

TMOS: Tetramethyl orthosilicate

***Tt*-BOD:** Bilirubin oxidase from *Trachyderma tsunodae*

***Tt*-laccase:** Laccase from *Trametes troggii*

***Th*-laccase:** Laccase from *Trametes hirsuta*

tVA: Thiolated veratric acid

***Tv*-laccase**: Laccase from *Trametes versicolor*

PPY: Polypyrole

1. Introduction

About 2.5 billion years ago, oxygen became an important component of the earth atmosphere[1] due to the emergence of cyanobacteria, organisms that produce oxygen during photosynthesis. One of the consequences of this event is the biological utilization of copper, a transition metal now omnipresent in biology, while only iron used to be predominant in the first living forms. In the oceans, oxygenation led to a shift from high-iron to high-copper contents, because oxygen favors the oxidation state +III of insoluble Fe^{3+}, while Cu is preferentially in the Cu^{2+} form which is soluble and therefore bioavailable.[2] In living organisms, copper is still linked with oxygen metabolism : a recent study examining copper utilization by 450 bacteria demonstrated that around 80% of anaerobes did not depend on copper, while more than 90% of aerobes were copper dependent.[3]

Copper can be found in numerous metallo-proteins, in which the metal is coordinated by amino-acids. Copper-containing proteins are present in bacterial, fungal, plant and mammalian organisms.[4] In some of the proteins, copper is frozen in the reduced or oxidized state. Of particular importance in the frame of electrochemistry are the proteins in which copper centers are able to undergo the redox Cu^{2+}/Cu^{+} reaction. These metallo-proteins contain either one or several copper centers, and the latter are either mononuclear (type T1, T2 or Cu_B sites) or binuclear (type T3 or Cu_A sites).[5] Copper ligands and protein environment modulate the potentials of the +II/+I transition that varies accordingly from ≈85 mV to >1000 mV,[6] while in water the apparent standard potential E°' of the Cu^{2+}/Cu^{+} couple is 150 mV *vs*. the normal hydrogen reference electrode (NHE).[7]

Copper-containing proteins cover different functions ranging from electron transfer to catalysis, and are involved in a wide variety of mechanisms among which the most important are energy conversions in respiration or metabolism. It must be noted however that copper is also toxic at high concentrations so that many proteins are linked to copper regulation and

homeostasis.[2] Copper based enzymes are associated with the metabolism of N_2O (nitrous oxide reductase), NO_2^- (nitrite reductases), $O_2^{\cdot -}$ (superoxide dismutase), or O_2.[5] More relevant are the two classes of enzymes involved in oxygen reduction: terminal oxidases, and multi-copper oxidases (MCOs). Terminal oxidases can be divided in cytochrome or quinol oxidases, and contain both copper centers and hemes. Oxygen reduction occurs with cytochrome or reduced quinone as a primary electron donor. The reaction is coupled to proton transfer and the enzyme-catalyzed reactions create the proton gradient necessary for ATP synthesis.[8] MCOs catalyze the 4-e^- oxygen reduction coupled to oxidation of various organic or metallic substrates.[5] In MCOs, inner sphere electron transfers are involved in binding, activation and reduction of O_2.

Among the desperately sought, but rarely well-engineered devices envisioned for sustainable energy conversion, fuel cells could harvest energy from fuels like dihydrogen, alcohols, etc.[9,10] Their advantages stem from direct conversion of chemical energy into electricity, and long-term operation enabled by continuous fueling. The reaction involved in fuel cells requires a combustive, and O_2 is the most widely used because of its availability and high O_2/H_2O redox potential.[11] Designing catalysts for O_2 reduction in conventional fuel cells (CFCs) is challenging. They generally require high overpotentials,[12] or only catalyze the incomplete O_2 reduction to H_2O_2.[13,14] Ideally, the platinum-based catalysts widely used in CFCs would be replaced by less expensive biological oxidation catalysts. Enzymatic biofuel cells (EBFCs) are a sub-class of fuel cells in which enzymes replace the conventional catalysts used in CFCs. They offer numerous advantages such as selectivity and specificity, allowing in particular operating without the separation membrane otherwise required to avoid cross-reactions at the electrodes. Moreover, they can operate in mild environments, and are also renewable and biodegradable.

The glucose/O_2 biofuel cell, with a glucose oxidizing anode and a O_2 reducing cathodes could become the *in vivo* source of electricity that would power sometimes in the future integrated medicals devices.[15] In this context, the enzymatic MCO catalysts are especially interesting because they provide Efficient 4-e^- O_2 reduction[5] with almost no overpotential.[16] In the last decades, electrochemical research of redox proteins showed ways to connect MCOs at electrodes, and to use them as Efficient and specific electrocatalysts for O_2 reduction,[17,18] making some the enzymes of choice in EBFCs.

In this review we cover the challenges and advances in the electrochemistry of MCOs and their use in EBFCs since their first connection at an electrode 40 years ago, with a particular emphasis in the last 6 years. The interested reader will find in Table 1 additional reviews on this topic, with a particular focus on electrode materials for EBFCs. Here, we first briefly present basic features of MCOs and EBFCs, before focusing on the electrochemical approach of MCO study and applications. We describe what electrochemistry teaches us about these enzymes, and how they behave once connected at electrodes. We then discuss the progresses realized in the development of Efficient biocathodes for O_2 reduction relying both on direct and mediated electron transfer mechanism (DET and MET respectively). Finally, we present some implementation in EBFCs.

Table 1: Reviews related to O_2 reduction by MCOs and in Biofuel cells

2004	
Enzymatic Biofuel Cells for Implantable and Microscale Devices	Barton *et al.* [19]
Biological fuel cells and their applications	Sukla *et al.* [20]
2006	
Challenges in biocatalysis for enzyme-based biofuel cells	Kim *et al.* [21]
Biofuel cells and their development	Bullen *et al.* [22]
Potentially implantable miniature Batteries	Heller [23]
2007	
Biofuel cells--recent advances and applications	Davis *et al.* [24]
Enzyme-based biofuel cells	Minteer *et al.* [25]

2008

Energy harvesting by implantable abiotically catalyzed glucose fuel cells	Kerzenmacher *et al.* [26]
Enzymes as working or Inspirational Electrocatalysts for Fuel Cells and Electrolysis	Cracknell *et al.* [27]
Enzyme catalysed biofuel cells	Cooney *et al.* [28]
Extended lifetime biofuel cells	Moehlenbrock *et al.* [29]

2009

Integrated Enzyme-Based Biofuel cells - A review	Willner *et al.* [30]
Hemoproteins in Design of Biofuel Cells	Ramanavicius *et al.* [31]
Microfluidic fuel cells: A review	Kjeang *et al.* [32]

2010

An overview of enzymatic Biofuel cells	Aquino Neto *et al.* [33]
Biofuel Cells with Switchable Power Output	Katz [34]
Protein Engineering – An Option for Enzymatic Biofuel Cell Design	Guven *et al.* [35]
Recent Advances in Enzymatic Fuel Cells: Experiments and Modeling	Ivanov *et al.* [36]
Biofuel Cells for portable power	Gellet *et al.* [37]
Enzymatic Biofuel Cells—Fabrication of Enzyme Electrodes	Hao Uy *et al.* [38]
A perspective on microfluidic biofuel cells	Lee *et al.* [39]
Mediated Biocatalytic Electrodes and Enzyme Stabilisation for Power Generation	Brito *et al.* [40]
Biosensors and biofuel cells with engineered proteins	Caruana *et al.* [41]

2011

Strategies to extend the lifetime of bioelectrochemical enzyme electrodes for biosensing and biofuel cell applications	Rubenwolf *et al.* [42]
Bioelectrochemical interface engineering: Toward the fabrication of electrochemical Biosensors, Biofuel cells and self-powered logic biosensors	Zhou *et al.*[43]
Recent Developments of Nanostructured Electrodes for Bioelectrocatalysis of Dioxygen Reduction	Opallo *et al.* [44]
Self-powered sensors	Arechederra *et al.* [45]
Recent progress and continuing challenges in bio-fuel cells. Part I: Enzymatic cells	Osman *et al.* [46]
Biofuel cells for Self-Powered electrochemical biosensing and logic biosensing: A Review	Zhou *et al.* [47]
Bioelectrochemical systems: Microbial versus enzymatic catalysis	Freguia *et al.* [48]
New materials for biological fuel cells	Minteer *et al.* [49]
Immobilization technology: a sustainable solution for biofuel cell design	Yang *et al.* [50]
Enzymatic fuel cells: Recent progress	Leech *et al.* [51]
Carbon nanotube/enzyme biofuel cells	Holzinger *et al.* [52]
Features and applications of bilirubin oxidases	Mano [53]
Enzymatic versus Microbial Bio-Catalyzed Electrodes in Bio-Electrochemical Systems	Lapinsonnière *et al.* [54]
Direct electron transfer based enzymatic fuel cells	Falk *et al.* [55]

2013

Biofuel Cells for Biomedical Applications: Colonizing the Animal Kingdom	Falk *et al.* [56]
Direct Electrochemistry based biosensors and biofuel cells enables with nanostructures materials	Liu *et al.* [57]
Bilirubin oxidases in bioelectrochemistry: Features and recent findings	Mano *et al.* [58]
Implanted biofuel cells operating *in vivo* – methods, applications and perspectives	Katz *et al.* [59]
New Energy Sources: The Enzymatic Biofuel Cell	Aquino Neto *et al.* [60]
A perspective on microfluidic biofuel cells	Lee *et al.* [39]

2014

Enzyme Biofuel Cells: Thermodynamics, Kinetics and Challenges in Applicability	Luz *et al.* [61]
Enzymatic Biofuel Cells on Porous Nanostructures	Wen *et al.* [62]
Biohydrogen for a New Generation of H2/O2 Biofuel Cells: A Sustainable Energy Perspective	De Poulpiquet *et al.* [63]
New trends in enzyme immobilization at nanostructured interfaces for Efficient electrocatalysis in biofuel cells.	De Poulpiquet *et al.* [64]
Paper-based Batteries: A review	Nguyen *et al.* [65]
Recent advances in carbon nanotubes-based enzymatic fuel cells	Cosnier *et al.* [66]
Hybrid Electric Power Biodevices	Pankratov *et al.*[67]

Electrochemical and electrophoretic deposition of enzymes: Principles, differences and application in miniaturized biosensor and biofuel cell electrodes	Amman *et al.* [68]
Is graphene worth using in Biofuel cells?	Filip *et al.* [69]
QM/MM Molecular Modeling and Marcus Theory in the Molecular Design of Electrodes for Enzymatic Fuel Cells	Vasquez-Duhalt *et al.*[70]
Towards glucose biofuel cells implanted in human body for powering artificial organs: Review	Cosnier *et al.* [71]
2015	
Recent progress in oxygen-reducing laccase biocathodes for enzymatic biofuel cells.	Le Goff *et al.* [72]
Wired enzymes in mesoporous materials: A benchmark for fabricating biofuel cells	Catalano *et al.* [73]
Graphene based enzymatic bioelectrodes and biofuel cells	Karimi *et al.* [74]
2016	
Recent advances on enzymatic glucose/oxygen and hydrogen/oxygen biofuel cells: Achievements and limitations	Cosnier *et al.* [75]
Paper electrodes for bioelectrochemistry: Biosensors and biofuel cells	Desmet *et al.* [76]
Progress on implantable biofuel cell: Nano-carbon functionalization for enzyme immobilization enhancement	Babdai *et al.* [77]
Wearable Biofuel Cells: A Review	Bandodkar *et al.* [78]
BioCapacitor: A novel principle for biosensors	Sode *et al.* [79]
Tear Based Bioelectronics	Pankratov *et al.* [80]
Laccase: a multi-purpose biocatalyst at the forefront of biotechnology	Mate *et al.* [81]
Microfluidic fuel cells for energy generation	Safdar *et al.*[82]
2017	
Recent advance in fabricating monolithic 3D porous graphene and their applications in biosensing and biofuel cells	Qiu *et al.* [83]
Review—Wearable Biofuel Cells: Past, Present and Future	Bandokar *et al.* [84]
The applications and prospect of fuel cells in medical field: A review	Xu *et al.* [85]
Biological fuel cells and membranes	Ghassemi *et al.* [86]
Nanostructured inorganic materials at work in electrochemical sensing and biofuel cells	Holade *et al.* [87]
Advanced Materials for Printed Wearable Electrochemical Devices: A Review	Kim *et al.* [88]
Quo Vadis, Implanted Fuel Cell?	Shleev [89]
Mathematical modeling of nonlinear reaction–diffusion processes in enzymatic biofuel cells	Rajendran *et al.* [90]
Nanostructured material-based biofuel cells: recent advances and future prospects	Zhao *et al.* [91]

2. Background

2.1 Multicopper oxidases

In this paragraph some reminders about MCOs will be given. Detailed enzymology, kinetics, electronic structure, and mechanism can be found elsewhere.[5,92-99]

Multicopper Oxidases (MCOs) family is ubiquitous in nature and can be divided in three categories depending on the enzymes' specificity towards substrates.[5,95] The first category includes laccases (EC 1.10.32) which oxidize a broad range of organic substrates. The second category, metalloxidases, includes for example ceruloplasmin (EC 1.16.3.1) or

cuprous oxidase that oxidize metal substrates. The last category includes ascorbate oxidase (EC 1.10.32) or bilirubin oxidase (EC 1.3.3.5) which can be specific towards single substrate (*i.e* ascorbate or bilirubin) while also being able to oxidize other organic substrates.[100] A general trait of MCOs is the presence of at least four copper ions which permit oxidation of substrates while reducing O_2 to water without production of any toxic intermediates. Each copper is classified according to its optical and magnetic properties. Type I Cu displays an intense absorption band near 600 nm resulting from a charge transfer transition from Cys to Cu (II) and is responsible for the name, blue copper oxidases, given to these enzymes (Fig 1A). It also exhibits a small Cu(II) A|| hyperfine coupling constant in EPR (Fig 1B).

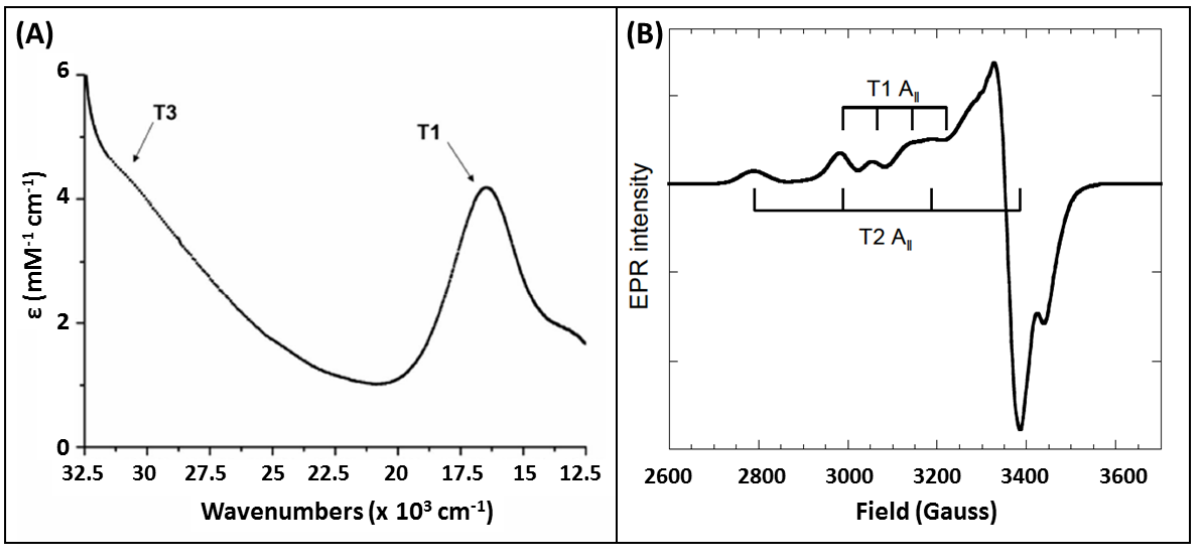

Figure 1. UV-visible (A), X-band EPR (B) of purified BOD from *Bacillus pumilus* highlighting the spectral feature in MCOs. Reprint with permission from ref [101] Copyright 2010 Elsevier.

Type 1 copper accepts electrons from the electron-donating substrates and shuttles them to the O_2 reduction site composed of three coppers. The tri-nuclear cluster (TNC) consists in a Type 2 copper ion active in EPR with a normal Cu(II) A|| hyperfine coupling constant and a pair of Type 3 cupric ions with a characteristic 330 nm absorption shoulder and

antiferromagnetically coupled via a bridging hydroxide (Fig 1B). Electrons are relayed from the T1 to the TNC through ~13 Å of Cys-His residues (Fig 2).

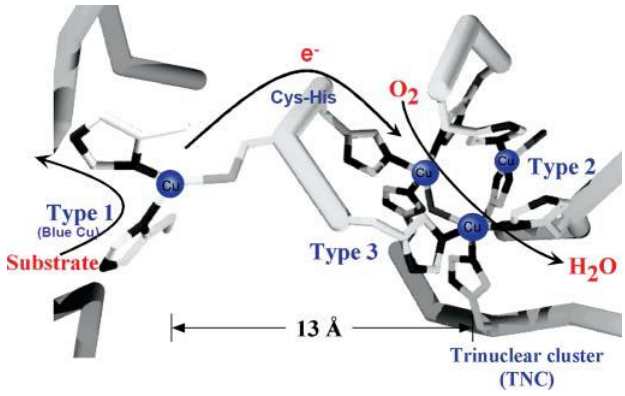

Figure 2. The structure of the MCO active site with arrows marking the flow of substrates, electrons (e^-), and O_2. Reproduced with permission from ref [93]. Copyright 2012 Royal Society of Chemistry

The exact nature of the electron transfer has been the subject of numerous investigations and is summarized in Figure 3.[5,92,94,97,98,102-106]

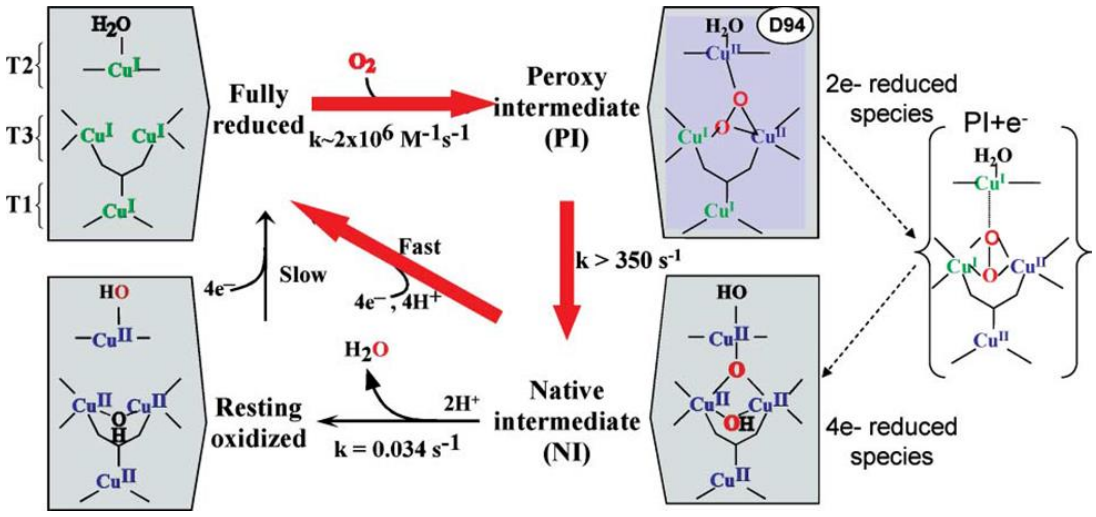

Figure 3. Mechanism of O_2 reduction to water by the MCOs. Red arrows indicate the steps that take place in the catalytic cycle of the MCOs. Black arrows indicate steps that can be experimentally observed but are not part of the catalytic cycle. The dashed arrows at the right indicate the transfer of an electron from the T1 Cu to the T2 Cu to create PI + e-, that occurs in going from PI to NI but is not experimentally observed in the wild type enzyme. Reproduced with permission from ref [93]. Copyright 2012 Royal Society of Chemistry

Briefly, after oxidation of the substrate at the T1, electrons are shuttled to the TNC where the two two-electron steps of O_2 reduction to H_2O occurs.[93,107,108] The formation of the peroxide intermediate (PI) results from the first two-electron step with a fast reaction rate (~ 10^6 $M^{-1}.s^{-1}$). In the second two-electron step, the O-O bond is cleaved with a fast rate constant leading to the formation of the Native Intermediate (NI). In presence of substrate, NI is reduced to the fully reduced form of the enzyme and is ready for another catalytic cycle. In absence of substrate, NI slowly decays to the resting oxidized (RO) form and only reintegrates the catalytic cycle upon reduction with a substrate.

2.1.1 Laccases

Laccases (Fig 4A) are the most studied MCOs because of their use in different biotechnological applications; ranging from food applications, pulp bleaching, hair-coloring to organic synthesis.[81,109-111] More than 220 species have been identified in insects, fungi or bacteria.

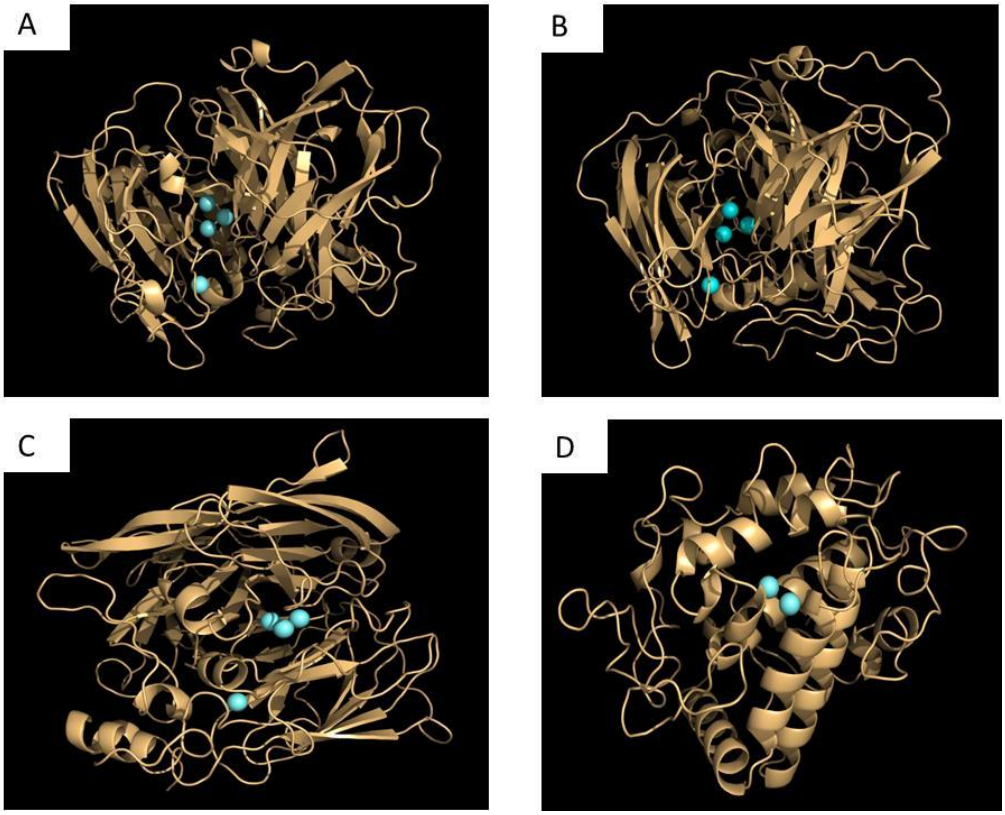

Figure 4. X-rays structure of different MCOs. A) Native fungus laccase from *Trametes hirsuta* (PDB: 3FPX); B) BOD from *Myrothecium verrucaria* (PDB: 2XLL); C) Copper

efflux Oxidase CueO (PDB: 4NER); D) Tyrosinase from *Bacillus megaterium* (PDB : 5I38). All Coppers are displayed in blue

Among them, fungal laccases have been the most studied.[5,112-114] Laccases are known to oxidize a variety of polyphenolic compounds concomitant with the reduction of O_2. Due to this latter property, Tarasevich *et al.* have pioneered the use of laccases for O_2 reduction. In 1979, they reported the immobilization of monolayers of laccases on vitreous carbon electrodes, generating O_2 reduction currents of 175 $\mu A.cm^{-2}$ at pH 5.[115] The geometry/coordination of the T1 copper deserves attention since this is the entry point of electrons coming from the electrode or from the redox mediator. It has been shown that its redox potential was modulated by the nature of its coordination. A T1 with a weakly coordinating Met in the axial position exhibits generally a lower redox potential than MCOs where Met has been replaced by non-coordinating Phe or Leu.[116] However, many exceptions exist and the type of coordination cannot explain alone the difference in the observed electrochemical potentials. Other factors such as electrostatic interactions and hydrogen bonds must be taken into account, making therefore difficult to predict the redox potential of MCOs.[117] We list here some of the most commonly studied laccases in bioelectrochemistry. Fungal laccases have been identified in basidiomycetes. Among them we use the abbreviation *Th*-laccase to call without differentiation the two isoenzymes from *Trametes hirsutus*, also known as *Coriolus hirsutus*[118], and *Tv*-laccase to call the laccase from *Trametes versicolor*, also known as *Coriolus versicolor* or *Polyporous versicolor*. Other laccases are extracted from trees, among which *Rv*-laccase the laccase from the Japanese lacquer tree *Rhus vernicifera*.

2.1.2 Bilirubin oxidases

BODs (Fig 4B) have been discovered in 1981 by Tanaka and Murao.[119] Because of their ability to oxidize bilirubin, they were classified as BODs and not laccases, even though BODs can also oxidize a variety of phenolic compounds.[53] BODs have been primarily used in the medical field to elaborate bilirubin biosensors.[53,58] Only 7 BODs have been identified/characterized so far, among which BOD from *Myrothecium verrucaria* (*Mv*-BOD), the most studied BOD, BOD from *Trachyderma tsunodae*[120] (*Tt*-BOD), BOD from *Magnaporthae orizae*[121] (*Mo*-BOD) and BOD from *Bacillus pumilus* (*Bp-BOD).*[101] Unlike *Tt*-BOD or *Mv*-BOD, the two newly identified *Mo*-BOD and *Bp*-BOD display good thermal stability, a high activity at pH 7 and high temperature, a low sensitivity towards NaCl and no sensitivity to urate. Bilirubin is not a substrate that has been systematically tested with laccases or other MCOs. Therefore, it is not unlikely that MCOs already identified and characterized also display BOD-like activity. The use of *Mv*-BOD for the electrocatalytic O_2 reduction at neutral pH has been reported for the first time in 2001 by Tsujimura *et al.*[122] Ever since, the number of studies relying on BODs has been flourishing for one main reason: unlike laccases, BODs display a high activity and stability at neutral pH and in presence of chloride. Two points deserve attention. The first concerns the denomination of the enzyme. Reiss *et al.* recently identified a CotA enzyme from *Bacillus pumilus*[123] which was classified as a laccase while Durand *et al.* classified an enzyme sharing 98% identity as a BOD.[101] BOD-like activity has also been observed in a CotA from *Bacillus subtilis* but the enzyme was classified as a laccase.[124] Reiss *et al.* have suggested that the denomination of BOD was improper since these enzymes could oxidize a variety of substrates. Therefore, they suggested to introduce the term of laccase-like MCOs (LMCOs).[125] On the other hand, not all laccases oxidize bilirubin. Therefore, the denomination of BOD would permit to differentiate between those MCOs that oxidize bilirubin or those that do not. The question of classification remains

open. The second point deserving attention, which is linked to the first, is the core structural difference between laccases and BODs. Detailed analysis of amino acid sequences does not permit to differentiate BODs and laccases.[126] Combining different analytical tools such as molecular modeling or X-rays analysis would definitely help, but only two X-rays structures of BODs are available so far, for *Mo*-BOD[127] and *Mv*-BOD.[128,129]

2.1.3. Cuprous oxidase and tyrosinase

The two enzymes have been rarely used in O_2 biocathodes. Cuprous oxidase, or copper efflux oxidase (CueO) (Fig 4C) is involved in copper efflux in *E.coli.*[130,131] CueO possesses the same catalytic site as other MCOs but exhibits a strong activity towards cuprous ion and, unlike other MCOs, no activity towards phenolic compounds. Tyrosinase, or polyphenol oxidase (Fig 4D), only carries a couple of T3 copper atoms and is involved in the ortho-hydroxylation of monophenols and two-electron oxidation of diphenols.[95]

In the following, we will not consider cerulosplasmin and ascorbate oxidase (EC 1.10.3.3) which have not yet proven their utility in O_2 reduction.[11] It has been shown that direct electron transfer (DET) between ceruloplasmin and an electrode surface was feasible under non turnover conditions, but in most cases electrocatalytic reduction of O_2 was not achieved.[18,132-135] The only example of O_2 reduction with ceruloplasmin on gold modified with ferromagnetic particles encapsulated in carbon was reported in 2015 by Matysiak *et al.*[136] However, the current density is too low to envision, so far, application in EBFCs. The DET of ascorbate oxidase has been reviewed by Shleev[18] and also investigated by Atanassov *et al.*[137]

2.2 Basic feature of enzymatic biofuel cells

Detailed thermodynamic and kinetic analyses of enzymatic biofuel cells (EBFCs) have been provided in earlier reviews.[19,22,24,61] Therefore, in the following, we only briefly summarize key points and advantages of EBFCs.

Despite the fact that electrochemical reactions are catalyzed by enzymes at one or both electrodes of the EBFCs, there is no conceptual difference between the latter and conventional fuel cells (CFCs).[9] The fuel is oxidized at the anode while the oxidant is reduced at the cathode, and electrons are exchanged between the two electrodes in an external electrical circuit. The driving force of the reactions is the difference in electrochemical potential between the two electrodes. The transport of charges in the electrolyte solution (or polymer) is ensured by ions. However, unlike CFCs, EBFCs operate at near-neutral pH and ambient temperature. Enzymes also have advantages as electrocatalysts: specificity towards their substrates, renewability, biodegradability, high turnover frequencies, and low intrinsic overvoltages. Moreover, the great diversity of enzymes allows envisioning EBFCs working with diverse fuels and oxidants. In addition, if the bioelectrodes are properly designed, no membrane is needed in EBFCs to separate anodic and cathodic compartments, allowing thereby miniaturization of the devices.

An EBFC is characterized by its current intensity, I, its voltage E_{cell}, and its power, defined as the product of these latter:

$$P\ [W] = E_{cell}\ [V] \times I\ [A] \quad \textit{Eq. 1}$$

The electrical current intensity I is the charge flux entering the anode or leaving the cathode. In lots of studies the current density, defined as the ratio of current I by surface area A and denoted j, is preferred. Similarly, the power is often expressed in terms of power density. This makes actually hard to compare the efficiency of different devices because in some (rare)

cases the real electroactive surface area of the electrode is considered for the calculation, whereas it is more common to use the projected geometric area.

This point deserves a particular attention. While the normalization of the current is critical for comparing the results of the numerous publications, normalization is difficult. Other difficulties for comparison arise from the fact that experimental conditions (pH, temperature, scan rate, electrode rotation…) differ and in some studies, experimental details (enzymes activities and purities, loading…) are not provided. Natural convection which is often underestimated may also significantly affect current densities.[138] Comparisons are even more difficult when porous materials are used and particularly when detailed characterization of the materials are not provided (BET, thickness, porosity, mass,..). In addition, the different electrochemical techniques used to evaluate the power profile of EBFCs may also be problematic in some cases. For example, using linear sweep voltammetry at a quite fast scan rate (>5 $mV.s^{-1}$) to evaluate the power profile of EBFCs based on highly porous electrode materials may induce errors. Since porous materials usually have a high capacitance, it is more than likely that the measured currents are composed by both catalytic and capacitive current, which artificially enhances the biofuel cell performances. In order to evaluate the actual power, the effective catalytic currents have to be determined using chronoamperometry (for individual bioelectrodes) and under continuous discharge (for the biofuel cell setup) at different imposed potentials, or using linear sweep voltammetry at very low scan rates so that the steady-state can be reached. For all the above considerations, it would undoubtedly be useful to develop a protocol for comparison of data, as was already suggested by Minteer and others,[139-141] but was not favorably received. The authors of this review believe that such normalization is much needed, after answering the question of the best way to normalize performances, taking into account the variety of electrode materials, EBFC designs and enzymes used.

While in CFCs currents can be measured in A, they are mostly in the range of few tenths of µA to few hundreds of µA (resp. few $\mu A.cm^{-2}$ to few $mA.cm^{-2}$) in EBFCs, or more generally at enzymatic electrodes. Similarly, power (resp. power densities) are in the range of kW to MW in CFCs whereas they are mostly between few µW and few mW in EBFCs. Some impor

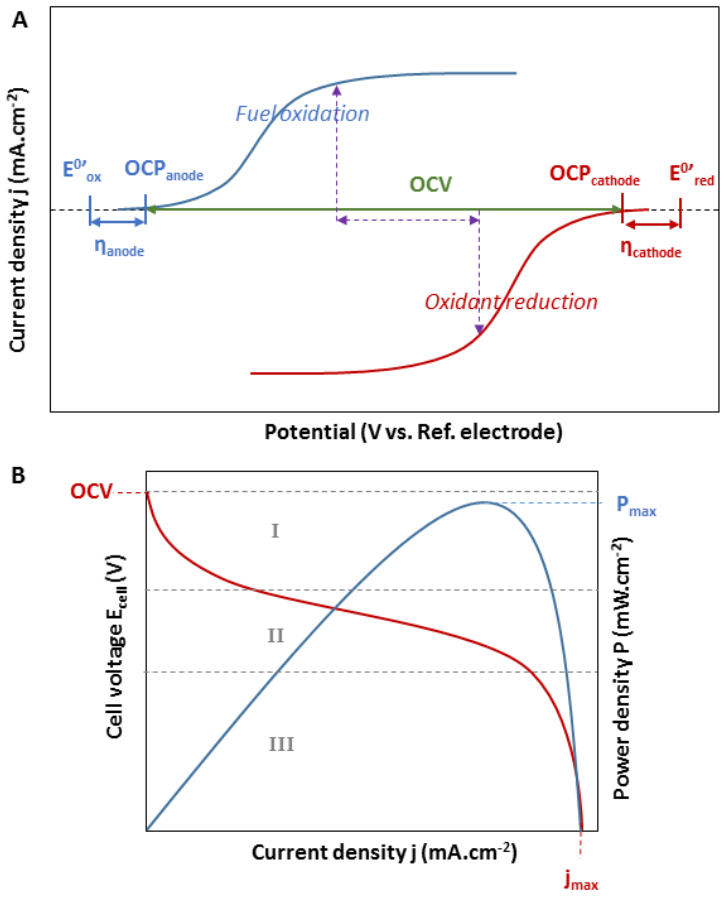

Figure 5. Electrochemical characterization of an EBFC. A: Current/Voltage response of the bioanode (blue curve) and of the biocathode (red curve). The purple arrows indicate the current density and the cell voltage giving the maximum power density. B: Polarization curve (red) and power curve (blue) of the complete EBFC. Adapted from [27]. Copyright 2008 American Chemical Society.

The potential adopted by the electrode at j = 0 is the open circuit potential (OCP). It is close to the onset potential, the starting potential of catalysis. It must be underlined that the

definition of “onset potential” is quite fuzzy since it is difficult to define the exact point at which catalysis actually “starts”. The difference between the OCP and the apparent standard redox potential, the overvoltage (η), characterizes the deviation to ideality of a catalyst and is a significant measure of its efficiency. Enzymes and MCOs in particular, are potentially powerful catalysts since for most of them electrochemical overvoltages are lower than for conventional catalysts. The difference between the OCP of the biocathode and the bioanode determines the maximal electrochemical driving force or open circuit voltage (OCV, also E_{cell} for $j = 0$) of the EBFC. The OCV of biofuel cells lies below the thermodynamic limit of 1.23 V for H_2/O_2 EBFCs, but sometimes very close to it,[142,143] and below the maximal OCV of 1.18 V for glucose/O_2 EBFCs, where glucose is oxidized into gluconolactone at the anode.

EBFC performances can be characterized in terms of OCV, polarization curve and power curve. These two curves show respectively the evolution of the cell voltage and of the power density with the current density (Fig 5B). Particular data are the maximum power density P_{max}, and the maximum current density j_{max} which corresponds very often to the short-circuit current (*i.e.* current density for $E_{cell} = 0$). As seen in Figure 5B, the polarization curve can be divided into three regions. In Segment I, the steep decrease of the cell voltage corresponds to kinetic losses, which are related to the slow rate of the electrode reaction due to e.g. slow electron-transfer kinetics. After this first decrease of the cell voltage, the polarization curve continues decreasing more linearly with a smaller slope over a wide range of current density values. This decrease, which can be seen in Segment II, corresponds to the ohmic voltage drop originating from the system’s intrinsic resistance as well as from the resistance to the flow of ions within the electrolyte. Finally, (concentration polarization) losses related to mass transport limitations result in the final decrease of the potential until it reaches zero (Segment III). At that point, the current reaches its maximal value and the system behaves as if the electrodes were in a short circuit. Each of the mentioned potential losses can

be described with corresponding overpotentials (Eq. 2). This allows calculating the cell voltage as:

$$E_{cell} = E_{eq} - \eta_{act} - \eta_{diff} - I \sum R \qquad Eq. 2$$

where: E_{cell} and E_{eq} are respectively measured and theoretical (thermodynamic) voltages, η_{act} and η_{diff} are respectively kinetic (activation) and mass transport based overpotentials, I is the current that flows through the cell and $\sum R$ is the sum of all resistances that are present in the system. The challenge is to minimize all kinetic losses by optimizing each ingredient of the biofuel cell; the electrode material, enzymes, and redox mediators if needed; and by Efficiently integrating them together. It could be done for example by optimizing the cell design and the immobilization of the enzymes.

2.3 Electronic connection of immobilized enzymes

One of the major challenges of using an enzyme as an electrocatalyst is to establish an Efficient electronic connection between the enzyme and the electrode, particularly because of the important size of the protein molecule, and the anisotropy of its electronic properties. A poor electrical connection will induce consequent kinetic losses. Two mechanisms allow electron transfer between an enzyme and an electrode. On one hand, in direct electron transfer (DET), electrons tunnel directly between an enzyme and an electrode. This mechanism relies on the ability of the enzyme to accept electrons not only from its natural substrate but also from artificial electron donors like the electrode. On the other hand, in mediated electron transfer (MET), electrons are shuttled via a redox molecule, called mediator, which exchanges electrons with the enzyme and is reversibly oxidized or reduced at the electrode surface (Fig 6).

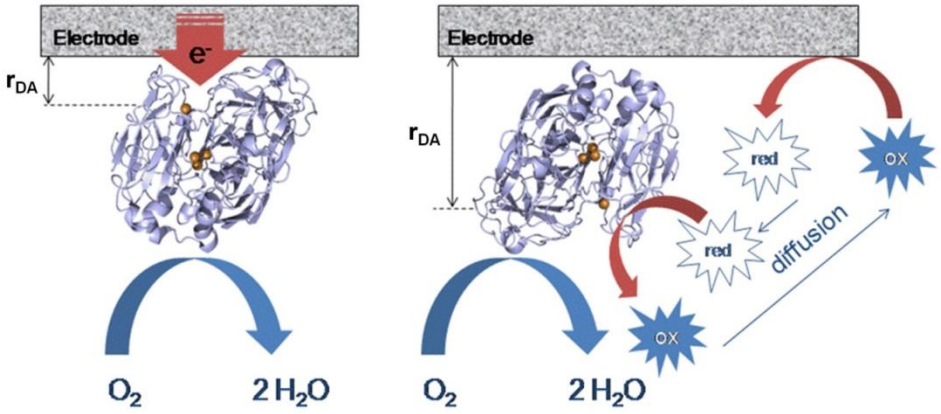

Figure 6. Two different mechanisms of electron exchange between an enzyme (here a laccase) and an electrode. Left: Direct Electron Transfer (DET) and Right: Mediated Electron Transfer (MET), here with a diffusive mediator.

DET can only occur if the enzyme active site or an electron relay is close enough to the electrode surface. The rate of interfacial electron transfer k_{ET}, described by Marcus semi-classical theory[144,145] (Equation 3), depends on the driving force of the reaction (ΔG°), the nuclear reorganization energy (λ), and the electronic coupling (H_{DA}) between donor D and acceptor A.

$$k_{ET} = \frac{1}{h}\frac{H_{DA}^2}{\sqrt{4\pi\lambda RT}} e^{\frac{-(\Delta G^\circ+\lambda)^2}{4\lambda RT}} \qquad Eq.3$$

The simplest model to describe the electronic coupling in case of proteins is the « square-barrier model », according to which H_{DA}^2 decreases exponentially with increasing distance between donor and acceptor (r_{DA}):

$$H_{DA}^2 = (H_{DA}^0)^2 e^{-\beta(r_{DA}-r_0)} \qquad Eq.4$$

where H_{DA}^0 is the electronic coupling at Van-der-Waals distance (r_0). The tunnel parameter β reflects the protein efficiency for electron transfer and depends on the protein structure.[146,147]

In DET, the catalytic wave is centered on a potential that is only affected by the properties of the enzyme molecule. This is discussed further in section 3.4.5 and 3.4.7. The

distribution of orientations allowing DET results in distribution of electronic transfer rates[148] reflected by the trailing edge in the catalytic cyclic voltammogram (Fig 7A).

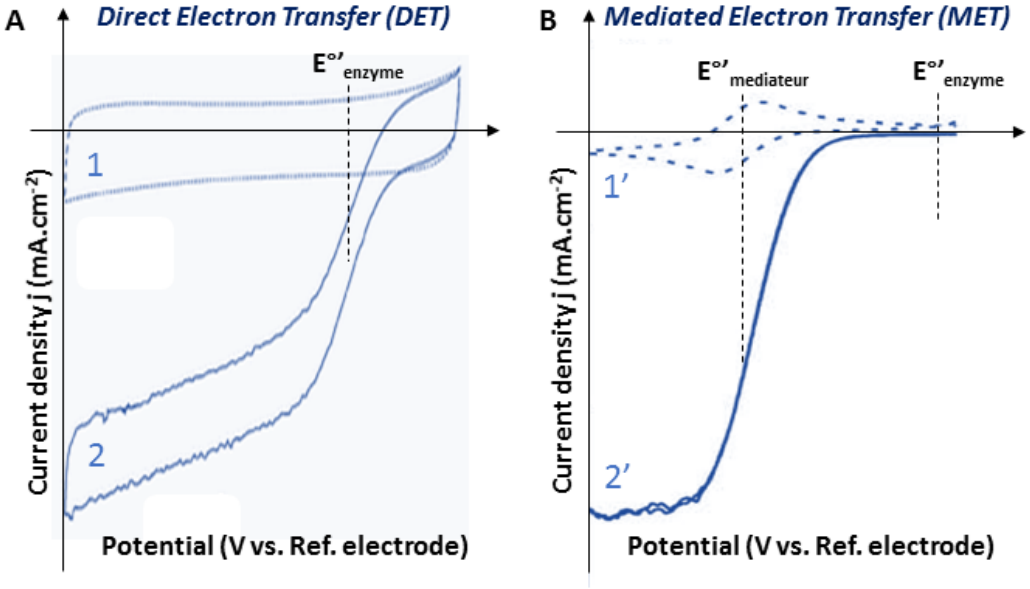

Figure 7. Representative cyclic voltammograms of a MCO in DET (A) and MET (B). Curves 1 and 1' are recorded in non-catalytic conditions in the absence of O_2. Curve 1' clearly shows the redox process of the mediator. Curves 2 and 2' are recorded in catalytic conditions under O_2. The dotted vertical bars indicate the apparent standard potentials of the enzyme ($E°'_{enzyme}$) and of the mediator ($E°'_{mediator}$).

Therefore, a performant DET can only be obtained for a monolayer of enzymes properly oriented. Experimentally, it has been verified for redox proteins including MCOs immobilized on SAMs with different alkyl lengths that the efficiency of electron transfer decreases exponentially with increasing numbers of methyl groups.[149-151] In proteins, electrons tunnel through a maximum distance of ~ 14 Å.[146]

MET is possible if the affinity between the enzyme and the mediator is high enough, and if the difference in their redox potentials induces a driving force for the electron transfer. Both the oxidized and the reduced forms of the mediator must be stable chemically, and of course none of them must inhibit the bioelectrochemical reaction. The mediator can be for example

another protein like cytochrome *c*,[152] diffusive species like ABTS or transition metal complexes, or a metal complex bound to a polymer, like osmium complexes.[153] The corresponding polymers are used in the form of a hydrogel, whose reticulated structure allows permeation of solvent and diffusion of ions and non-charged species. Unlike most hydrogels, osmium based redox polymers are also capable of conducting electrons via self-collision between neighboring oxidized and reduced osmium redox moieties. The "diffusivity" of electrons in the hydrogel depends on the length of the tether that links the osmium complex to the polymer backbone, the characteristic electron-hoping distance between neighboring redox sites, the self-exchange rate constant, and the concentration of redox sites.[154] In MET configuration, the catalytic wave is centered on the mediator potential (Fig 7B).

The two approaches have advantages and drawbacks. DET is reasonably simple and cheap, and allows working with overvoltages close to zero thanks to intrinsic properties of enzymes. However, it requires a unique orientation and only allows the simultaneous connection of a maximum of one monolayer of enzymes. In contrast, MET allows to wire electronically lots of enzymes regardless of their orientation and even in multilayers. The hydrogel especially is a convenient matrix for enzyme immobilization that even protects enzymes from inhibitors. However, electron-hopping in the redox polymer introduces additional steps that can lower the catalytic efficiency of the bioelectrode. A drop of cell voltage is also induced because catalysis is recorded at the potential of the mediator which must be lower than that of the enzyme. Finally, in case of diffusive mediators, a cell membrane is required to avoid cross reactions.

3. Mechanistic studies of MCOs

The catalytic mechanism of MCOs in homogeneous solution has been largely investigated by different spectroscopic techniques, crystallography and density functional

theory (DFT) calculations and only partly elucidated.[92,93,95] For example, the mechanisms of MCO inhibition at high pH or high concentrations of halides, or the differences between BODs and laccases are still unclear.

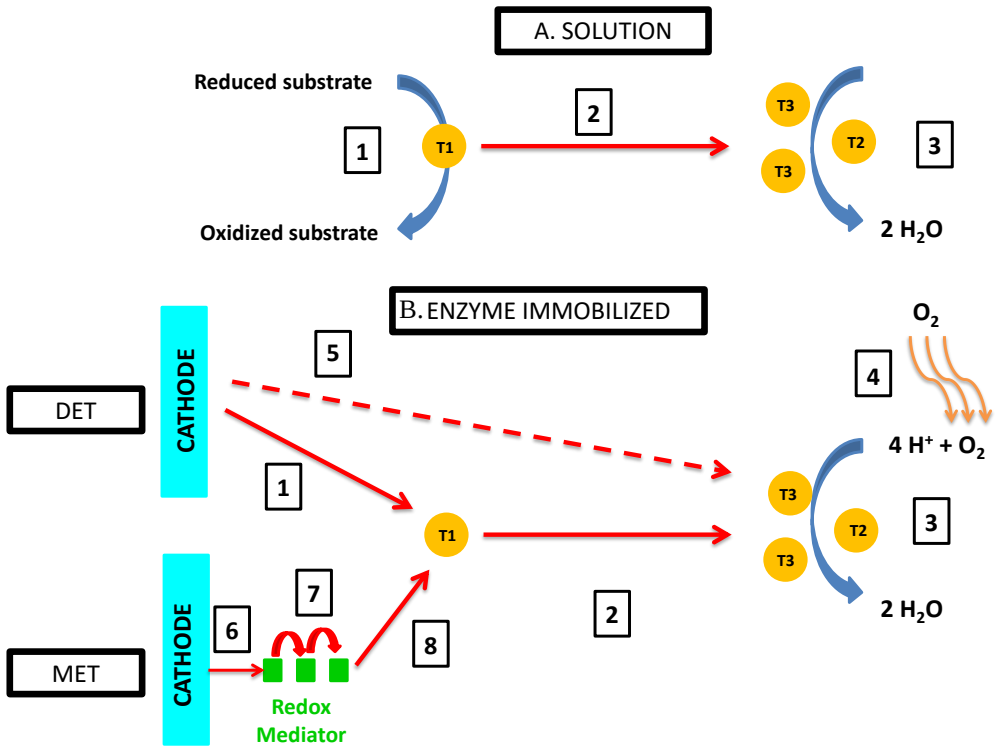

Figure 8. Comparison of different steps for electron transfer for enzymes in solution (A) and immobilized (B) with Direct electron transfer (DET) or Mediated electron transfer (MET). A) Step 1: Substrate oxidation at the T1; Step 2: IET; Step 3: O_2 reduction. B) Step 1: Electron transfer from the electrode to the T1; Step 2: IET; Step 3: O_2 reduction; Step 4: O_2 diffusion; Step 5: hypothesized electron transfer from the electrode to the TNC; Step 6: Electron transfer from the electrode to the redox mediator; Step 7: electron transfer within the redox mediator; Step 8 electron transfer from the redox mediator to the T1. Adapted with permission from [155] Copyright 2017 Elsevier

During homogeneous catalysis, oxidation of organic substrates occurs via a ping-pong type mechanism. T1 is the primary center at which electrons from the reducing substrates are accepted,[92,93,95,155,156] and O_2 is reduced at the TNC (Fig 8). One of the major questions,

however, is whether the mechanism is the same for an enzyme immobilized at the electrode. Intuitively, we may for example expect different rate limiting steps, depending whether the MCOs are connected at the electrode in DET or in MET.

The influences of pH and chloride on the MCOs activity are of particular importance, especially if MCO-based biocathodes are envisioned for BFCs operating in physiological media. In this section, we first present commonly adopted opinion about how pH and halide inhibitors impact on MCO mechanism in homogeneous solutions. Due to the general similarity between mechanism in homogeneous solution and in electrochemistry in MET connection, we simultaneously develop investigations realized in electrochemistry in MET. The reader can find more information about mechanism in homogeneous solution in different specialized reviews.[93,157-161] The following part presents a comprehensive view of DET connected immobilized enzymes. We also consider two less-known inhibitors, hydrogen peroxide and methanol, without differentiating DET and MET, because *a priori* their effect is similar in both modes.

3.1 Effect of pH on MCOs

The effect of pH on the MCO catalytic mechanism has been the subject of intense research and has only recently been partly elucidated. The first studies were reported in homogenous solution in 1997 by Xu.[162] They demonstrated that both high- and low-potential laccases from *Trametes villosa*, *Rhizoctonia solani* and *Myceliopthora thermophila* were inhibited at neutral pH and above. It was hypothesized that laccases were inhibited upon increasing the pH due to the binding of OH^- to the T2 site, therefore interrupting intramolecular electron transfer between the copper sites.[157,158]

Solomon *et al.* investigated in details how pH influences laccases reaction mechanism.[93] They particularly tried to decipher which step of the reaction cycle was

inhibited at high pHs. Since the rates of formation of the PI and NI states are pH-independent[163], these steps cannot be associated to the pH inhibition (Fig. 3). The remaining possibilities are therefore the formation of the fully reduced form, either from NI or from the resting oxidized form, or an alternative mechanism. More recently, by combining protein film volammetry,[164] computational modeling and numerical analysis, Blanford *et al.*[165] investigated the pH dependence of O_2 reduction of two high and two low-potential MCOs immobilized in DET mode. They attributed the pH inhibition to another redox state of the enzymes, unknown so far, called "X state". This point is detailed further in section 3.4.8. However, since there are no direct spectroscopic or crystallographic features of the "X state", it cannot be totally excluded that the inhibition effect may come from the NI state. If the formation of NI has been studied extensively, this is not the case of the protons involved during the reduction of NI.[105]

While the residual activity of laccases is almost nil at neutral pH, irrespective of the redox mediator used, this is not so for BODs.[53] Since the specific activity of BODs is declining with the pH (when ABTS is used as a substrate), one can hypothesize that OH^- also inhibits BODs. Nevertheless, detailed kinetics studies on BODs still have to be performed. Another question remains open: why are BODs less sensitive to pH than laccases?

Different strategies have been explored to prevent laccases inhibition at neutral pH, or to get around it. For example, by switching from a fungal *Tv*-laccase to the small bacterial laccase from *Steptomyces coelicolor*, which was reported to be highly active at pH 7, Calabrese-Barton *et al.* reached 1.5 $mA.cm^{-2}$ at 40°C and 900 rpm while they only reached 0.2 $mA.cm^{-2}$ with the fungal one.[166] The exact reason for the higher activity of *Sc*-laccase at neutral pH still has to be identified. Enzyme engineering and molecular biology are also powerful tools to evolve laccases.[167] For example in 2009, Cusano *et al.*[168] succeeded in shifting the pH profile of chimeric laccases and in 2013, Alcalde *et al.* widened the pH profile

of a fungal laccase.[169] The same authors later used directed molecular evolution to evolve a basydiomycete laccase.[170] After several rounds of evolution, they succeeded in getting a high redox potential laccase with an optimum activity shifted towards neutral pH and more resistant to chloride. Surprisingly, all mutations were located in the second coordination sphere of the T1. All these engineered enzymes have yet to be tested in electrochemistry. Pita, De Lacey *et al.*[171] proposed a different approach. By locally acidifying the pH at pH 5 near a modified electrode with *Th*-laccase, the authors succeeded in keeping the enzyme active while the pH of the bulk solution was 6.5. To create an acidic local pH around the *Th*-laccase electrode, they used magnetic particles modified with glucose oxidase.

3.2 Halides inhibition

The first detailed studies in homogeneous solution on the effect of halides (Cl^-, F^-, Br^-) on MCOs activity have been reported in 1996 by Xu using ABTS as a substrate.[172] In the study, the author tested 5 different laccases and *Mv*-BOD. He concluded that the inhibition order was following the general trend $F^- > Cl^- > Br^-$ and depended on the accessibility of ions to the TNC. The author also noticed that the magnitude of the inhibition was dependent on the species of laccases, particularly because the latter influences the size of the channel leading to the TNC. All MCOs were inhibited by F^-, and *Mv*-BOD was 1000 times more tolerant to Cl^- compared to laccases. In 2001, Xu reviewed the effect of pH and anions on the inhibition on 5 laccases from different species.[157] In 1998, Hirose *et al.*[173] specifically studied the effect of halides inhibition on bilirubin ditaurate oxidation by *Tt*-BOD. The inhibition order was SCN^- (thiocyanate) > F^- >> Cl^- > Br^-, and the inhibition was non-competitive.

Mechanistically, the affinity between fluoride and the TNC is a general trait of MCOs and has been the subject of numerous investigations particularly by combining EPR, X-ray crystallography and modeling.[158-161] In 2005, Quintanar *et al.*[174] proposed a model in which

the binding of F^- only occurs in presence of the fully oxidized TNC. It is explained by strong electrostatic interactions between the negatively charged fluoride and the positively charged fully oxidized TNC. On the contrary, the exact mechanism of chloride inhibition of MCOs in homogeneous solution is not yet elucidated. It is not excluded that Cl^- may interact with the T1 or with the TNC but spectroscopic and crystallographic evidence is still missing.

Because of the envisioned applications of MCOs, the effect of halides on the catalytic reduction of O_2 by MCOs immobilized at electrodes has been studied. The current density of the "wired" *Mv*-BOD and *Tt*-BOD electrodes with osmium redox polymer only declined respectively by 6% and 3% in presence of 140 mM NaCl at pH 7.4.[120,175] Moreover, even though fluoride has a very high affinity with the MCOs, the presence of 100 mM F^- did not significantly affect the current density. It can be hypothesized that the electrostatic adduct formed by the enzyme and the redox polymer acts as a shield against Cl^- and to some extent F^-. A similar effect has been seen by Calvo *et al.* with a self-assembled layer of laccase and osmium bound to poly(allylamine), when the concentration of Cl^- in solution was below the concentration of chloride bound to positively charged groups in the polycationic film.[176] When the same redox polymer used to wire BODs was quaternized,[177] the effect of fluoride was much more pronounced, the current declining already by 40% in presence of 20 mM F^-. Quaternization introduces positive charges within the redox polymer and may therefore affect the interaction between enzymes and polymer, exposing the TNC to fluoride. Although BODs already share a relative tolerance to chloride, to prevent even more the inhibition by Cl^-, a different strategy consists in identifying new BODs with increased resistance to it. Durand *et al.* have for example reported a new BOD from *Bacillus pumilus* which only loses 20% of its activity towards SGZ oxidation in presence of 500 mM NaCl in a 100 mM citrate–phosphate buffer pH 7.[101] Once immobilized within an osmium redox polymer, this new enzyme showed a high tolerance to chloride.

In contrast to BOD electrodes, the effect of Cl^- on laccase-modified electrodes is pronounced. The activity of an electrode modified with osmium polymers and *Th*-laccase declined by 60% at pH 5 when the chloride concentration was raised from nil to 100 mM.[178] It has been hypothesized that Cl^- was a competitive inhibitor towards redox mediators, blocking their access to the T1 site.[179] Even though this hypothesis still has to be clearly proven, strong evidence has already been reported. For example, Bey *et al.* designed a new osmium redox polymer with the objective to improve the interaction between the T1 and the osmium, therefore restricting the access of anions to the catalytic site. It resulted in the formation of a chloride-resistant cathode based on *Trametes hirsuta*.[180] The authors also applied the same strategy to shield CotA from *Bacillus subtilis* from chloride.[181] With the same objective but a different strategy, Leech *et al.* used a laccase from *Melanocarpus albomyces*, which displays an optimal activity near neutral pH,[182] co-immobilized with $(polyvinylimidazole)_{10}[Os(2,2'\text{-}bipyridine)_2\ Cl\ ]^{+/2+}$. They could reach 3.8 mA cm^{-2} at 0.2 V in a physiological buffer solution containing 100 mM NaCl,[183] the highest current density reported for laccase at neutral pH, and later used it in a glucose/O_2 BFC.[184] The inhibition effect of Cl^- on laccase modified electrodes is also observed in DET, to some extent. For example, when *Cerrena maxima* laccase was immobilized on graphite particles, the current declined by 30% upon addition of 0.1 M NaCl.[185] Salaj-Kosla *et al.* showed that the activity of nanoporous gold electrodes modified with a laccase from *Trametes hirsuta* was strongly dependent on halides in a citrate-phosphate buffer pH 4.[186] Addition of fluoride completely inhibited the enzyme because, as discussed above, F^- blocks the electron transfer between the T1 and the TNC. The addition of 200 mM Cl^- decreased the current by 50%. In contrast, when the same enzyme was immobilized on graphite carbon electrodes through phenyl derivatives, De Lacey *et al.* did not observe any inhibition by Cl^-.[187] Interestingly, the addition of ABTS as a diffusing redox

mediator made the modified electrodes sensitive again to Cl^-. This observation tends to confirm that Cl^- may act as a competitive inhibitor towards redox mediators.

3.3 Model of mediated electron transfer

3.3.1 Model

Mathematical models predict and describe the observed steady-state electrochemical currents and concentration profiles of enzymes, substrates and redox mediators. The models consider mass and charge transport, enzymatic reactions and electrode reactions. Modeling coupled reaction/diffusion problems leads to a set of non-linear differential equations that cannot always be solved analytically. Therefore, either analytical solutions are derived under certain hypothesis or simplifications (*i.e* describing limiting cases), or alternatively numerical full solutions can be simulated. We give below a brief introduction of the models of an MCO cathode based on mediated electron transfer (MET) mechanism. Further details and last achievements can be found in a recent review.[90]

MET mechanism includes two substrates, O_2 and the redox mediator. The mechanism is described by a non-sequential, or "ping-pong" mechanism, where all steps of enzyme reaction with O_2 are included in a global oxygen reduction reaction (ORR) mechanism (Fig 9). The redox mediator transfers one electron to the electrode.

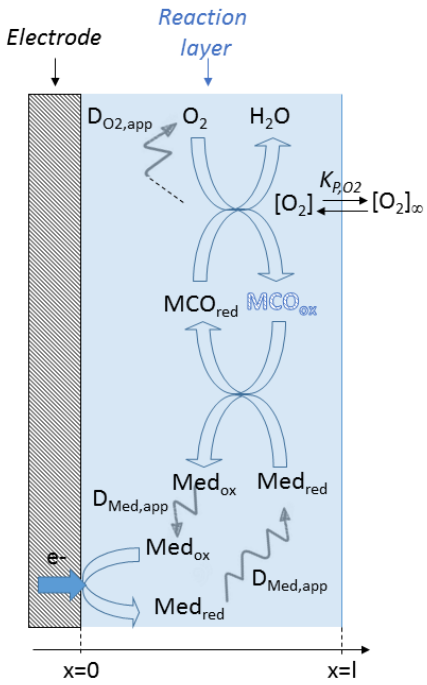

Figure 9. Schematic illustration of a MCO-based oxygen-reducing cathode. The processes described in the mathematical model occur throughout the film from x = 0 (electrode surface) to x = l (film thickness). Partition of oxygen between the film and solution is described by the partition coEfficient $K_{P,O2}$. The motion of charges is described by the apparent diffusion coEfficient $D_{Med,app}$ of the redox mediator. Oxygen diffusion occurs within the film with a diffusion coEfficient $D_{O2,app}$. O_2 is reduced by the reduced MCO to H_2O, the oxidized MCO is reduced by the mediator, and the mediator is re-reduced at the electrode surface. Adapted with permission from [188]. Copyright 1995 Elsevier.

The reaction mechanism for MCO can therefore be described by the following equations, derived from a general model of ping-pong mechanism[188-191]

$$O_2 + 4H^+ + MCO_{red} \rightarrow MCO_{ox} + 2H_2O \qquad Eq.5$$

$$4Med_{red} + MCO_{ox} \rightarrow 4Med_{ox} + MCO_{red} \qquad Eq.6$$

and the mediator reduction at the electrode can be expressed as:

$$Med_{ox} + e^- \leftrightarrows Med_{red} \qquad Eq.7$$

Typically only the case where both the enzyme and the redox mediator are confined by a membrane or a polymer in the reaction layer at the electrode surface was considered.[188-194] In this case, the enzyme is immobile while the mediator is diffusing with an apparent

diffusion coEfficient $D_{Med,\ app}$ to/from the electrode surface where it is reduced. Alternatively, in case of a linked redox mediator, charges are propagating by electron-hopping between the neighboring redox sites across the hydrogel layer and the model is formally unchanged. Oxygen is diffusing in the film with an apparent $D_{O2,app}$. The bulk solution is supposed to be ideally mixed (*i.e.* $[O_2]_{x=l}$ = constant) and the convection in the catalytic layer can be neglected. Assuming a one-dimensional diffusion, the following differential equations can then be derived (for $0 < x < l$):[188,189,193]

$$\frac{\partial[Med_{red}]}{\partial t} = D_{Med,app}\frac{\partial^2[Med_{red}]}{\partial x^2} - 4v_{Enz} \quad Eq.8$$

$$\frac{\partial[O_2]}{\partial t} = D_{O2,app}\frac{\partial^2[O_2]}{\partial x^2} - v_{Enz} \quad Eq.9$$

where v_{Enz} is the rate of the enzymatic O_2 reduction. In some studies, only the substrate consumption rate was supposed to exhibit a Michaelis-Menten kinetics,[188] while in other cases the catalytic rate constants of the enzymatic reaction were supposed to be independent on both O_2 and mediator concentrations.[192] The pH-dependency of enzymatic activity was not taken into account.

It may reasonably be proposed that the model assuming a Michaelis-Menten kinetics both for O_2 and the redox mediator, first derived for a stoichiometric coEfficient for electrons, can be extended to the case of MCOs for which 4 electrons are necessary to reduce 1 molecule of O_2. In these conditions, v_{Enz} at steady-state is therefore defined as:[189,191,193]

$$v_{Enz} = \frac{k_{cat}[MCO_{Tot}]}{1 + {K_{M,Med}}/{[Med_{red}]} + {K_{M,O_2}}/{[O_2]}} \quad Eq.10$$

k_{cat} is the effective rate constant and K_{M,O_2} and $K_{M,Med}$ are the effective Michaelis-Menten constants for the ping-pong mechanism. This allows introducing two additional kinetic

constants, k_{O_2}, the maximal catalytic rate constant at saturating mediator concentration and k_{Med}, the maximal catalytic rate constant at saturating O_2 concentration. With the notations used above, theseconstants are respectively defined as:

$$k_{O_2} = \frac{k_{cat}}{K_{M,O_2} + [O_2]} \qquad Eq.11$$

$$k_{Med} = \frac{k_{cat}}{K_{M,Med} + [Med_{red}]} \qquad Eq.12$$

The kinetics of equation 7 defines the boundary conditions of $[M_{red}]$ at x = 0. It is reasonable to consider that the electrochemical reaction is reversible and that its kinetics follows a Butler-Volmer law. In most cases, diffusion is considered to be the only mass transport mechanism. In some recent models however, an additional term has been introduced to take into account the mass transport by migration (*i.e.* the influence of electric field),[194]or convection.[192]

3.3.2 Mathematical modeling

Both analytical and numerical methods have been used to derive the equations describing the behavior of an enzymatic electrode[188-193,195,196] or more rarely of complete EBFCs.[90,194]

3.3.2.1 Analytical solutions

In a first fundamental study Bartlett *et al.*[188] built a case diagram based on complete analytical solutions derived for a set of limiting cases. In their study, they only considered a Michaelis-Menten kinetics for the substrate conversion (*i.e.* O_2 reduction in our case). Figure 10 shows the 2D case diagram corresponding to the further assumption that diffusion/reaction of redox mediators are well balanced with diffusion/reaction of substrate in the reaction film

(in our case it would correspond to $D_{O2,app}\frac{K_{M,O_2}}{k_{O_2}} = D_{Med,app}\frac{K_{M,Med}}{k_{Med}}$), while substrate concentration is below the saturation condition in the film ($K_{P,O2}[O_2]_\infty << K_{M,O2}$).

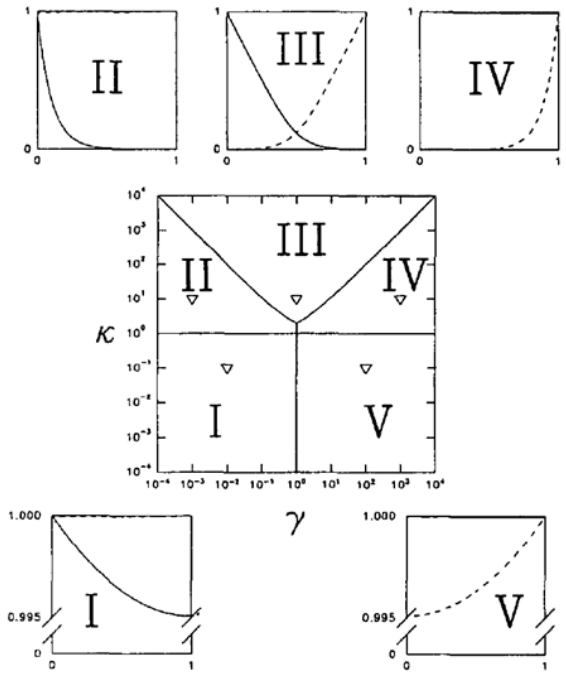

Figure 10. Two-dimensional case diagram showing the five limiting cases predicted analytically. The concentration profiles surrounding the case diagram are from simulations at the points marked (∇) on the case diagram: case I, κ = 0.1, γ = 0.01; case II, κ = 10, γ = 0.001; case III, κ = 10, γ = 1; case IV, κ = 10, γ = 1000; case V, κ = 0.l, γ = 100. The continuous lines indicate dimensionless mediator concentration profiles ($[Med_{red}]/[Med_{Tot}]$, assuming that the mediator is confined in the film); and the dotted lines the dimensionless substrate concentration profiles ($[O_2]/K_{P,O2}[O_2]_\infty$). Horizontal scale is from x = 0 (electrode) to x = 1 (bulk solution). Vertical scale is dimensionless concentration. Note the compressed vertical scale for profiles I and V. Reprinted with permission from [188]. Copyright 1995 Elsevier.

The two dimensionless coordinates of the resulting case diagram are κ, which describes the relative thicknesses of the film and diffusion layer; and γ, the relative concentrations of enzyme in its reduced or oxidized forms. In the first case (I), the limiting step is the enzyme-mediator reaction (*i.e.* mass and charge transport of substrates and redox

mediators within the film are faster than the enzymatic reaction). The second case (II) corresponds to limitation by the mass and charge transport of the redox mediator. In case III, the reaction kinetics are much faster than substrate and mediator diffusion, so that the enzymatic reaction is limited by the substrate in one part of the film, while it is limited by the mediator in the other part of the film. This situation results in the reaction occurring only in a very thin region inside the film. The fourth case (IV) corresponds to limitation by the mass and charge transport of the substrate. Finally, in case V the limiting step is the enzyme-substrate reaction (*i.e.* mass and charge transport of substrate and redox mediators within the film are faster than the reaction).

More recently, analytical solutions were derived using the homotopy perturbation method (HPM) combined with the inversion conjuncture in the Laplace plane.[192,195,196] While limiting cases mostly describe steady-state electrochemical responses, this method allowed describing current densities in chronoamperometry at different potentials both in the transient and steady states. It was applied to an electrode based on MET of laccase in an osmium redox hydrogel. The time to reach steady-state was determined, and proved to depend on the potential of the redox mediator. Interestingly this approach could show how much the steady state current densities were influenced by the enzyme characteristics (catalytic and Michaelis-Menten constants), concentration of substrate in the bulk, and film thickness.[192] In a further study, the same approach showed its significance for the derivation of analytical expressions of steady-state current densities and O_2 and mediator concentrations, valid in the potential step methods. Moreover, two graphical procedures were proposed for the estimation of Michaelis-Menten constants. In both cases, the model was validated by fitting with experimental data of oxygen-reducing laccase cathodes.[192,196]

3.3.2.2 Full numerical derivation

In the first study of Bartlett mentioned above, numerical simulations of the one dimensional model were performed based on the relaxation method, and were in good agreement with the analytical study.[188] This 1D model was then applied to an enzymatic O_2 reducing porous cathode.[193] The composite electrode was modelled as cylindrical conducting fibers around which the reaction layer film was coated. The influence of morphology (in terms of film thickness, composite porosity and fiber diameter) was evaluated. The authors also studied how to improve mass transport of the oxygen substrate, and predicted that the maximum current densities could be close to 100 $mA.cm^{-2}$ for a pure O_2-breathing electrode, and 60 $mA.cm^{-2}$ for an air-breathing electrode.[193] While this study mainly focused on thick films, another proposed to consider high-surface area electrodes grafted with thin polymer layers.[189] In that case also it was proposed that currents around 100 $mA.cm^{-2}$ could be achieved with the porous electrode.

Another important contribution[190] used modeling to determine the effect of ΔE_{et} (difference between the T1 and the redox mediator potentials) on the bimolecular rate constants of the enzymatic reaction; k_{cat}/K_m and k_{cat}/K_S towards mediator and oxygen respectively (corresponding to $k_{cat}/K_{M,Med}$ and $k_{cat}/K_{M,O2}$ with our notations). Using a finite difference method, expressions of substrate and redox mediator concentrations were determined, from which the expression of current density was derived. This expression was used to extract kinetic parameters from experimental CVs recorded with *T. hirsuta* laccase immobilized in redox hydrogels with osmium based redox mediators covering a wide range of potentials.[190] The bimolecular rate constants were found to be slightly lower in the film than those determined in free solution.[156] In addition, the performance of the cathode was found to vary linearly with ΔE_{et} for $\Delta E_{et} < 300$ mV, and to be independent on ΔE_{et} for $\Delta E_{et} > 300$ mV (Fig 11).[190]

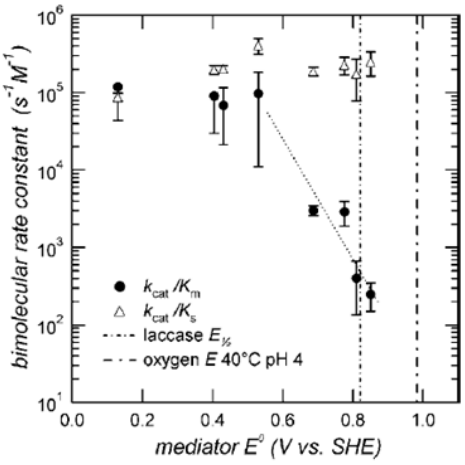

Figure 11. Effect of mediator redox potential, E^0, on laccase-mediator bimolecular rate constant, k_{cat}/K_m, and laccase-oxygen rate constant, k_{cat}/K_s. Also shown are redox potentials of laccase and O_2/H_2O at pH 4. A linear free energy region is observed for high E^0 (small ΔE_{et}) and constant mediation rate at lower E^0 values. Reproduced with permission from [190]. Copyright 2008 American Chemical Society.

A model of a complete glucose/O_2 EBFC composed of a cascade of enzymes and a redox mediator at the anode, and an air-breathing cathode based on BOD with ferricyanide has also been reported.[194] This model was used to describe an EBFC formerly reported by Sakai *et al.*[197] where both enzymatic systems were immobilized on porous carbon-fiber electrodes. The simulated data agree with the experimental results. Clues could be obtained concerning the evolution of concentrations and currents over time at a given cell voltage, but also concerning the evolution of several parameters in space. For example, pH was shown to vary in the cell, being maximal at the anode. When a voltage was applied across the cell for a long time, the overpotential at the carbon-fiber cathode was found to drop drastically with the distance from the electron collector/carbon-fiber interface.[194]

3.4 Studies of the mechanism of direct electron transfer

In this part, we discuss the electrochemical behavior of enzymes at the electrode interface in DET and explain general mechanistic clues provided by electrochemical studies. In the DET mode, electrons could theoretically be transferred directly to the TNC, provided that this latter is accessible and close enough to the electrode surface, thus bypassing the internal electron transfer. Therefore, one of the major questions is whether the O_2-reduction mechanism remains unchanged for an enzyme directly connected at the electrode (DET mode).

3.4.1 Redox potentials of the Cu sites

Redox potentials characterizing the different Cu sites of various MCOs have been determined by redox titration in homogeneous solutions. T1 Cu, whose oxidation state can only vary between +I and +II, is well characterized by a single redox transition at a determined apparent standard potential E°'. Slightly different values for the same enzyme can however be found in literature. MCOs can be classified according to the redox potential of their T1 site in low (340-490 mV *vs.* NHE), middle (470-710 mV *vs.* NHE) and high (730-780 mV *vs.* NHE) redox potential MCOs.[18,198] Tree laccases belong to the first group and fungal laccases to the third one,[18,199,200] while BODs are part of the 2nd with for example T1 potentials of 660 mV and 670 mV *vs.* NHE at pH 7 for *Tt*-BOD and *Mv*-BOD.[201-204] Moreover, the T1 titration curve is indicative of a one electron process since the potential varies by 49-90 mV per unit of log(Abs).[118,202] The molecular origin of these potential differences is discussed in section 2.1. It is more difficult to attribute redox potentials to the TNC because this cluster can be characterized by several redox transitions. In very early studies, the redox potentials of the T3 sites of *R. vernicifera* and *T. versicolor* laccases have been determined at 480 and 780 mV *vs.* NHE resp.,[199,200] while a redox potential of ≈390 mV

vs. NHE was attributed to the T2 Cu of the low-potential *Rv*-laccase.[199,200] In this section, unless stated otherwise, we quote redox potentials against the NHE reference electrode for the sake of consistency with the literature.

Determination of the redox potential of T1 in MCOs has also been realized by non-mediated spectroelectrochemistry following the vanishing of the blue band at 600 nm upon application of reductive potentials and its re-apparition upon re-oxidation.[118] Direct electron transfer between a gold electrode and a high-potential laccase was also observed for the first time with this technique, with *Trametes hirsuta* in a gold capillary.[118] Non-mediated spectroelectrochemistry furthermore confirmed the possibility to establish DET with the T1 Cu for several fungal laccases from different basidiomycetes (*Trametes hirsuta*, *Trametes ochracea*, *Cerrena maxima*).[205] Simultaneous detection of T1 and T3 Cu (at resp. 600 and 300 nm) also proved that enzymes could be fully reduced via DET from an electrode.[205] Here again, analysis of the titration curves gave information about the electron transfer mechanism. In case of high potential *Th*-laccase and *Mv*-BOD, DET to the T1 was very slow, and the curve showed a hysteresis and 2 noticeable electron transfer (ET) processes. This was attributed to ET to the T1 (resp. at 860 mV for *Th*-laccase and 805 *vs*. NHE for *Mv*-BOD) mediated by another redox site in the MCO (resp. at 290-370 and 460 mV *vs*. NHE for *Th*-laccase and *Mv*-BOD).[118,202] Since only ascorbate can fully reduce the laccase, implying that the redox potential of the T2 might be considerably more negative than the T1, it was proposed that the T2 redox potential for high-potential laccases was about 400 mV *vs*. NHE at pH 6.5. Therefore, although in these cases electron transfer from the electrode to the T1 was realized without the help of an external redox mediator, it was not, strictly speaking, “direct electron transfer” to the T1. It proceeded via another enzymatic redox site of lower potential and most likely the T2 Cu. [118]

3.4.2 Non-catalytic faradaic processes under anaerobic conditions

In several cases, direct electron transfer (DET) between MCOs and electrodes has been observed under anaerobic conditions and characterized by the appearance of reversible or quasi reversible redox peaks in cyclic voltammetry (CV), linear sweep voltammetry (LSV) or square wave voltammetry (SWV). For high-potential laccases, different redox peaks have been observed corresponding to either a high or a low-potential process, or both. The midpoint redox potentials (given by $E_m = \frac{E_a+E_c}{2}$ where E_a is the potential of the anodic peak and E_c is the potential of the cathodic peak) were usually observed in the 300-450 mV *vs.* NHE range for the low-potential processes, and between 600 and 900 mV *vs.* NHE for the high-potential processes respectively.

3.4.2.1 Strongly oxidizing laccases

3.4.2.1.1 Low redox potential

In 1999, a low redox quasi reversible process at E_m = 411 mV *vs.* NHE was observed at pH 6 for a recombinant truncated *Tv*-laccase immobilized on a thiol-modified gold electrode.[206] Numerous other examples of this low-potential redox process can be found in the literature: a pair of peaks with a midpoint at E_m = 337 mV *vs.* NHE at neutral pH was recorded for *T*v-laccaseat thiol modified monocrystalline gold (111) surfaces;[207] a single quasi reversible redox process at E_m = 405 mV *vs*. NHE was observed for *Th*-laccase in a gold capillary.[118] *Th*-laccase adsorbed on a bare gold disc, and laccases from *Cerrena maxima*, *Trametes hirsuta* and *Trametes versicolor* covalently bound on 4-aminothiophenol (AMT) on gold exhibited two pairs of redox peaks. One of them had a low-potential resp. at E_m = 486 mV *vs*. NHE for *Th*-laccase on bare gold, and approx. 400 mV for the three laccases on aminothiophenol.[205] *T. versicolor* and *T. hirsuta* laccases entrapped in a cationic polymer matrix on a gold electrode also exhibited two pairs of peaks, with one in the low-potential

range (resp. E_m = 394 ± 3 mV *vs*. NHE for *Tv*-laccase and E_m = 408 ± 4 mV *vs*. NHE for *Th*-laccase at pH 6.5).[208]

This low-potential process, mostly observed with a gold working electrode,[18,118,205-208] can hardly be assigned to the T1. It was hypothesized that it could be related to the T2 redox transition. To confirm this hypothesis, experiments were realized with T2-depleted enzymes.[118] While a 50% T2-depleted *Th*-laccase gave 50% peak current, no low-potential redox peak was observed for the apo-enzyme. In addition, in presence of F^-, whose affinity for the TNC has been shown in homogeneous solution, the midpoint potential increased by about 35 mV. All these experiments tended to confirm that T2 potential is around 400 mV *vs.* NHE, and that in all the above mentioned cases, at least a fraction of laccases were oriented with the T2 Cu facing the surface.[118] Experiments performed with a recombinant laccase bearing a Cys-tag, inducing different orientations of the enzyme on gold via the S-Au bond, also supported the attribution of the peak at lower potential to a TNC intermediate. When upon immobilization the T1 was repelled far from the electrode surface, and the T2/T3 approached close to it, a redox process at E_m = 377 mV *vs*. NHE was observed and attributed to the T2. On the contrary when T1 and T2/T3 were at the same distance from the electrode surface, a more irreversible pair of redox peaks with E_m = 470 mV *vs*. NHE was observed and attributed to simultaneous effect of both T1 and TNC Cu clusters.[209]

3.4.2.1.2 High redox potential

For high-potential laccases, a high-potential redox process, more certainly corresponding to the T1 has also been identified (Fig 12).

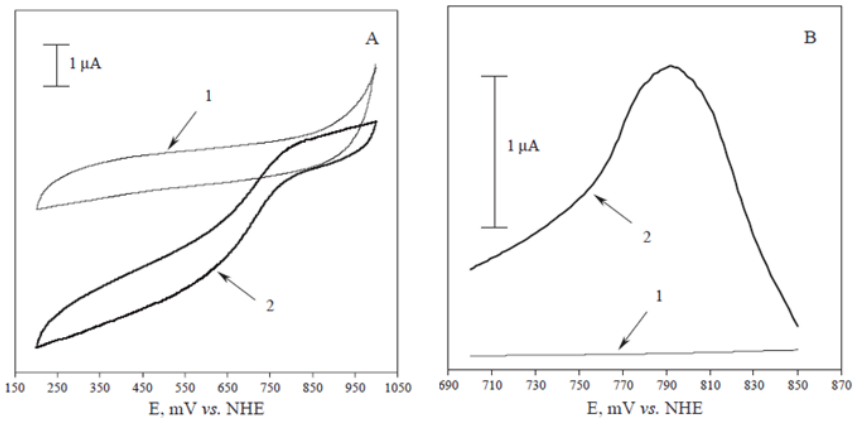

Figure 12. Voltammograms recorded with HOPG electrodes (1) without and (2) with *T. hirsuta* laccase (30 mg.mL^{-1} laccase solution) entrapped under a dialysis membrane at the electrode surface. (A) Cyclic voltammograms recorded in air-saturated 50 mM citrate-phosphate buffer pH 3.5 containing 100 mM $NaClO_4$; scan rate: 10 mV.s^{-1}. (B) Osteryoung square wave voltammograms recorded under anaerobic conditions in 100 mM phosphate buffer pH 6.5; amplitude: 10 mV, frequency: 10 Hz. Reprinted with permission from [210]. Copyright 2005 Elsevier.

A reversible redox process on a graphite electrode at 645-700 mV *vs.* NHE at pH 5 has been observed for *Tv*-laccase, but only in the presence of a promotor (2,6-dimethoxyphenol (DMP) or 4,4'-bipyridine).[211] Later, *Tv*-laccase adsorbed on edge-plane pyrolytic graphite exhibited a reversible redox process at 790 mV *vs.* NHE.[212] Similarly, redox peaks between 780 and 800 mV *vs.* NHE at pH 6.5 were recorded by SWV for *T. hirsuta*, *T. ochracea*, and *C. maxima* laccases adsorbed on HOPG.[210] The same enzymes adsorbed on gold electrodes exhibited high redox processes (between 857 and 903 mV *vs.* NHE), which lowered to approx. 800 mV when the enzymes were covalently bound on AMT.[205] Similarly, the high potential redox peak of laccases from *T. versicolor* and *T. hirsuta* entrapped in a cationic polymer matrix on a gold electrode were respectively 784 ± 3 and 778 ± 4 mV *vs.* NHE, in good agreement with the T1 potential. [208]

3.4.2.2 Low-potential laccases

For low potential laccases, electrochemical studies described only one pair of redox peaks coinciding with the T1. A non-catalytic process with semi reversible behavior was observed for *Rv*-laccase on a gold electrode modified with an anionic polymeric film at 410 mV (pH 5.5) or 400 mV *vs.* NHE (pH 7),[213] and at 410 mV *vs.* NHE at pH 7 for the same laccase covalently bound on mercapto-propionic acid (MPA) on gold.[214] This anaerobic process did not change upon addition of F^-,[214] and T2-depleted enzyme still exhibited the same redox process while the apo-protein was electrochemically silent.[213] *Melanocarpus albomyces* and *Rv*-laccases entrapped in a cationic polymer matrix on a gold electrode also exhibited only one redox process at resp. 422 ± 4 and 449 ± 5 mV *vs.* NHE at pH 6.5, in good agreement with T1 potential.[208]

3.4.2.3 Bilirubin oxidases

BODs behave approximately like laccases with respect to their electrochemical response in absence of O_2. For *Mv*-BOD adsorbed on SPG, a unique and very small quasi reversible process at E_m = 51[illegible] ge peak separation was first recorded.[215] Later, two pairs [illegible] ified at E_m = 690 mV (resp. 700 mV) and E_m = 390 mV [illegible] or *Tt*-BOD (resp. *Mv*-BOD) adsorbed on SPGE (Fig 13).[20[illegible]

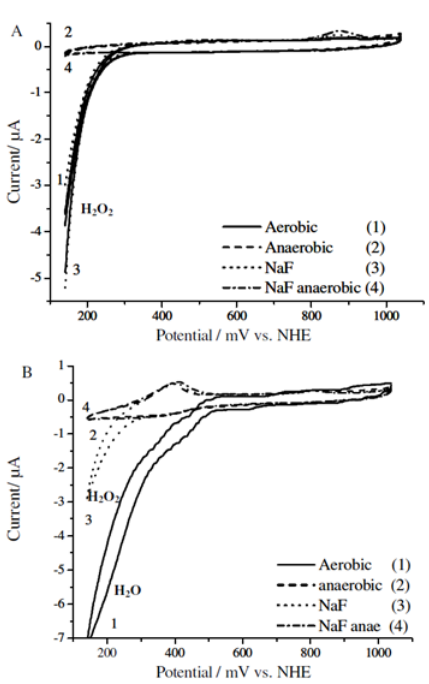

Figure 13. Representative cyclic voltammograms of (A) *Cerrena maxima* and (B) *Trametes hirsuta* laccases immobilized on (A) bare and (B) 4-aminothiophenol self-assembled monolayer (SAM) modified gold disc electrodes (0.1 M phosphate buffer pH 5.0; scan rate: 10 $mV.s^{-1}$; second scan). (A) CVs of *Cerrena maxima* laccase under aerobic and anaerobic conditions, and in the absence or presence of sodium fluoride starting at 1040 mV *vs.* NHE. (B) CVs of *Trametes hirsuta* laccase under aerobic or anaerobic conditions, and in the absence or presence of sodium fluoride starting at 1040 mV *vs.* NHE. Reprinted with permission from [205] Copyright 2006 from Elsevier.

Furthermore, a quasi-reversible redox process at E_m = 360 mV vs. NHE at pH 7, observed for *Tt*-BOD covalently bound on MPA on gold, was attributed to a resting form of the enzyme because it was almost not influenced by F^-.[203] This led to the suggestion that an endergonic tunneling from the T1 to T2/T3 could be involved in MCO mechanism.[203] A non-catalytic low-potential redox signal of *Mv*-BOD (360 mV *vs.* NHE at pH 7), attributed to a resting form of the enzyme, also appeared when the enzyme was oriented with the TNC facing the electrode surface.[216] 3 non-catalytic cathodic peaks (at resp. ≈ 693, 574 and 403 mV *vs*. NHE), and only one anodic (at the lowest potential) were visible on a CV at pH 6 for *Mv*-BOD entrapped in a matrix of Ketjen black (KB), carbon nanotubes (CNTs) and chitosan. The highest was assigned to the T1, consistently with previous studies, and it was proposed that the 2 others might be attributed to different redox states of the TNC, containing or not bridging oxygen species.[217] It is noteworthy however that a low potential redox peak at ≈ 420 mV had previously been assigned to a surface group of the enzyme.[218,219] The simultaneous presence of two pairs of peaks suggested that for different fractions of BOD only the T1 or the T2 was in contact with the electrode.[208] The appearance of the low-potential redox process was attributed to either the T2 or to a coincidental electrochemical response of the 4 Cu

ions,[18] while the high potential peak was attributed to the T1. Since different redox processes could be observed for the same enzyme immobilized at different materials, it was proposed that different protein sites were communicating with the electrode, depending on the electrode material.[203]

3.4.3 Two- *versus* four-electron reduction of dioxygen

The redox processes observed in anaerobic conditions, especially those at low potential, could not always be correlated to a catalytic current in aerobic conditions. This means that some enzymes were immobilized in a configuration that permitted direct electron exchange with the electrode, without however enabling the catalytic mechanism. This remark suggested that in these cases the enzymes were not connected via the proper redox center.[118,207] This hypothesis was confirmed in some cases by the addition of a redox mediator that enabled MET.[203,220]

The onset of catalysis was observed in some rare cases in the low-potential range for high- or middle-potential MCOs. Onset at ≈ 300 mV *vs.* NHE at pH 5 was for example reported for the fungal *Th*-laccase on bare gold[221] or AMT self-assembled monolayer (SAMs) on gold.[222] Similarly, oxygen reduction by *Mv*-BOD in solution started at ≈ 450 mV *vs.* NHE, when a gold wire modified with a mixed mercapto-undecanol/mercapto-undecanoic acid SAM was used as the working electrode.[223] Only low catalytic currents were observed with these systems, while non-catalytic signals were not detected.[221-223]

The influence of F^-, which is known to inhibit the IET in homogeneous catalysis, has been also studied. For example, *Th*-laccase covalently bound on 4-AMT-modified gold electrode exhibited a first reduction current starting at 510 mV *vs.* NHE at pH 5, which was followed by a second more steeper increase at 240 mV. F^- inhibited only the high-potential (E

> 240 mV) reduction, while the current at lower potentials remained unchanged (Fig 13). Similar observation was done for *Cm*-laccase on a bare gold disc: O_2 reduction started at a quite low potential, 320 mV *vs.* NHE, and was not influenced by F^-. This led to the supposition that in both cases no IET was occurring.[205]

Moreover, the catalysis starting at low potential has been correlated to the incomplete O_2 reduction to H_2O_2 in several cases. For example, when a fungal laccase was adsorbed on bare gold electrodes, H_2O_2 production in the low potential range (E < 240 mV *vs*. NHE) was 3 times higher than for naked gold alone. It was lower both in presence or absence of enzyme at higher potentials (240-440 mV *vs.* NHE).[205] Similarly, for an engineered laccase adopting different orientations on a gold electrode, oxygen reduction was observed either at 495 mV *vs*. NHE or at 340 mV *vs*. NHE and assigned respectively to DET by the T1-TNC or by the TNC alone. It was associated with H_2O_2 production of resp. 2.75 and 7.53 µM.[209] It seems therefore that DET from the electrode to the T2/T3 is possible but leads either to no catalysis or in the best cases to the 2-e^- reduction of O_2 to H_2O_2. It clearly appears that the orientation of the enzyme at the electrode influences both the electron transfer pathway and the electron efficiency of O_2 reduction.[209]

Contrary to the catalysis observed at low potential and assigned to the reduction of O_2 to H_2O_2, no significant formation of hydrogen peroxide has been reported for catalysis starting at the T1 potential. H_2O_2 evolution was for example estimated with a porphyrin-coated electrode in a solution in which O_2 had been reduced by a *Tv*-laccase electrode. Direct ORR started at ≈ 0.84 V *vs.* NHE at pH 5.5 with the fungal *Tv*-laccase adsorbed on graphite. The experiment confirmed that no more than 5% O_2 could have been reduced to H_2O_2.[211] A similar experiment was performed with *Mv*-BOD attached to multi-wall carbon nanotubes (MW-CNTs) on the disc of a rotating ring disc electrode (RRDE), for which the ORR onset was ≈ 0.7 V *vs.* NHE at pH 7.5. During the CV, the platinum ring was polarized to measure

the reduction of H_2O_2. Zero hydrogen peroxide was detected on the disc, and according to the mass and charge balance of the RRDE no more than 7.5% O_2 in total could have been reduced to H_2O_2.[224] In both cases, Koutecky-Levich analysis of the rotating electrode matched a 4-electron reduction to water and not H_2O_2.[211,224]

It is therefore of interest to determine the number of electrons exchanged by an enzyme respectively in high- *versus* low-potential anaerobic redox processes. For a peak at high potential, the ratio of anodic to cathodic currents were shown to vary from 1:1 (which actually can be converted to 4:4 by normalizing the peak intensity i_p by the scan rate *v*) at very low scan rates (below 1 $mV.s^{-1}$) to 4:1 at fast scan rates (above 200 $mV.s^{-1}$).[208,214] Further analysis of the peak separation ΔEp as a function of Δlog(f) in SWV indicated that 3.65 electrons were transferred for *Tv*- laccase and 3.85 for *Th*-laccase.[208] These results support a 4 e^- transfer to/from the T1 site, which would correspond to a possible full reduction/oxidation of the enzyme via the T1, with the full reduction being much slower than the oxidation. For a low-potential peak of high-potential laccases, the width of the peak (given by the difference between the half-wave potential E_{HW} and the peak potential E_P) was consistent with a 1 e^- transfer.[118] The anodic to cathodic Qa/Qc charge ratio increased from 1:1 to 3:1 with increasing *v*; and SWV analysis gave numbers of electrons of 2.78 for *Tv* and 2.9 for *Th*-laccase[208] which suggests that full reduction of the enzyme cannot occur via the low-potential intermediate whereas it is possible via the T1 Cu. For the unique redox peak of low-potential *Ma* and *Rv*-laccases, Qa/Qc varied from 1:1 for $v < 100$ $mV.s^{-1}$ to 4:1 for scan rates above 800 $mV.s^{-1}$, and SWV gave n values close to 4 (n = 3.9 for *Rv* and 3.8 for *Ma*-laccases).[208] The general observation that the reduction peak is lower than the oxidation peak[118,205] or that the rate of oxidation is faster than the reduction in CV or SWV[208,214] is consistent with the hysteresis noticed in spectroelectrochemistry, which also shows that the oxidation process is

significantly faster than the reduction process.[205] All this suggests that IET might be the rate-limiting step.

3.4.4 Causes of the low catalytic efficiency and stability on gold electrodes

Different behaviors were observed for BODs and laccases on gold electrodes. On bare gold, besides the H_2O_2 related mechanism described above, no catalysis at high potential or no catalysis at all was recorded for *Th*-laccase,[205,225] *Cm*-laccase,[205] or small laccase from *Fusarium proliferatum.*[226,227] On the other hand, a clear DET catalysis was observed for *Mv*-BOD on bare monocrystalline gold[17,225] or platinum electrodes,[17] with an onset above 0.7 V *vs*. NHE at pH 5.8 consistent with the T1 redox potential. With this latter enzyme, the observed electrocatalytic responses vanished however relatively quickly[17] with for example half-lives of resp. 15 minutes and 2.5 hours at pH 4 and 7.4, rather due to gradual deactivation than to desorption of the enzyme.[225]

The efficiency and stability of catalysis at gold electrodes was investigated by coupling electrochemistry to other techniques like quartz crystal microbalance (QCM),[151,228] QCM with dissipation monitoring,[229-231] surface plasmon resonance (SPR),[220] ellipsometry,[225] atomic force microscopy (AFM)[225-227] or dual polarization interferometry (DPI).[231] No desorption of either BOD or laccase immobilized on bare or on thiol-modified gold electrodes was measured by ellipsometry, SPR or QCM, confirming the irreversible character of the adsorption of the enzymes on these surfaces.[220,225,228,230,231] Therefore, the decrease in cathodic current observed in numerous studies cannot be related to enzyme loss but most probably to enzyme denaturation or structural rearrangement.[220,228,229] The enhancement of stability observed with amide bonding of MCOs on the electrode surface was more likely due

to a stiffening of the immobilized layer preventing conformational changes, rather than due to a better binding of enzymes to the electrode.[220,229]

3.4.4.1 Denaturation by enzyme-metal interaction

For MCOs adsorbed on bare metal surfaces, a certain loss of activity towards oxidation of organic substrates was demonstrated. DMP oxidation was 7.5 times less Efficient for *Fp*-laccase adsorbed on bare gold than on HOPG.[227] Enzymatic assay with 2,2'-azino-bis(3-ethylbenzothiazoline-6-sulphonic acid) (ABTS) showed that *Th*-laccase was completely deactivated on bare polycrystalline gold, while some activity was still recorded for *Mv*-BOD.[225] Denaturation of MCOs adsorbed on bare metal has already been suggested.[232] Very fast adsorption of *Fp*-laccase on bare gold was observed by atomic force microscopy (AFM), and the formation of aggregates with a wide variety of sizes suggested an intense interaction with bare gold.[227] For *Mv*-BOD and *Th*-laccase on bare gold, the size of globular features (≈ 20 nm) was considered normal, taking into account the tip dilation effect of the AFM.[225] Similarly, the low heights of the molecules, ranging between 2.5 and 3 nm, was attributed to a tip compression effect that makes soft biological molecules appear always smaller with AFM,[225,227] although it could also correspond to a flattening of enzymes at the surface.[231] *Mv*-BOD was also more stable on MPA-modified gold than on bare gold.[225] BOD faster deactivation on single crystal might be due to tighter holding.[17] These observations can be correlated with the faster denaturation caused by stronger electrostatic interactions observed when MCOs are adsorbed on N-doped carbon nanotubes. (see section 4.1.2 for further details)

3.4.4.2 Applied electrode potential

A potential-induced structural change of the enzyme was evidenced by in situ STM studies of *Streptomyces coelicolor* laccase adsorbed on butanethiol modified Au (111)

surface.[233] This technique allowed at the same time the first single-molecule resolution in aqueous buffer. Interestingly the oxidized enzyme (at 0.89 V *vs*. NHE) appeared transparent, while bright spots were observed for the enzyme under turnover (at 0.44 V *vs*. NHE under air) (Fig 14A).

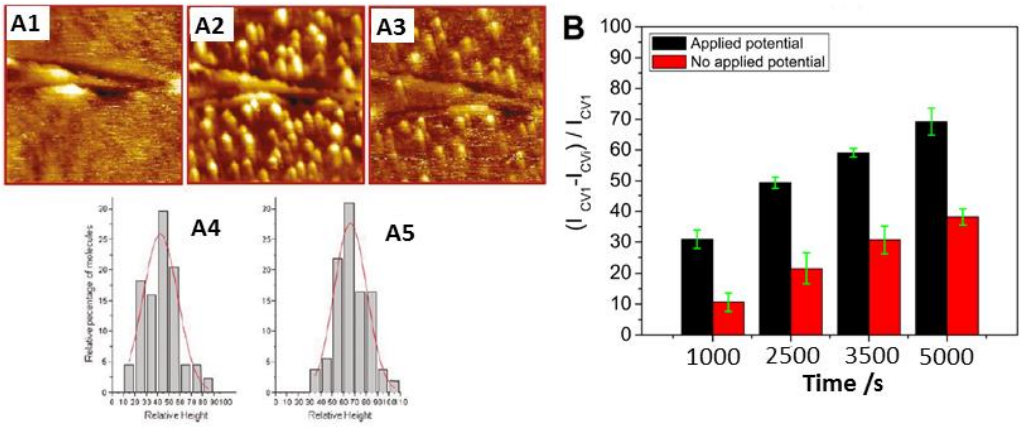

Figure 14. Influence of applied electrode potential on enzyme. (A): structural change induced by potential, evidenced by in situ STM of *Streptomyces coelicolor* laccase on a butanethiol-modified monocrystalline gold under pure O_2 atmosphere. A1: Initial image at 0.84 V *vs.* NHE. Bias: 0.70 V. A2: Image at 0.44 V *vs.* NHE. Bias: 0.30 V. A3: Image after returning at 0.84 V *vs.* NHE. Bias: 0.70 V. Tunneling current in all cases: 0.035 nA. Scan area: 100 × 100 nm^2. A4 and A5 are histograms showing the height distribution of the bright spots in A2 and A3, respectively. Height normalization was done against the maximum height measured in A2. Lines are best fits to a normal distribution. Adapted with permission from [233], copyright 2012 American Chemical Society. (B): Comparison of the catalytic current loss measured in cyclic voltammetry after the *Mv*-BOD electrode has been left at OCV (red columns) or submitted to an applied potential E = +0.2 V *vs.* Ag/AgCl (black columns). The error bars are represented in green. For better accuracy with respects to the original figure, the timescale is not linear. Adapted with permission from [220]. Copyright 2016 American Chemical Society.

Under O_2, a stronger STM contrast was observed and the process was less reversible than under air. This study therefore highlights a structural change of the protein, that enables current tunneling through the enzyme only in its oxidized form.[233] Other studies suggested

either a conformational change or reorientation under applied potential.[220,229,234] For *Mv*-BOD adsorbed or covalently bound to thiol-modified gold electrodes, currents decay did not coincide with the mass decay[228,229] but with the energy dissipation change,[229,230] indicating a non-desorptive degradation and most probably structural changes. Since no activity was recovered upon addition of a diffusing redox mediator; the current loss could not be explained by reorientation of some enzymes.[220]

The current was even less stable when the potential was applied continuously, compared to punctual measurements (Fig 14B).[220,229] At the same time, the dissipation losses were much higher, meaning that the BOD layer stiffened under application of a potential, and supporting a potential-induced enzyme denaturation. Moreover, under potential cycling, a mass drop was also recorded, therefore suggesting protein dehydration.[229] This could be an important cause of activity loss, since different studies have shown that drying the BOD electrode in a desiccator led to complete loss of the enzymatic activity, which was attributed to denaturation of the enzyme by losing water.[235,236]

To rationalize the direct influence of potential on the active site, the behavior of the fraction of enzymes that were not directly connected at the electrode was investigated in MET upon addition of a redox mediator. A more stable current was observed for *Mv*-BOD adsorbed or covalently bound on NH_2 terminated SAM on gold electrode in MET configuration, *i.e*. when the enzyme was not directly submitted to potential cycling.[220] However, on carboxylate SAMs, the fraction of enzymes oriented in MET also lost its activity. These results suggest that direct influence of the potential on the active site is not the only origin of denaturation.[220] The electric field created at the electrode interface could also be deleterious for the enzyme structure, but to the best of our knowledge, no direct proof of this hypothesis has been reported. Since in the case discussed above the systems essentially differ by the chemistry of

the electrode surface, it also indicates that the electrode surface charges influence on the enzyme stability.[220] This effect is discussed further in section 4.1.4.

3.4.4.3 Enzyme concentration

Catalysis constants k_{cat} much lower than values for homogeneous catalysis (250 s^{-1}) could be calculated for a surface coverage close to one monolayer of *Mv*-BOD adsorbed on bare gold (ca 4 s^{-1})[228] or on 3-MPA-modified flat polished gold surface of a QCM sensor (35 s^{-1}).[229] The decrease in activity with time was higher for immobilized enzymes than for enzymes in solution.[220] This suggested that BOD was poorly oriented at the electrode, and that some denaturation occurred upon immobilization. Furthermore, at pH 4 more enzyme was adsorbed but the measured current was even smaller than at pH 7.[228] Similarly, a lower efficiency was recorded for a monolayer of *Mv*-BOD on mercapto-hexanoic acid (MHA)-modified gold (5 pmol.cm^{-2}) than for a sub-monolayer (0.6 pmol.cm^{-2}) with global k_{cat} of respectively 7 and 48 s^{-1}.[220] It was therefore likely that higher BOD concentrations were detrimental, due to the increased interactions between neighboring BOD molecules. However, the opposite effect has also been observed. The behaviors of *Mv*-BOD and *Th*-laccase upon immobilization on bare gold electrodes were compared. *Mv*-BOD-always led to higher surface coverages, and at the same time to the highest enzyme specific activity. It was consequently proposed that steric effect or electrostatic interactions between neighboring molecules, induced by higher enzyme coverage, could prevent the enzyme from flattening, thereby lowering inactivation due to conformational changes.[225,231]

The influence of the initial *Mv*-BOD concentration on the adsorption was investigated by DPI: intermediate concentrations (10-25 mg.mL^{-1}) were shown to lead to the most Efficient (in terms of k_{cat}) and persistent (in terms of k_{cat} stability) layers, with an optimized k_{cat} of 60 s^{-1}.[231] Adsorption was shown to occur in 2 stages: first an irreversible binding of a protein layer attributed to the spreading of the molecules at the surface, and then the

formation of a less rigid layer of proteins. Higher concentrations of the enzyme solution produced less rigid layers in the first phase, because faster adsorption prevented enzyme from relaxing and flattening at the electrode surface. This correlated well with higher enzymatic specific activity.[231] However too dense layers also led to decreased efficiency.[231]

3.4.5 Catalytic mechanism on carbon electrodes

When BOD and laccase are immobilized on bare polished GC, catalytic currents have not always been observed.[235,237] Therefore unless stated otherwise, this paragraph is only focused on studies of MCOs adsorbed on graphite electrodes. A well-defined catalytic wave for O_2 reduction was recorded for most enzymes (Fig 15). To determine the primary electron acceptor in heterogeneous electron transfer (HET), characteristic potentials of the ORR under aerobic conditions as well as their variation with pH have been first considered. This follows the general assumption that catalysis is controlled by the potential of the redox center at which electrons enter/leave the enzyme, and not by the potential of the actual catalytic center.[238,239] E_{cat}, the potential corresponding to the maximum acceleration of the catalysis (*i.e.* E for maximal di/dE) is a convenient tool to describe values of characteristic potentials in catalysis, because it contains both thermodynamic information and clues about kinetics of the transformation.[165,240] However the steady-state potential of the electrode (OCP), onset potential or half-wave (E_{HW}) potential of the catalytic ORR wave are more widely described in the literature.

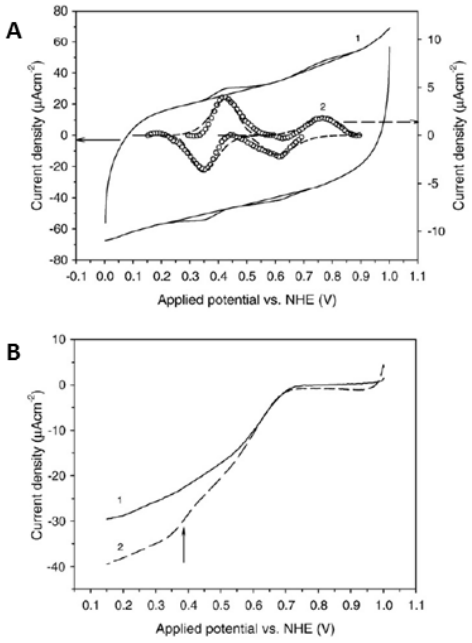

Figure 15. (A) Cyclic voltammogram of BOD adsorbed on SPGE in the absence of O_2. pH 7.0, 0.1 M phosphate buffer; scan rate: 100 $mV.s^{-1}$; starting-scan potential: 1000 mV *vs.* NHE. Curve 1: uncorrected for the background current; Curve 2: circles, background current subtracted. The broken line curve represents the calculated theoretical voltammograms. (B) Effect of the scan rate on the background-corrected voltammograms under O_2. Curve 1: 10.mV s^{-1}; Curve 2: 100 $mV.s^{-1}$. Reprinted with permission from [203] Copyright 2008 Elsevier.

OCP for *Th*-laccase increased from 780 to 910 mV *vs*. NHE for pH decreasing from 6 to 3;[210] and changed by 20-30 mV/pH unit between pH 4.5-6 for *Th*-, *To*-, *Cf- and Cm*-laccases, and by 65, 33, 33, and 13 mV/pH resp. for the same laccases between pH 3 and 4.5.[210] Approximate values of ORR onset were also reported: ≈ 840 mV and ≈ 490 mV *vs*. NHE at pH 5.0 for *Th*- and *Rv*-laccases resp.,[221] ≈ 840 mV *vs*. NHE for *Tv*- laccase at pH 3.8,[211] and values between 840 and 900 mV *vs.* NHE at pH 6.5 for *Th*-, *To*-, *Cu*-, *Cm*-, and *Cf*-laccases.[210] Similar values were recorded for both *Mv*- and *Tt*-BOD. The ORR onsets were 800 mV *vs.* NHE at pH 4 and 700 mV *vs.* NHE at pH 7.4 resp. for *Mv*-BOD,[204,215,217,241] which coincided well with the high-potential quasi-reversible redox transformations observed under anaerobic conditions, and 810 mV at pH 4, *i.e.* 120 mV above $E°'_{T1}$, for *Tt*-BOD.[204] All

these values of onset potential are slightly higher than the redox potential of the T1 Cu center, indicating that the T1 might be the electrochemical control center of catalysis.

The onset pH-dependence was precisely 60 mV/pH unit in the first report for laccase,[242,243] which was consistent with a 1 proton-1 e^- exchange, but slightly higher than 52 mV/pH unit reported later for *Mv*-BOD on SW-CNTs.[244] Furthermore it was more than twice higher than slopes of 20-25 mV/pH unit described for *Mv* and *Tt*-BODs on graphite.[204] These latter values were consistent with 23 mV/pH unit observed for the non-catalytic signal of both BODs, and close to the pH dependence described for laccase T1 potential.[200] This is a further indication that T1 controls the potential of catalysis.

In the absence of diffusion limitation, it is also consistent to consider the half-wave potential E_{HW}, which coincides with the redox potential of the electrochemical control center in catalysis, under kinetic limitation. For *Mv*-BOD, E_{HW} was 670 mV *vs*. NHE at pH 7.4 in one study,[241] while a lower value of 600-605 mV *vs*. NHE at pH 7.4 can be found elsewhere.[215] This latter value shifted to 700 mV *vs*. NHE at pH 4.0, consistent with a change of 30 mV/pH unit.[215,217] Potentials lower than expected were ascribed to a slow HET. On the other hand, E_{HW} for *Tt*-BOD coincided well with E_m of the high-potential redox process (690 mV).[203] E_{HW} was between 740 and 800 *vs*. NHE and changed by 5-30 mV/pH unit in the pH range 3-5 for *Cf*- and *Cu*-laccases.[210] An approximation of the standard apparent potential of the redox center involved in catalysis, E°', was determined for *Mv*-BOD by fitting the curves with the model developed by Ikeda.[235] E°' was found quasi constant in the pH range 2-5.5 (≈ 670 mV vs NHE) and a shift to less positive values with an average variation of 45 mV/pH unit was recorded between pH 6 and 8. [245]

For the different MCOs adsorbed on various graphite electrodes, reproducible values were obtained for characteristic potentials of catalysis (OCP, onset, E_{HW} and E°') and all

correlated with values of the T1 Cu potential. Although one must be careful that CV curves are not in all cases centered on the potential of the first electron relay when enzymes present several redox centers,[246] it is clear that the T1 Cu strongly influences the potential of catalytic O_2 reduction. Moreover, the catalytic potential correlates in numerous cases with a non-catalytic signal centered on the T1 potential, indicating that this latter must be directly facing the electrode surface. This strongly supports that DET at graphite electrodes under turnover conditions occurs via the T1 Cu, similarly with the O_2-reduction mechanism in homogeneous catalysis. [18,198,202]

This conclusion is furthermore supported by the electrochemical behavior of a mutant of *Mv*-BOD, Met467Gln in which the axial methionine ligand of T1 Cu was replaced by a glycine residue, and its comparison to that of the recombinant wild type BOD.[247] The onset potentials for O_2 reduction by both enzymes were consistent with the previously-determined T1 potentials, with a negative shift for the mutant at 230 mV *vs.* Ag/AgCl instead of 460 mV *vs.* Ag/AgCl at pH 7.[248]

A further indication that a similar reaction mechanism is adopted is the consistency of the enzyme activity with that observed in homogeneous solution. pH dependence of maximal currents under kinetic control display a bell shape typical of reaction rate of MCOs *vs.* pH.[17,215,221,242] K_M for O_2 of resp. 0.11 mM and 0.27 mM at 500 and 50 mV *vs*. NHE at pH 7,[204] and 0.7 mM at 342 mV *vs*. NHE at pH 5 were determined for graphite-adsorbed *Mv*-BOD.[17] These values are close to ≈ 0.2 mM at pH 7 measured in homogeneous system, which suggests that *Mv*-BOD preserves its native state after adsorption at the carbon material.

Even though the same tendency has been reported in the literature concerning the characteristic potentials at steady state and catalysis, the pH dependence of activity, K_M constants…, slight variations have been observed. They are probably due to different surface

states of the electrode, which result in varying affinities with MCO molecules (see section 4.1.4). However, no considerable deviation from homogeneous catalysis has been observed. The same general conclusion can therefore be drawn for both laccases and BODs: since the properties of heterogeneous electron transfer at graphite electrode are similar to those in homogeneous reaction, the T1 copper must be the first electron acceptor of DET between MCOs and carbon electrodes. This is furthermore consistent with T1 being situated not further than 8 Å from the enzyme surface. Electrons accepted from the T1 are then transferred to the TNC where the $4e^-$-O_2 reduction occurs.

Similarly, at modified gold electrodes, DET occurring at the T1 was also observed for both high and low-potential laccases.[233,249] *Rv*-laccase covalently bound on MPA-modified gold showed an onset at ≈500 mV *vs*. NHE, and a half-wave potential E_{HW} = 400 mV *vs*. NHE at pH 7.[214] For *Rv*- and *Ma*-laccases in a cationic polymer on gold, the onset was 450 mV *vs*. NHE at pH 6.5 and E_{HW} was close to the non-catalytic process at 350 mV.[208] Addition of fluoride inhibited the catalysis both for BOD and laccase,[17,214] while no change of the anaerobic voltammogram was observed,[214] which pointed to the inhibition of the internal electron transfer. All these data showed that a similar mechanism accounts for homogeneous and heterogeneous O_2 reduction by MCOs, provided that DET to the T1 can be established. The effect of surface modification on DET bioelectrocatalysis is discussed further in section 4.1.4

3.4.6 Possibility of endergonic electron-transfer

The general mechanism at carbon (or conveniently-modified gold) electrodes has been described in previous paragraph. However, a more intriguing phenomenon has sometimes been observed. Two consecutive catalytic waves in the cyclic voltammogram of O_2 reduction were detected in following cases. When *Th*- and *Tv*-laccases were immobilized within a

polymer on a gold electrode, an onset at 730 mV *vs*. NHE at pH 6.5 followed by a more drastic increase at 620 mV was recorded.[208] For both *Mv*- and *Tt*-BODs at graphite electrodes, two consecutive reduction waves were observed in the absence of diffusion limitation (Fig 15).[203,204] These processes coincided well with 2 quasi-reversible redox transformations at low and high potential observed under anaerobic conditions (Fig 15).[203,204,208]

This curious phenomenon was particularly investigated for BOD electrodes.[203,204] Several hypotheses had to be examined before considering that it was catalytically relevant. First, a damaged and a native active fraction of enzyme could have been simultaneously immobilized onto electrodes. Second, two different catalytically active BOD fractions could coexist. The catalytic currents decreased over time but did not result in change of the voltammogram shape, thus ruling out the first possibility. Moreover, since BODs had been purified the second hypothesis was very unlikely.[204] It was therefore proposed that a single enzyme form could adopt 2 different orientations at the electrode interface. Several redox centers of the oxidoreductase could therefore be addressed simultaneously.[204,208] This proposition is not contradictory with published BOD structures, in which both Cu clusters are situated within tunneling distance from the enzyme surface.[129,146]

The low-potential wave was attributed to a catalytically active intermediate of the TNC[118,203,204] with a potential close to 400 mV *vs*. NHE. The redox transformation of this intermediate was shown to be O_2-independent and pH-dependent. As a consequence, it was attributed to the redox transformation between the first and second partly reduced TNC intermediates, *i.e*. to the proton-coupled redox transformation from the peroxide intermediate to another state.[95,250] This latter enzyme state would be comprised between peroxide and native intermediates. It is noteworthy that, later, catalytic oxygen reduction by *Mv*-BOD starting exclusively at low potential could be observed when the controlled immobilization of

the enzyme at CNTs specifically approached the TNC close to the electrode surface. In that case, the low potential was attributed to a resting form of the enzyme.[216]

Despite the disputable opinion concerning the redox intermediate involved in the above described catalytic mechanism, it is not unreasonable to consider that at least one IET is uphill. Page *et al.*[146] and other studies[251] have indeed calculated for a series of redox enzymes that endergonic ET can occur, as long as neighboring redox centers are not separated by more than 14 Å. Taking into account this maximal distance, reorganization energy λ calculated from quantum mechanical and molecular mechanics (QM/MM) evaluations, and ΔG° calculated from the measured potential difference between the two detectable sites, pH-dependent internal electron transfer rate constants between T1 and the TNC low redox intermediate were calculated. They ranged from 3 s^{-1} up to 138 s^{-1}, in agreement with experimental k_{cat} values.[204]

3.4.7 Mathematical modeling of the catalytic current

Different DET models can account for the mechanism of the O_2 reduction by MCOs electronically connected to the electrode via the T1. Importantly, all models are derived considering non-limiting O_2 diffusion. In the first general model proposed by Tsujimura *et al.*,[235] the internal electron transfer (IET) and the different steps of O_2 reduction at the TNC are included in a general "catalytic" mechanism (Fig 16 A).

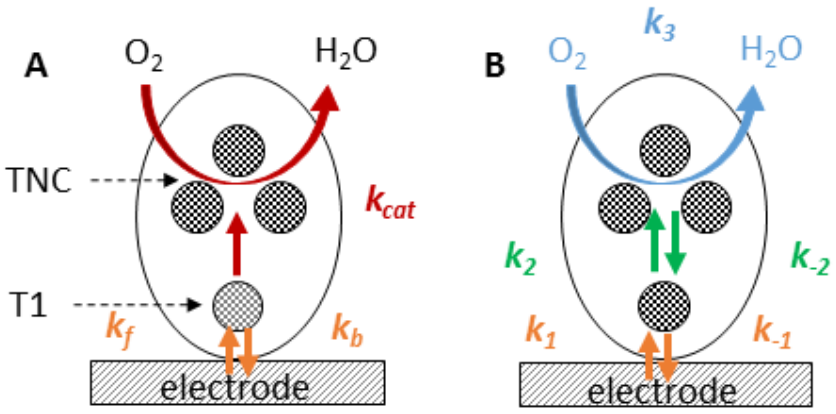

Figure 16. Schematic representation of DET mechanism for O_2 reduction by MCOs. (A): model proposed by Tsujimura *et al*. (adapted from [235]). k_f and k_b are the rate constants of the reversible heterogeneous electron transfer , and k_{cat} is the global catalytic constant for O_2 reduction by the BOD including intramolecular electron transfer and all steps of O_2 reduction at the TNC. The second step is considered irreversible in the model. (B): refined model. The heterogeneous electron transfer is considered reversible and characterized by the rates for forward and reverse electron transfers k_1 and k_{-1}. Similarly, the internal electron transfer is considered reversible and characterized by the rates of forward and reverse electron transfers k_2 and k_{-2}. The only irreversible step is the O_2 reduction at the TNC characterized by the rate constant k_3. Adapted with permission from [204,233]. Copyright 2012 Wiley-VCH Verlag GmbH & Co. KGaA, and American Chemical Society.

O_2 reduction by MCOs can therefore be decomposed in two parts, heterogeneous electron transfer between enzyme and electrode, and catalysis. If the second step is considered irreversible, two rate constants, k°, the standard surface rate constant, and k_c, the catalytic rate constant, are enough to describe the kinetics of O_2 reduction. It is noteworthy that k_c normally follows a Michaelis-Menten dependence on O_2 partial pressure. Moreover, only HET rates are supposed to be dependent on the electrode potential, and this dependency can be described in a first approximation by Butler-Volmer kinetics (equations 13 and 14).

$$k_f = k° e^{-\alpha \frac{nF}{RT}(E - E°')} \quad Eq.13$$

$$k_b = k° e^{(1-\alpha) \frac{nF}{RT}(E - E°')} \quad Eq.14$$

where k_f and k_b are forward and reverse interfacial electron-transfer rate constants, resp. for the reduction and oxidation, and k° is the standard heterogeneous electron-transfer rate constant at the apparent standard potential E°' of catalysis. α is the charge transfer coEfficient (usually considered equal to 0.5), and R is the universal gas constant. Missing parameters can

be determined by fitting the experimental CV curves with the expression of steady-state current density given by:

$$j = \frac{n_E F k_c \Gamma_t}{1 + {k_c}/{k_f} + {k_b}/{k_f}} \quad Eq.\,15$$

where n_E is the number of electrons exchanged (a single electron exchange at the T1 copper is considered), F is the Faraday constant, and Γ_t is the total surface concentration of the enzyme (in mol.cm^{-2}). This model was also extended for enzymes diffusing in a reaction layer, just replacing Γ_t by μ[E] in eq. 15, where [E] is the total concentration of enzyme in the reaction layer, and μ is the thickness of this latter.[252] μ is given by $\mu = \sqrt{{D_E}/{k_c}}$, with D_E being the diffusion coEfficient of the enzyme in the layer.

This model considers a very fast internal electron transfer (IET), therefore the enzyme behaves as if only one redox center able to take 2 different redox states (reduced or oxidized) were present. Although this is a strong simplification, the resulting equation is able to generate curves that closely fit to the experimental voltammetry data. However it is quite disputable if E°' can account for a real thermodynamic potential of one of the Cu centers.

A refined, yet still simplified, model is described in Figure 16B.[204,233] The internal electron transfers between T1 and TNC are separated from the catalytic O_2 reduction at the TNC and considered reversible, while all steps of O_2 reduction at the TNC are still included in a global catalytic mechanism considered irreversible. 5 kinetic rate constants are therefore needed to account for the forward and reverse HET (k_1 and k_{-1}), forward and reverse IET (k_2 and k_{-2}) and irreversible catalysis (k_3). Heterogeneous electron-transfer can still be described by Butler-Volmer type equations (equations 13 and 14, with $k_f = k_1$ and $k_b = k_2$), while catalysis is best described by Michaelis-Menten kinetics (equation 16).[233,253]

$$k_3 = \frac{k_{3,max}[O_2]}{K_M + [O_2]} \qquad Eq.16$$

In this approximation, IET is considered to occur as a bimolecular reaction of electron exchange between T1 and TNC. If forward and reverse IET rates are considered equal (*i.e.* $k_2 = k_{-2}$), the total current can be expressed as:[233]

$$j = \frac{-k_1 k_2 k_3 n_E F \Gamma_t}{k_1(k_2 + k_3) + k_{-1}(k_2 + k_3) + k_2 k_3} \quad Eq.17$$

It is interesting to note that by then considering fast IET, *i.e.* when catalysis and HET are the limiting steps, equation 17 can be further simplified to give back equation 15, with $k_c = k_3$, $k_f = k_1$ and $k_b = k_2$.[233,253] On the contrary, when IET is the rate limiting case, *i.e.* when catalysis is very fast ($k_3 >> k_2$), eq. 17 becomes :

$$j = \frac{n_E F k_2 \Gamma_t}{1 + {}^{k_{-1}}/_{k_1} + {}^{k_2}/_{k_1}} \qquad Eq.18$$

Importantly, as evidenced by the absence of k_3 in the equation, no dependence of the catalytic current on O_2 concentration is expected in this latter case.[233] This catalytic scheme is however still incomplete as it does not consider all electron transfer steps and catalytic intermediates of the general mechanism of O_2 reduction by MCOs. Blanford *et al.* proposed a complete general mechanism for O_2 reduction by immobilized MCOs, based on that developed by Solomon *et al.*[92,93] for homogeneous conditions (Fig 17A, see sections 3.1 and 3.4.8 for more details).

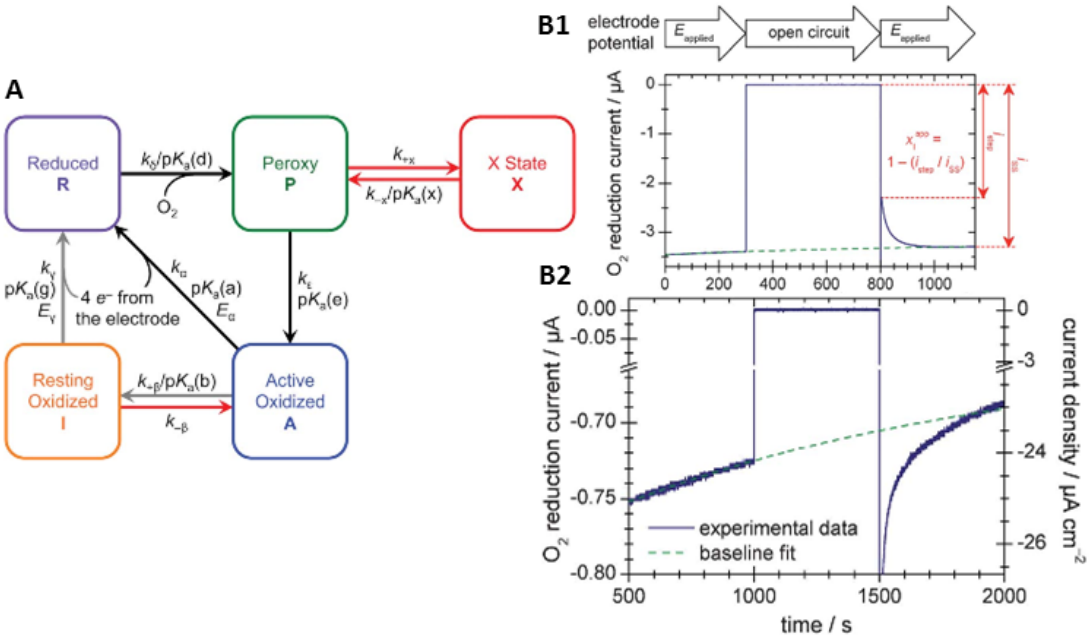

Figure 17. A: A mechanism for MCO-catalyzed O_2 reduction based on that of Solomon and co-workers, with additions from Blanford *et al*. shown in red. B: Evidence for the formation of the Resting Oxidized (B1) and X state (B2) in response to a series of applied potentials. $E_{applied}$ is the experimental potential used, typically 0.4 V *vs.* NHE at pH 4; when the electrode is at OCP no potential is applied. B1 indicates how the fraction of enzymes in the RO state is calculated. B2 is observed in some particular combinations of pH and time at OCP. Adapted with permission from [165] Copyright 2012 Royal Society of Chemistry.

Due to the complexity of the mechanism, and since their purpose was to explain the transient phenomena, they did not use a steady-state approximation and did not derive a general expression of current density. They proved however that all kinetic parameters could be experimentally elucidated. Gray *et al*. proposed an expression of the O_2 reduction current that takes all the catalytically-relevant intermediates into account (Fig 18).[254]

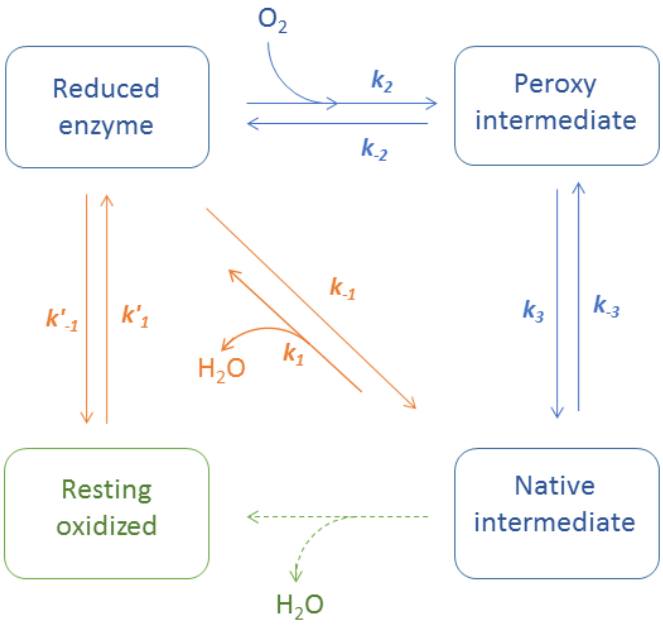

Figure 18. Mechanism for MCO-catalyzed O_2 reduction used in the analytical model developed by Agbo *et al*. The steps including HET are indicated by orange arrows, the catalytically relevant intermediates and internal steps are indicated in blue, and the resting form outside of the catalytic cycle is indicated in green. For the n^{th} step, the forward rate constant is indicated by k_n and the reverse by k_{-n}. Adapted with permission from [254]. Copyright 2014 American Chemical Society.

However, contrary to Blanford *et al*., they considered that the resting oxidized form was formed irreversibly from the native intermediate, and did not consider the formerly introduced X state. Moreover, as in the previous models, they considered reversible HETs. Based on the assumption that the limiting step is O_2 binding, they could derive an expression of the cathodic current that contains 8 rate constants (Fig 18):

$$j = \frac{n_E F \Gamma_t k_1' (k_2[O_2] - k_{-2} f)}{g(1 + \frac{k_1}{g}(1 + f + \frac{k_3 f + k_{-1}}{k_{-3} + k_1})} \quad Eq.19$$

Where f and g are respectively given by:

$$f = \frac{k_2[O_2](k_{-3} + k_1)}{(k_{-3} + k_1)(k_{-2} + k_3) - k_3 + k_{-3}} \quad Eq.20$$

$$g = k_{-1} + k'_{-1} + k_2[O_2] - k_{-2}f - k_1\frac{k_3 f + k_{-1}}{k_{-3} + k_1} \quad Eq.21$$

The potential-dependent HET rate constants k_1, k_{-1}, k'_1 and k'_{-1} can be described by Butler-Volmer kinetics, where k°, the exchange rate at 0 overpotential, can be further expressed by the semi-classical Marcus equation (equations 3 and 4 in part 2.3). This allowed to evaluate both the electronic coupling and the mean distance between enzyme and electrode. This theoretical approach was validated with experiments performed with *Thermus termophilus* laccase.

3.4.8 Resting forms of MCOs

Electrochemical experiments did not only allow to determine all rate constants of O_2 reduction on MCOs modified electrodes, but were also useful to evidence and study different resting forms.[127,165,255,256] The resting oxidized (RO) form, an inactive fully oxidized form of MCOs, already characterized by spectroscopic, crystallographic and DFT techniques, is known to re-enter the catalytic cycle only upon reduction. Similarly, activation of a fraction of enzymes at reducing potentials was evidenced in electrochemistry both in CV or in chronoamperometry (CA) (Fig 17B), but only for high-potential MCOs (*Tv* and *Coriolopsis gallica* laccases, and *Mv*-BOD) and not for low potential (*Bs*-BOD or *Rv*-laccase).[165] The inactive state, formed outside the catalysis, was identified as the RO form. By simple electrochemical experiments, the formation rate of this RO form was proved to increase with decreasing pH. In addition, while the formation of RO was usually considered to be reversible, the fraction of inactive form did not tend to 1, thus supporting an equilibrium between RO and an active state (indicated by the red arrow for the reverse reaction added in the catalytic cycle on Fig 17A). The existence of another inactive "X-state", to the best of our knowledge not described elsewhere, was also evidenced, based on the observation that under certain conditions of pH and potential a fraction of enzymes seems to inactivate during

catalysis and to reactivate outside of catalysis.[165] Different scenarios were envisioned to elucidate the origin of the "X-state": it could either be formed from the PI and then evolve to give the NI; or be the result of reversible transformation of NI or PI. Experimental data permitted to eliminate the first hypothesis since the PI to NI transition is pH-independent. The second hypothesis was also ruled out by a modeling approach. The "X state" was therefore assumed to be in a "dead-end" equilibrium with PI. (Fig 17)

Pronounced hysteresis with shift of O_2-reduction onset towards a more negative potential, characteristic of an inactivation, followed by reactivation at reductive potentials, has also been observed for fungal BOD from *Magnaporthe oryzae*[127,255] and in the presence of Cl^- for bacterial BODs from *Bacillus subtilis* and *Bacillus pumilus* (Fig 19).[256] Complementary UV-Vis and spectroscopic studies allowed to assign this feature to the "alternative" resting form (AR), a partially reduced resting form of MCOs.[127,255] Its formation and reactivation were then fully characterized by electrochemistry, showing that its rate of formation increased upon decreasing pH and increasing Cl^- concentrations. AR formation did not require the presence of O_2 which is therefore not involved as bridging species in this form, and sufficiently oxidizing potentials were needed to partially oxidize the Cu centers. Contrary to the case of RO formation, all enzymes were converted to the AR form, supporting the hypothesis that this transformation is irreversible. Enzymes in the AR form only reenter the catalytic cycle upon full reduction.

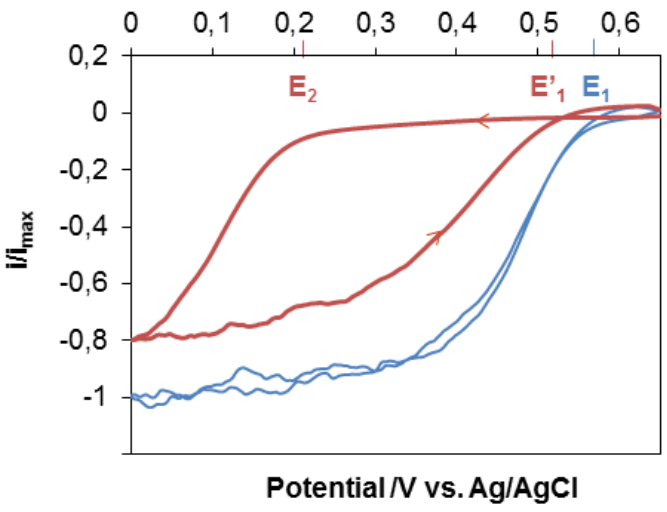

Figure 19. Electrochemical evidence of the alternative resting form in *Bp*-BOD in presence of NaCl at pH 4 and 37°C, observed in cyclic voltammograms of O_2 reduction at 5 $mV.s^{-1}$ in 200-100 mM phosphate-citrate buffer. Blue curve: usual catalytic response in the absence of NaCl. Red curve: hysteresis observed after 15 mM NaCl addition. The arrows indicate the direction of the potential sweep. *Bp*-BOD was adsorbed on a pyrolytic graphite electrode first modified with carbon nanofibers. Reproduced with permission from [256]. Copyright 2017 American Chemical Society.

3.4.9 Halides affecting the direct electron transfer

As discussed above, in homogeneous solution, by using combined spectroscopic and DFT studies, Cl^- has been shown to bind to T1, and F^- to the TNC. In terms of inhibition mechanism, Cl^- and I^- are competitive inhibitors while F^- is non-competitive with respect to electron donor. In DET mode, MCOs are also to some extent inhibited by halides.[234,257,258] Inhibition of high potential catalysis by F^- for BOD or laccase both in DET and MET[186,203,204,220,221,257,259] is in agreement with F^- binding at the TNC and/or inhibition of the IET. Inhibition by Cl^- has been also observed. For example, the current delivered by *Cerrena maxima* laccase immobilized on graphite particles declined by 30% upon addition of 100 mM NaCl.[258] Addition of 200 mM Cl^- decreased the current by 50% for laccase from *Trametes hirsuta* adsorbed in nanoporous gold electrodes at pH 4.[186] However, higher resistance to Cl^- even for laccases has been sometimes observed in DET. It suggests that the electrode, in particular when it is nanostructured, prevents Cl^- access to the T1.[257,259] For example, when *Th*-laccase was covalently bound on LDG electrodes, DET was stable in presence of 150 mM NaCl, while MET with a diffusing mediator was completely inhibited for the same chloride concentration.[259]

Potential shifts similar to those described above, have also been observed in DET upon addition of halides. E_{HW} of *Cerrena maxima* laccase shifted 94 ± 3 mV in the negative direction in presence of 150 mM Cl^- at pH 5. This effect disappeared as soon as the electrode was transferred in a chloride-free buffer.[258] The E_{HW} shift observed with *Trametes* laccase immobilized on SW-CNTs increased with increasing Cl^- concentration, being respectively 60 mV at 10 mM and 150 mV at 100 mM Cl^-.[257] For the same enzyme, similar potential shifts were observed upon addition of I^-.[257] This potential shift can be explained by Cl^- or I^- binding at the T1. In presence of F^-, the low-potential anaerobic redox process observed for *Mv*-BOD decreased, consistently with F^- binding to TNC.[204] More surprisingly, a negative shift of the high potential catalysis has also been observed upon addition of F^-.[234,256,257] The slight 30 mV-decrease in conjunction with 90% current loss was attributed to F^- binding both at the T1 and the TNC, thus shifting the T1 potential and blocking IET at the same time.[257] A higher 100 mV-decrease for *Didymocrea* laccase at pH 4, with lesser-pronounced inhibition, was attributed exclusively to F^- binding to the TNC. In this case, surface-enhanced Raman spectroscopy (SERS) studies of the enzyme orientation suggested that the T1 was relatively far from electrode surface, so that DET was more likely occurring through the TNC.[234] Interestingly this study is the first to propose a DET via TNC occurring at a higher potential than T1.[234] However, this is not a direct demonstration that DET to TNC is feasible and additional experiments with T2-depleted MCOs would be required. A redox titration showed that the T1 potential, ca. 100 mV lower than the half-wave potential correlated to TNC, was little affected by F^- addition. Exactly the same shift was observed for *Bp*-BOD, while the primary electron acceptor in that case was supposed to be the T1 Cu.[256]

3.4.10 Rate limiting steps of O_2 reduction

Different studies have shown that the rate limiting step during O_2-reduction catalysis by MCOs connected in DET mode varied depending on the experimental conditions and

applied potentials. The enzyme affinity for O_2 was shown to depend on electrode potential, which means that "apparent" Michaelis constants are measured at a given potential. This led to the conclusion that the rate determining steps of the catalytic mechanism also depend on the electrode potential.[233] In the case where an endergonic IET was considered, the calculated IET rates were influenced by pH, due to the different pH dependencies of the high and low-potential intermediates. The thermodynamic driving force decreased at basic pH, so that IET started to be the rate limiting step in alkaline solution.[204] The same conclusion was drawn from analysis of the O_2-reduction CV shape in the absence of O_2 diffusion limitation. At low pH, the CV exhibited a trailing edge well described by the model introduced by Léger *et al.*, whereas it was almost sigmoidal at high pH.[17] This was attributed to fast IET and catalysis at low pH. In this case, both current and turnover rate are determined by the rate of HET, which increases at high overvoltage. On the contrary, at high pH, slow IET and catalysis are determined by the turnover rate. T1 is therefore the electrochemical control center, and defines the potential of electro-catalysis. The authors proposed that the process at high pH is limited because the deprotonated carboxylate D105 close to TNC cannot supply the required protons.[17]

3.4.11 Inhibition by H_2O_2

While studies describing the effect of pH and halides on MCOs activity are widespread in the literature, the impact of hydrogen peroxide on laccases and bilirubin oxidases has only more recently attracted attention. In the context of a glucose/O_2 biofuel cell where glucose oxidase is used at the anode, it is hypothesized that H_2O_2 generated during the oxidative half reaction of glucose may affect BOD or laccase. The first paper addressing this issue was reported in 2010 by Calvo *et al.*[260] Their cathode was composed of a self-assembled layer of laccase from *Trametes versicolor* or *Trametes trogii* and osmium complex bound to poly(allylamine). They evidenced the inhibition of biocathodes by H_2O_2 during oxygen

reduction. In 2015, they extended their work and demonstrated the reversible non-competitive inhibition of laccase by H_2O_2 both in MET[261] and DET.[253] The authors attributed the inhibition of the laccase to the oxidation of the T3 Cu by H_2O_2, earlier hypothesized by Solomon *et al.*,[262,263] which therefore interferes with the mechanism of oxygen reduction.[95] Minteer and co-workers also demonstrated the reversible non-competitive inhibition of laccase by H_2O_2 whether the laccase operated in DET or MET (when ABTS was used as a redox mediator).[264] They furthermore studied the effect of H_2O_2 on bilirubin oxidases.[265-267] They demonstrated that, unlike laccases, *Mv*-BOD was irreversibly inhibited by H_2O_2 (Fig 20).

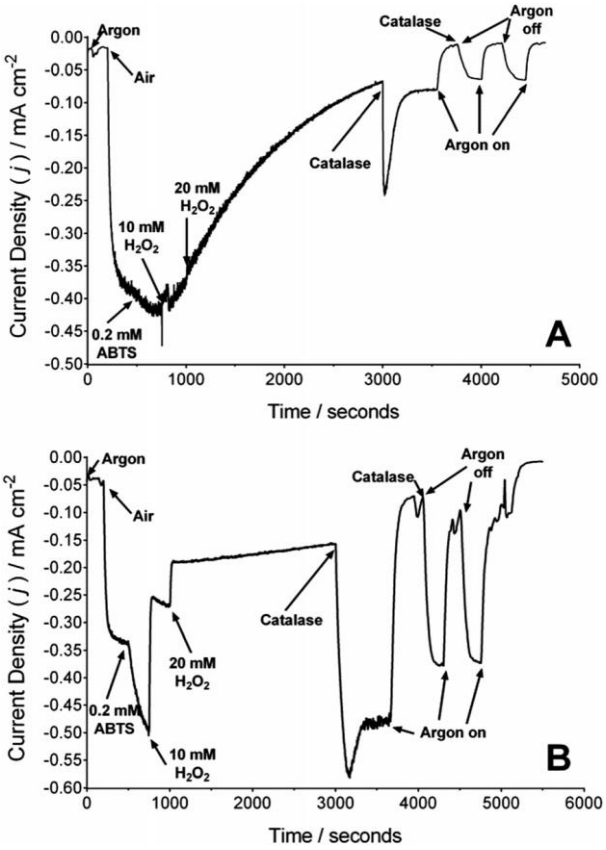

Figure 20. Chronoamperometric trace for a (A) BOD/Anthracene-MWCNTs (pH 6.5) and (B) laccase/Anthracene-MWCNTs (pH 4.5) Toray-paper electrode in a hydrodynamic citrate/phosphate buffer solution (0.2 M), poised at 0.2 V (*vs.* Ag/ AgCl). *NB*: air and argon

gasses were purged individually – air purging was terminated at t = 3600 seconds. Reproduced with permission from [266]. Copyright 2014 The Royal Society of Chemistry.

However, the exact mechanism of inhibition still has to be understood. Fortunately, it is less complicated to overcome the problem of H_2O_2 than the pH or Cl^- effect. Different strategies have been developed to protect the MCO cathode. To prevent the formation of the inhibiting H_2O_2, O_2-independant glucose-oxidizing enzymes such as glucose dehydrogenase can be used. Alternatively, H_2O_2 can be degraded via the formation of bi-enzymatic systems such as glucose oxidase/horseradish peroxidase, glucose oxidase/catalase or BOD/catalase. In this latter case, H_2O_2 is dismutated to water by the second enzyme, thus protecting the MCO. Although these studies on H_2O_2 inhibition are of interest from a mechanistic point of view, they are not necessarily relevant for the field of biofuel cells since highly concentrated solutions of H_2O_2 have been used (~mM range and up to 20 mM). For example, a carbon fiber coated with 35 wt% of an engineered glucose oxidase[268] and an adequate redox polymer for a total loading of 2000 $\mu g.cm^{-2}$, would generate 20 mM H_2O_2 after 4.2 months of continuous operation in presence of 5 mM glucose in a saturated O_2 buffer pH 7.2.

3.4.12 Effect of methanol

Palmore *et al.* envisioned the use of enzymatic electrodes in direct methanol fuel cells, which typically operate with concentration of MeOH comprised between 1 and 5 M.[269] The authors showed that the activity of laccases either in solution or entrapped in polypyrrole film was decreasing upon increasing MeOH concentrations.[270] However, the decline was slower for the immobilized enzymes. They attributed the loss of activity to the replacement of water molecules by MeOH within the enzyme.[271] In a series of three papers, Calabrese-Barton *et al.* also investigated the impact of methanol on the oxygen reduction current delivered by an electrode modified with an osmium polymer and *Tv*-laccase. When the bioelectrocatalysts

were immobilized on a carbon-fiber paper support incorporated in a membrane-electrode assembly, the authors demonstrated the tolerance of laccase to methanol. A 6% increase in current density at E_{cell} = 0.2 V was found for 10 M methanol as compared to 1 M methanol.[272] They later demonstrated that in presence of 1 M methanol, the performance of a biocathode based on *Th*-laccase on carbon cloth was only reduced by 4.5%. This decrease was explained by a de-swelling of the redox polymer rather than by the enzyme deactivation.[273] In 2011,[274] they showed that the sensitivity of O_2 reduction to methanol depended not only on the concentration of MeOH, but also on the osmium polymer used and particularly on its redox potential. The loss in current was nil below 2.5 M methanol, it was 30% between 2.5 and 5 M, while 100% current was lost above 7.5 M. For a 7.5 M methanol concentration, the authors showed that *Tv*-laccase inactivation was irreversible. Blanford *et al.*[275] also studied the effect of MeOH on *Tv*-laccase immobilized on pyrolitic graphite edge electrode modified by reduction of diazonium salts. In presence of 2.7 M and 5 M methanol the current density was reversibly decreased by respectively 10 and 20%, while at 9.7 M the current loss was irreversible. Xiao *et al.* have reported a *Mv*-BOD based biocathode which could operate in acetonitrile, acetone and various alcohols (*vide infra*).[276] De Andrade *et al.*[277,278] have designed laccase-based EBFCs operating at pH 5 in presence of 100 mM methanol.

4. Enzymatic O_2 reduction

4.1 Direct electron transfer

Catalysis of O_2 reduction by laccase in DET was demonstrated for the first time almost 40 years ago. In this early study, *Tv*-laccase was immobilized on carbon black.[243] As for BOD, connection in DET was reported much later, in 2004, with *Mv*-BOD adsorbed on different carbon electrodes.[235] In the first studies of DET catalysis by MCOs, the main efforts were directed towards elucidation of O_2 reduction mechanism by enzymes directly connected

at the electrode (see section 3.4), and less importance was attributed to electrocatalytic performances. In this section, we describe works performed to achieve Efficient enzyme connection in DET, with the purpose to use MCOs as cathodic enzymes in EBFCs. Important parameters are therefore high onset potential, high current densities and stabilities. To obtain high onset potentials the enzyme must be connected to the electrode via the T1. Lots of efforts have been devoted to reach large current densities at sufficiently high potentials. This involves immobilization of high amounts of enzymes, and high apparent catalytic rates. We consider first random orientation of the enzyme at the electrode, and describe current densities reached at different planar electrodes. Since current densities remained limited in that configuration, two main strategies have then been developed. On one hand, current magnitudes could be increased by immobilizing higher number of catalysts at a given geometric surface. Nano- or micro-structuration of the electrode surface has been envisioned in this context, to multiply the real electroactive surface area of an electrode. We develop this in part 4.1.2 and 4.1.3. On the other hand, the enzyme electronic connection had to be optimized, which mostly relied on achieving functional orientation of the enzyme at the electrode surface. We describe strategies developed to ensure optimal orientation of MCOs at both planar and structured electrodes in part 4.14. Then, we discuss the stability issue in part 4.1.5.

Contrary to previous section describing the mechanistic study of MCOs, and still for the sake of consistency with the literature, we will here quote the potentials versus the Ag/AgCl reference electrode, unless stated otherwise. The potentials are therefore typically ≈ 200 mV lower than when quoted *vs*. the NHE reference electrode.

4.1.1 Planar electrodes

4.1.1.1 “Planar” Carbon electrodes

In the first studies, MCOs have been immobilized on various kinds of carbon electrodes: glassy carbon (GC),[235] various types of graphite (low density graphite (LDG), spectroscopic graphite (SPG), pyrolytic graphite (PG), basal plane or edge plane highly oriented pyrolytic graphite (HOPG)…),[203,210,215,221,235] and screen printed carbon.[279] Except glassy carbon, carbon surfaces are however rarely strictly planar. While it is clear that DET catalysis has been observed with different MCOs simply adsorbed on most of these materials, it is difficult to compare their efficiency as enzyme support. Indeed, it is well-known that carbon electrodes differ from one another as far as microstructure, roughness, and chemical functions are concerned.

To give an idea of the magnitude of currents or current densities recorded with MCOs adsorbed on carbon electrodes, we list below some values obtained at 0 V *vs.* Ag/AgCl. *Tv*-laccase adsorbed on edge plane graphite gave currents of ≈ 40 µA. In that case, the maximum rate at which O_2 could be reduced, deduced from the intercept of a Koutecky Levich plot, indicated a turnover rate of ca. 20 s^{-1}.[211] *Rv*-laccase was adsorbed on two carbon materials (RWII and RW0), and the higher electrocatalytic current, 60 µA.cm^{-2} at neutral pH, was observed with RWII. It was attributed to a higher porosity and the presence of more oxygen functions. With laccases of different origins, *T. ochracea*, *C. maxima*, *C. unicolor*, *C. fulvocinerea*, adsorbed on SPG or HOPG, currents were in the range 2-20 µA.[210] It is interesting to note that *Tv*-laccase adsorbed on HOPG was observed by STM, revealing that the enzyme was not homogeneously distributed at the electrode surface and probably forming aggregates.[271]

In the very first study of DET by a BOD, *Mv*-BOD was also adsorbed on different electrode materials: GC, HOPG and PFC (plastic formed carbon). PFC and edge-plane HOPG gave the best results (200 µA.cm^{-2} with HOPG at pH 7), even exceeding the highest current densities obtained at that time with laccase. It was proposed that surface functional groups

and/or nanostructure governed the surface ET kinetics and adsorption property of BOD, but no more details were provided.[235] In the following reports, the current densities diverged. The differences cannot be assigned merely to different operating conditions; they may be explained by the fact that, as already mentioned, the electrode surface was not well characterized. For example ≈ 25 µA.cm^{-2} at pH 7 were recorded with *Mv*-BOD adsorbed on HOPG,[245] and ≈ 30 µA.cm^{-2} for the same enzyme adsorbed on SPG.[215] *Tt*-BOD adsorbed on SPG led to 20 µA.cm^{-2} at pH 7[203] and ≈ 0.5 mA.cm^{-2} under O_2 at pH 4,[204] *i.e.* the results differed by more than one order of magnitude. Although it is not possible to identify the exact origin of this difference, we can note that it is much higher than those observed in studies of pH influence performed in homogeneous solution.

DET on carbon electrodes was also routinely used to characterize less widespread or newly discovered MCOs.[166,181,280,281] Interestingly, the proof of concept of some EBFCs was established with enzymatic planar carbon cathodes. *Tv*-laccase adsorbed on graphite provided the cathode of the first totally enzymatic H_2/O_2 BFC.[282,283] Similarly, the first mediator- and cofactor-free EBFC based on cellulose dehydrogenase (CDH) operating in neutral chloride-containing buffers as well as in serum relied on *Mv*-BOD adsorbed on SPG electrode as a cathode.[241] A cathode based on *Mv*-BOD adsorbed on a LDG electrode was also combined to a bi-enzymatic anode for the 6 e$^-$-oxidation of glucose in a membrane-less EBFC operating in a buffer mimicking human physiological fluid.[284] This is detailed further in section 6.

4.1.1.2 Other planar electrodes

DET was also achieved for different MCOs on bare or modified gold surfaces. Since this is explored in details in section 3.4.4. and 4.1.4., we only remind here some current densities obtained when MCOS were randomly immobilized.[221] For most laccases, no DET

current was recorded when they were adsorbed on bare gold. *Rv*-laccase on MPA-modified gold gave 84 µA.cm^{-2} at pH 7.[214] With *Mv*-BOD, very different values ranging between 5 and more than 100 µA.cm^{-2} were recorded on bare gold electrodes.[17,225,228,231]

Some less conventional materials have been proposed, like boron doped diamond (BDD) or semiconductors. BDD has a wide working potential window, low background current, high stability, tunable hydrophilicity and optical transparency. Direct O_2 reduction by *Cerrena unicolor* laccase was demonstrated on BDD[285] with the enzyme either in solution or immobilized in a liquid crystalline cubic phase at the electrode. However, DET currents were very low (< 1 µA.cm^{-2}) while much higher currents were achieved upon addition of a redox mediator (25 µA.cm^{-2}). This proved that the enzyme orientation was not optimal.[285] *Tv*-laccase was immobilized on p-type nanostructured silicon (111) as a model semiconductor.[286] Under illumination with visible light, the material was theoretically able to supply electrons for the enzyme activation. O_2 reduction started about 200 mV more positive when laccase was present, but still at a very low potential (-0.24 V *vs.* SCE). The plateau current was 30 µA.cm^{-2}.[286]

4.1.1.3 Strategies for increasing the enzyme loading

To overcome the limitation in current densities, and reach values usable in EBFC, the surface concentration of enzymes on electrode surfaces had to be improved. A study by Ikeda *et al*. showed that multiple layers of enzymes could be connected in DET configuration on a planar electrode.[252] Multilayers of *Mv*-BOD were entrapped electrostatically in poly-L-lysine (PLL) on a PFC electrode. In O_2 saturated buffer, the process was diffusion controlled. A plateau at 845 µA.cm^{-2} was reached upon stirring at 1400 rpm, while only 300 µA.cm^{-2} were recorded when BOD was simply adsorbed on this PFC electrode. Calculations according to the model presented in section 3 indicated that the reaction layer was 0.2 µm-thick, *i.e*. much smaller than the real thickness of the BOD-PLL film (50 µm). HET standard rate constant was

19 s^{-1}, *i.e.* about 10 times smaller than for adsorbed BOD (178 s^{-1}). These two calculations highlight that this design was not optimized, although it allowed to connect more enzymes and to reach higher currents.[252]

Another option for immobilizing more enzymes is to increase the roughness of the electrode surface. Following this strategy, graphitized carbon cloth treated with H_2SO_4 was developed for the covalent binding of laccase,[287] while *Mv*-BOD was adsorbed on thorn-like nanostructures with an average roughness of 3.5-4 Å homogeneously distributed on a nano-carbon film (Fig 21).[288]

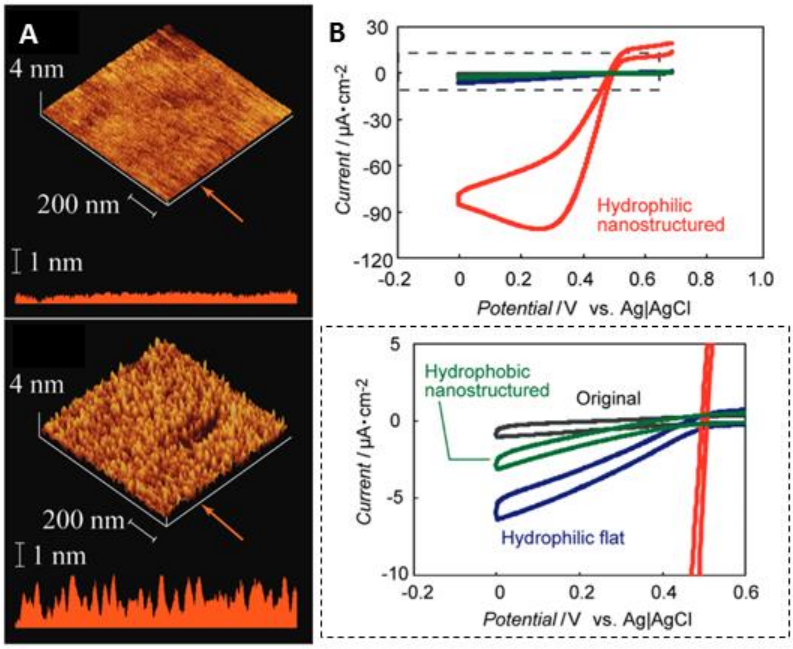

Figure 21. (A) AFM topographical images and height line profiles at points indicated by the arrows. Top: before UV/ozone irradiation. Down: after irradiation for three hours. The thorn height distribution is centered at 2,25 nm. (B) Voltammograms of BOD physically adsorbed on original and nanostructured carbon films with different surface wettabilities. 50 mM PB pH 7.0, scan rate 20 $mV.s^{-1}$ and electrode area 0,0314 cm^2. Top: real scale and down: enlargement of the dotted square in Top. Adapted with permission from [288]. Copyright 2017 American Chemical Society.

In both cases, currents increased compared to the planar electrode: 0.27 $mA.cm^{-2}$ were reached at 0 V in the first case, supposedly due to higher number of electrochemically active laccases[287], and 102 $\mu A.cm^{-2}$ in the second thanks to the nanostructure.[288] The importance of the roughness has also been highlighted with *Mv*-BOD immobilized on a planar electrode together with platinum group metal-free catalysts. Current densities did not only increase because of the inherent properties of the catalysts, but the contribution of the increased roughness was also important, providing better results when pores within the ratio 3-5 nm where formed. No significant increase occurred with larger pores (12-20 and 40-80 nm).[289]

Alternatively, a large variety of materials can be used to enlarge the electroactive specific surface area (ESSA) of the electrode. Matrices based on nanomaterials with a high surface/volume ratio have been developed. Typical nanomaterials are carbon nanotubes, nanoparticles or nanofibers (resp. CNTs, CNPs or CNFs), and gold nanoparticles (AuNPs). Various metallic nanoparticles (Fe, Pt...) have also been described. Ideally, it would be beneficial to find materials with hierarchical porosity allowing Efficiently immobilizing enzymes and preventing mass transport limitations. Therefore, highly porous 3D materials like mesoporous gold or carbon with the adequate and tailored porosity have also been engineered. In the following of this section we will focus on studies where the nano-structuration of the electrode has been evaluated, first with carbon and then with gold-based materials.

4.1.2 Carbon nanostructures

Carbon based materials are especially available, cheap, biocompatible, and can be produced in a variety of structures. Moreover, they are chemically and electrochemically inert.

4.1.2.1 Carbon nanotubes

Discovered in 1991, carbon nanotubes (CNTs)[290] are rolled layers of sp^2 carbon atoms. Single-wall (SW) CNTs consist of one single graphene layer, while multi-wall (MW) CNTs are composed of several layers. Their typical diameters range from 1 to few nm (SW-CNTs) or 20-50 nm (MW-CNTs), and their lengths are in the range of few µm to few tens of µm. Their nanometer-sized dimensions impart them a high aspect ratio. Moreover, they possess a high electronic conductivity, and a huge mechanical strength.[291] Their surface chemistry can be divided into two types. Their walls, made of sp^2 graphene carbon atoms, are hydrophobic pristine, while the defects on the side walls and edge sites at the open ends are full of hydrophilic carboxy groups. As for their electrochemical properties, it is widely accepted that atoms at the ends are like edge planes of HOPG and favor electrochemical activation; and atoms at the sidewalls are like basal plane of HOPG and show very slow electron transfer kinetics.[292,293] However, recent SECM studies have demonstrated that electrochemical properties are more likely to be similar at the ends and at the walls.[294]

It is often stated that DET is favored by the appropriate dimensions of CNTs. It is true that DET has been often reported on CNTs, whether it was a catalytic[295-297] or a non-catalytic signal,[295-298] while the same enzyme on a planar electrode gave no DET. It must however be noted that in the case where no DET was observed on the planar electrode, this latter was most of the time made of bare gold or GC.[295,296,298] The properties of these surfaces towards DET have already been discussed in previous section. Therefore, the reasons why DET is appearing are most of the time unclear. It could be due to an increase in ESSA, and thus an increase in enzyme loadings, that makes visible a signal non detectable with fewer enzymes. Alternatively, it could come from chemical functions inducing appropriate immobilization of the enzyme, to the increase in roughness, or to the peculiar properties associated to nano-size of CNTs. The very few fundamental studies will be discussed herein.

4.1.2.1.1 Preparation of the biocathode

Both SW-CNTs[142,296,297,299-304] and MW-CNTs[218,244,295,298,303,305-308] have been used to immobilize the MCOs. No clear trend could be established if one of these two kinds of CNTs induces more Efficient O_2 reduction. With the purpose to allow for Efficient DET, CNT-based 3D-structures for MCO immobilization have been built following various methods. In many studies, a CNT suspension in water, buffer, or organic solvent was deposited on a planar electrode and left to dry to allow for the formation of a 3D network.[142,244,299,309] However, CNTs tend to aggregate due to Van-der-Waals interactions, so that their high surface area is not entirely exploited for the electrochemical reaction. Since it is desirable to form electrodes with a high degree of CNT dispersion, a specific care has to be used for homogenization of the suspension in different solvents. Surfactants, or biopolymers like cellulose, can for example help the dispersion and improve compatibility with biomolecules.[295,310,311] Another issue arising from this method is the effective electrical connectivity of CNTs with the electron collector surface. A model based on Monte Carlo simulations has recently shown that the CNT-connectivity drops off once the distance to the electrode surface becomes higher than the CNT size (Fig 22).[312]

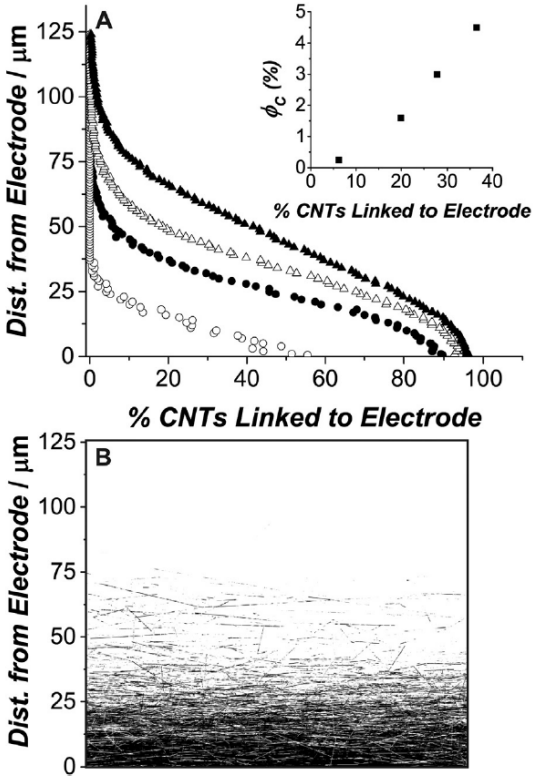

Figure 22. (A) Percentage of CNTs connected to the electrode in a 125-mm thick film for various volumes. % CNT fill, Φ_C: 0.25% (o); 1.6% (•); 3% (Δ); 4.5% (▲). (B) MATLAB image displaying only those CNTs connected to the electrode, shown as black lines. Reproduced with permission from [312]. Copyrigth 2016 Elsevier

Another possibility is to fabricate ordered arrays of CNTs grown by chemical vapor deposition on the electrode, [257,313,314] or by electrophoretic deposition.[313] Covalent binding of CNTs on Au[218] has also been performed. Free standing CNT-based electrodes have been designed, either in the form of buckypaper (BP),[315] fibers[310] or 3D pellets.[316-318] These structures have ensured DET for different MCOs: *Mv*-BOD,[142,296,302,303,305,308,311,319,320] *Mo*-BOD,[310] *Th*-laccase, *Rv*-laccase,[320] *Tv*-laccase,[295,299,321] *Cerrena unicolor* laccase,[301,322] *Agaricus bisporus* laccase,[313] or even tyrosinase.[317] Similar protocols have been used for the immobilization of MCO, whatever their origin, and their peculiar surface properties have been little considered. This latter point will be discussed further in section 4.1.4.

CNTs were often treated with HNO_3[299,300,323] or H_2SO_4 before use, which eliminates impurities but also introduces defects and oxygenated functions.[142,313,320] Enzymes have been directly adsorbed on the CNTs network,[299,320] mixed with CNTs prior to the formation of the network,[297] covalently bound using EDC-NHS on CNT carboxy groups, [142,244] or cross-linked with glutaraldehyde.[295,296,323] Another possibility has taken benefit of the π-conjugated systems of CNT walls to induce functionalization, using a bi-functional molecule that bears a defined aromatic functionality to bind by π-π stacking to the CNT walls, and a functional tether group for attachment of the enzyme.[324,325] This method has been used for example to introduce pyrene-butyric succinimidyl ester (PBSE) [306,307,321,326,327] or pyrene butyric acid.[308] The impact of the chemical functionalization is discussed further in section 4.1.4. The strong interaction between concavalin A immobilized on SW-CNTs and the glycosylated laccase has been exploited.[328] The laccase presented a higher activity towards oxidation of organic

substrates than the enzyme directly adsorbed, however no electrochemical catalysis was proved in this case.

4.1.2.1.2 CNT properties affecting direct electron transfer to MCOs

Very few studies have been performed to establish a clear link between the different kinds of CNTs, or the different protocols used to immobilize the MCOs, and the efficiency of the DET. The electrocatalytic activity of cross-linked *Tv*-laccase[329] and *Mv*-BOD[309] on two types of CNTs has been compared. The first kind had a uniform inner diameter (10-30 nm), carboxylic surface groups, a higher graphitization degree, a better conductivity and a higher electroactive surface area. The second kind had tapered inner tube diameter and mostly quinone surface groups. Without much surprise both enzymes exhibited a nicer behavior on the first kind. For *Tv*-laccase, a faster electron transfer, a clearer non catalytic signal, and 6 times higher current densities in catalysis (reaching 25 $\mu A.cm^{-2}$) were observed.[329] For *Mv*-BOD, the non-catalytic signal was observed only on the first kind that led also to 5 times higher current densities (90 $\mu A.cm^{-2}$). However, currents did not reach a plateau for any of these CNT-types, meaning that the interfacial electron transfer was a quite slow process.[309] In another report, the authors tried to compare electrophoretic deposition and chemical vapor deposition (CVD) of SW-CNTs on porous silicon.[313] Better DET for a covalently linked laccase was obtained with electrophoretically-deposited CNTs, but these results have to be considered carefully since porous silicon was covered with a conductive gold layer, while an insulating layer was formed during CVD growth. Therefore, higher cathodic currents could be assigned to a better conductivity of the electrode/nanomaterial interface rather than to better inherent properties of the material. Highly crystalline SW-CNTs (grown by CVD on a gold wire) were also compared to Toray carbon paper treated with UV-ozone.[257] Adsorbed laccase

from *Trametes sp*. led to catalysis on both materials but k_{ET} constants were respectively 1200 and 800 s^{-1}, reflecting higher degree of appropriate orientations on SW-CNTs. The coverage of electrochemically active enzymes was also much higher on these latter ($3.6.10^{-12}$ against $0.31.10^{-12}$ $mol.cm^{-2}$), translating a higher affinity.

Recently, the effect of the length of MW-CNTs has also been evaluated[330] for *Mv*-BOD in a kinetically controlled regime. The intermediate length (1-4 µm) led to the highest current densities (6.1 $mA.cm^{-2}$ at 0.1 V) while performances decreased for longer (10 µm) and shorter (<1 µm) CNTs sharing the same diameter (10-15 nm) (Fig 23). This quite complex behavior was explained by considering determinant the ratio of hydrophobicity to density of carboxy groups. Since the walls are mostly hydrophobic, while carboxy groups are mostly at the ends, this ratio is driven quasi exclusively by the length of the CNTs.

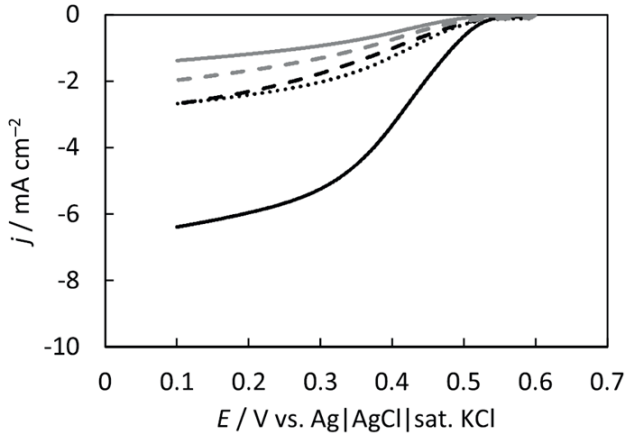

Figure 23. Influence of the length of MW-CNTs on ORR by *Mv* BOD. LSVs in O_2- saturated 100 mM phosphate buffer (pH 7) at 41 C, ω = 4000 rpm, and v = 5 $mV.s^{-1}$. Mv BOD is adsorbed at MW-CNTs of different lengths (L) and outer diameter (OD), or at CNPs. Black solid line: L = 1-4 µm and OD = 10-15 nm ; black broken line: L = 1-4 µm and OD = 10-15 nm and a surfactant is added ; black dotted line : L < 1 µm and OD = 8-10 nm ; and gray solid line : L = 10 µm and OD = 10-15 nm. The gray broken line represents CNPs. Adapted with permission from [330]. Copyrigth 2016 Elsevier

Considering that substituting carbon atoms by heteroatoms in graphene sheet of CNTs change the local electron density and should affect DET, qualitative effects of N-doping of SW-CNTs on the DET reaction of laccases were also studied.[331] A laccase from *Trametes* sp. was adsorbed onto SW-CNTs and N-doped SW-CNTs grown by CVD on a gold electrode, for N/C ratios of 0.1, 2.4 and 4.1%. Enzyme loading per BET surface and onset for DET did not depend on doping, but DET currents decreased with increasing doping. It was proposed that the induced positive charge led to increase electrostatic interactions with the slightly negative patch surrounding the T1 Cu, therefore denaturating the laccase. This explanation was furthermore confirmed by thermodynamic investigation showing that enthalpy change ΔH of laccase binding becomes more negative with increasing doping. This observation can be correlated with what happens on bare gold electrodes, where strong interactions between the enzyme and the electrode leads to enzyme denaturation (see section 3.4.4).

The spatial homogeneity of the mediator-less bioelectrocatalysis in a CNT composite was also evaluated by SECM. *Cerrena unicolor* laccase was encapsulated in a sol-gel silicate matrix with SW-CNTs. ORR was recorded in the presence of the laccase at $E_{applied}$ = 0.3 V and compared to a control experiment with the laccase at OCP. The activity was more evenly distributed than in a silicate film without CNT where proteins were shown to aggregate. [332]

4.1.2.1.3 Increasing the current densities through CNT networks

In evaluating the benefits of CNTs, performance improvements are reported most of the time in terms of higher current densities. Importantly, very little change in onset potentials has been reported. Although CNTs were shown to increase DET efficiency, currents were small when MCOs were first immobilized in CNT-networks: ~5 µA at the plateau with *Mv*-BOD and *Tv*-laccase cross-linked with glutaraldehyde on MW-CNTs for the first demonstration;[295] 28 $\mu A.cm^{-2}$ under air and 102 $\mu A.cm^{-2}$ under O_2 with *Mv*-BOD immobilized on SW-CNTs.[300]

Later the increase in current was mostly assigned to the higher electroactive surface area rather than to a better electrical connection. We give below some examples of MCOs immobilized in 3D networks constructed by drop casting of a CNT-solution on the electrode.

A 300-fold current increase was reported for *Mv*-BOD covalently linked on SW-CNTs compared to bare PG under 100% O_2 at 25°C, giving almost 1 mA.cm^{-2}.[142] Laccase embedded in a bioceramic (Hydroxyapatite)-CNTs self-assembled nanocomposite led to around 100 µA.cm^{-2} under air with an OCP of 0.56 V *vs.* Ag/AgCl at pH 6, and the currents were diffusion limited.[323] When *Mv*-BOD was immobilized in a MW-CNT/cellulose network, ~800 µA.cm^{-2} were reached under air at pH 5, and 60% were still recorded after 45 h at the constant potential 0.2 V *vs.* Ag/AgCl.[311] *Cerrena unicolor* laccase incorporated in SW-CNTs covered with a transparent and highly viscous cubic phase of monoolein gave 200 µA.cm^{-2}. This was however not optimal since the addition of covalently bound ABTS raised the current to 400 µA.cm^{-2}, indicating that some enzymes could not participate in DET currents.[301] In another study, when *Mv*-BOD was covalently attached at MW-CNTs, themselves covalently attached on a gold electrode, currents increased up to 500 µA.cm^{-2} in an unstirred solution.[218] Although these results already represented a considerable increase compared to most bare carbon electrodes, the current densities remained limited. Therefore, specific and oriented attachment of the enzymes has been the main concern in most of the following studies (section 4.1.4.).

Some of the developed cathodes were successfully used in EBFCs, for example with MW-CNTs oxidizing ascorbate at the anode,[295] or with glucose dehydrogenase (GDH) on SW-CNTs at the anode.[296,299,300,302] The first Glucose/O_2 EBFC based on SW-CNTs showed OCV = 0.8 V and P_{max} = 9.5 µW.cm^{-2} at E_{cell} = 0.52 V at pH 6.[299] Other devices included a H_2/O_2 EBFC with a hyperthermophilic hydrogenase at the anode leading to OCV = 1.1 V, more than 300 µA.cm^{-2} at E_{cell} = 0.65 V, and less than 40% loss after 24 h at an applied E_{cell} = 0.65 V.[142] A CNT-based cathode was also used as a proof of concept in a photosynthetic

electrochemical cell for the light-to-electricity conversion with water as the only input. Water was oxidized by thylakoid membranes while the laccase reduced O_2, regenerating water in the system. The maximal generated power was 5 $\mu W.cm^{-2}$.[306] The hydroxyapathite-CNT cathode combined with glucose oxidase (GOx) also gave an OCV of 0.58 V and P_{max} = 15.8 $\mu W.cm^{-2}$ at 0.28 V. [323] In a fructose/air one chamber EBFC, OCV = 663 mV and P_{max} = 126 $\mu W.cm^{-2}$ at pH 5 were obtained. 90% of the initial power remain after 12 h, and 52% after 87 hours at E_{cell} = 0.35 V.[311]

To obtain a hierarchical porosity, CNTs were also deposited in an already porous material. 3D hierarchically structured composites were built by growing MW-CNTs by CVD on CMF with diameters ranging from 6 to 9 µm,[314,333,334] or by depositing CNTs on a porous carbon fabric to form a gas diffusion layer (GDL),[305] or by coating CNTs-Anthracene or CNTs-COOH in a highly porous carbon felt.[335,336] In the latter case, after deposition of CNTs-COOH by LBL, ESSA increased 5 times, and cathodic currents reached almost 1.5 $mA.cm^{-2}$ at 0 V. This allowed the development of a H_2/O_2 EBFC with an OCV of 1.12 V and net currents of 765 µA at short circuit. Absolute P_{max} was 410 ± 5 µW which represented a successful scale-up compared to a previously reported device,[142] indicating that the diffusion limitation of O_2 was overcome by the porosity of the electrode.[335]

4.1.2.1.4 Free-standing CNT-based 3D layers

Besides porous random networks, CNTs can be used as electrospun fibers[310,337] or buckypaper.[319-321,326,327,338,339] BP is a flexible self-supporting membrane-type film made of densely packed CNTs maintaining close contact by Van der Waals interactions. It is obtained by filtration of CNTs dispersion. This nanoporous material has attractive properties such as very high surface area, high porosity, chemical and electrochemical stability, high mechanical

strength and high conductivity (a value of 51.2 $S.cm^{-1}$ has been reported[326]). Importantly for the construction of potentially implantable biodevices, it has also a low toxicity both *in vivo* and *in vitro*.[340] To quote some performances: BP enabled an enhancement in current densities for *Th* and *Rv*-laccases as well as *Mv*-BOD. Currents reached 120-220 $\mu A.cm^{-2}$ compared to 12-35 $\mu A.cm^{-2}$ for spectrographic graphite, leading to a mass-transport limited regime.[320] An EBFC based on BP had an OCV of 710 mV and P_{max} > 100 $\mu W.cm^{-2}$ [319] and this device was furthermore able to work in urine and saliva.[338] BP was also compared to "conventional" MW-CNTs electrodes where CNTs formed aggregates of ~500 µm in diameter. *Tv*-laccase was adsorbed on a 30 µm thick BP made of 0.9 $mg.cm^{-2}$ MW-CNTs homogeneously dispersed, and presenting a median pore diameter of 48 nm.[315] Reporting the current to the mass of material showed that properties of MW-CNTs were better exploited in BP: at ≈ 0.54 V *vs.* Ag/AgCl, the current was 471 ± 64 $\mu A.mg^{-1}$, which represented a 68-fold increase. In terms of current densities, they were an order of magnitude higher than previously reported: 487 ± 117$\mu A.cm^{-2}$ against only 50 $\mu A.cm^{-2}$. [315,326]

Miyake *et al.* constructed an innovative free-standing CNT-based enzymatic film.[341] After introducing *Trametes* sp. laccase in a forest made of 1 mm-long CNTs separated by 16 nm, further drying induced shrinkage to a close packed structure, whose total thickness was 20 µm (Fig 24). Current densities of 2.1 ± 0.3 $mA.cm^{-2}$ were reached with stirring, and further increased to 4 $mA.cm^{-2}$ when 2 films were joined (Fig 24).

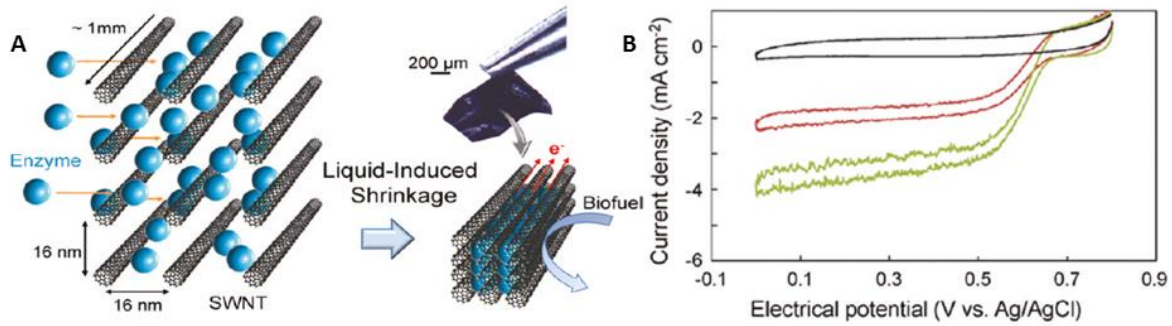

Figure 24. (A) Schematic diagram of laccase entrapment in a CNT forest by "liquid-induced shrinkage". The photograph shows a free-standing enzyme-CNT film that can be manipulated with tweezers. (B) Corresponding CV of the so-formed single-piece electrode in N_2 (black curve) and O_2-saturated stirred Mc Illvaine buffer pH 5 (red curve). The green curve shows the currents obtained with a double-piece electrode, v=10 $mV.s^{-1}$. The electrode films were prepared using a 20 µm thick CNT film and 0.25 $mg.mL^{-1}$ laccase solution. Adapted with permission from [341]. Copyright 2011 American Chemical Society.

In a fructose/O_2 EBFC, where fructose dehydrogenase was used at the anode, P_{max} was 1.8 $mW.cm^{-2}$ at 0.45 V in a stirred oxygenated fructose solution. More than 80% of P_{max} was maintained after 24 h of continuous operation at an external load of 35.3 kΩ. It is noteworthy that this technique allowed both anodic and cathodic enzymes to be closely surrounded by CNTs. In contrast with the commonly used surface-coating technique where the enzymes are deposited on an electrode surface, in this case, enzymes are trapped within the CNT networks. Such homogeneous entrapment was also achieved by trapping *Magnaporthe oryzae* BOD and SW-CNTs in wet-spun fibers.[310] Homogeneous distribution of enzymes in the resulting material was confirmed by fluorescence imaging and energy dispersive X-Ray analysis (EDX). Amounts of immobilized BOD were higher than when the enzyme had to diffuse in a previously made CNT-fiber. The currents increased 3 times, and no further increase was recorded upon addition of ABTS, indicating a proper orientation of the enzymes. In the previous system, 50% increase in current was recorded after ABTS addition.

Cosnier *et al*. developed free standing pellets obtained by mechanical compression of CNTs mixed with enzymes. They showed that a 3D porous network was formed with 10 nm thick CNTs, and that pores inter CNTs were ranging between 50 and 100 nm.[317] The CNT matrix had a high surface area and high porosity. With 250 mg MW-CNTs and ≈50 mg enzyme, the electroactive surface area was 52 cm^2, the conductivity 3300 $S.m^{-1}$, and the percentage of void 43%.[316] This technique allowed in particular to record the first DET-based

O_2 reduction by a tyrosinase[317], and to develop highly powerful cathodes and EBFCs. Cathodes exhibited for example 5.8 $mA.cm^{-2}$ at 0 V under O_2 with the quantities mentioned above,[316] or a current plateau of 0.17 mA at pH 7 with a smaller electrode made of 35 mg MW-CNTs and 15 mg enzyme.[342] The cathode OCP was shown to increase from 740 to 820 mV *vs.* NHE with increasing enzyme amounts.[316] The first glucose/O_2 BFC using these electrodes had an OCV = 0.95 V and P_{max} = 1.3 $mW.cm^{-2}$ at E_{cell} = 0.6 V in a pH 7 buffer containing 50 mM glucose.[316] Upon improvement of the bioanode, P_{max} was 1.54 $mW.cm^{-2}$ in an air-saturated buffer pH 7 containing 50 mM glucose.[342] Impressive stabilities were recorded.[316-318] An EBFC based on 35 mg MW-CNTs and 15 mg laccase at the cathode and both GOx and catalase at the anode had an initial P_{max} of 160 $\mu W.cm^{-2}$ and OCV of 0.75 V at pH 7, with a buffer containing 5 $mmol.L^{-1}$ glucose under air. It was operated regularly during one year with 1 hour constant-load discharges, and kept in a pH 5 buffer when not used. 22% of the initial power was still recorded after 1 year.[318] However, this corresponds to the "apparent stability" described by Armstrong *et al.*[27] With a high amount of enzymes, the current is indeed limited by the substrate diffusion, therefore enzymes can be lost from the electrode surface or inactivated without altering the current magnitude.

4.1.2.2 Graphene

Discovered in 2004, graphene is a honeycomb crystalline lattice of sp^2 carbon atoms with high in-plane electron conductivity, mechanical strength, and transparency.[343] It can be obtained via mechanical exfoliation of graphite, chemical synthesis like chemical vapor deposition, or by chemical or electrochemical reduction of graphene oxide (GO).[237,344-346] This latter method restores partially the sp^2 structure and electron conductivity of graphene, while conserving oxygen functionalities. Despite its promising properties, graphene has not yet been

widely used in EBFCs.[74,347] Graphene has been used as a building block for the construction of 3D networks, either alone or in combination with CNTs or AuNPs.[348-350] Unless otherwise stated, in the cases described here ORR started at a potential close to T1 of the enzyme, proving that currents were due to DET between the MCO and the electrode. Moreover, like in most studies, the DET performances will be described in terms of current densities.

In earlier studies, it was not obvious that graphene could be of any interest for DET of MCOs, and that DET was obtained at all. An ORR onset at potentials below 0 V *vs.* Ag/AgCl was for example reported for *Mv*-BOD immobilized on graphene, while no control without the enzyme was presented, suggesting that direct electroreduction of O_2 on graphene was more likely recorded.[351] In another case, with a graphene-modified electrode, *Tv*-laccase in solution reduced O_2 at 0.25 V *vs.* Ag/AgCl. This potential was attributed to a redox process of hydroxyle, which suggests a MET mechanism with hydroxyle acting as a redox mediator.[345] A combination of GO and cobalt hydroxide with chitosan was described for a glucose/O_2 BFC employing laccase at the cathode. An OCV of 0.6 V and a P_{max} of 517 $\mu W.cm^{-2}$ were reported, but from the article it is not clear if a redox mediator has been used or not.[352]

In case of assessed DET mechanism, the current densities were very low at the beginning of the use of graphene. *Tv*-laccase adsorbed on electroreduced GO gave currents inferior to 5 $\mu A.cm^{-2}$, probably due to aggregation of the enzymes.[345] With BOD adsorbed on graphene, reduction current 74 times higher than at GC were obtained, but they still only reached 1.5 µA.[353] BOD covalently attached to a block copolymer bearing carboxylate moieties modified with graphene was employed in an EBFC using GOx at the anode. In an oxygenated solution containing 5 mM glucose at pH 7.4, power and current densities reached 0.115 $\mu W.cm^{-2}$ and 0.16 $\mu A.cm^{-2}$, and 3.7 $\mu W.cm^{-2}$ and 5.1 $\mu A.cm^{-2}$, respectively without and with graphene. Not many details about the electrodes were however given.[354]

However, DET currents could be increased by simply optimizing the electrode preparation protocol. Different protocols were evaluated for *Mv*-BOD: 1/ layer-by-layer deposition of electrochemically reduced GO and BOD; 2/ electrochemical reduction of BOD mixed with GO flakes presenting a wide size distribution of 0,5-5 µm; 3/ the same protocol as in 2 but with a narrower size distribution of 200-650 nm, and 4/ the same protocol as in 3 but with an increased mixing duration. This led to current densities of respectively 2.6, 46 ± 4, 120 ± 19 and 280 ± 30 µA.cm^{-2}, *i.e.* a more than 100-fold increase between the least and the most Efficient parameters (Fig 25).[346,355]

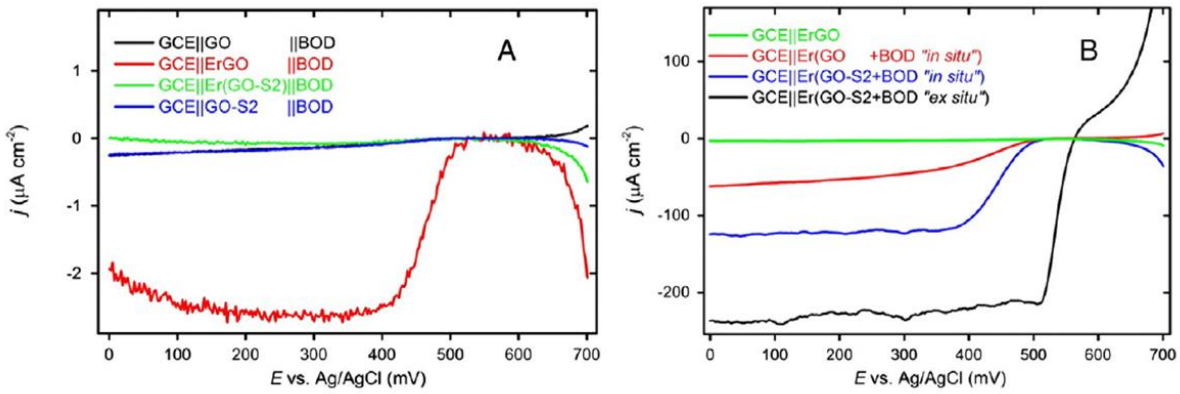

Figure 25. Comparison of different protocols for *Mv*-BOD immobilization on GO flakes. Small GO flakes are labelled GO-S2. (A): The LBL biocathodes with BOD adsorbed on layers of GO (black), electrochemically reduced GO (red), GO-S2 (blue) and electrochemically reduced (GO-S2) (green). (B): The biocathodes prepared by *in-situ* mixing of BOD on the GCE with GO (red) and GO-S2 (blue) with their subsequent reduction. The biocathode prepared by "ex situ" incubation of BOD with GO-S2 and consequent electrochemical reduction is shown in black and control electrode with only electrochemically reduced GO layer is shown in green. Adapted with permission from [355]. Copyrigth 2014 Elsevier

The total pore volume of a network of graphene nanoplatelets could also be increased by adding in the graphene suspension NaH_2PO_4 that crystallized in the carbon thin film during

the drying process, thereby acting as a mold.[356] The adsorbed *Trametes sp*. laccase gave catalytic currents of 1.6 $mA.cm^{-2}$ at pH 3, a 2-fold increase compared to the network without Na_2HPO_4. This enhancement corresponded to an increase of enzyme coverage thanks to a more appropriate porosity. Competitive ORR currents of respectively 2.1 $mA.cm^{-2}$ at pH 4 and 0.4 $mA.cm^{-2}$ at pH 7.4 were obtained with *Mv*-BOD and *Th*-laccase covalently bound on graphene after simultaneous electrodeposition and electroreduction of GO. A rotation rate of 1500 rpm had to be used to overcome mass transport limitation.[237] Finally, BOD adsorbed on graphene and coated on a carbon fiber cloth rendered hydrophilic by UV-ozone treatment led to a plateau current of 0.2 $mA.cm^{-2}$. [357]

Very recently, parameters influencing adsorption and electrocatalytic properties of BOD integrated in an electrochemically reduced GO matrix were investigated.[358] GO flakes with different negative charge densities were studied. It was found that the current density (j), the heterogeneous electron transfer rate (k_{ET}) and the coverage of electrochemically active enzyme (Γ_a) depended on the negative surface charge density of graphene, and that j was more influenced by Γ_a than k_{ET} (*i.e.* the electron transfer was fast enough not to be limiting). The maximum current density was 597 ± 25 $\mu A.cm^{-2}$.

Hierarchical 3D graphene-based structures have also been designed. A graphene-laccase composite was electrodeposited and covalently bound on carbon micropillars (50 µm in diameter, 200 µm in height) of a 3D array. The cathode was combined to a GOx-based anode developed following the same procedure. The power density of this EBFC was 7 times higher than that of the graphene-less EBFC. However, the stability was lower, which could be related to enzyme denaturation within the graphene matrix.[359] *Tv*-laccase was also immobilized on carbon fiber electrodes decorated with graphene nano-sheets produced in situ by an electrochemical procedure. This cathode was coupled to a PQQ-dependent GDH in a

glucose/O_2 EBFC leading to j_{max} = 70 µA.cm^{-2} and P_{max} = 5.5 µW.cm^{-2} at an external load of 6 kΩ.[360]

4.1.2.3 Other carbon-based 3-dimensional structures

4.1.2.3.1 Carbon nanoparticles

Widely used carbon nanoparticles (CNPs) offer a more or less cost-effective alternative as well as an Efficient tool for production of high surface area matrices for enzyme immobilization and improved bio-electro-catalysis. They are easily available using fast, simple and cheap synthetic routes. Most are strongly adsorbent, have a high specific surface area and a good biocompatibility, a high electrical conductivity and excellent chemical stability. However, the general term "CNPs" covers a large variety of materials more or less defined, with different sizes, microstructures, internal porosity, so that it is difficult to precisely determine them. The described materials include carbon nano-dots, *i.e.* discrete quasi spherical carbonaceous nanoparticles with average diameter of 50-60 nm;[361] glassy carbon double-shelled hollow spheres with a porous shell of about 480 nm,[362] carbon Vulcan,[253,363] hydrophilic or hydrophobic CNPs,[258,364] Black pearl 2000 carbon particles,[365] carbon coal or carbon black,[366,367] Ketjen Black (KB),[219,367-371] carbon nanofibers made of stacked graphene cones,[372] mesoporous CNPs with diameters below 500 nm and 6.3 nm pores,[373] carbon aerogels with average pore size 22 nm,[374,375] or carbon cryogel with average radius of 20 nm.[376]

More generally, CNPs seem to promote DET but in many cases poor results were obtained. The protocols mostly involved drop-casting of CNP-suspensions with Nafion® or PVDF as a binder.[361-363] When *Mv*-BOD was adsorbed or cross-linked with glutaraldehyde, less than 5 and 10 µA.cm^{-2} were respectively obtained under air and O_2, while no DET at all

was observed with a GC electrode. This corresponds likely to an increase of ESSA.[361,362] A biocomposite of *Cerrena maxima* laccase, glutaraldehyde and CNPs delivered 43 µA.cm^{-2}, while only 17 µA.cm^{-2} were obtained on graphite.[258] For *Mv*-BOD adsorbed on Carbon Vulcan 0.27 mA.cm^{-2} were obtained in O_2 at 600 rpm without a mediator, and 1.6 mA.cm^{-2} upon ABTS addition. This underlines that despite the structuration of the electrode not all enzymes were favorably connected for DET.[363] Different polymers have also been introduced for the dispersion of CNPs, like chitosan[346] or polylactic acid (PLA),[377] leading respectively to 83 ± 19 µA.cm^{-2} and 255 ± 42 µA.cm^{-2} and underlying the influence of the charge of the polymer. Interestingly, the example of *Trametes trogii* laccase adsorbed on large surface area graphite and Vulcan carbon electrodes showed that current densities were in the nA.cm^{-2} range when referred to the real electroactive surface area, while they reached 600 µA.cm^{-2} when calculated with the geometric surface.[253] It is therefore questionable if DET was really promoted or if a "zoom factor" was more likely observed.

4.1.2.3.2 Enzymatic BFCs based on carbon nanoparticles

Despite generally relatively low performances, the described mesoporous carbonaceous cathodes were used for EBFC development. A glucose/air EBFC with GOx at the anode had a 0.93 V OCV, and P_{max} = 40.8 µW.cm^{-2} at E_{cell} = 0.41 V with a pH 7.2 air-saturated buffer containing 4 mM glucose. Connected 24 h at an external load of 1 MΩ, the EBFC lost 7.1% power density in 24 h and 37.4% in 7 days while the OCV remained constant.[361] A compartmentless lactate/O_2 BFC had a 0.6 V OCV and P_{max} = 3.13 µW.cm^{-2} at E_{cell} = 0.4 V. Connected 24 h at 1 MΩ, in a pH 7 buffer containing 40 mM lactate and 20 mM NAD^+ under ambient air, the power losses were 6% in 24 h and 41% in 7 days.[362] A

compartmentless fructose/O_2 EBFC with FDH immobilized on KB at the anode gave a 790 mV OCV, j_{max} = 2.8 mA.cm^{-2} and P_{max} = 850 µW.cm^{-2} at E_{cell} = 410 mV at pH 5, room temperature, and in presence of 200 mM fructose under stirring. In a quiet solution, performances were lower: j_{max} was 1.1 mA.cm^{-2}, while P_{max} was 390 µW.cm^{-2} at E_{cell} = 410 mV. 63% of power was lost after 12 h of continuous operation under stirring. But the delivered power was already usable: 4 EBFCs connected in series lighted a red LED (1.8 V) during ~60 days.[374] CNFs also allowed the development of a H_2/O_2 EBFC delivering P_{max}= 1.2 ± 0.2 mW.cm^{-2} at E_{cell} = 0.75 V while the OCV was 1.1 V at pH 6 and 50°C. The biocathode was quite stable, with 90, 70 and 50% current remaining after 30 minutes cycling at 50, 60 and 70°C.[372]

4.1.2.3.3 Importance of porosity

What seems nevertheless important for entrapping an enzyme is the adequacy between the size of the enzyme and the size of the meso-pores. The increased current densities observed with pores of appropriate sizes were attributed not only to the ESSA enlargement but also to a "curvature effect" promoting DET.[371] Contrary to low current densities reported previously, currents of 4 mA.cm^{-2} were obtained under stirring for *Trametes sp* laccase adsorbed on carbon aerogels with an average pore size of 22 nm,[374] reaching even 10 mA.cm^{-2} with a RDE at 8000 rpm.[375] Stabilization in the meso-pores was observed with stable currents recorded continuously during 10 days.[375] *Mv*-BOD immobilized in the same carbon aerogel gave 6 mA.cm^{-2} at 3000 rpm and pH 7[375] while *Bp*-BOD adsorbed in a mesoporous matrix of carbon cryogel with average radius of 20 nm gave 3 mA.cm^{-2} at -0.1 V *vs.* Ag/AgCl, 37°C and pH 7.2.[376] The same enzyme *Bp*-BOD adsorbed on carbon nanofibers made of stacked graphene cones presenting a large volume of mesopores gave 4 mA.cm^{-2} under O_2 at 60°C

and pH 4.[372] Similarly, around 1 mA.cm^{-2} was obtained when *Mv-BOD* was adsorbed at KB with mesopores in the range 2-100 nm, while only 3.5 µA.cm^{-2} were recorded at a planar electrode.[371] On the contrary, with too small pores of 6.3 nm, currents delivered with immobilized BOD were only ~20 µA.cm^{-2} in DET and twice more in MET, showing that both enzyme immobilization and orientation were not optimized.[373]

A mathematical model of random orientation of enzymes on planar and mesoporous electrodes was derived from Laviron's model[378] for the non-catalytic signal[379] and from Léger's model[148] for the catalytic signal.[371] It estimated the possibility to establish DET between enzyme and electrode. BOD was chosen as a model protein, among others. It was assimilated to a sphere with a radius r = 3 nm, and a distance between enzyme center and active site r_{AS} = 2 nm (a unique redox center was considered), while electrode pores were considered to be spherical with a radius R_p. Computation showed that no clear non-catalytic redox process in the absence of substrate was expected with the BOD model on planar or mesoporous electrode with $R_p >> r$, but a clear redox peak when R_p was close to r.[379] Catalytic currents on the contrary were predicted both for planar and mesoporous electrodes, but they were much higher when pore and enzyme sizes were close to each other.[371] Although the model showed that an adequate porosity should promote DET, it did not take into account the problems related to adsorption of enzymes in the pores, that may be sterically restricted in case of small pores radii (typically adsorption is not expected for pores smaller or of the same size than enzymes).

Besides the pores needed for enzyme immobilization, a network for Efficient transport of substrate is also important. *Mv*-BOD was for example adsorbed in macro/mesoporous carbon with different ratios of meso/macropores, obtained by carbonization of magnesium oxide hard template (MgOC). This technique ensures the control of morphology and pore size, and the material was composed of interconnected macropores (150 nm) with an

additional morphology of 40 nm mesopores. The highest current density was obtained with the material containing 33% macropores, with which around 12 $mA.cm^{-2}$ was reached in O_2 saturated pH 5 buffer at 25°C and 10000 rpm, *i.e*. approx. twice more than when either only meso or only macropores were present. Mesopores are important for enzyme immobilization, and ensure better stabilization. For the materials containing only mesopores, only macropores or the 33% mixture, respectively 80%, 66% and 75% of the current density was retained after 100 CV cycles. However, additional macropores are necessary to ensure O_2 mass transport, as demonstrated by the high increase in current densities recorded with increasing macropores contents.[380]

4.1.2.3.4 Free-standing carbonaceous films

Free-standing carbonaceous materials have been developed, either with micro/macroporous carbonaceous monoliths made from hard macrocellular silica templating[141] or cylinders of compacted nanomaterials: CNTs (see above), graphitized mesoporous carbon[143] or mixtures of graphite and MW-CNTs[381]. The first presented excellent mechanical properties, and tunable size, geometry and porosity. Small pores of diameters slightly bigger than enzymes were present for effective immobilization of enzymes, micro-pores of 5.4 Å representing a total microporous area of 600 $m^2.g^{-1}$ were supposed to help the enzyme attachment, and larger pores (> 10 µm) were introduced to allow mass transport of fuels. In the second case, mixing different nanoparticles in various proportions influenced the ratio of pores with diameters larger than 10 nm. With a ratio of 60/40 graphite/MW-CNTs, these latter pores represented 0.42 $cm^3.g^{-1}$, *i.e*. 75% of the total pore volume. Currents delivered with adsorbed *Tt*- and *Mv*-BOD were respectively 2.1 $mA.cm^{-2}$ at 1000 rpm, 25°C and pH 7.2, *i.e.* a 500-fold increase compared to GC,[141] and 1.23 $mA.cm^{-2}$ at 25°C and pH 6.[381] Interestingly, catalytic currents increased linearly with electrode thicknesses and volumetric current densities were constant, reflecting that the same intrinsic efficiency was

obtained. It is also interesting to note that when currents were normalized by the specific area, values of 1.58 µA.cm^{-2} in mesoporous carbon and 2 µA.cm^{-2} at GC were calculated (resp. at 7500 and 1000 rpm).[141] Similarly, with mixtures of graphite and MW-CNTs, currents were divided by 2 when electrodes were cut in half. For higher thicknesses, a linear scale up of the current was however not observed.[381] Despite the tuned microstructure in carbon monoliths, systems were still limited by random orientation of enzymes, as shown by the wide distribution in ET interfacial rate constants reflected by the CV shape, and mass transport was not fully optimized.[141] In the second system, designed for H_2/O_2 fuel cells, intrinsic limitations were induced because non-explosive gas mixtures were used to design a membrane-less EBFC. A low level of O_2 (4.6%) was therefore present. This, combined with a poor affinity of *Mv*-BOD towards O_2, explains why cathodic currents were much lower than anodic currents where a hydrogenase was oxidizing H_2. The electrodes were scaled to compensate this cathodic limitation, and ultimately permitted to get an EBFC delivering 1.67 ± 0.24 mW.cm^{-2} (relative to the anode area).[143] Power densities could be further multiplied by a simple stack design. For example, assembling in series two composed cells, themselves made by parallel assembling of 4 individual cells, gave: OCV = 2.1 V and P_{max}= 7.5 mW (0.18 mW.cm^{-3}) with the same gas mixture at pH 6 and 20°C.[381] Enzyme stability inside the pores was comparable to that in solution. The current kept a constant value of 0.7 mA.cm^{-2} during 18 hours at 0 V *vs.* Ag/AgCl and 25°C, while the current at a GC electrode was nil after 2 h in the same conditions.[141] In an EBFC configuration, 90% of the initial current densities were retained after 1 day, and 54% after 1 week at an applied voltage of E_{cell} = 0.8 V. 76% were retained after 24 h when the voltage was E_{cell} = 0.55 V.[381] This last point underlines that estimated stability is not only an intrinsic characteristic of a system, but also depends on the conditions chosen for the test (See section 4.1.5.).

4.1.2.3.5 Comparison of carbon nano-structures

To conclude, it is interesting to quote a study comparing the efficiency of different carbon-based nanomaterials or porous 3D materials as DET promoters for MCOs. Catalysis was described both in terms of volume and surface current densities for the various materials. To calculate surface current densities, the real surface (BET) was taken into account. *Tv*-laccase was adsorbed on graphite felt, CNFs, SW and MW-CNTs or porous carbon tubes, and ORR was recorded at ≈ 0.45 V *vs.* Ag/AgCl. In terms of volumetric current densities, the least Efficient was graphite felt with less than 10 $\mu A.cm^{-3}$, and the most Efficient were MWCNTs and CNFs with resp. 77 $\mu A.cm^{-3}$ and 70 $\mu A.cm^{-3}$. SW-CNTs and porous carbon tubes gave intermediate results (resp. 40 $\mu A.cm^{-3}$ and 37 $\mu A.cm^{-3}$). The rankings were totally different when surface current densities were compared. CNFs and graphite felt gave the highest current densities (resp. 129 and 125 $\mu A.cm^{-2}$), SW-CNTs gave the lowest (2 $\mu A.cm^{-2}$), while intermediate results were recorded with porous carbon tubes and MW-CNTs (resp. 14 and 10 $\mu A.cm^{-2}$, *i.e.* 1 order of magnitude lower than the CNFs or graphite felt). When the current was normalized by the surface, the results highlighted a possible limitation: CNTs may form aggregates so that their surface is not entirely available for enzyme adsorption.[382] This study also demonstrated that nanomaterials have to be selected carefully depending on the envisioned application.

4.1.3 Gold nanostructures

Besides widespread carbon, metallic 3D electrodes have also been designed for MCOs immobilization and DET bioelectrocatalysis. The most described metal for this purpose is gold, either as gold nanoparticles (AuNPs) for the nanostructuration of planar electrodes, or

by direct synthesis of porous gold materials. Gold has a good electronic conductivity, a high chemical stability, and superior surface tunability by chemisorbed thiols, used to form self-assembled monolayers (SAMs), or by other techniques like electrochemical reduction of diazonium salts.[383,384] AuNPs in particular present a high surface area, a controllable size and are easily synthesized. Immobilization of already synthesized AuNPs, or direct synthesis of AuNPs at the electrode surface allowed the development of a 3D network. The first method involved deposition by drop casting,[385-390] layer-by-layer,[391,392] or covalent bonding.[393,394] The second method relied on electrochemical or chemical reduction of gold salts,[395-397] or on de-alloying of Au alloys.[398] Porous gold electrodes could also be formed by covering with gold a 3D silicon material,[399] by electrodepositing a porous gold film on a gold electrode,[400] or by bottom-up templating approach.[401-403] Pores of different sizes, depending on the Au/Ag ratio,[398] or a nanoporous gold structure displaying 3D networks of interconnected pores with typical pore diameters of ca. 30-40 nm, were also obtained via de-alloying of Au alloys.[404] Calculation of the real electroactive surface area of 3D gold electrodes is then possible by integrating the peak associated to the reduction of gold oxide, which corresponds to a theoretical charge density of 390 ± 10 $\mu C.cm^{-2}$.[405]

The use of other metallic nanoparticles has also been reported. Thioaniline modified BOD and Pt nanoparticles (Ø ≈ 2 nm) were simultaneously electro polymerized on a gold electrode. The presence of BOD increased the onset potential, and higher current densities (ca 90 $\mu A.cm^{-2}$) were recorded, as a synergic effect of Pt and BOD.[406] Nano-structuring the electrode surface with nano-crystalline hematite semiconductor (αFe_2O_3) allowed DET currents to be multiplied by 20 compared to a flat surface. However, the onset was ≈50 mV *vs*. Ag/AgCl at pH 6.4, which is quite low for *Mv*- BOD.[407] No DET was recorded for the same enzyme with other metal oxides like TiO_2 or WO_3.[407] Alloys were also used. For example, a BFC was built with a cathode based on *Mv*-BOD encapsulated in a mesoporous

Pd-Pt aerogel. The electrode delivered a maximum current density of ≈ 200 µA.cm^{-2}, with combined contributions of the enzyme and the alloy to catalysis.[408]

DET was observed when *Tv*-laccase was immobilized at TiO_2 nanoparticles, but the catalysis was more Efficient when ABTS was added.[409] For a laccase covalently bound on ordered arrays of polyaniline-coated polycrystalline copper nanotubes (200 nm in diameter and 30 µm in height) the plateau current density was 1.2 mA.cm^{-2} (which corresponded to an absolute current of 220 µA).[410] To the best of our knowledge, no DET current was observed for a laccase covalently bound on 40-nm magnetite Fe_3O_4 nanoparticles,[411] nor with platinum nanoparticles.[412]

As already stated for carbonaceous nanostructures, there is a discussion whether AuNPs increase DET efficiency by enhancing the electroactive area and thus by connecting more enzyme molecules, or favor a better relative orientation of the enzyme towards the conducting material. Actually one can imagine that when the size of the AuNP is comparable or smaller than the enzyme, the nanoparticles should approach closer to the active site and therefore drive a better electronic communication while allowing more freedom of orientations. This must be carefully evaluated in the case of MCOs. There is sometimes a clear evidence that DET appears on nanostructured gold, while not on planar gold (all other parameters being kept constant),[413,414] or that catalytic currents are enhanced. Nonetheless, precise evaluation of electron transfer rate is rarely performed. Contradictory results can even be found in the literature. We will first discuss this point in the following, then address the increase in current densities via surface increase and finally discuss the actual usefulness and limitations of gold nanostructured electrodes.

4.1.3.1 Effect of the size of AuNPs on DET

First studies that compared the influence of different sizes of AuNPs showed quite contradictory results. 5 and 16-nm spherical AuNPs were used for oriented attachment of *Th*-laccase (see section 4.1.5.). The recorded efficiency of DET was attributed not only to an appropriate orientation but also to an adequate size of the AuNPs. Results were indeed better when the particle dimensions were close to those of *Th*-Laccase (5 nm), leading to catalytic O_2 reduction in DET, and only 6% increase in currents after addition of the diffusing redox mediator ABTS.[393] *Mv*-BOD was also covalently bound to small nanoparticles (5 ± 3 nm), giving 375 $\mu A.cm^{-2}$ under pure O_2, with only 5% increase upon ABTS addition.[415] The catalytic efficiency decreased when nanorods (average size 31 ± 6 nm) were used instead of nanoparticles, supporting the assumption that when the nano-elements are bigger than the immobilized MCO, the improvement effect in the electronic coupling does not take place.[394] Higher values of βd_0 (16.6) than on AuNPs (11.0), representing higher dispersion of orientations, were also attributed to the presence of different crystalline facets of the nanorods.[394] Yet, on the other hand, another study suggested that better electronic coupling was favored with bigger AuNPs. Diameters of 7, 15 and 70 nm, leading to the same electrode roughness, were used as a support for *Mv*-BOD. The highest current density was obtained with the biggest AuNPs, bringing the conclusion that the most important parameter is the size of the spaces between the AuNPs where the enzyme must penetrate.[416]

Moreover, the presence of AuNPs is not enough by itself to allow for Efficient DET, as shown by the following examples. *Rv*-laccase covalently bound on small nanoparticles (1.7 ± 0.4 nm) encapsulated in polyamidoamine (PAMAM) dendrimers exhibited a non-catalytic redox peak which increased with AuNPs compared to dendrimers only, but no O_2 reduction catalysis was recorded.[417] In another study *Tv*-laccase was cross-linked with glutaraldehyde on AuNPs forming uniform aggregates of 200-500 nm. While AuNPs increased the conductivity of the ITO electrode, only MET catalysis could be observed.[396] Polypyrrole

nanotubes were decorated with AuNPs whose sizes ranged between 40 and 1000 nm. When attached on them, neither *Tv*-laccase nor *Mv*-BOD exhibited DET but only MET, probably due to the high abundance of repulsive amino groups on polypyrrole.[418]

Calculations suggested also that even at AuNPs not all enzymes were in DET configuration.[413,414] The number of *Th-laccase*s per AuNP (22 nm) was evaluated at 44 by QCM-D coupled to electrochemistry.[413,414] On the other hand, the maximum current density, obtained for a monolayer of AuNPs, was 31.10^{-18} A at a single nanoparticle. The low value of k_{cat} (13 s^{-1}) was explained by unfavorable orientation of some enzymes.[413,414] Interestingly, another laccase from *Trichaptum abietinum* (*Ta*-laccase) showed the same electronic coupling with AuNPs, but a better catalytic activity was recorded.[419] This latter result was attributed to the smaller size of *Ta*-laccase reducing conformational changes at the AuNPs surface.

Shleev *et al.* proposed to rationalize the influence of the size of the nanoparticles by taking into account not the geometric area but the real area of the electrode.[386,387,419] The study was performed with *Mv*-BOD immobilized on sub-monolayers of AuNPs with uniform sizes significantly bigger than that of enzymes (20, 40, 60, 80 nm). i_{max} clearly increased with AuNPs size, but when the current was reported to the real area of the electrode, the same value of 15 ± 3 µA.cm^{-2} was obtained for all particle sizes (Fig 26).

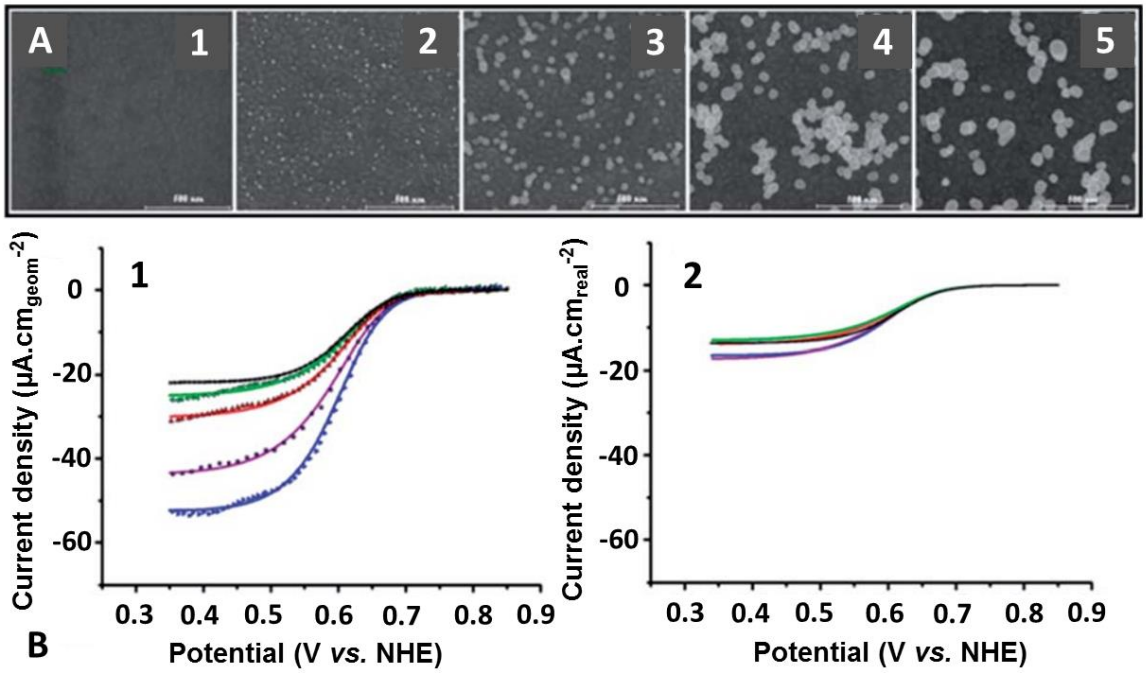

Figure 26. AuNPs: (A) SEM images of bare electrode (1) and electrode modified with 20 (2), 40 (3), 60 (4) and 80nm (5) AuNPs. (B) Experimental (points) *vs.* modelled (lines) voltamogramms of electrodes modified with *Mv*-BOD in O_2 saturated buffer. In 1 currents are reported to the geometric area and in 2 they are reported to the real area. Black: bare gold; Green: 20 nm AuNPs; Red: 40 nm; Purple: 60 nm and Blue 80 nm. Adapted with permission from [386]. Copyright 2014 The Royal Society of Chemistry

$k_{cat,\ app}$ and k_{ET}, resp 15.0 ± 1.5s^{-1} and 10.4 ± 0.4s^{-1}, were also not influenced by the AuNPs size. These results demonstrated that kinetic constants were not influenced by the addition of AuNPs nor by their size. The increase in DET on AuNPs was in general more likely due to an increase in electroactive surface than to an accelerated heterogeneous electron transfer or biocatalytic rate. However, as the authors stated it, these conclusions are not necessarily true for all enzymes and for particles smaller than enzymes. Recently, Bilewicz's group designed a fructose/O_2 EBFC with *Cerrena unicolor* laccase immobilized on macroporous reticulated vitreous carbon (RVC) covered with a gold thin layer and decorated with very small AuNPs (~1.8 nm) at the cathode.[420] The maximal current density, calculated with the BET surface of bare RVC, was 301 ± 26 µA.cm^{-2}, *i.e.* approx. 1.5 times more than

when bigger AuNPs (14 nm) were used instead. It is nevertheless hard to conclude on the effect of the size of AuNPs, since the calculation does not take into account the developed surface of AuNPs.

4.1.3.2 Increasing the current density by enlarging the electroactive surface

We list in this section some examples of increase in current density attributed to a greater electroactive surface area. A ~70-fold increase in surface area with AuNPs (Ø ≈ 50 nm) provided currents of 5.2 $mA.cm^{-2}$ with *Mv*-BOD at 4000 rpm.[390] Catalytic O_2 reduction with *Th*-laccase on 5-nm AuNPs reached 1.3 $mA.cm^{-2}$ at ~200 mV *vs.* Ag/AgCl,[393] and 0.6 $mA.cm^{-2}$ on gold nanorods at the same voltage.[394] *Mv*-BOD directly adsorbed on AuNPs (Ø ≈ 20 nm) on a gold disk gave 110 $\mu A.cm^{-2}$ (= 2.2 µA) in an air-saturated quiescent solution.[385] When the 3D structure was built with 17-nm AuNPs on a gold wire (3 mm in length, 100 µm in diameter), the ESSA increased around 100 times and *Mv*-BOD O_2 reduction reached 1.5 $mA.cm^{-2}$ in an O_2-saturated buffer at pH 7.[391,421-423] For a surface ratio of AuNPs (22 ± 3 nm) to planar electrode of 40, *Mv*-BOD adsorbed on carboxylate-bearing SAMs gave 0.4 $mA.cm^{-2}$.[392] In all the above mentioned studies, ESSA increases more than the current densities, which means that the surface is not entirely exploited.

4.1.3.3 Hierarchical porosity

To obtain a hierarchical porosity, besides mixing AuNPs with other nanomaterials,[424] different structures have been developed. A nano/microstructured porous silicon was covered with a gold thin layer, further chemically modified for covalent binding of *Trametes* sp. laccase. The structure presented micrometer-size channels (≈ 1-2 µm in diameter) and an

additional nano-morphology (50-300 nm). However, DET was limited and currents of 70 µA.cm^{-2} were only obtained in MET configuration.[399] In another study, *Mv*-BOD[236] and *Th*-laccase[186] were adsorbed in nano-porous gold electrodes of roughness factor 26. Currents of 0.3 mA.cm^{-2} and 2 µA.cm^{-2} were obtained with BOD and laccase respectively, which further increased to 0.8 mA.cm^{-2} and 28 µA.cm^{-2} when the enzymes were covered with an epoxy polymer. For both enzymes the current was nil on planar gold. Currents increased even further with addition of an Os polymer, proving that not all enzymes were in DET configuration.[186] Another article reports the use of porous gold consisting of large micropores connected with nanopores, with a wide pore size distribution (10 nm-30 µm), at both electrodes of a glucose/O_2 EBFC. P_{max} was 6 µW.cm^{-2} at E_{cell} = 0.2 V, but no details were given on the electrochemistry of the cathode.[400] *Tv*-laccase was also covalently bond in an orientation favoring DET in a 3D macroporous sponge-like network based on gold "supraspheres", themselves made of 20-nm AuNPs. The current density reached 0.61 mA.cm^{-2} compared to 0.13 mA.cm^{-2} on a planar electrode, while the ESSA was multiplied by 45 (Fig 27).[401]

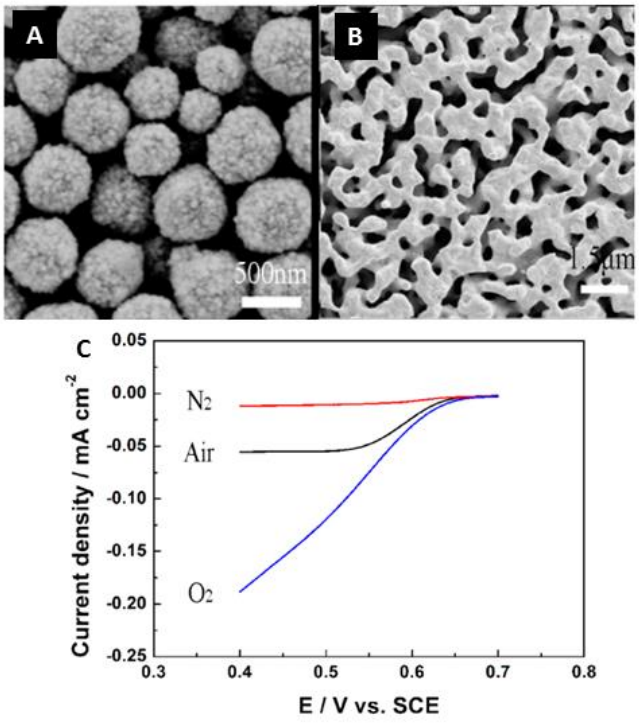

Figure 27. (A) SEM images of the building blocks, gold supraspheres. (B) top view of the resulting porous gold surface. (C) Polarization curves of the biocathode for O_2 reduction in 50 mM acetate buffer pH 5.5 under saturated N_2, ambient air and saturated O_2 conditions. Scan rate 1 $mV.s^{-1}$. Adapted with permission from [401]. Copyright 2014 American Chemical Society.

Mv-BOD was also adsorbed on nanostructured gold electrodes obtained by nanoimprint lithography, presenting cavities of 300 nm in lateral dimension and 100-200 nm in depth. Currents reached 186 $\mu A.cm^{-2}$ compared to 48 $\mu A.cm^{-2}$ at the planar electrode, and the increase was attributed to surface increase, the electrode roughness being multiplied from 1.06 to 1.7.[425]

Recently a more rational approach of the effect of the pore size has been proposed. *Mv*-BOD was adsorbed under vacuum in nanostructured gold, consisting in a 3D network of channels with evenly distributed pores, and obtained by de-alloying Ag/Au alloys.[398,426] The maximal currents of 65 $\mu A.cm^{-2}$ were obtained with pores of 8 ± 2 nm (*i.e* close the enzyme size), while increasing the pore size to 24, 42 and 62 nm decreased the current densities.[398]

4.1.3.4 Mass transport issues and stabilization in pores

In some cases, O_2 mass transport limitation was also reported and clearly evidenced by the shape of the cyclic voltammogram (a peak shape characteristic of diffusion-limitation was observed in some cases), or by using a rotating electrode.[385,390] In other cases, even with elevated current densities, this limitation was absent.[399] This can be related to the size of the channels of the porous network: nanometer-sized in the case of mass transport limitation and micrometer in its absence, but other parameters like the length of the diffusing distance for the substrate, could also intervene. A stabilization effect has also been noticed. The stability was

enhanced compared to a flat gold electrode and attributed to the confinement of enzymes or their retention in the mesopores.[390,426,427] The confinement could not only prevent their leaching but reduce their flattening at the electrode surface, thus reducing the activity loss.[425] Some of the gold nanostructures described above have been implemented successfully in EBFCs.[385,388,390-392,400,421,426] This point is detailed later in section 6.

4.1.4 Tailored orientation of MCOs at the electrode interface

We have already discussed that increasing the amount of immobilized enzymes allowed reaching higher catalytic currents. However, the magnitude of these latter was still limited, and most of the time not all immobilized enzymes could take part in the catalysis. Another requirement is therefore to ameliorate the enzyme electronic connection.

Whatever the material of the electrode, there is a huge interest in controlling and optimizing the heterogeneous electron transfer at the enzyme/electrode interface. The major parameter involved, the distance between the active site of the enzyme and the electrode surface, has to be minimized. A first possibility, previously developed, is to use nanomaterials with adequate porosity/dimensions, while random orientation is allowed. However, the limitations encountered in terms of current densities and percentage of favorable connection underline that this approach is rarely completely successful. On the other hand, particularly when the dimensions of the electrode surface structure are big compared to the enzyme, this distance mainly depends on the relative orientation of the protein towards the electrode surface. Enormous efforts have been accomplished to understand the parameters that drive this orientation, and to engineer adequately the chemistry of the electrode surface to obtain the desired positioning of the enzyme molecule, both on planar and on structured electrodes. It is easy to understand that rationalization and improvement of the orientation necessitate a

precise knowledge of the enzyme structure. Both the positioning of the active site in the protein molecule, and the chemical properties of the enzyme surface are important parameters. Several examples showed that different enzymes, even originated from the same class and sharing very close amino-acid sequences, did not display the same behavior with respect to their orientation at a given interface. Most chemical modifications intend to approach the T1 Cu closer to the electrode surface, although there is still some controversy about which Cu atom is the electron entry point during bioelectrocatalysis (see above). In the following we classify the different developed strategies according to the nature of the main interaction involved: hydrophobic interactions, supramolecular arrangement, electrostatic interactions, and covalent bonding.

Surfaces can be chemically functionalized via different methodologies. To quote only a few used here, monolayers can be formed by chemisorption of thiols (SAMs) on gold or reduction of diazonium salts on carbon, gold or platinum.[216,249,348,428] This theoretically allows grafting of any desired chemical function. The reduction of diazonium salts is supposed to be more stable than SAMs that can be easily oxidatively or reductively desorbed, but can lead to more than one monolayer.[429] It can then possibly increase the distance between enzyme and the conductive surface, or even lead to the formation of insulating layers. Oxygen groups can be created by oxidative chemical or plasma treatments[430] or by UV/ozone treatment.[431] A fast and easy way to functionalize CNTs is to use the non-covalent π-π interactions with aromatic molecules, which is stronger than simple electrostatic interactions or physical adsorption but conserves electronic properties of CNTs contrary to covalent grafting.[325,337,432-436] This even allowed wrapping CNTs in DNA, enabled by the presence of π-electrons in stacked base pairs of DNA.[437]

To evaluate the efficiency of the adopted strategy towards enzymes orientation, it is possible to evaluate the increase in DET, which however reflects also the increase in enzyme

loadings. The comparison DET/MET, that is a reciprocal function of the amount of properly oriented enzymes, is therefore more rigorous. Kinetic models that extract information from voltammograms give useful and precise information. Several models have been developed by Tsujimura *et al.*[235], Léger *et al.*[148], Hexter *et al.*[239] The first one, already described in section 3.4.7, assumes that all electrocatalytically active enzymes have the same orientation. Therefore, heterogeneous electron transfer can be described by a unique average rate constant, k^0.[235] In the second model, it is assumed that enzymes adopt a distribution of slightly different orientations.[148,238,239] The distance between the electrode surface and the enzyme redox center is evenly distributed between a minimal distance d_{min}, and a distance $d_{min}+d_0$. The product βd_0 reflects the scattering of orientations (β is the decay constant in the Marcus theory), and determines the wave shape at high driving force where the slope of i *vs.* E is given by:

$$\frac{di}{dE} = \frac{i_{lim}}{\beta d_0} * \frac{F}{2RT} \qquad Eq.22$$

4.1.4.1 Laccases immobilized by supramolecular/hydrophobic interactions

This approach is quite simple and cheap since the enzyme is directly adsorbed on the chemically modified electrode. The idea to orientate the laccase via a "lock and key" or "plug-in-the socket" interaction with a substrate-like function at the electrode surface was first introduced by the group of Armstrong.[438] They considered that the T1 Cu in the structure of *Tv*-laccase (PDB ID 1KYA) was surrounded by a hydrophobic and electron-rich region, the "substrate-binding pocket", where the oxidation of the substrate takes place. In their first studies, a wide variety of polycyclic aromatic molecules[275,438] was covalently grafted on a "planar" PG electrodes. This led to more uniform and higher enzyme coverage of the electrode, as evidenced by epifluorescence microscopy. Importantly, the wave shape and the

onset of O_2 electro-reduction were not affected by the chemical functions, thus attesting no mediation nor change of the enzymatic mechanism. This result also underlines that the grafted chemical functions do not have to possess redox properties. However, the chemical modification, especially with anthracene and chrysene moieties, proved to be very good both for increasing the current density and improving the stability (Fig 28); leading to up to 4-fold increase in the current density. These results were attributed to the presence of specific hydrophobic and π-electron conductor recognition sites with the right length, angle and rigidity.

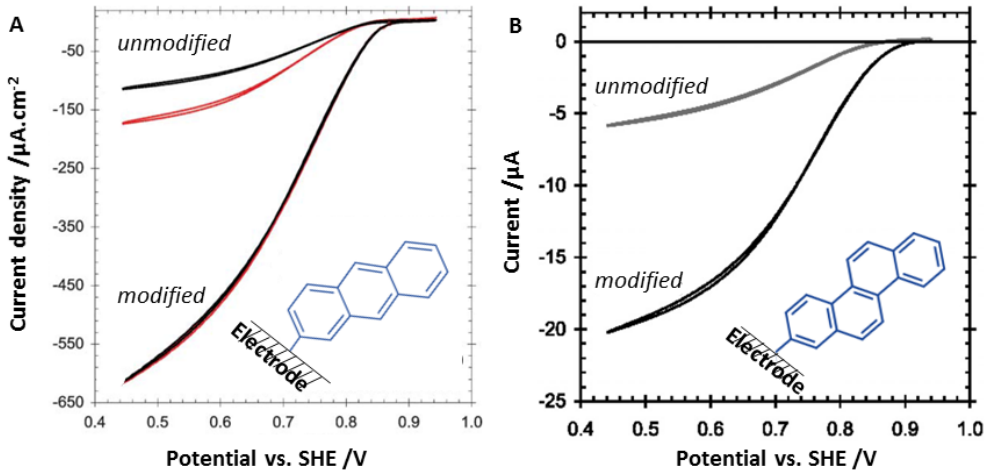

Figure 28. Catalytic cyclic voltammogramms of a laccase at a modified or unmodified PG electrode. Inserts show the grafted surface groups. (A) *Pc*-laccase at an electrode modified with anthracene groups. The black curves are the catalytic waves immediately after spotting on laccase solution and the red curves are the catalytic wave after cell solution was changed for fresh buffer. (B) *Tv*-laccase at an electrode modified with chrysene groups. Adapted with permission from [438] and [275]. Copyright 2007 and 2008, Royal Society of Chemistry.

In the following, most studies were performed with laccases from *Pycnoporus cinnabarinus*,[275,438] *Trametes versicolor*,[275,435,439,440] *Trametes hirsuta*,[438], *Cerrena unicolor*,[441,442] but also with other enzymes with considerably different structure like the low-potential laccase from *Streptomyces coelicolor*.[443]

The use of very smooth planar surfaces like monolayers obtained by protecting the electrode during the electrochemical grafting on polished glassy carbon electrodes[444] or closely packed SAMs on gold surface, [445,446] raised the question whether a good orientation is only due to chemical modification or also to the roughness of the electrode. Very low DET was observed in these cases, although the electrode surface was decorated with anthracene or anthraquinone moieties. This result was explained by the fact that on a smooth surface, or on a well-organized monolayer, the chemical functions are less accessible. On the contrary, when a mixed (antracene-methanethiol/ethanethiol) SAM was formed on an electrochemically roughened gold surface, the grafted moieties became accessible to the laccase and the current doubled.[445] A direct proof that isolated accessible molecules are needed for an Efficient immobilization of laccase via supramolecular interaction was given by a SECM study of mixed SAMs on monocrystalline gold (111).[446] Mixed thiolated veratric acid (tVA) / mercaptopropionic acid (MPA) SAMs were built with different water contents, leading either to separated pure tVA or MPA phases or to a unique well-mixed phase. In the case of the pure phase, neighboring tVA moieties were closely interacting, thus forming clusters bigger than the enzyme hydrophobic substrate-binding pocket. This was directly linked to quasi-inexistent DET for adsorbed *Tv*-laccase on this SAM. On the contrary, tVA molecules were widely separated by MPA molecules in the well-mixed phase. Adsorbed *Tv*-laccase exhibited in this case a clear cathodic wave with j = 0.58 µA.cm^{-2} at 0.4 V *vs.* Ag/AgCl.[446]

This approach was further extended to different electrode materials and nanostructured architectures: carbon cloth,[275] carbon nanotubes covalently modified with anthracene, anthraquinone, naphthalene or related compounds at their ends or walls,[424,439,441,442,447-450] CNTs covalently modified with bisphenyl groups,[451] or CNTs non-covalently modified with pyrene molecules bearing the desired chemical functions.[440,452] Even on nanostructures, a considerable increase in catalytic currents was observed.

A major problem with CNTs is that the terminal « substrate-like » moieties are rich in aromatic electrons and can also bind to CNTs by π-stacking, thus reducing the amount of available anchoring groups for the attachment of the enzyme. Better availability of anchoring groups at the electrode surface can be induced by bi-functionality where at least one functional linker is not bound to CNT walls due to steric hindrance,[436,452] as it has been done with pyrene-bis anthraquinone,[452] pyrene-bis naphtoquinone,[436] or by functionalization of graphene oxide further immobilized by π-π interactions on MW-CNTs.[348] Another possibility is to use another hydrophobic moiety unable of π-stacking like adamantane.[433] Interestingly, although the binding energy of anthraquinone (evaluated by theoretical calculations) is almost twice higher than that of adamantane, catalytic currents for the reduction of O_2 were much higher with adamantane, reaching 2.2 $mA.cm^{-2}$. This result, combined with QCM-D experiments showed that more enzyme was immobilized, supporting the idea that more groups were accessible and allowed for enzyme binding and orientation.

The hydrophobic interactions between electrode and substrate-binding pocket was also exploited for SW-CNTs modified with a steroid biosurfactant bearing a large, rigid and planar hydrophobic moiety.[453,454] This allowed very fast heterogeneous electron transfer rates between T1 Cu site and SW-CNTs (3000 s^{-1}). Hydrophobic polymers were also able to act as a conductive wire approached to the T1 via π-π stacking.[455,456]

However, a possible limitation of this approach is the lack of specificity of the hydrophobic interaction, since several hydrophobic regions co-exist at the surface of the enzyme, and not only close to the T1. This was evidenced in several cases by different experimental observations. Either a trailing edge was observed in the cyclic voltammograms[275] or currents were consistently enhanced upon addition of a soluble mediator, whatever the surface modification,[444] consistent with the assumption that a unique molecule orientation was probably not achieved. In addition, the immobilization of *Tv*- and

Sc-laccases on SW-CNT modified with the molecular tether PBSE was investigated *via* molecular dynamic. SW-CNTs (2.71 nm in diameter) were positioned near the hydrophobic substrate binding pocket of the laccases (position 1) and close to 2 other regions where adsorption was also likely (positions 2 and 3). In case of *Tv*-laccase, T1 Cu was situated resp. at 0.5, 2.1 and 3.0 nm from the surface in the considered positions 1, 2 and 3. Calculations demonstrated that adsorption was favored in region 1 over region 2 by 20-40 kcal.mol^{-1}, but by only 11-15 kcal.mol^{-1} in region 1 over region 3. For *Sc*-laccase, the distance between T1 Cu and the protein surface was resp. 0.7, 3.5 and 1.6 nm in the regions 1, 2 and 3. No preferential adsorption was shown between regions 1 and 3. This modeling study is a further indication that several positions of the enzyme at the electrode surface have approximately the same probability.[457]

4.1.4.2 Electrostatic interactions

4.1.4.2.1 Laccases

Although in most studies laccase orientation has been performed via the supramolecular orientation strategy, another approach relies on electrostatic interaction. This approach was proposed for *Cerrena unicolor* laccase (pI = 3.95) immobilized on CNPs[364] or SW-CNTs[458] bearing sulfonate functionalities in a silicate sol-gel matrix. This surface chemistry induced better reproducibility and at least twice higher currents. However, the increased performances observed in this case are more likely favored by the hydrophilicity of the structured matrix, rather than due to better orientation on negative charges, since for the same laccase a better orientation on positive charges was confirmed by PM-IRRAS studies.[428] Electrostatic interactions could also drive an enhanced immobilization for an engineered enzyme, as demonstrated with an unusual homo-trimeric laccase bearing a His-

affinity tag at the C-ter close to the T1.[459] In contrast, QCM studies performed with different laccases showed that the nature of the charges did not influence the enzyme coverage.[428,459]

Studies performed with various laccases highlighted that electrode surface chemistry has to be customized according to the specific structure of each enzyme. Ulstrup *et al.* compared the influence of electrode surface charge for 3 different laccases: *Coprineus cinereus* (*Cc*-laccase), *Streptomyces coelicolor* (*Sc*-laccase), *Myceliophtora thermophila* (*Mt*-laccase), and *Mv*-BOD.[233] The differences in electrocatalytic behavior were notable, and could be easily correlated with the residues surrounding the T1 Cu atom. *Mv*-BOD and *Cc*-laccase, who share a positive charge area around the T1 center, displayed the highest activity on carboxylate-terminated SAMs. On the contrary, *Sc*-laccase showed the best activity on alkyl-terminated thiols, consistently with a hydrophobic pocket around the T1 Cu. *Mt*-laccase, the only one bearing a negative patch around the active site, was also the only one not to display a catalytic current.[233]

4.1.4.2.2 Bilirubin oxidases

A considerably different behavior between most laccases and *Mv*-BOD was observed: contrary to laccases, adsorbing *Mv*-BOD on molecules with a single aromatic ring or presenting a hydrophobic end lowered catalytic currents.[17,233] When a complete structure of *Mv*-BOD was obtained,[129] this could be explained by the presence of a narrow hydrophilic substrate binding site close to T1, with basic amino acid residues positively charged at acidic and neutral pH. The differences in terms of amino-acid sequence between bacterial BODs and fungal BODs also resulted in different behaviors.[434]

Due to the difficulty to rationalize how DET with *Mv*-BOD could be obtained on carbon surfaces, which generally bear lots of functionalities and have a porous structure,[460] studies were performed on well-ordered and atomically flat single gold crystal [151] and then

extended to carbon or more complex architectures: KB,[461] GO, ECR-sputtered CNFs[431] and CNTs.[152,216,338,437,462,463] Here also DET was proved because the catalysis started at a potential that could be attributed to the T1 whatever the chemical functions at the electrode surface,[151] even when the surface was modified with redox active groups.[152,338,458] Studies globally showed the importance of the electrode charges,[151,437,463] catalytic currents being low for positive charges, and higher for negative charges (most studies were performed at neutral or near-neutral pH). This proved that amino-acids near the T1 are more important than the global charge of the BOD whose isoelectric point is 4.1. Especially the adequacy of carboxylic functions[17,151,220,432] has been highlighted. On carbon presenting carboxylate functions on aromatic protrusion,[17] kinetic analysis[148] evidenced that the enzyme adopted a narrow cone of orientations. This can be partly attributed to an increase of hydrophilicity, or a better wettability of the electrode[431,437,462] rather than to enhanced enzyme loadings. As a matter of fact, similar enzyme loadings have been calculated for different electrode surface charges.[216]

However, the interactions favoring a functional immobilization could be more complex than simply electrostatic. Indeed, some studies have suggested that for optimal immobilization of *Mv*-BOD, the anchoring molecules need to possess both aromatic properties and negative charges.[432,461] This is consistent with previous studies where *Mv*-BOD adsorbed on MW-CNTs modified with different compounds, all bearing carboxylic functions, showed no special difference with unmodified CNTs, except when the compound was Pyrroloquinoline quinone (PQQ). For this latter the catalytic currents almost doubled.[152,319,338] Consistently also, *Mv*-BOD was perfectly oriented on MW-CNTs bearing carboxy-naphthalene moieties. DET currents reached 4 ± 0.4 mA.cm^{-2} in a stirred oxygenated solution, and no increase was observed upon ABTS addition.[216] On the contrary, when *Mv*-BOD was immobilized on CNTs bearing positively charged amino groups, O_2 reduction was observed at much lower potential (E_{HW} = 0.19 V *vs.* Ag/AgCl at pH 7). This was attributed to DET to the

TNC.[216] In that case, addition of ABTS led to high MET currents (≈ 2.5 mA.cm^{-2}). This is also consistent with DET at T1 requiring negative surface charges at the electrode.

Quite contradictory results were however recorded, with *Mv*-BOD showing a better orientation than *Tv*-laccase on anthracene-modified MW-CNTs. Upon addition of ABTS only 11% increase in current densities were observed, while 59% increase was recorded for *Tv*-laccase.[266,267,464,465]

Mv-BOD immobilized on PG modified with naphthyl-2-carboxylate moieties was compared with platinum. The limiting current density, j_{lim}, was 10 mA.cm^{-2} for the platinized PG electrode, with an estimated platinum concentration of 2150 pmol.cm^{-2}. For *Mv*-BOD, j_{lim} was 0.7 mA.cm^{-2}, which represents a much better efficiency since the enzyme concentration was supposed to be lower than 10 pmol.cm^{-2}. In addition, the reaction overpotential for oxygen reduction was much smaller at the *Mv*-BOD naphthyl-2-carboxylate modified PG electrode than at Pt under all experimental conditions.[17]

Although electrostatic interactions have enabled Efficient immobilization of different MCOs, the specificity of the electrode modification towards immobilization of each particular enzyme is of crucial importance. A few examples underline it. The presence of COO^- on the electrode surface did not improve the bioelectrocatalytic activity for a CueO, whose T1 is surrounded by acidic residues, while an improvement was recorded with positively charged modification.[461] Two different BODs, the bacterial *Bp*-and the fungal *Mv*-BODs, sharing only 36% sequence homology had also very different behaviors on CNTs with different surface charges.[434] The comparison of DET/MET currents, and modeling with Armstrong's model,[148,239] showed that *Mv*- was correctly oriented on negative surfaces (as already demonstrated), while *Bp*- was much better on positive. This result was consistent with their respective positive and negative charges surrounding the T1 in the considered pH range. This

difference was also observed for naphtoate-CNTs, which were favorable for *Mv*-BOD but detrimental for *Bp*-BOD.[466]

4.1.4.3 Orientation of bilirubin oxidase with substrates

The supramolecular arrangement involved in orientation of BOD with its substrate is also consistent with the fact that both aromatic and negative functions are needed.[129,461] The onset of catalysis did not change[467] but currents increased when *Mv*-BOD was adsorbed on PG electrode or MW-CNTs modified with bilirubin.[129,468,469] A shift in half wave potential towards more oxidizing potentials was ascribed to a better control of the orientation when BOD was adsorbed on Ketjen black modified with bilirubin or other bilirubin related compounds.[470] Both the coverage of electrochemically active enzyme (λΓ) and standard surface electron-transfer rate constant (k°, determined according to Tsujimura's model) increased with bilirubin.[470] This latter induces rearrangements in the binding pocket that favor the interaction of BOD with the electrode, as was recently demonstrated by molecular docking and DFT.[471]

The idea of binding the BOD through its substrate was extended to other compounds; syringaldazine on CNTs,[472] or CNTs with different porphyrins (by considering that bilirubin is a decomposition product of protoporphyrin IX),[432] leading to current densities up to 4.66 $mA.cm^{-2}$. This furthermore showed that the aromatic moiety (here the porphyrin skeleton) influences the enzyme coverage, while carboxylate groups help orientating the proteins.

4.1.4.4 Covalent attachment

Covalent binding has also been introduced to force the desired MCO orientation by attaching a specific part of the enzyme, mostly a determined amino-acid residue or a

carbohydrate of the glycosylation shell, at the electrode surface. Linking is ideally performed at a site that does not affect the catalytic activity of the immobilized enzyme, and is also enhanced when the enzyme is linked via several points[307] due to a more constraint orientation. It is of course necessary to identify the appropriate site. In a first approach, this was often done by trial and errors rather than by extensive modelling analysis. Even if a good position is identified, this does not guarantee the success of the immobilization.

Different chemistries for the covalent binding have been compared in terms of DET/MET ratios for *Th*-laccase on planar gold[249], gold nanoparticles[393], gold nanorods[394] or on a composite of carbon microfibers and carbon nanotubes (CNT/CMF).[333] The Schiff's base or imino-bond formation involving glycosylated residues close to the T1 binding pocket led consistently to a preferential orientation, contrary to amide bond formations involving carboxylic functions located at the opposite of T1.[222,249,333,394,473-475] Therefore, chemical modification can be used to tune the electrode surface for the enzyme: for example, amino aryl functions were introduced on graphene for amide bonding with oxidated sugar residues of *Th*-laccase, and naphtoic acid was grafted to enable amide bond formation with Lys residues of *Mv*-BOD.[237] An Efficient DET cannot however always be attributed to optimal orientation, as shown by the covalent anchoring of *Mv*-BOD on a CNT/CMF material. The best results were obtained when a lysine of the enzyme was linked to the CNTs via a phenylbutanoic acid or glutaraldehyde spacer, *i.e.* a very long chain (23 atoms in the case of glutaraldehyde).[314] An explanation is that the flexibility of the long chain allowed repositioning of the enzyme at the CNT surface for an Efficient electron transfer.[314]

Covalent binding often leads to random immobilization because the involved residues are in most cases distributed over the protein surface. For example, *C. gallica* laccase bears 7 reactive lysines that can be involved in a covalent bond, but none of them is situated close to T1.[476] In case of laccase covalently bond on NHS-SAMs, DET was evidenced but no

electrocatalytic activity was recorded, suggesting that the copper ion undergoing electron transfer was not the primary electron acceptor in electrocatalysis.[207] In another case, addition of ABTS improved the current density by respectively 20% (laccase) and 24% (BOD) indicating that not all molecules were correctly oriented for DET.[237] In case of *Mv*-BOD, reactive dye labelling was performed to identify lysine involved in covalent attachment: all of these groups would position the metal center at least 2 nm from a planar electrode surface.[229]

4.1.4.5 Engineered enzymes

To be even more specific, the orientation of MCOs could be driven via supramolecular chemistry as described above, and followed by covalent binding for example via carbodiimide chemistry.[337,476] But another solution was to artificially introduce amino acids at a desired location via site-directed mutagenesis. This approach exploited the well-known ternary metal-chelate complex formed between His-tagged proteins and nitrilo-triacetic acid, which is easily grafted on a planar electrode.[477] With His-tagged laccases,[478,479] although the specific binding of the protein was proved, this approach did not allow a DET probably because of a too long distance between T1 and electrode, even in case of a proper orientation. But importantly the activity towards mediators in solution was not affected neither by the tag nor by the immobilization. With a His-Cys tag at the N- or C-terminus, a laccase from *Trametes sp.* could also be directly attached to a gold surface. A DET communication could be established with the electrode, but the quite low onset potential was attributed to either the TNC alone, or a mixed T1-TNC signal, and the incomplete O_2 reduction to H_2O_2 was recorded.[209] An unnatural amino acid, 4-azido-L-phenylalanine, was also genetically introduced at different positions of *Sc*-laccase to enable specific attachment at the electrode surface via click-chemistry. Surprisingly however, the best results in terms of O_2 reduction were obtained with positions that were supposed to keep the Cu sites away from the electrode surface.[480] More

recently, a recombinant laccase from *Trametes sp.* was engineered to present a unique surface lysine residue close to the T1 copper atom.[481] A pyrene was grafted at this lysine enabling immobilization on β-cyclodextrine decorated AuNPs (3 nm) on MW-CNTs. O_2 reduction currents reached 2.75 mA.cm^{-2}, and this ten-fold increase compared to random adsorption was attributed both to a better coverage, and to an excellent DET proved by a pure Nernstian behavior (Fig 29).

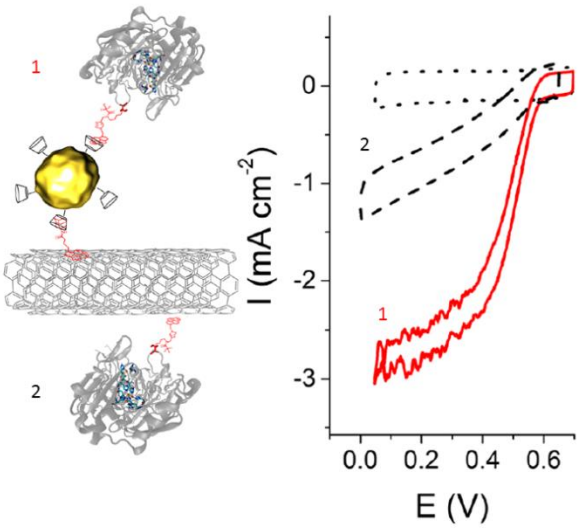

Figure 29. Site-specific pyrene modified laccase immobilized either at β–cyclodextrin-AuNPs/MW-CNTs (1) or directly via π-π stacking of the pyrene on MW-CNTs (2) and the corresponding cyclic voltammogramms under O_2. Reproduced with permission from [481]. Copyright 2016 American Chemical Society.

4.1.4.6 Other strategies

Some more anecdotic studies rely on oriented immobilization of the MCO under the influence of an external magnetic field.[482,483] *Tv*-laccase was immobilized on a GC electrode modified with nanomagnets, made of carbon nanocapsules (Ø ≈ 30-70 nm) with an iron core. O_2 reduction currents were doubled under application of an external magnetic field $\vec{B}$,[482,483] reaching 5 mA.cm^{-2} when PPY and GA were added.[483] $\vec{B}$ was supposed to influence on the

migration of paramagnetic O_2, but also on the enzyme orientation via attraction of the paramagnetic T1 Cu(II).

A very recent study proposed MCO orientation assisted by organic solvents.[484] *Tv*-laccase was mixed with SW-CNTs in the presence or absence of 20% organic solvent. Results were particularly detailed in case of ethanol. When the mixtures were immobilized on an electrode surface, currents were increased by 70% in presence of ethanol compared to controls made in absence of ethanol, leading to 711 $\mu A.cm^{-2}$ at 0.4 V *vs*. Ag/AgCl at pH 6 and 500 rpm. The enzyme structure was studied by circular dichroism (CD) and attenuated total reflectance infrared (ATR-IR) spectroscopy in presence of CNTs and ethanol, either in solution or dried at the electrode surface. Surprisingly, no drastic influence of ethanol on enzyme denaturation/unfolding was observed. An orientation change was recorded instead, with β sheets of the enzyme aligned perpendicularly to CNT sidewalls, indicating that the substrate binding pocket was facing the sidewalls.[484]

4.1.5 Stability issues

Bioelectrochemical devices, either single electrodes, complete EBFCs or various biosensors, generally share a relatively poor operational stability. Enzymes in solution are typically active for a few hours to a few days[485], and most enzymatic systems are rarely stable for more than few hours under continuous operations.[27] However, it is important to be aware that the stability is not only an inherent property of the device, but that numerous other parameters such as the experimental conditions, the method to evaluate the stability or the storage conditions have a huge influence on it. The problems encountered in assessing, and therefore comparing, the stability of various devices are comparable to those encountered for the normalization of current, since in both cases there is no specific guidelines or established protocol.

An interesting study published by Minteer and coworkers underlined for example the impact of the measurement method. They compared galvanostatic and potentiostatic measurements, and different experimental conditions for both techniques.[486] For a laccase from *Trametes* sp. immobilized on anthracene-modified MW-CNTs, at pH 4.5, 25°C and in atmospheric conditions, galvanostatic measurement (at 30% of the electrode maximal current) led to a 3% decrease over 24 hours, while 15% were lost in potentiostatic measurement (at ≈ 0.44 V *vs*. Ag/AgCl, *i.e*. 200 mV more negative that the onset potential) (Fig 30). Stability in potentiostatic conditions also decreased with increasing overvoltage, 21 ± 6% being lost after 24 hours at ≈ 0.54 V *vs*. Ag/AgCl, and 42 ± 12 % at ≈ 0.24 V *vs*. Ag/AgCl. In galvanostatic conditions, the stability also decreased with increasing applied currents, only 3.0 ± 0.9% being lost after 24 hours at 10% of the electrode limiting current, and 100% at 90% of the limiting current.[486]

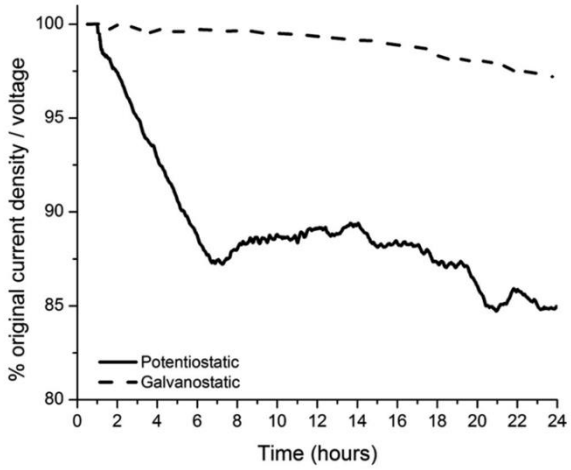

Figure 30. Comparison of operational stability of the anthracene-MW-CNTs/laccase cathode in potentiostatic (solid line) and galvanostatic (dashed line) mode. Potentiostatic: cathode was poised at 0.4 V vs. SCE in 50 mM citrate buffer, pH 4.5 at 25°C for 24 h in atmospheric conditions and the current was measured as a function of time. Galvanostatic: Under the same conditions, 30% of the individual electrode current was passed through the electrode for 24 h, and the voltage measured as a function of time. Reproduced with permission from [486]. Copyright 2014. The Electrochemical Society.

Many mechanisms could account for the relative instability of an enzymatic electrode: lack of intrinsic stability of the enzyme itself;[27] denaturation, change of conformation or configuration, reorientation, and chemical inactivation upon immobilization;[27,229,320] or just enzyme leaching from the electrode surface due to a weak enzyme/electrode interaction. Electrochemistry by itself does not permit to link the catalytic stability with the structure/conformation of proteins, so combined approaches have been put forward. Efforts to elucidate the nature of the damage on gold electrodes involved the coupling of electrochemistry to other analytical techniques (QCM, PM-IRRAS, ellipsometry, AFM, SPR: see section 3.4). The problem is more complex with carbon electrodes due to the lack of Efficient analytical tools. Therefore, it is still unclear which factor is mainly responsible for instability.

In this context, different techniques have been envisioned to improve the stability of enzymatic electrodes. Most are directed towards retaining the enzyme molecule at the electrode surface, or ensuring a stabilizing environment for the enzyme at the electrode.

4.1.5.1 Reducing damaging surface-interactions with a promoter

Promoters used to favor enzyme orientation have also shown to stabilize the electroenzymatical O_2 reduction current. When *Pycnoporus cinnabarinus* laccase was adsorbed on a 2-anthracene modified PG electrode, 57% of the initial current was retained after 8 weeks. On the contrary, on an unmodified electrode, more than 95% were lost after 4 weeks. The stability was measured by daily cycling in O_2-saturated solution.[438] The stability of *Tv*-laccase on carbon cloth modified by reduction of anthracene-2-diazonium (A2D) was measured continually over 2000 hours. Without A2D the current dropped from 75 to 10 $\mu A.cm^{-2}$ in 72 hours; with A2D a rapid decrease was observed, followed by a stabilization at 75% of the initial current density (50 $\mu A.cm^{-2}$).[275] An electrode modified with *Th*-laccase

coated on monolayers of anthracene or anthraquinone exhibited still half of the initial current after 30 days of storage in the buffer. However, no comparison was reported with the promoter-free electrode.[444] For *Tv*-laccase adsorbed on CNTs bearing bis-anthraquinone moieties, 48% of the initial signal were retained after 20 days with one hour discharge every day, while all the current was lost for the same experiment without the promoter.[452] Similarly, *Tv*-laccase was more stable when adsorbed at MW-CNTs bearing adamantane moieties than immobilized on pristine MW-CNTs. The stability was evaluated over one month with a daily 1 h discharge at 0.24 V vs. Ag/AgCl. On bare MW-CNTs, currents were below 5% of their initial value after 20 days, while 66% was conserved after one month on adamantane-MW-CNTs.[433]

Similar observations were made when *Mv*-BOD was immobilized at an interface covered with bilirubin or related compounds. Lifetime of the BOD-PG electrode assessed by chronoamperometry or cyclic voltammetry was increased by 50% when the surface was coated with bilirubin.[129] An increase in the stability was also recorded when KB CNPs were modified with bilirubin. With daily measurements, 60% of initial current densities were left after 7 days at bilirubin-coated KB, while only 20% were left after 7 days (or 40% after 3 days) when *Mv*-BOD was adsorbed at bare KB (Fig 31).[470] With phenylcarboxylate-modified KB, 60% of initial current densities were retained after 4 days.[461] In all these cases, the stability increase could be due to a better retention of the enzyme at the electrode surface, or to the promoter reducing conformational change or reorientation.

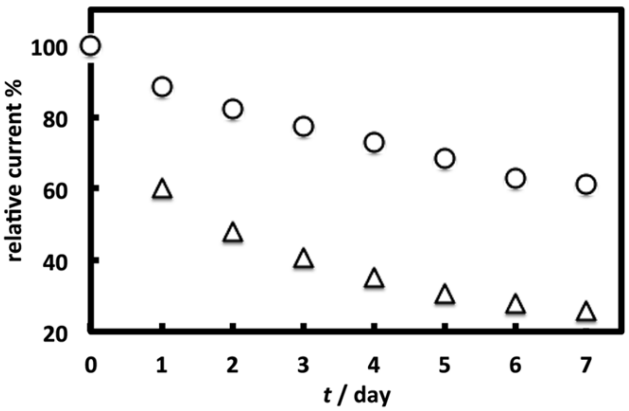

Figure 31. Long-term stability of the BOD adsorbed at a KB-GC electrode modified with bilirubin (circles) and at an unmodified KB-GC electrode (triangles). The activity was measured from the steady-state catalytic current in CA at 0 V vs. Ag/AgCl and 60 s after the potential step in an O_2-saturated phosphate buffer (pH 7) at ω= 4000 rpm. The current is plotted as the relative value. Reproduced with permission from [470]. Copyright 2014. Published by the PCCP Owner Societies

4.1.5.2. Covalent bonding

To prevent enzyme leaching from the electrode, covalent binding has also been envisioned. An electrode based on BOD covalently bound at PQQ-modified MW-CNTs had a half-life of about 20 days compared to ~5 days for a MW-CNT electrode with only adsorbed BOD.[152] For *Th*-laccase covalently bound at PG bearing aminophenol moieties, ≈ 75% of the initial current was retained after 10 days of continuous chronoamperometry at 0.2 V *vs.* Ag/AgCl, with pure O_2 bubbled through the electrolyte solution.[259] Stability of the covalently bound *Th*-laccase at 6-mercapto-1-hexanol modified gold electrode was evaluated by continuous operation at $E_{applied}$ = 200 mV *vs.* Ag/AgCl, at ω = 500 rpm and under O_2. 70% of the initial current was left after 24h. Unfortunately, control experiments were not provided.[249] When the same enzyme was covalently bound on AuNPs on a LDG electrode, 40% of the catalytic current was maintained after 4 days of continuous operation in chronoamperometry.[393] When AuNPs were replaced by gold nanorods, the electrodes were stable during a day and kept their stability during few days of storage at 4 °C. The stability was not tested longer in continuous operation.[394]

4.1.5.3. Encapsulation

It has been reported that the lifetime of an enzyme in solution could be extended to ~ one year[29] when enzymes were included in micellar polymers. Similarly, at electrodes, MCOs

have been embedded in sol-gel matrices, sometimes with conductive nanomaterials.[364,458,463] A composite film formed of tetramethyl orthosilicate sol-gel (TMOS), CNPs and laccase was deposited on an electrode and tested by chronoamperometry at 0.2 V *vs.* Ag/AgCl. The dioxygen reduction current decreased by ca. 60% in the first hour, but only ~17% were lost over the next 30 h.[364] *Mv*-BOD was adsorbed on SW-CNTs modified with pyrene sulfonic acid in a TMOS sol-gel. The current density, measured in air-saturated buffer at 0.2 V *vs.* Ag/AgCl, dropped from ~20 µA.cm^{-2} to ~16 µA.cm^{-2} in the first 12 hours, and was then stable for another 60 hours.[463] This represents an interesting stability, however the influence of the different elements was not tested separately. An increased stability at medium temperatures (37°C) was also recorded when *Mv*-BOD was embedded with CNTs in a TMOS matrix, and attributed to the stabilizing environment of the sol-gel.[487]

Other matrices have also been proposed to stabilize the enzyme. *Mv*-BOD was for example immobilized in a network of naphtylated MW-CNTs and AuNPs in a lipidic cubic phase (monoolein). The stability was evaluated by realizing daily cyclic voltammograms. 70% of the initial current density was left after 9 days, whereas only 10% were retained in the absence of the lipidic cubic phase (Fig 32).[424] *Mv*-BOD in solution was stabilized by polyammonium cations.

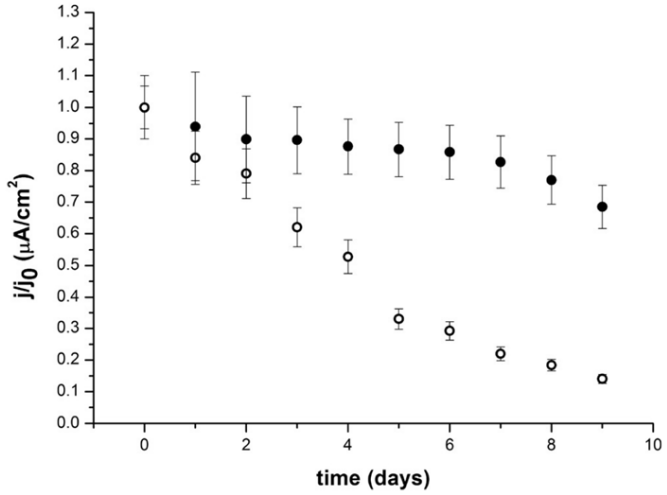

Figure 32. Long-term stability of *Mv*-BOD adsorbed on a composite of naphthalene-MWCNTs and AuNPs on a GC electrode (empty circles) and *Mv*-BOD + AuNPs embedded in the lipidic cubic phase on naphthalene-MWCNTs on a GC electrode (full circles). The activity of the electrode in time is shown as the limiting catalytic current measured at 0.3 V in oxygen-saturated phosphate buffer (pH 7). Reproduced with permission from [424]. Copyright 2017. Wiley-VCH Verlag GmbH & Co. KGaA.

This remained true for the immobilized enzyme, but so far it has indisputably been shown only in MET.[488] A biocathode based on *Tv*-laccase adsorbed at SW-CNTs was coated with a hydrophobic room-temperature ionic liquid.[489] This protected the laccase in a buffer neutral pH and in the presence Cl^-, probably by forming a weakly acidic layer at the electrode surface. In cyclic voltammetry, the signal was stable over 50 cycles.[489] Efficient O_2 reduction by *Mv*-BOD adsorbed on AuNPs (15 nm) has also been reported in non-polar ionic liquids with small quantity of water, however a stabilization effect has not been described.[490]

Nafion® is often used as a binder or as a covering membrane for laccase electrodes. To the best of our knowledge, indisputable evidence of its stabilization effect has however not been reported so far. For example, a laccase physically adsorbed on carbon coal or carbon black and covered by Nafion®[366] was more stable than in solution, retaining 55% activity after one month of storage in buffer. However, the relative influence of Nafion® and nanoparticles has not been deciphered. A *Trametes* laccase was embedded with anthracene-MW-CNTs in different polymer matrixes to compare their influence on stability. Three matrixes were used: Nafion® modified with tetrabutylammonium ions (TBAB Nafion®), hydrophobically modified linear polyethyleneimine presenting surfactant like properties (C8 LPEI), and vapor deposited TMOS sol-gel.[486] We give here the results obtained in potentiostatic mode, since it has been proved to be harsher than galvanostatic mode.[486] The 3 different electrodes, TBAB Nafion®, C8 LPEI and TMOS, respectively lost 4.1 ± 0.4%, 9.6 ± 0.5% and 10 ± 2% of the initial current densities after 24 hours at $E_{applied} \approx 0.44$ V vs.

Ag/AgCl at pH 4.5 and 25 °C in atmospheric conditions. According to this study, Nafion®-TBAB was therefore the most suitable matrix for laccase entrapment.[486] Elsewhere, authors from the same group demonstrated that Nafion® modified with ammonium cations provided a suitable matrix for immobilization of enzymes,[491] which could also explain the results obtained here.

Stabilization was also noticed in some cases when the enzyme was confined in a 3D network and closely surrounded by nanomaterials. A CNTs-enzyme composite induced by liquid shrinkage allowed a laccase to be closely surrounded by CNTs. The so-formed cathode was used in a fructose/O_2 EBFC, which retained 80% of its initial power density after 24 h of continuous operation at an external load of 35.3 kΩ.[341] A one-year stability of an EBFC was also reported with enzymatic electrodes made of compressed enzyme-CNTs pellets. After one year of regular discharges, 22% of the initial power was still recorded.[318] (see section 4.1.2.1)

4.1.5.4 Other strategies

Other strategies have also been proposed to extend the lifetime of a bioelectrochemical device, without necessarily stabilizing the enzyme at the electrode. The lifetime of an enzymatic cathode based on *Tv*-laccase and bucky paper was extended 2.5 fold by resupplying fresh enzyme in the electrolyte.[492] Untreated culture supernatants containing laccase were also used instead of purified enzymes. Here also fresh supernatant was periodically introduced in the catholyte. The potential was stable during 120 days under continuous application of 50 µA.cm^{-2} (i.e. ≈ 40% of the limiting current) while the half-life of the electrode was ≈ 10 days when no fresh enzymes were supplied.[493]

4.2. Mediated electron transfer

Direct electrical communication between MCOs and electrodes has been largely exploited in the recent past, and nowadays 60% of the published papers concern DET-based MCO cathodes, and 40% MET-based electrodes. Although DET efficiency has been greatly enhanced over the last decade, MET still possesses numerous advantages, as described above. An obvious asset of MET, beside its versatility, is that multilayers of enzymes can be simultaneously connected at an electrode surface whatever their orientation. This might be an explanation why between 1982 and 2004, most of the published papers on MCOs for O_2 reduction were based on mediated electron transfer connection. This ability to electronically connect multilayers of enzymes is a precious tool to enhance the current densities. This is the major focus of this section. We will willingly not compare the stabilities obtained for such MCOs electrode (except in some particular cases) because all the necessary information for a fair evaluation are, most of the times, not provided.

MET connection is often optimized on planar rotating or non-rotating electrodes, made of glassy carbon, platinum or gold, and then usually scaled to 3 dimensional electrodes to enhance specific surface and enzyme loading. Diffusive redox mediators are commonly used to probe enzymatic kinetics while immobilized redox mediators are rather used to elaborate devices. For the latter, 80% are osmium based redox polymers, and 20% other redox mediators including conducting polymers, proteins or organic/inorganic compounds. In this section, we will first discuss MET on various types of bare electrodes with diffusive or immobilized redox mediators. In a second time, we will describe the use of 3D materials in MET based cathodes.

4.2.1 Bare electrodes

4.2.1.1 Diffusing redox mediators

Diffusing redox mediator are used to probe electrochemically the kinetics between enzymes and redox mediator,[201,494] to probe the effect of mutations on MCOs[247,488,495] or to

evaluate the potentiality of an enzyme as a bioelectrocatalyst.[496,497] For this purpose, the most common diffusive redox mediator is 2,2'-azinobis(3-ethylbenzothiazolin-6-sulfonate) (ABTS),[216,363,498-502] first introduced in 2001 by Tsujimura *et al.*[122] with *Mv*-BOD. In an air-saturated pH 7.0 buffer containing 0.5 mM $ABTS^{2-}$ and 0.11 μM of enzyme, they could reach 2 mA on a carbon felt electrode. ABTS is also used routinely as a control to verify the efficiency of enzymes connected in DET.[503-507] However, at neutral pH, ABTS has the disadvantage to undergo gradual decomposition[122,494,508] and other redox mediator should be preferred. For example, Cavaco-Pualo *et al.*[509] used 6 redox mediators (ABTS, promazine, hydroquinone, syringaldazine, Ferrocyanide, hydroquinone) with redox potentials ranging from +150 mV to +800 mV *vs.* Ag/AgCl to mediate the reduction of O_2 by a glassy carbon electrode modified with the fungal laccase *T. villosa* in a pH 5 buffer. Leech *et al.* were the first to report the use of an osmium complex, $[Os(2,2'\text{-bipyridine})_2(N\text{-methylimidazole})Cl]^+$, as a diffusing redox mediator for the reduction of O_2 to water.[135] They determined the homogeneous second order rate constant for tyrosinase from *Agaricus bisporus* in a 0.1 M phosphate buffer pH 7.4 (3×10^4 $M^{-1}s^{-1}$) and for laccase from *Trametes versicolor* in a 0.1 M acetate buffer pH 4.7 (3.3×10^6 $M^{-1}s^{-1}$). Other cyano-metal complexes such as $[W(CN)_8]^{3-/4-}$, $[Os(CN)_6]^{3-/4-}$, $[Mo(CN)_8]^{3-/4-}$ and $Ru(bpy)_3^{2+}$ have also been used in this context.[497,510] In presence of 0.25 mM $[W(CN)_8]^{3-/4-}$ in an O_2 saturated pH 7 buffer at 4000 rpm, Tsujimura *et al.* reached 17 $mA.cm^{-2}$ at +0.25 V *vs.* Ag/AgCl with a carbon felt electrode modified with *Mv*-BOD.[511] Later Ikeda *et al.* used $[Fe(CN)_6]^{3-/4-}$ as a redox mediator to study the effect of poly[oxyethylene(dimethylimino)propyl-(dimethylimino)ethylene][495] and of polyammonium cations as enzyme stabilizers for *Mv*-BOD.[488]

From an engineering point of view, the use of diffusive redox mediator is not the "ideal" strategy when designing electrochemical devices. In the case of EBFCs, a membrane separating anodic and cathodic compartments is required to avoid cross over of the redox

mediator. Diffusive redox mediators therefore complexify the system and introduce new limitations, kinetic losses and additional costs.[496,512] For example, Palmore *et al*. reported one of the first membrane EBFC using ABTS and laccase from *Pyricularia oryzae* generating P_{max} = 42 μW.cm^{-2} at E_{cell} = 0.61 V in a 0.2 M acetate pH 4 buffer. However, Nafion® had to be used as a separating membrane.[513]

4.2.1.2 Immobilized redox mediators

4.2.1.2.1 Osmium based redox polymers

The use of osmium based redox polymers has been pioneered by Adam Heller in the 90's.[514-519] These hydrogels have been first used with glucose oxidase to make glucose sensors.[520,521] Due to its success, this system was then extended to numerous other enzymatic devices.[522-525] Os-based polymers constitute the only hydrated electron conducting system which allows for rapid diffusion of ions, substrates (glucose, O_2,…) and products.[154] Such systems permit to immobilize simultaneously enzymes and redox mediators on the electrode surface. Phase separation is avoided by creating an electrostatic adduct between the polycationic osmium redox polymer and enzymes, which are polyanionic at neutral pH (for example, the pI of most MCOs lies between 3 and 6). In addition, this adduct can be further cross-linked to enhance its stability. Because the enzymes are surrounded by the redox hydrogel, they are electrically wired irrespective of their orientation. This allows the electrical connection of multiple layers of enzymes in 3 dimensions. Conduction within the hydrogel results from the collisions between neighboring oxidized and reduced osmium moieties tethered to the polymer backbone (Fig 33A).[514]

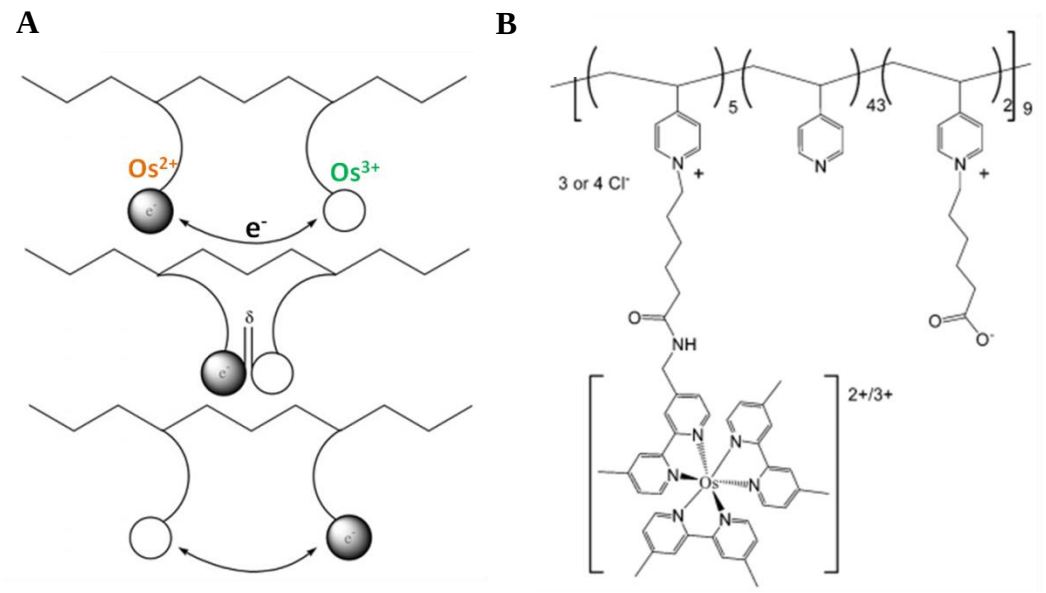

Figure 33. (A) Schematic representation of electron conduction in an Os-based redox polymer. Electron transfer in between reduced and oxidized osmium centers is based on a self-collision phenomenon. Introducing a long tether increases electron "diffusivity" along the polymer "wire" (Adapted from [526] with permission from the PCCP Owner Societies); (B) Chemical structure of a tris(4,4'-dimethyl-2,2'-bipyridil)osmium complex tethered to a partially quaternized polymer (poly(4-vinilpyridine)) backbone through an eight atoms long link. Reprinted with permission from [527]. Copyright 2003 American Chemical Society

In addition, these hydrogels are particularly versatile. Their redox potential can be tuned at will to be close to the redox potential of the enzymes, by choosing the adequate ligands around the osmium atom. The concentration of osmium, the nature and composition of the polymer backbone,[528-532] but also the spacer that connect osmium complexes to the backbone,[527,533] can be designed depending on the enzymes and the future applications. Furthermore, quaternization of the pyridine rings permits to introduce positive charges in the osmium redox polymer, enhancing both the rate of electron transport and the strength of the electrostatic complex formed between the polycationic redox polymer and the polyanionic MCO.[534,535] The electrochemical properties of the modified electrodes can be for example optimized by tuning the ratio between enzymes, redox polymer and cross linker[536], by

choosing an adequate film thickness[537] and/or by optimizing the temperature and drying time.[538]

In 2004, Leech *et al.*[539] reported the co-immobilisation of *Tv*-laccase with an osmium based redox polymer (E°' = +0.4 V *vs.* Ag/AgCl) on GC electrodes which reached a current density of 240 $\mu A.cm^{-2}$ in pH 5.0 buffer, at +0.3 V *vs.* Ag/AgCl. At pH 7.5, the current was only 7% of the catalytic current observed at pH 5. The authors attributed this loss in current to the low activity of laccases at neutral pH, but also to a change in electron transport upon hydrogel swelling.[540] The same authors later optimized the cathodic redox polymer and increased its redox potential by 90 mV. Their objective was to improve the OCP of an EBFC, and to demonstrate it was possible to yield a significant power density in a 0.05 M phosphate buffer pH 7.4 containing 0.1 M NaCl, even though laccases are sensitive to chloride and less active at neutral pH.[541] The cathodic current was increased by 20%, and a maximum power density of 16 $\mu W.cm^{-2}$ was reached at a cell voltage of 0.25 V when a glucose oxidizing anode was used. To improve the stability of their modified electrodes, they specifically tailored Os redox polymers to three enzymes *Mv*-BOD, *Ma*-laccase and *Th*-laccase and evaluated their performance and stability.[542] They showed that the magnitude of the O_2 reduction current densities depended on the enzyme selected, the thermodynamic driving force induced by the difference between the enzyme and the polymer redox potentials, and also on the chemical structure of the osmium complex. The same authors pre-treated graphite electrode by reduction of diazonium salts, or gold electrodes with cysteamine, to introduce anchoring amine groups[543] to further improve the stability, and particularly improve the interface between the osmium polymer and the electrode surface. After functionalization and modification with osmium polymer and enzymes, the authors showed for example that a pre-treated graphite electrode retained 90% of the original redox signal after 48 hours. By replacing GC electrodes with their newly developed pretreated graphite electrodes, they

showed a four-fold increase of the power density of their EBFC.[544] In 2003, Mano *et al*. demonstrated that the overpotential of an enzymatic cathode was lower than platinum for the reduction of oxygen at any current density (Fig 34).[545]

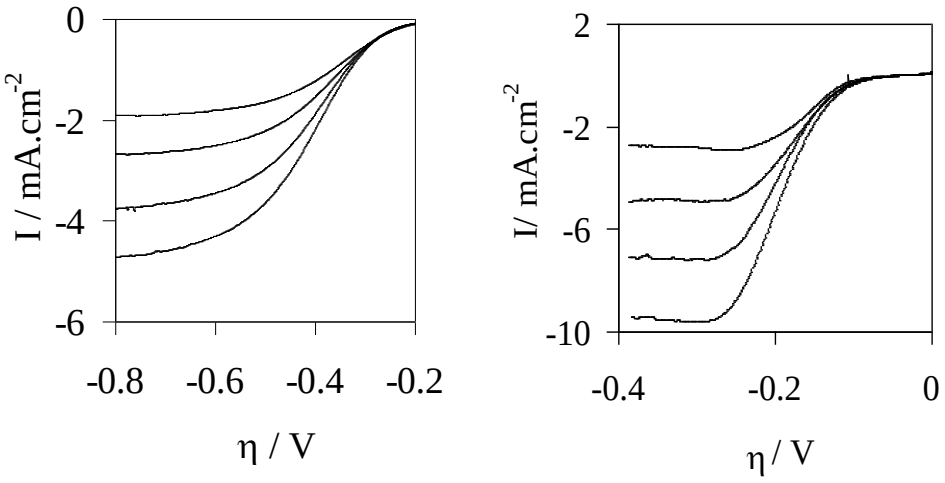

Figure 34. Dependence of the current density on the overvoltage for electrodes rotating at 500 rpm (top curve) 1000 rpm, 2000 rpm, and 4000 rpm (bottom curve) under 1 atm O_2 at 37°C. Scan rate. 5 $mV.s^{-1}$ *Left*. Polished Pt in 0.5 M H_2SO_4. *Right.* "Wired"-BOD on polished vitreous carbon in a pH 7.2 saline (0.15 M NaCl) phosphate (0.02 M) buffer. 32.3 wt% BOD, 60.2 wt% polymer, 7.5 wt% PEGDGE, at 0.17 $mg.cm^{-2}$ loading. Reprinted with permission from [545]. Copyright 2003 American Chemical Society.

For example, under 1 atm O_2 pressure, 9.5 $mA.cm^{-2}$ at an overpotential of -0.31 V was reached on the enzymatic electrode and only 0.6 $mA.cm^{-2}$ (16-fold lower) on a polished platinum cathode in 0.5 M H_2SO_4. The electrode consisted in the cross-linked adduct of *Mv*-BOD and a copolymer of polyacrylamide and poly(N-vinylimidazole) (PAA-PVI) complexed with [Os (4,4'-dichloro-2,2'-bipyridine)$_2$Cl]$^{+/2+}$ whose redox potential is +340 mV *vs.* Ag/AgCl. The modified electrode reached 5 mA cm^{-2} when poised at -0.18 V *vs.* the reversible O_2/H_2O electrode potential in a phosphate buffer saline. With the same redox polymer, the same authors reported the wiring of *Bp*-BOD which led to an Efficient biocathode that could operate in physiological conditions with a high tolerance to chloride,[101] in serum with less than 9% of current loss after 3.3 h of continuous experiments[546] and at

temperatures up to 70 °C[376,547] making it particularly suitable for the design of high-temperatures H_2/O_2 biofuel cells in combination with a thermophilic hydrogenase.[372,466] With the high redox potential *Mo*-BOD, it was possible to reach 1.37 $mA.cm^{-2}$ for the enzymatic O_2 reduction at +0.2 V *vs.* Ag/AgCl under physiological conditions by designing a new Os redox polymer with an increased density of catalytic sites.[531] The onset for O_2 reduction was +0.46 V *vs.* Ag/AgCl at pH 7. By combining *Tt*-BOD and PVI−Os(4,4-dimethyl-bpy)$_2$Cl on carbon rod electrodes, Scherson *et al*. reached 40 $\mu A.cm^{-2}$ at neutral pH. They further combined this cathode with a bi-enzymatic anode composed of trehalase and glucose oxidase to build an EBFC able to operate in a living insect.[548,549]

The wide variety of developed protocols is another proof of the versatility of osmium polymers. Apart from the original method developed by Heller, different authors have proposed alternative synthesis and immobilization strategies. Gao *et al*.[550] developed a cross linking technique taking advantage of the labile Cl^-, which is substituted upon electrodeposition by nitrogen-containing amino acid residues (histidine, lysine and arginine) naturally present in enzyme. This new immobilization technique was used to successfully wire bilirubin oxidases[551,552] and laccases.[553,554] Photoinitiated polymerization using poly(ethyleneglycol)diacrylate and 2-hydroxy-2-methyl propiophenone has also been shown to be an Efficient method to co-immobilize *Mv*-BOD and osmium based redox polymers.[555] This new protocol permitted to reduce the preparation time of electrodes from 18 h to 1 h. The possibility to modify electrodes by self-assembling alternating layers of polycationic redox polymers and polyanionic enzymes has also been exploited. Calvo *et al*. designed a biocathode made by self-assembling laccase from *Trametes troggii* and an osmium complex bound to polly(allylamine).[176] For three enzymes layers, the authors reached 80 $\mu A.cm^{-2}$ at +0.3 V *vs.* Ag/AgCl in a citrate buffer. Leech *et al*. used the same approach to elaborate a

membrane-less EBFC with a cathode made by layer-by-layer self-assembling of *Th*-laccase and osmium polymers.[556]

A new synthesis route for osmium based redox polymers has been elaborated by Schuhmann *et al*. (Fig 35).[557] Instead of using the classical "ligand exchange method", they proposed a covalent binding approach with an osmium complex already bearing the suitable ligands.

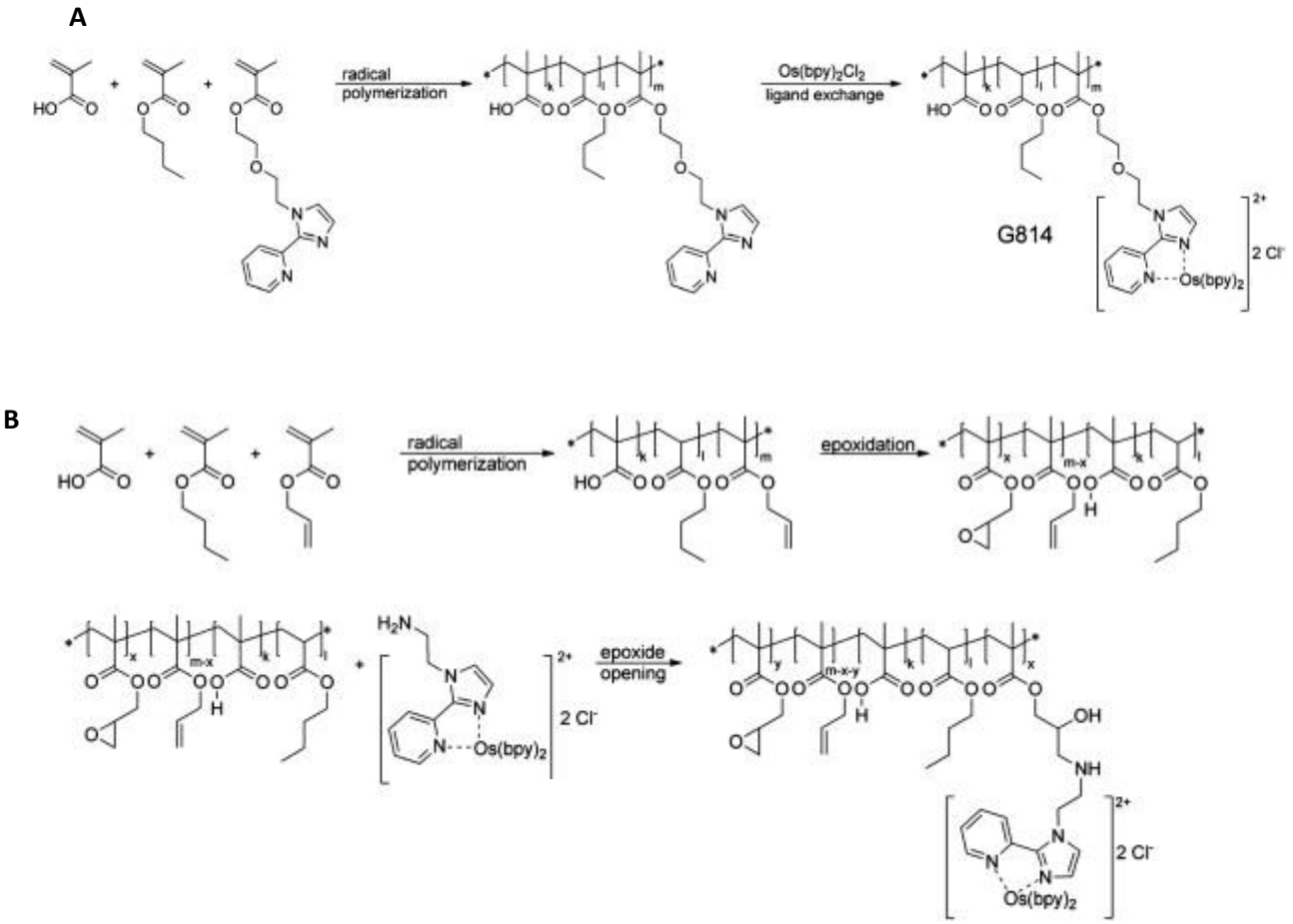

Figure 35. (A) Synthesis route for redox polymers synthesized by the ligand exchange approach; (B) Synthesis route for redox polymers synthesized by the covalent binding approach. Adapted with permission from [557]. Copyright 2012 Elsevier

The authors successfully used this strategy to wire laccase from *Trametes hirsuta*. In 2008, Banta *et al*.[558] proposed a particularly original strategy to immobilize a small laccase from *Streptomyces coecicolor* and an osmium redox complex by creating a bioelectrocatalytic

supramolecular hydrogel (Fig 36). This hydrogel was composed of two building blocks. The first one consisted in two α-helical leucine zipper domains separated by a randomly coiled domain rendered conductive by the addition of an osmium complex. The second building block was composed of a α-helical leucine zipper domain attached to a random coiled domain genetically fused to *Sc*-laccase. Upon mixture, the helical domains assemble into tetrameric coiled coils, thus forming an ordered and conductive supramolecular hydrogel. As seen in Fig 36B, after drop casting such hydrogel on a GC electrode, the authors could reach 15 $\mu A.cm^{-2}$ at +0.2 V *vs.* Ag/AgCl in an oxygenated 100 mM phosphate buffer pH 7 at 900 rpm and 25 °C.

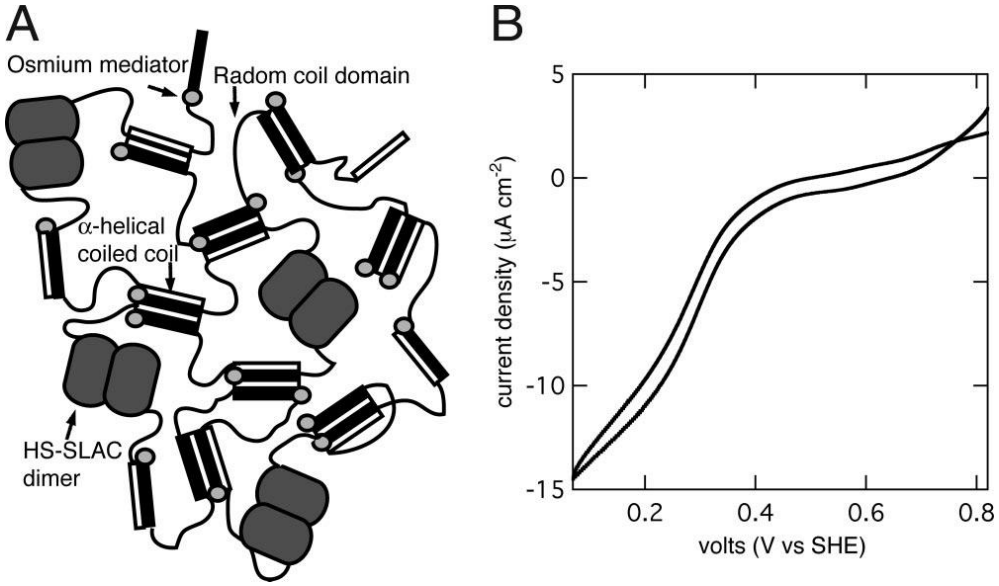

Figure 36. Bioelectrocatalytic hydrogel. (A) Schematic diagram of the supramolecular hydrogel. (B) Bioelectrocatalysis of a mixed hydrogel of 7.5 wt% OsHSH-1 and 2.5 wt% HS-SLAC on a 3-mm glassy carbon rotating disk electrode. Buffered to pH 7.0 with 100 mM phosphate buffer, 900 rpm, 25°C, 1 mM O_2. Adapted with permission from [558]. Copyright (2008) National Academy of Sciences, U.S.A.

More recently, Le Goff *et al.*[559] reported the synthesis of original osmium complexes bearing chelating N-heterocyclic and bipyridine ligands to wire *Mv*-BOD. These complexes were easily grafted at the surface of both planar and nanostructured CNT electrodes, either by

electrogeneration of a redox polymer, or by supramolecular π-π interactions. The immobilization of diazonium derivatives of an osmium bipyridine complex has also been reported, but has not been used with an enzyme so far.[560]

4.2.1.2.2 Conducting polymers

Different examples of the use of conductive polymers and particularly polypyrole (PPY) can be found in the literature. PPY is a versatile polymer which can be easily functionalized to introduce functional groups for the covalent binding of enzymes.[561] However, since PPY is a poor electronic conductor, redox mediators are preferably added to ensure a better electronic conduction. The use of PPY with laccase was first described in 2007 by Palmore *et al.*[270] Films of PPY doped with ABTS and laccase were grown on glassy carbon electrodes. Under 1 atm O_2, a current density of 3 $mA.cm^{-2}$ was reached at +0.33 V in a pH 5 buffer at 500 rpm. The same system has also been grafted by Yoo *et al.* on a gold electrode.[562] With the same idea, PPY was used by Mousty *et al.* to entrap laccase and modified anionic clays with ABTS.[563] Fransaer *et al.*[564] reported the electrodeposition of a solution containing PPY, a derivative of ruthenium as a redox mediator, 4-sulfonyldiphenol and *Tv*-laccase, yielding 50 $\mu A.mm^{-2}$ at 0 V in a pH 7.4 phosphate buffer. The same author also reported a biocathode made by adsorbing laccase and ABTS on MW-CNTs, further stabilized by an electrodeposited film of PPY.[565] In their later system, they also added catalase to benefit from an extra boost at their EBFC by dismuting H_2O_2, which is naturally present in bodily fluids.[566] PPY has also been used by Tingry *et al.*[567,568] In a series of papers, they immobilized *Mv*-BOD or laccase and ABTS in a PPY film[569] and for example used it as a cathode in a concentric EBFC generating P_{max} = 42 $\mu W\ cm^{-2}$ at E_{cell} = 0.3 V.[570] To improve the stability of the biocathode, functional groups were also introduced on PPY to covalently attach BOD.[571] Redox mediators such as porphyrin, ferrocene, osmium, and ruthenium

complexes were also entrapped in electropolymerized PPY.[572] Shimomura *et al*.[573] used different conductive polymers, polythiophene derivatives, but also had to dope them with ABTS. Upon immobilization with *Mv*-BOD on a modified gold electrode, 0.4 $mA.cm^{-2}$ was reached at +0.2 V *vs*. Ag/AgCl in a 0.1 M pH 7 phosphate buffer. The use of conductive polymers such as polyaniline has also been reported more recently. Shleev *et al*. elaborated a composite electrode comprising *Mv*-BOD, polyaniline and CNTs.[574] In a pH 7.4 phosphate buffer complemented with active blood components, a current density of 0.48 $mA.cm^{-2}$ was reached at 37°C. This demonstrated the ability of such system to operate in a blood-like medium.

4.2.1.2.3 Proteins as redox mediators

The use of Cytochrome *c* (Cyt *c*) as a redox mediator in homogeneous solution has been reported by Sakurai in 1992.[575] The authors studied the kinetic parameters of the electron exchange between horse heart Cyt C and *Rhus vernicifera* laccase as a function of pH, ionic strength, and temperature. Cyt C was subsequently used as a redox shuttle between immobilized enzymes and gold electrode surfaces. This has been reviewed in deeper details by Siveria *et al*.[576] Of particular interest is the work of Lisdat *et al*.[577] In 2007,[223] they demonstrated that *Mv*-BOD could accept electrons from Cyt C, whether this latter was used as a diffusive redox mediator or electrostatically immobilized with the enzyme. It was then possible to achieve a direct inter-protein electron transfer. In 2008,[578] they built an electrode by alternating layers of poly(aniline sulfonic acid) and a mixture of *Mv*-BOD and Cyt C, and demonstrated the possibility to electrically connect multilayers of both proteins. The electrochemical properties of such electrode depended on the number of deposited layers of proteins. Later, they extended this concept to other enzymes such as laccases,[579,580] and in

2011, used different forms of Cyt C, including mutant forms of human Cyt C, in their self-assembled protein multilayers (Fig 37).[581]

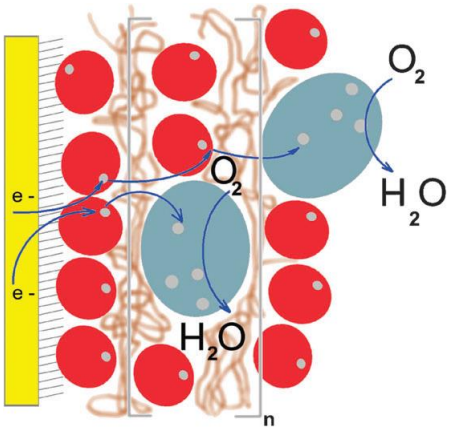

Figure 37. Schematic illustration of the redox chain in Cyt C/BOD multilayer electrodes. Red circles = Cyt C protein, blue shapes = BOD enzyme, arrows indicate electron transfer pathways between Cyt C and BOD within the polyelectrolyte network and the four-electron oxygen reduction process. Adapted with permission from [579]. Copyright 2009 The Royal Society of Chemistry

Surprisingly, the authors considered their system as a DET. Even though organic/inorganic redox mediators are not used, it may not be considered as a DET *per se* since electrons are shuttled from one protein to another one, *i.e.* from Cyt C to BOD, and not directly transferred between enzymes and electrode. With the same idea of using proteins as redox mediators, a paper by Altamura *et al*. is of particular interest (Fig 38).[582] The authors designed an electroconductive bionanowire which resulted from the attachment of a prion domain with a rubredoxin. The newly formed bionanowire was then used as a redox mediator for the reduction of O_2 by *Tv*-Laccase in a sodium phosphate buffer pH 5. The current density obtained for such system was higher than those obtained with Cyt C. This technique may provide a new strategy to elaborate enzymatic electrodes.

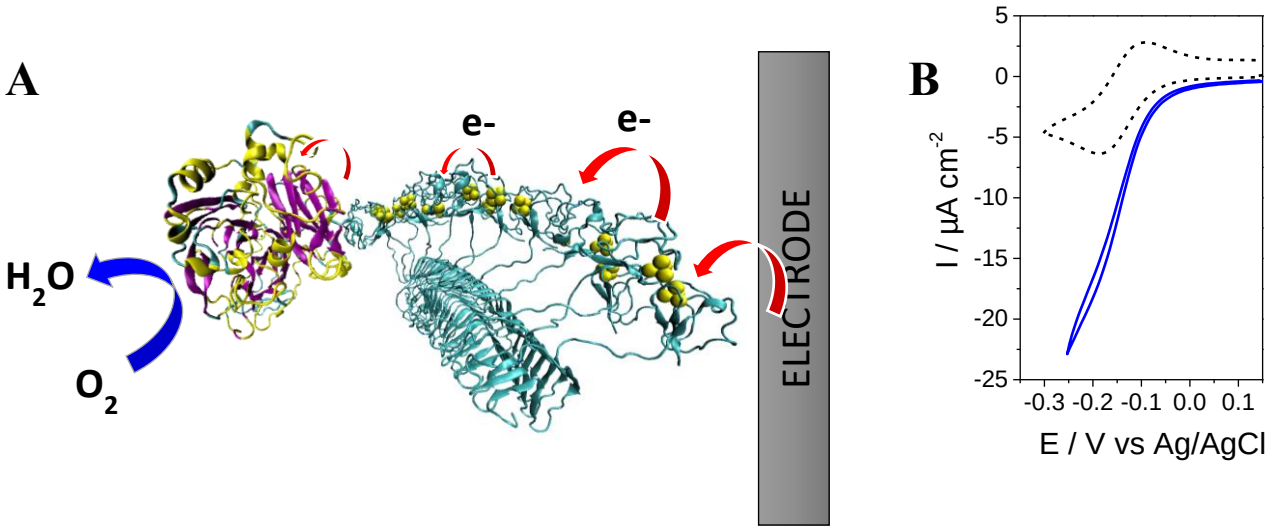

Figure 38. Chimeric Rubredoxin (Rd) as a redox mediator for the bioelectrocatalytic reduction of oxygen by laccase. A) Graphical depiction of the electron transfer from the electrode towards laccase through Rd-HET bionanowires. B) CV of electrocatalytic-mediated oxygen reduction of Rd-HET/laccase in sodium phosphate buffer (pH 5) at 37 °C. Both the redox couple of Chimeric-Rd/laccase in deoxygenated sodium phosphate buffer (dashed black line) and the catalytic oxygen reduction of Rd-HET/laccase in the presence of oxygen (blue line) are shown. Reproduced with permission from [582]. Copyright 2016, Nature Publishing Group

4.2.2 Carbon electrodes

4.2.2.1 Nanomaterials

4.2.2.1.1 Carbon particles

Carbon particles of various shapes and sizes (graphite, graphene, carbon black, ketjen black, carbon vulcan,..) have been used to make carbon electrodes.[376] The common point of these electrodes is the preparation method which comprises the mixture of the particles with a binder to form a paste, further deposited onto electrode surfaces. It is a very easy way to increase the specific surface, however without controlling or maximizing the porosity. For example, Kondo *et al*. mixed *Mv*-BOD, ABTS and carbon paste to elaborate a biocathode, further used in a starchy biomass EBFC delivering 99 µW.cm^{-2} at 0.55 V.[583] The second

common point of this preparation method is the frequent need to add a membrane to prevent the leaching of the redox mediator. For example, Kokoh *et al*. used Carbon Vulcan XC72 to elaborate an electrode further modified by adsorbing *Mv*-BOD and ABTS. Nafion® was added on top of the modified layer, or in the mix of enzyme and ABTS, to prevent the leaching of the bioelectrocatalyst.[363,584] Nafion® was also used by Cosnier *et al*. in their compressed electrode made of graphite, laccase and ABTS.[585] Sol-gel[586], poly-L-lysine[497] or lipid liquid crystalline cubic phases[587] were also used to prevent the leaking of redox mediators.

4.2.2.1.2 Carbon nanotubes

The general properties and advantages of CNTs have been presented in section 4.1.2.1. These outstanding nanomaterials have also been implemented in MET-based electrodes. They were generally used to formulate carbon ink. Such carbon ink was developed by Viikari *et al*.[588] by mixing carbon nanotubes, ABTS and *Trametes hirsuta* laccase. After coating on different printing substrates, they could reach current densities up to 39.1 $\mu A.cm^{-2}$ at 0.25 V *vs.* Ag/AgCl on Whatman filter paper. Such methodology has also been reported later by Leech *et al*.[589] CNTs can also be incorporated to the enzyme solution prior to casting on an electrode. For example, in 2013, Leech *et al*. used osmium redox polymers to elaborate three different biocathodes with two laccases and *Mv*-BOD.[590] To enhance the electroactive surface of their electrodes, they added MW-CNTs in the mixture containing enzymes and redox polymer. In presence of MW-CNTs, the current density was increased by a factor of 2.5 compared to the corresponding planar electrode without MW-CNTs. Such increase was attributed to higher loading of enzymes enabled by the addition of carbon nanotubes. The authors exploited this advantage to elaborate various EBFCs.[591,592] In 2010, Sadowska *et al*. described the first deposition of single-walled carbon nanotubes (SW-CNTs) covalently

modified with ABTS[593] on glassy carbon electrodes, and further cover with a mixture of laccase/Nafion®. Covalent linking of ABTS to SW-CNTs prevented its leaking from the electrode surface and allowed a better interaction with laccase molecules. The presence of Nafion® also prevented the leaching of the enzyme without impeding the diffusion of O_2. The combination of CNTs and graphene has also been reported by Chen *et al*.[594] After growing 3D graphene networks, the electrode was first modified with SW-CNTs, and then laccase was covalently immobilized on the composite electrode. Poor electron transfer was observed on the graphene modified electrode compared to the composite electrode. However, even in presence of SW-CNTs, ABTS was needed to improve the electron transfer.

4.2.2.1.3 Carbon fibers

Even if carbon fibers usually do not offer a large volumetric area, their geometry allows them to reduce mass transport limitations.[595] Radial diffusion with electrode diameters smaller than the diffusion length of the reactants allows for faster mass transport compared with semi-infinite planar electrodes. In addition, the use of carbon fibers allows for miniaturization of EBFCs. 7 μm diameter-2 cm long commercial carbon fiber electrodes have been used by Mano *et al*. in biocathodes and EBFCs with *Mv*-BOD and *Tt*-BOD,[545,596-601] *Tv*-laccase[533] and *Bp*-BOD.[602] Current densities ~1mA.cm^{-2} were reached in PBS buffer. Home-made carbon fibers were also designed by Tingry *et al*.[603] by electrospinning polyacrylonitrile followed by carbonization. The carbon fiber electrodes were then modified with PPY, ABTS and laccase. 1 mA.cm^{-2} at +0.1 V *vs.* Ag/AgCl in a 0.1 M pH 3 phosphate buffer was reached.

4.2.3 3D materials

Although on planar electrodes MET permits to significantly enhance O_2 current densities compared to DET, the performances are still not sufficient to envision the

elaboration of high power EBFCs. In such a context, the most intuitive way to enhance the power densities is to increase the specific surface of the electrode, to allow for higher enzyme loading. It is especially crucial to develop a microstructure suitable both for enzyme immobilization and mass transfer of substrates. Regarding that, different carbonaceous or metallic matrices based on conductive nanomaterials, as well as free-standing 3D structures, have been proposed for MET electrodes and will be discussed in the following. Of particular interest is the recent paper from Eychmuller *et al.*[62] and Zhao *et al.*[91] reviewing the use of porous nanostructures for enzymatic EBFCs.

4.2.3.1 Porous carbon electrodes

4.2.3.1.1 Carbon cloth

Carbon cloth is usually made with carbon fibers of different diameters, which can be further functionalized with CNTs to enhance even more the specific surface.[604] It is usually fixed on a planar electrode with a conductive carbon paint, and further modified with polymer and enzymes (Fig 39). Calabrese-Barton *et al.*[605,606] were the first to report the use of a 375 μm thick carbon cloth with a porosity of 78% and made with 10 μm diameter carbon fiber. Their electrode was composed of PVI-Os(tpy)(dme-bpy)$^{2+/3+}$ (with 1/5th of the imidazoles complexed with [Os(tpy)(dme-bpy)]$^{2+/3+}$ (tpy = terpyridine; dme-bpy = 4,4'-dimethyl-2,2'-bipyridine)]) and *Th*-laccase. They reached a current density of 5 mA.cm^{-2} at 0.57 V *vs.* Ag/AgCl in a pH 5 chloride-free citrate buffer at 37.5ºC (Fig 39B).

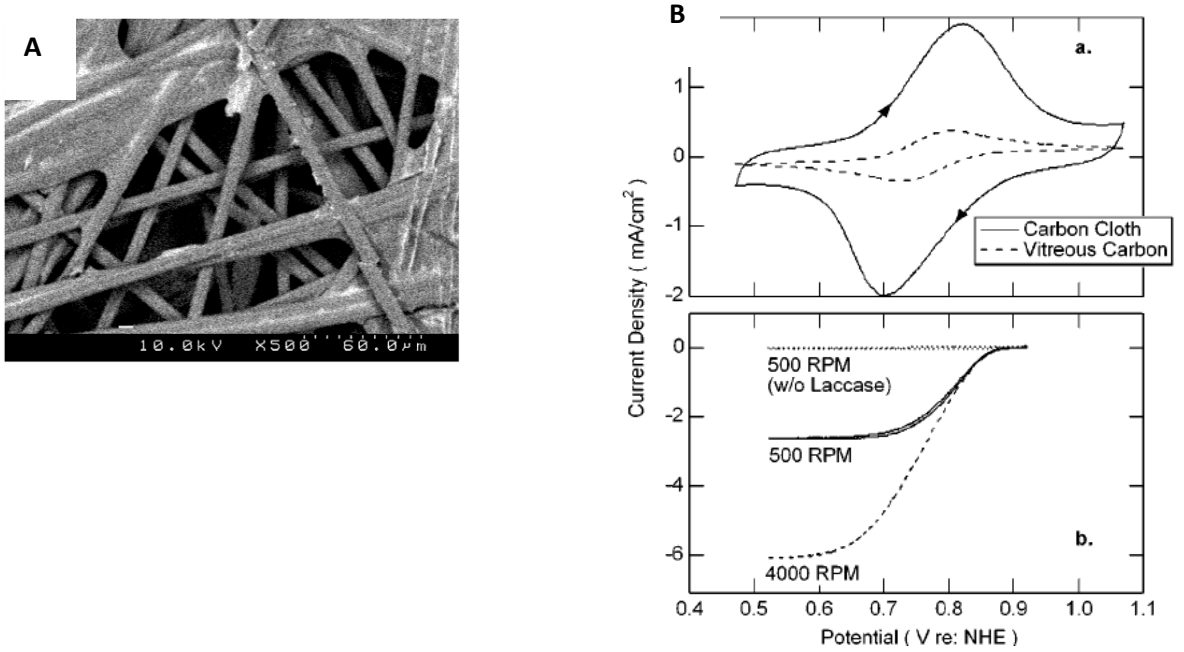

Figure 39. (A) SEM (electron backscattering mode) of the composite 350 µm thick carbon cloth cathode loaded with 0.78 mg.cm^{-2} "wired" laccase (45 wt % laccase, 49 wt % redox polymer, 6 wt % PEGDGE) The lighter areas are coated with more heavy atoms (osmium). (B) (a) Cyclic voltammograms (50 mV.s^{-1} sweep rate, 500 rpm) of the vitreous carbon and the composite carbon cloth electrodes under argon. (b) Potential-dependence of the O_2 electroreduction current density at 1 mV.s^{-1} sweep rate at 1 atm O_2 pressure. Current densities were based on the projected area of the 4-mm carbon cloth disk (0.13 cm^2). Reprinted with permission from [606]. Copyright 2001 American Chemical Society.

In this pioneering work, the authors demonstrated that a 50-fold increase in surface area lead to a multiplication of the O_2 reduction current by a factor of 5. A glucose/O_2 EBFC built with this cathode had a five-fold higher power density than the earlier cells.[606] At neutral pH and in presence of 0.14 M chloride, the current density of this cathode was almost nil, due to the inactivity/inhibition of this laccase species in physiological conditions. However, when using laccase from *Pleurotus ostreatus*, the same authors could obtain ~100 µA.cm^{-2} at +0.4 V *vs.* Ag/AgCl at pH 7 in a phosphate buffer containing NaCl.[178] In 2008, Gallaway *et al.* reached 6.25 mA.cm^{-2} at +0.3 V *vs.* Ag/AgCl in an oxygenated pH 7 buffer when *Sc*-laccase was used in a porous composite electrode.[166] To build a faster O_2 cathode operating at pH 5, a spacer has been introduced between the backbone and the osmium polymer to enhance the

rate of collisions between neighboring osmium complexes and therefore the apparent electron diffusion from $(6.2 \pm 0.8)\times10^{-9}$ $cm^2.s^{-1}$ to $(7.8 \pm 0.4) \times 10^{-7}$ $cm^2.s^{-1}$.[533,607] As seen in Fig 33B, the presence of the tether permitted to significantly increase the current. 500 $\mu A.cm^{-2}$ was reached at only +0.63 V *vs.* Ag/AgCl for the polymer with the tether while it was at +0.54 V *vs.* Ag/AgCl for the polymer without spacer. A glucose/O_2 biofuel cell built with this new cathode operated at E_{cell} = 0.88 V while producing P_{max} = 350 $\mu W.cm^{-2}$ in a stagnant pH 5 buffer at 37°C.[533] At the cathode, a current density of 3 $mA.cm^{-2}$ at +0.54 V *vs.* Ag/AgCl at pH 5 was reached, which is at only -140 mV *vs*. the potential of the reversible O_2/H_2O electrode. In 2002, Mano and Heller were the first to report the reduction of O_2 under physiological conditions (pH 7.4, 0.15 M NaCl, 37°C) with immobilized redox mediators.[175] The electrode consisted in the crosslinked adduct of *Mv*-BOD and PAA-PVI-[Os (4,4'-dichloro-2,2'-bipyridine)$_2$Cl]$^{+/2+}$ with a redox potential of +340 mV *vs.* Ag/AgCl. The modified electrode reached 5 mA cm^{-2} when poised at +0.3 V *vs.* Ag/AgCl. The same year, to upshift the operating voltage of the EBFC, a new cathode was elaborated with the same redox polymer but with a new BOD from *Trachyderma tsunodae*.[120] Cardoso *et al*. have also reported the use of carbon cloth modified with polyamidoamine dendrimers for the immobilization of *Tv*-laccase using ABTS entrapped into polypyrrole films.[278]

Minteer *et al*. used a different approach.[510] Their carbon cloth electrode was first coated with a suspension of Nafion® modified with quaternary ammonium salt and containing bilirubin and *Mv*-BOD, and further soaked in 1 mM $Ru(bpy)_3^{2+}$ to pre-concentrate the redox mediator in the membrane. In addition to be ethanol tolerant, the advantage of this cathode was its extended active lifetime provided by the treated porous Nafion® membrane.[491] The authors postulated that the modified structure of Nafion® with ammonium salts could help stabilizing and increasing the enzyme activity, by providing a protective outer shell and an ideal chemical environment resisting to a decrease in pH within the pore

structure. This cathode was used in an ethanol/oxygen biofuel cell which displayed an active lifetime of ~30 days and power densities of up to 0.46 $mW.cm^{-2}$. With the same idea of improving the active lifetime of *Mv*-BOD, Heller *et al*. adopted a different strategy.[608] After modification of their carbon cloth electrode with osmium polymer, crosslinker and BOD, they coated their electrode with lyotropic liquid crystals. The authors demonstrated that such coating permitted to prevent mechanical stripping of the bioelectrocatalyst upon shearing. Moreover, it reduced the damage due to urate electro-oxidation without affecting the reduction of O_2. A similar strategy has been recently developed by Jian *et al*. with the same system, but using a supramolecular coating made with glycosylated nucleoside fluorocarbon amphiphile instead of liquid crystals.[609] Carbon nanotubes were also controllably grown on carbon cloth as reported by Schuhmann *et al*.[610] With such electrode modified with osmium polymer and *Th*-Laccase, the authors could increase 125 fold the power density of their EBFC compared to an EBFC made with a bare carbon cloth electrode and identical bioelectrocatalysts.

4.2.3.1.2 Buckypapers

Buckypaper (BP)-based nanostructured electrodes have been widely used due to their simplicity of fabrication. BPs are usually obtained by classical filtration technique of a CNT suspension. Redox mediators may be added during the filtration or *a posteriori* to functionalize the electrode surface. However, with this filtration process, it is not possible to control neither the porosity, nor the orientation of the nanotubes, and non-homogenous papers are usually obtained.

Cosnier *et al*. developed free standing buckypaper electrodes by combining multi-walled carbon nanotubes (MW-CNTs) and bis-pyrene modified with ABTS. The latter acted both as a cross linker between the nanotubes and as a redox mediator for the *Tt*-laccase. The

authors could reach 1.6 mA at 0 V *vs.* Ag/AgCl in a 0.1 M pH 5 buffer with an operational stability evaluated at two weeks.[611] Hussein *et al*.[612,613] also described the use of buckypapers. Novel BPs fabricated from commercially available multi-walled carbon nanotubes (MW-CNTs) were coated with *Mv*-BOD, ABTS and Nafion®.[613] The authors demonstrated that they could obtain a higher electrocatalytic activity of BOD for the ORR than at a commercially available carbon black (Vulcan XC-72R).[613] In their last report,[614] BP was modified with *Mv*-BOD and ABTS and further coated with Nafion®. When this electrode was implemented in an EBFC with a glucose oxidizing anode, a power density of 26 $\mu W.cm^{-2}$ at E_{cell} = 0.2 V was attained at 37°C in a quiescent O_2-saturated physiological buffer containing 5 mM glucose.

4.2.3.1.3 Carbon-nanotube fibers

3D-structured carbon fiber is the ideal candidate to develop miniaturized EBFCs. It is the ideal combination for achieving large surface area and fast mass transport while maintaining the geometric surface as small as possible. In 2010, Gao *et al*. developed a new porous cylindrical electrode combining radial transport and large specific surface area allowing for fast mass transport. It was made of assembled and oriented nanotubes further coated with osmium redox polymer and *Mv*-BOD.[615] In a PBS buffer and under air, the current density was 10 folds higher on the newly engineered porous microwire electrode compared to a conventional modified carbon fiber. It also allowed smaller overpotentials for O_2 reduction. In addition, the mechanical stability was considerably enhanced due to the presence of nanotubes. Such strengthening effect has also been reported for numerous electrodes made with CNTs. For example, Kang *et al*.[551,616] observed a similar effect on glassy carbon electrode modified with oxidatively treated carbon nanotubes on top of which was deposited an adduct of *Mv*-BOD and osmium polymers. Imbrication of BOD and CNTs

in the core of the fiber was later made possible by developing a one-step fabrication of microfibers.[310] Baughman *et al.*[617] reported the fabrication of biscrolled yarn electrodes produced from MW-CNTs sheet and coated by PEDOT (Fig 40).

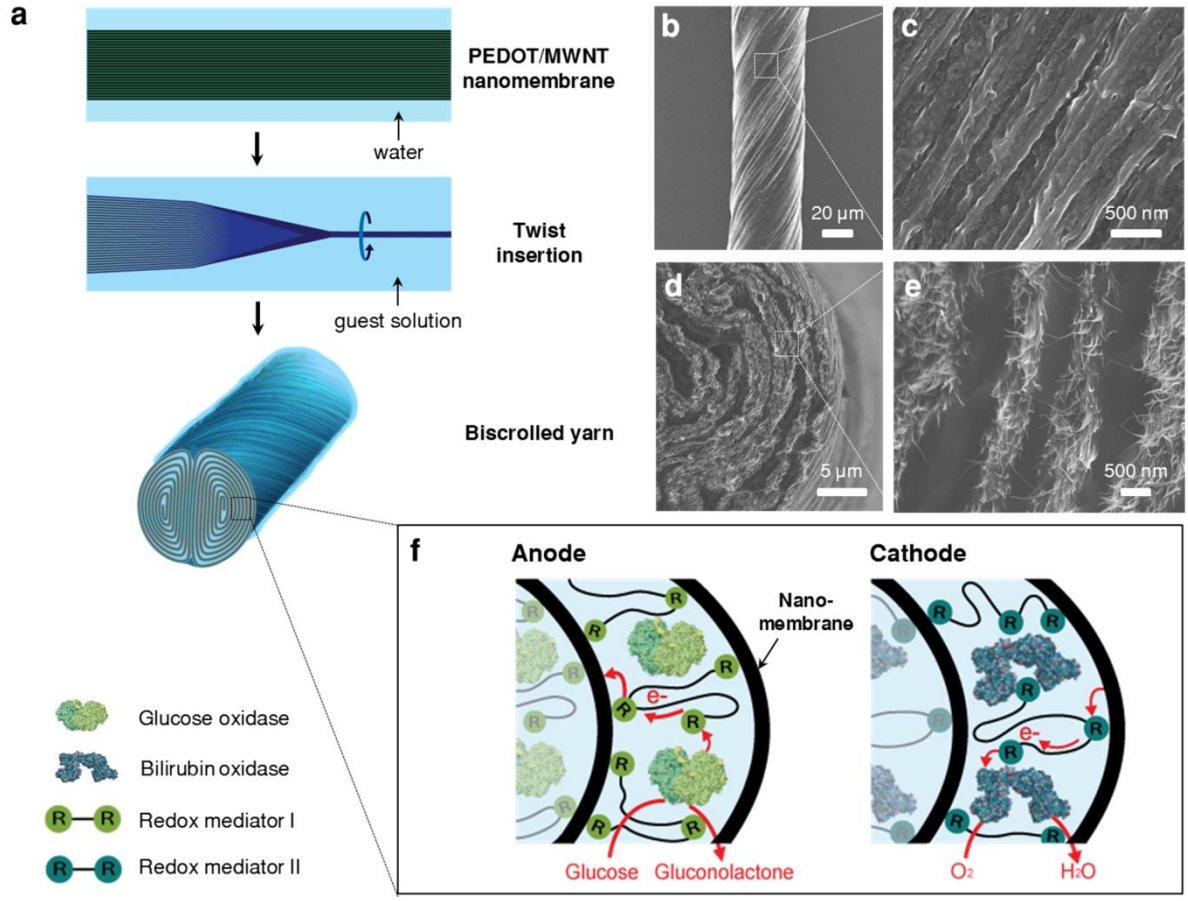

Figure 40. The fabrication and structure of biscrolled yarn electrodes for BFCs. (a) Schematic illustration of the fabrication method for biscrolled yarn electrodes. (b,c) SEM micrographs showing the surface of a 50-mm diameter biscrolled yarn cathode based on PEDOT/MW-CNT host. The scale bars were 20 mm and 500 nm, respectively. The yarn bias angle (the angle between the MW-CNT fiber direction on the yarn surface and the yarn direction) is ~37°. (d,e) SEM cross-section images at low and high magnifications of the fracture surface of a biscrolled yarn cathode, which shows yarn corridors between scrolled PEDOT/MW-CNT sheets that contain the yarn guests. The scale bars were 5 mm and 500 nm, respectively. (f) Schematic illustration of the structure and function of BFC anode and cathode, which indicate associated electron transfer processes and chemical transformations. The enzyme and redox mediator polymer used were glucose oxidase (GOx) and (poly(N-vinylimidazole)-[Os(4,4'-

dimethoxy-2,2'-bipyridine)$_2$Cl])$^{+/2+}$ for the anode. The enzyme and redox mediator polymer used were bilirubin oxidase (BOD) and (poly(acryl acid)-poly(N-vinylimidazole)-[Os(4,4'-dichloro-2,2'-bipyridine)$_2$Cl])$^{+/2+}$ for the cathode. Reproduced with permission from [617]. Copyright 21014, Nature Publishing Group

After twisting to obtain a yarn, the electrodes were modified with osmium polymer and *Mv*-BOD. The authors could reach 6 mA.cm^{-2} at +0.2 V *vs.* Ag/AgCl in an O_2-saturated PBS buffer at 37°C. The high current density resulted from the presence of the hydrophilic PEDOT layer which permitted to enhance the connectivity, conductivity and wettability of CNTs while providing electrolyte accessibility within the entire yarn. A different strategy has been developed by Cosnier *et al.*[337] The authors produced electrospun carbon nanofibers containing CNTs. After annealing, the fibers were first functionalized via the reduction of 4-carboxyphenyldiazonium to generate carboxy functions. Then, *Tt*-laccase was immobilized on the modified fiber by amide coupling. To further enhance the amount of wired enzymes, a bis-pyrene modified with ABTS was added on the fibers. Such modified fibers permitted to reach 100 μA.cm^{-2} at +0.2 V *vs.* Ag/AgCl in a 0.1 M phosphate buffer pH5.

4.2.3.1.4 3D carbonaceous electrodes

In 2014, Tsujimura *et al.*[618] reported the formation of Magnesium oxide-templated mesoporous carbon (MgOC, mean pore diameter 38 nm). The advantage of magnesium oxide templating is the possibility to tune at will the pore size. In 2015, they used this technique to elaborate a cathode modified with *Mv*-BOD and ABTS.[508] The adsorption of ABTS on the electrode surface improved both the BOD loading and the electron transfer rate from the electrode to the electro-active site of BOD. No significant leaching of the redox mediator was observed. Willner *et al.*[373] described the design of highly porous electrodes based on glassy carbon first modified with mesoporous carbon particles (~500 nm diameter, with pore

dimensions ~6.3 nm) perfused with ABTS after drying. The modified electrodes were then coated with *Mv*-BOD and Nafion®. According to the author, the advantage of this method was the combination of the high surface area, the close proximity between the redox mediator and the BOD, and the possibility to entrap the redox mediator within the matrix (Fig 41).

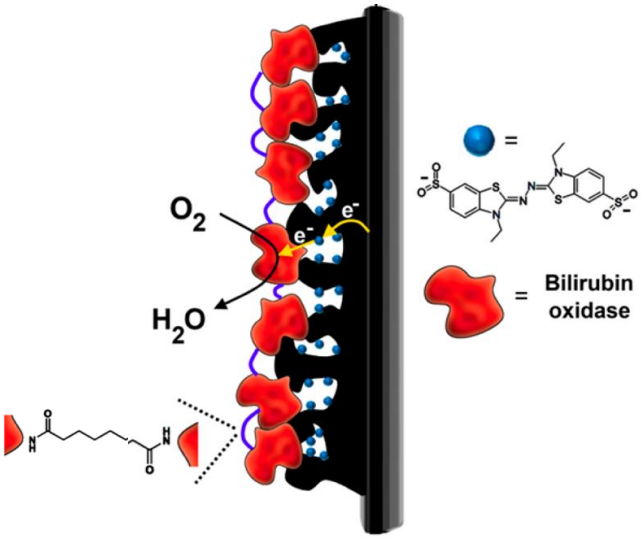

Figure 41. Schematic illustration of the modified cathode with BOD and $ABTS^{2-}$. Adapted with permission from [373]. Copyright (2013) American Chemical Society

With such design, a current density of 20 µA in a 0.1 M pH 7 HEPES buffer was reached. Wallace *et al*. reported nanostructured networks of carbon nanotubes grown by chemical vapour deposition onto reticulated vitreous carbon (RVC). After modification with *Mv*-BOD and osmium polymer, 175 $\mu A.cm^{-2}$ at +0.1 V *vs.* Ag/AgCl in a PBS buffer was obtained with or without rotation.[619] Additional examples can also be found in the review of Bellino *et al*.[73] who described in details the use of mesoporous materials for wired enzymes.

4.2.4 Gold electrodes

Magner *et al*.[620] fabricated and characterized nanoporous gold substrates, with different morphologies and roughnesses, which were attached to GC electrodes. After

modification with an osmium polymer and *Mv*-BOD, the authors reached 500 µA. cm^{-2} at neutral pH in unstirred conditions. Interestingly, the authors also demonstrated that the diffusion layer was exceeding the film thickness, resulting in the overlapping of the diffusion zone between adjacent nanopores, and therefore yielding to similar currents than a planar electrode. Leech *et al.* developed highly-ordered macroporous electrodes with 500 nm diameter pores (Fig 42).[621]

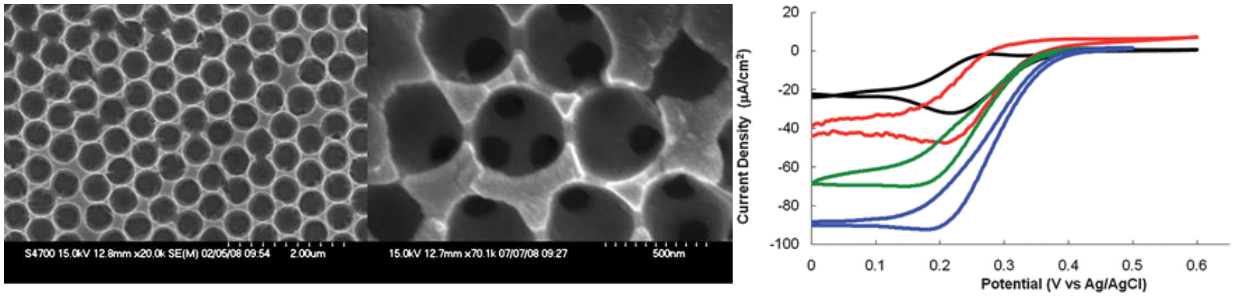

Figure 42. SEM images, at different magnification of a macroporous gold scaffold obtained upon electro-depositing though templates formed by vertical deposition of 500 nm diameter polystyrene spheres to yield 2½ deposited layers of gold. Cyclic voltammograms at planar (black), 1/2 sphere (red), 1½ sphere (green) and 2½ sphere (blue) gold layer electrodes modified with $[Os(2,2\text{-bipyridine})_2(PVI)_{10}Cl]^+$ and *Ma*-laccase recorded in 0.05 M phosphate buffer, pH 7.4, 0.15 M NaCl, 10 mM glucose. Scan rate 5 mVs^{-1} and current is normalised to projected geometric area of underlying gold substrate (0.1964 cm^2). Adapted with permission from [621]. Copyright 2012 The Royal Society of Chemistry

For electrodes made with 2 and a half layers, they could reach 100 µA. cm^{-2} in a 0.05 M phosphate buffer pH 7.4 containing 0.1 M NaCl when the electrode was modified with *Ma*-laccase and an osmium polymer.

4.2.5 Other enzymatic systems

If state-of-the art biocathodes mainly rely on the use of laccases or BODs, alternative approaches have been developed to enzymatically reduce O_2 to water. This includes the use of bienzymatic systems, or of different enzymes such as copper efflux oxidase (CueO) or tyrosinase (also called polyphenol oxidase, abbreviated PPO). Even if the reduction of oxygen

has been achieved with these systems, these approaches have not been widespread for two mains reasons: on one hand, CueO and PPO display an overpotential for O_2 reduction higher than BOD and laccase; and on the other hand the design of bienzymatic systems is often time consuming and more complicated to implement.

4.2.5.1 Glucose oxidase/horseradish peroxidase

In 2010, Ferontopava *et al.* proposed to elaborate a bienzymatic biocathode by assembling glucose oxidase (GOx) and horseradish peroxidase (HRP).[622] They first immobilized HRP on a graphite electrode, and after drying immersed the modified electrode in a GOx solution. The direct wiring of the HRP permitted to reduce H_2O_2 generated during the oxidation of glucose by GOx in presence of O_2. Therefore, we may consider that this bienzymatic electrode achieved the direct reduction of O_2 to H_2O, even though glucose had to be present. In 2012, Stoica *et al.* used the same strategy on their newly developed carbon microfiber (CMF)/carbon nanotubes (CNT) electrodes (Fig 43A).[623]

A

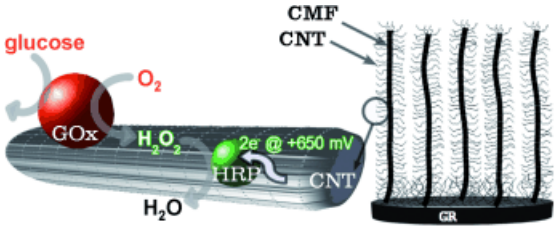

B

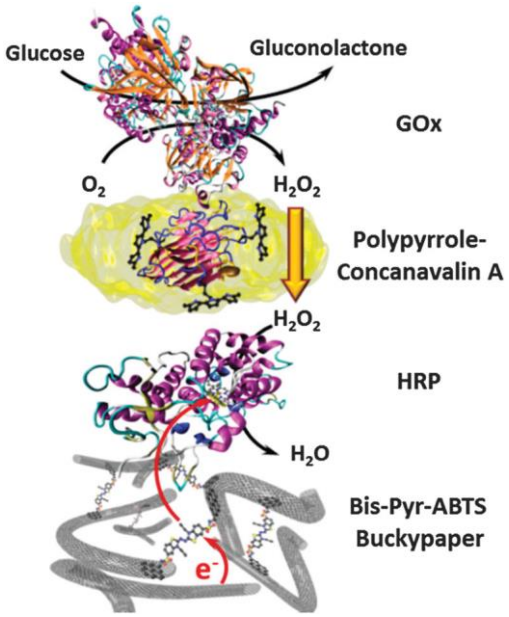

Figure 43. (A) Representation of CMF/CNT composite carbon structure onto Graphite rod and involved enzymatic/heterogeneous reactions responsible for reductive current at cathode. Reproduced from [623] with permission from John Wiley and Sons. (B) Sketch of the biocathode functioning based on bis-pyrene-ABTS BP after adsorption of HRP and subsequent electropolymerization of pyrrole–concanavalin A for the immobilization of GOx. Reproduced with permission from [624]. Copyright 2015 The Royal Society of Chemistry

After modification of the electrode with pyrenehexanoic acid, the modified electrode was sequentially modified with HRP and GOx. In an oxygenated PBS buffer containing 5 mM glucose, the authors could reach a current density of 280 μA. cm^{-2} at +0.3 V *vs.* Ag/AgCl. The onset potential was ~0.6 V *vs.* Ag/AgCl, close to the voltage that could be obtained with a high potential laccase. They also demonstrated that in presence of 6 mM glucose, the addition of 100 mM Cl^- did not affect the current density. Cosnier *et al.* elaborated two types of electrodes relying on the same concept. In the first, they used double-walled carbon nanotubes modified with HRP and GOx.[625] The authors reached 200 μA.cm^{-2} at +0.3 V *vs.* Ag/AgCl in an oxygenated 5 mM glucose solution. For their second biocathode, they developed a more complex system (Fig 43B).[624] First, they coated buckypaper with pyrene modified with ABTS, and then incubated it in a HRP solution. The modified electrodes were functionalized with pyrrole-concanavalin A and incubated in a GOx solution. Their freestanding electrode generated 11 mA.cm^{-2} at +0.1 V *vs.* Ag/AgCl during 1 hour of continuous discharge in an oxygenated 5 mM glucose buffer, and was insensitive to Cl^-. Ramanivicius *et al.* [626] used graphite rod electrode modified with GOx and HRP, and generated 150 μA.cm^{-2} in an aerated 100 mM glucose solution at 25°C.

4.2.5.2 Cytochrome *c* and cytochrome oxidase

In 1999, Katz and Willner reported the first membrane-less glucose/O_2 EBFC and paved the way for the development of such systems. They reached 4 μW for an external load

of 0.6 kΩ.[627] Their biocathode was composed of an assembly of Cyt *c* and cytochrome oxidase (COx) (Fig 44).

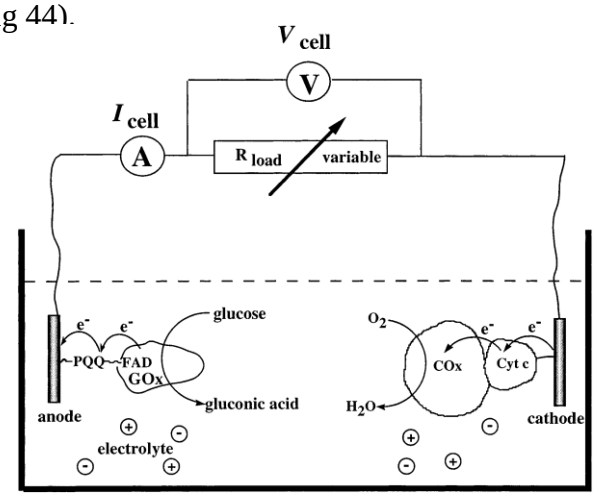

Figure 44. Schematic configuration of a biofuel cell employing glucose and O_2 as a fuel and an oxidizer, respectively, and PQQ-FAD/GOx and Cyt C/COx-functionalized electrodes as biocatalytic anode and cathode, respectively. Reproduced with permission from [627]. Copyright 1995 Elsevier

In 1982, it had already been shown that such protein-enzyme combination could undergo the 4-electron reduction of O_2 to water.[628] To allow for Efficient DET, the authors immobilized Cyt C to a maleamide modified gold electrode through a cysteine residue. Then, the assembled monolayer of Cyt C interacted with COx to generate a multiprotein complex. The resulting multilayers were then further cross-linked to provide stability. The authors used this kind of biocathodes for a variety of biocatalytic systems.[30,34,629-631] For example, in 2001, they reported the first self-powered biosensors with such bienzymatic cathode.[632] In 2003,[633] they developed an EBFC with an electrochemically switchable power output. Their cathode was composed of poly(acrylic acid) loaded with Cu^{2+} and further functionalized with Cyt *c* and COx. Depending of the applied potential, *i.e* -0.5 V or +0.5 V *vs.* Ag/AgCl, the authors could respectively tune the biocathode into a conductive or nonconductive state. In 2005,[634] they also developed a magnetically controlled EBFC still based on this biocathode and

demonstrated that a 3-fold increase in power output could be obtained when a magnetic field of 0.92 T was applied.

4.2.5.3 Copper efflux oxidase

The use of CueO has been proposed in 2007 by Kano *et al*. as an alternative to laccase or BOD, and has been mainly developed by this group.[635] After immobilization of the enzyme on highly oriented pyrolytic graphite electrodes by simple drop coating, the authors could reach 4 mA.cm^{-2} at pH 5, 25°C, with the electrode rotating at 1500 rpm. The authors also evaluated the redox potential of the T1 Cu at +0.3 V *vs.* Ag/AgCl by redox titration, which was later confirmed when CueO was immobilized in carbon aerogel.[636] In these conditions, they reached 8 mA.cm^{-2} at 0 V *vs.* Ag/AgCl in a pH 5 buffer and at 4000 rpm. They further improved their biocathode by using mesoporous carbon electrodes, and reached 12 mA.cm^{-2} at -0.4 V *vs.* Ag/AgCl in a pH 5 buffer and at 10 000 rpm (Fig 45).[637]

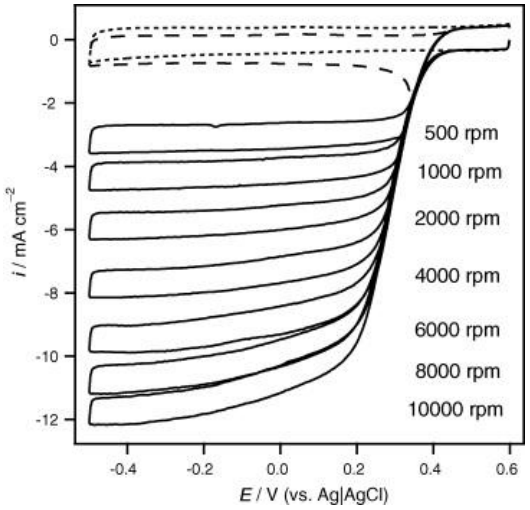

Figure 45. Cyclic voltammograms of CueO–KB-GCE in pH 5.0 McIlvaine buffer at 500 rpm (top curve), and 1000, 2000, 4000, 6000, 8000, and 10 000 rpm (bottom curve) at 1 atm O_2 and 25°C. The data were taken at the scan rate of 20 mV.s^{-1}. The dotted and dashed lines represent the CVs obtained in an Ar-saturated solution and in a quiescent O_2-saturated solution, respectively. Reproduced with permission from [637]. Copyright 2009 Elsevier

They also showed that the limiting current densities were pH independent in the 2-8 pH range. The exact kinetic mechanism of this enzyme, and particularly the role of the fifth copper, has yet to be elucidated. While it has been shown that the fifth copper of the enzyme is required to oxidize ABTS,[638] its presence is not necessary to achieve DET with an electrode surface. Kerzenmacher *et al*. have also reported the use of crude supernatants containing CueO.[639] The implementation of CueO in EBFCs using dissolved O_2 has however not been done so far.

4.2.5.4 Polyphenol oxidase

Because it was shown by Kang *et al.* that some BOD species were sensitive to urate,[640,641] which would prevent their use in blood, Cosnier *et al.* proposed to use instead the urate-tolerant tyrosinase as a cathodic enzyme. In 2010, they designed an EBFC implanted in rats with a biocathode composed of PPO, graphite and ubiquinone.[642] PPO could reduce O_2 to water in complex media, and the implanted EBFC generated P_{max} = 24.4 $\mu W.mL^{-1}$. Since a dialysis bag was needed to prevent the leaching of ubiquinone, the authors replaced ubiquinone with tetrathiafulvalene.[643] An original electrode has also been developed by Wang *et al*. A mixture of banana pulp, rich in PPO, and graphite particles, was used to elaborate a biocathode. In presence of hydroquinone, as diffusing redox mediator, the authors were able to reach 0.27 $mA.cm^{-2}$ in 0.1 M PBS pH 7.4.[644]

Non catalytic DET between PPO and graphite electrodes has been first reported in 1996 by Gorton *et al*., but the catalytic reduction of O_2 to water was not observed.[134] PPO has also been immobilized on nano titanium dioxide particles,[645] on silver electrodes,[646] on single-walled carbon nanotubes,[647] or onto glassy carbon electrodes,[648] but again catalytic electroreduction of O_2 was never achieved. The only success has been reported by Cosnier *et al.* in 2012.[649] The authors made an electrode by compressing MW-CNTs and PPO together.

With the resulting electrode, a current density of 0.55 mA.cm^{-2} was recorded at 0 V *vs.* Ag/AgCl in a 0.2 M PBS buffer pH 7 at 25°C (Fig 46A). The authors concluded that they succeeded in connecting the T3 copper to the electrode surface. Mechanistically, the authors proposed a kinetic model previously discussed for tyrosinase.[102,650] The oxy form might undergo an O-O cleavage via the DET, or via the formation of an intermediate which is further reduced at the electrode surface. After addition of 4 protons and 4 electrons, the generated deoxy form further reacts with O_2 which completes the catalytic cycle (Fig. 46B).

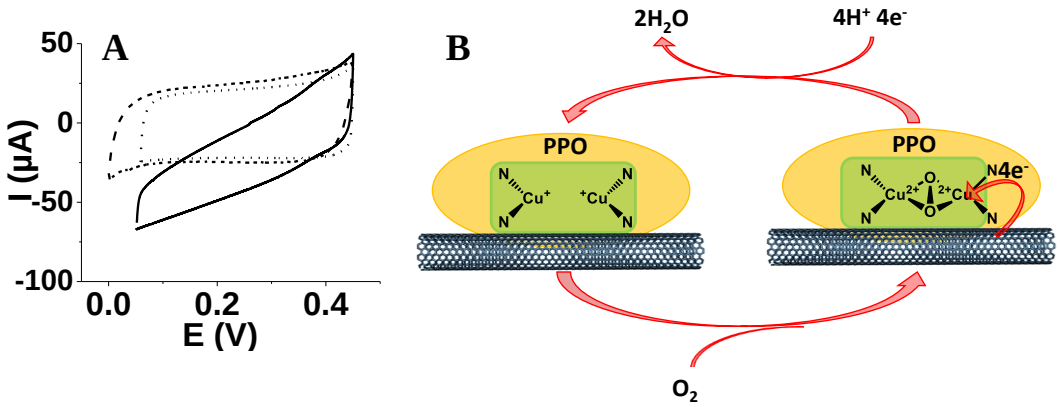

Figure 46. (A) Cyclic voltammograms recorded at MW-CNT/tyrosinase bioelectrodes in argon-deaerated solution (dotted line) or oxygen saturated solution (straight line). The dashed line corresponds to a MW-CNT electrode without tyrosinase in oxygen saturated solution (v = 0.2 mV.s^{-1}, 0.2 M PBS, pH 7, 25 °C). Adapted with permission from ref [649]. Copyright 2011 Elsevier. (B) Proposed kinetic mechanism of O_2 reduction.

5. MCOS based biocathodes in enzymatic biofuel cells

In this paragraph, we only give some examples of the implementation of MCO-based biocathodes in EBFCs. The interested reader will find in Table 1 a series of reviews published since 2004 that provide countless information on the history, applications and challenges of EBFCs. Of particular interest are the most up-to-date reviews by Rasmussen *et al.*[651] and Shleev.[89]

5.1 Glucose/O_2 EBFCs

5.1.1 Operated in buffer

As mentioned above, the first membrane-less glucose/O_2 EBFC was reported in 1999 by Katz, Willner *et al.*[627] This paper is important for the field as it was the first paper that demonstrated that by properly choosing and/or designing bioelectrocatalysts, a membrane separating anodic and cathodic compartments was not necessary. It also opened the way to miniaturized systems. However, both power density and operating voltage were quite low at that time. The next important step has been taken by Chen *et al.* two years later.[652] Their EBFCs consisted in two 7-μm diameter, 2-cm long carbon fibers respectively coated with glucose oxidase and an osmium redox polymer at the anode, and *Tv*-laccase and a second osmium redox polymer at the cathode. At 37°C, in a pH 5 aqueous solution containing 15 mM glucose, and under quiescent conditions, the EBFC reached P_{max} = 137 μW.cm^{-2} at E_{cell} = 0.4 V. Ever since, the numbers of MET and DET based glucose/O_2 EBFCs have been growing exponentially due to the envisioned applications in bodily fluids.[19,22,24,25,30,51,61,89] Laccases and BODs have been mainly used at the cathodic side in combination with glucose oxidase,[596,601,653,654] pyranose dehydrogenase,[655] PQQ-dependent glucose dehydrogenase,[426,590,656-658] FAD-dependent glucose dehydrogenase,[591,659] or cellobiose dehydrogenase[388,660-663] at the anode. It is worth mentioning that bionanodes based on enzyme cascades have also been developed[664-666] to improve the coulombic efficiency of EBFCs. One of the highest power densities was reported by Sakai *et al.* in 2009.[197] Their EBFC generated a maximum power density of 1.45 mW.cm^{-2} at 0.3 V under quiescent conditions, with a cathode based on *Mv*-BOD immobilized within a matrix composed of polylysine and $K_3[Fe(CN)_6]$.

The work of Xiao *et al.* deserves a particular attention because they reported the first and only example of EBFC operating in organic solvents containing 5 mM glucose.[276] Their

nanoporous gold EBFC was respectively modified with glucose oxidase and osmium redox polymer on the anodic side, and bilirubin oxidase and osmium redox polymer on the cathodic side. The EBFC could operate in acetonitrile, acetone and alcohols. In this latter case, the power output of the cell decreased with increasing hydrophobicity of the alcohols; methanol > ethanol > 1-propanol > 1-butanol >1-pentanol. More importantly, even though the power density was lower in organic solvents than in aqueous solvents, the anode and the cathode recovered their initial activities when transferred in aqueous buffer after operation in organic solutions. This inspiring work may lead to new applications of EBFCs, such as for example to their use in bioelectrosyntheses.

5.1.2 In fruits/vegetables

As a proof of concept of possible implantation in media containing glucose and O_2, EBFCs have been inserted in different fruits, vegetables or juices containing glucose and O_2 (Fig 47).[667-669] The first has been reported by Mano *et al.* in 2002 by inserting a Glucose/O_2 EBFC made with a *Tt*-BOD cathode within a grape (Fig 47A).[598] The O_2 mass transport limited EBFC could generate P_{max} = 2.4 $\mu W.mm^{-2}$ at E_{cell} = 0.52 V. Tsujimura *et al.* assembled in 2007 four DET based EBFCs in two oranges and two apples to light a LED (Fig 47B).[374] Miyake *et al.*[670] also implanted an EBFC in a grape, thus generating P_{max} = 111 $\mu W.cm^{-2}$ at E_{cell} = 0.25 V (Fig 47C). In 2010, Flexer *et al.*[671] reported the insertion of an EBFC in a cactus, generating P_{max} = 8 $\mu W.cm^{-2}$ at E_{cell} = 0.4 V while being able to harvest glucose and O_2 produced during photosynthesis (Fig 47D).

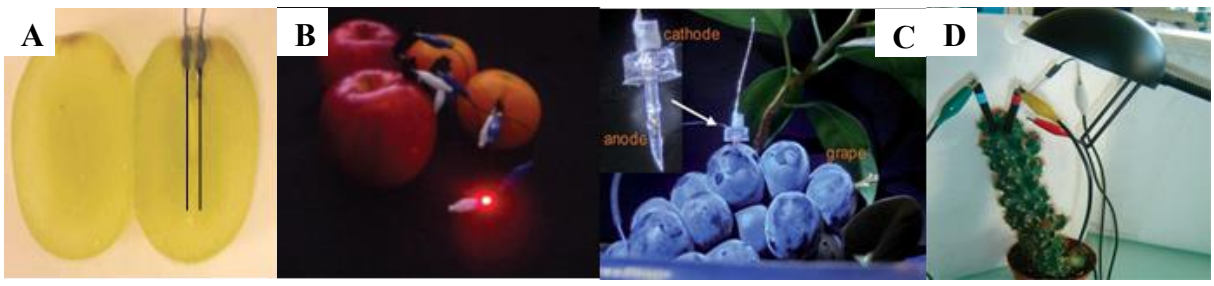

Figure 47. Different examples of EBFCs implanted in fruits and cactus. (A) in a grape[598] (Reprinted with permission from ref [598] Copyright 2003 American Chemical Society.); (B) in oranges and apples;[374] Published by the PCCP Owner Societies; (C) in grape[670] (Reproduced with permission from [670] Copyright 2011 The Royal Society of Chemistry); (D) in Cactus[671] (Reprinted with permission from [671]. Copyright 2010 American Chemical Society.

5.1.3 In vertebrates and invertebrates

40 years after the first implantation of abiotic electrodes in a sheep and a dog,[672,673] Cinquin, Cosnier *et al.* were the first to report an EBFC implanted in the abdominal cavity of a rat in 2010 (Fig 48).[642]

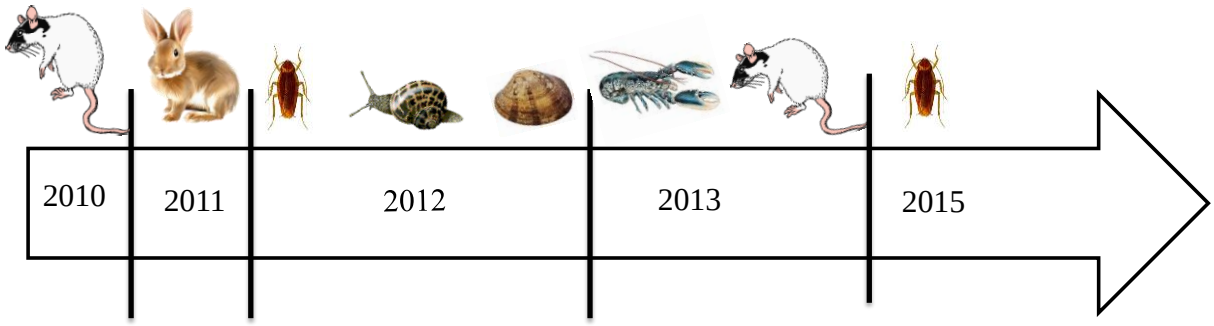

Figure 48. EBFCs implanted in animals. In rats in 2010[642] and 2013[674,675]; in rabbit in 2011[670]; in cockroaches in 2012[548] and 2015[549]; in snail [676] and clams[327] in 2012 and in lobsters in 2013 [677]. Adapted with permission from [678]. Copyright 2015, University of Bordeaux.

Their cathode was made by entrapping PPO and quinone in a graphite matrix. Their system produced P_{max} = 24.4 μW.cm^{-3} at E_{cell} = 0.13 V. In 2013, the same authors replaced PPO by *Tv*-laccase entrapped in CNTs and reached P_{max} = 193.5 μW.cm^{-2}, also upon implantation in rats.[674] In 2011, Miyake *et al.* [670] implanted an EBFC in a rabbit ear, generating P_{max} = 131 μW.cm^{-2} at E_{cell} = 0.56 V. Note that in this particular case, an air-breathing cathode made with *Mv*-BOD was used. These works were followed by a series of

implantations in various vertebrates and invertebrates which have been reviewed by Falk *et al.*[56] Because the dominant sugar in the body fluids of many insects is not glucose, the sugar of the vertebrates, but trehalose, Rasmussen *et al.*[548] designed a bi-enzymatic anode by combining glucose oxidase and trehalase. Coupled with a cathode made with *Tt*-BOD, the EBFC generated P_{max} = 55 μW.cm^{-2} at E_{cell} = 0.2 V when implanted in a cockroach. In 2015, the same authors reported[549] the wireless communication between a receiver and a cyborg cockroach modified with the same type of EBFC. In a series of paper, Katz *et al.* have implanted EBFCs in a snail (P_{max} = 30 μW.cm^{-2} at E_{cell} = 0.39 V),[676] in clams (P_{max} = 40 μW.cm^{-2} at E_{cell} = 0.17V),[327] in lobsters (P_{max} = 640 μW.cm^{-2} at E_{cell} = 0.28V)[677] and in rats (P_{max} = 70 μW.cm^{-2} at E_{cell} = 0.23V).[675] *Tv*-laccase based cathodes were used in all those EBFCs. Of interest is the experiment made by Southcott *et al.* in 2013.[679] To mimic the human blood circulating in a 8 μm capillary at 1 mm.s^{-1}, the authors elaborated a biofuel flow cell. When a human serum solution with 6.4 mM glucose concentration was used, a current density of 0.83 mAcm^{-2} was obtained with a laccase-based biocathode.

5.1.4 In serum and blood

Numerous examples of EBFCs operating in bovine or human serum can be found in the literature. To the best of our knowledge, the first EBFC operating in human serum has been reported by Gao *et al.* in 2007.[680] With a cathode based on *Mv*-BOD immobilized on carbon nanotubes, they obtained P_{max} = 5 μW.cm^{-2} at E_{cell} = 0.4 V. After further optimization of their electrodes with SW-CNTs, they reached P_{max} = 35 μW.cm^{-2} at E_{cell} = 0.39 V.[302] In 2010, P_{max} = 3 μW.cm^{-2} at E_{cell} = 0.37 V was reported for the first EBFC operating in DET with *Mv*-BOD coated on graphite electrodes.[241] In 2014, Scherbahn *et al.*[319] reached P_{max} = 45 μW.cm^{-2} at E_{cell} = 0.39 V in an unmodified serum for an EBFC cathode made with *Mv*-BOD immobilized on vertically aligned carbon nanotubes. With the same enzyme at the cathode,

P_{max} = 57.5 µW.cm^{-2} at 37°C in human serum containing 5 mM glucose was obtained by Milton *et al.*[464] Ammam *et al.* reported P_{max} = 160 µW.cm^{-2} at E_{cell} = 0.21 V on glassy carbon electrodes[564] and P_{max} = 69 µW.cm^{-2} at E_{cell} = 0.151 V on multi-walled carbon nanotubes when laccase was used.[681] The EBFC developed by Ó Conghaile *et al.*[591] generated P_{max} = 37 µW.cm^{-2} at E_{cell} = 0.26 V with a *Sc*-laccase immobilized within an osmium redox polymer, and P_{max} = 60 µW.cm^{-2} at E_{cell} = 0.3 V in artificial plasma when *Myceliophthora thermophila* laccase was used.[682] The highest power density obtained so far for an EBFC operating in human serum has been reported in 2015 by Kwon *et al.* using the device described in Figure 40. They first reached P_{max} = 1.02 mW.cm^{-2} at E_{cell} = 0.40 V in 2014[617] and then P_{max} = 1,1 mW.cm^{-2} at E_{cell} = 0.50 V in 2015.[683]

Experiments in human blood have been rarer, and only 5 can be found in the literature. In 2010, an EBFC made with a laccase entrapped within a matrix of Nafion® and poly(vinyl pyrrolidone) generated P_{max} = 5.56 µW.cm^{-2} at E_{cell} = 0.07 V.[684] However, neither the concentration of glucose nor the concentration of O_2 were provided in this work. P_{max} = 2.8 µW.cm^{-2} at E_{cell} = 0.47 V in presence of 4.6 mM glucose was reached by Wang *et al.*[663] with *Mv*-BOD immobilized in three-dimensional gold electrodes. More recently, P_{max} = 73 µW.cm^{-2} at E_{cell} = 0.3 V has been obtained by Ó Conghaile *et al.*[685] in whole blood containing 5.4 mM glucose. Their cathode was made with adsorbed *Mv*-BOD on a gold electrode modified with gold nanoparticles. The highest power density in whole and undiluted human blood so far has been reported by Cadet *et al.*[602] It was P_{max} = 129 µW.cm^{-2} at E_{cell} = 0.38 V with a glycaemia of 8.2 mM. The cathode was made with a combination of *Bp*-BOD and an osmium redox polymer (Fig 49A). The first *ex vivo* experiment in human blood under homeostatic conditions has been reported in 2016 in a vein replica.[686] The power generated by this EBFC made with a *Mv*-BOD cathode was enough to power a flexible low-voltage display (Fig 49B).

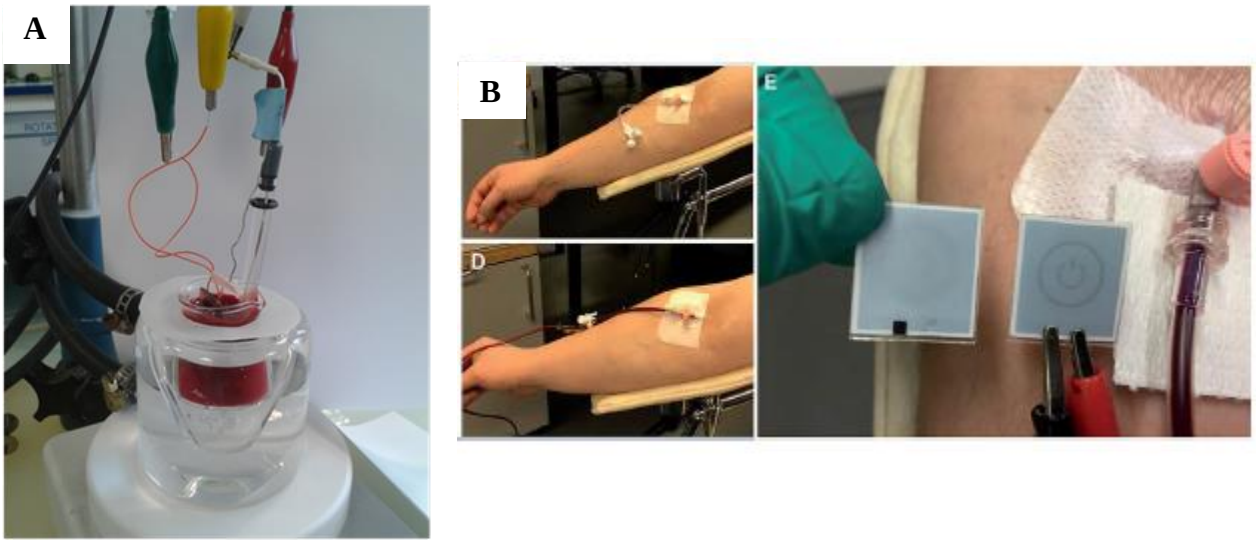

Figure 49. EBFCs operating in human blood: (A) *ex vivo* conditions. Reprinted from [602] with permission from Elsevier. (B) *ex vivo* conditions in a vein replica. Reproduced with permission from [686]. Copyright 2016 The Royal Society of Chemistry.

There are two major explanations for the low number of experiments in human blood. First, beyond respecting strict ethical guidelines for experimental practice, governmental authorizations are needed, which may be cumbersome in some countries. Then, blood contains numerous proteins, ions or molecules that may interfere, inhibit or passivate enzymes, redox mediators and electrodes. This is also the reason why power densities attained in whole human blood are lower than in serum, which is 90% water, and relatively interferent-free. In addition, the venous blood-dissolved O_2 concentration is lower than in aqueous buffers, making the cathode even more limiting than in buffer. The proof of concept that EBFCs can harvest energy for whole human blood has been, however, proven unequivocally. The first real *in vivo* experiment has yet to be done. To take this next step towards human implantation, other considerations will have to be taken into account such as biocompatibility and cytotoxicity. We note in this context that MCOs based cathodes have also been operated in other human fluids such as saliva, tears or urine.[339,391,421,685,687]

5.2 H_2/O_2 EBFCs

H_2/O_2 EBFCs have been reviewed in details by Lojou *et al*. in 2014[63] and some more recent developments have been described by Cosnier *et al*.[75] Except of the first device combining microbial H_2 oxidation and enzymatic mediated O_2 reduction by *Mv*-BOD and ABTS[496], these devices mainly rely on a hydrogenase (Hase) at the anode, and a MCO at the cathode, both operating in DET conditions (unless otherwise specified below). Even if high interests arise from the high OCV of H_2/O_2 EBFCs, and the high turnover frequencies and ability to establish DET of Hases, their story is rather short compared to that of glucose/O_2 EBFCs due to the problematic high sensitivity of most Hases towards O_2. The discovery of O_2-tolerant Hases allowed recently envisioning H_2/O_2 enzymatic BFCs. The publication in 2005 of the proof of concept of this kind of devices, that displayed a maximum power density of $5\ \mu W\ cm^{-2}$ at a cell voltage above 0.8 V at pH 5,[282,283] was followed by further developments and fundamental studies. Particular care is indeed required due to the specificities of Hase as an EBFC catalyst, and the inherent problems of the H_2 fuel that, combined with O_2, leads to explosive mixtures under certain conditions.[142,282,308] Power densities have overcome 100 $\mu W.cm^{-2}$ in 2012 thanks to the structuration of electrodes with CNTs.[142,308] The same kinds of performances were also obtained when the enzymes were immobilized at AuNP-modified electrodes.[392] H_2/O_2 EBFCs with power densities above 1 $mW.cm^{-2}$ have been developed in the groups of Armstrong[143] and Lojou.[372] In particular, the second was able to operate over a wide range of temperatures thanks to the combination of a hyperthermophilic Hase and the thermostable *Bp*-BOD, both immobilized in DET configuration at CNF-modified electrodes. In 2014 the first H_2/O_2 EBFC using an O_2-sensitive Hase was reported by Plumeré *et al.*[688] No membrane separated the anodic and cathodic compartments, and the Hase, operating via a MET mechanism, was protected from O_2 denaturation by a redox hydrogel.[689] The ability of these EBFCs to operate small devices

was also recently demonstrated.[335,381] A membrane-less H_2/O_2 EBFC using an air-breathing *Mv*-BOD cathode was reported in 2015[466], followed by the development of an EBFC using gas-diffusion electrodes both at the anode and the cathode by Kano *et al*. in 2016[467,690]. In this configuration, a maximal power density of 6.1 $mW.cm^{-2}$ at E_{cell} = 0.72 V was reached at room temperature and under quiescent conditions.[467]

Besides glucose or H_2, other fuels have been studied in combination with MCO-based biocathodes[666]: to name a few, methanol,[277,278,691] ethanol,[692-694] fructose,[470,695] ascorbate,[391] or sulfite[423] have also been reported in the literature. The interested reader will find additional information in the reviews listed in Table 1.

5.3 Microfluidic biofuel cells

MCOs based electrodes have also been used to elaborate microfluidic EBFCs even if, so far, their use for such applications is less widespread. This field has been reviewed by Kjeang *et al.*,[39] Sinton *et al.*[32] and more recently by Sanchez *et al.*[82] Microfluidic biofuel cells are usually composed of two channels, of various designs and geometries, into which circulate the respective anodic and cathodic substrates. Redox mediators and enzymes can also be added in this stream if they are not immobilized. The lack of convective mixing at low Reynolds numbers permits to eliminate the need for a membrane between the anode and cathode, therefore minimizing ohmic losses. Protons diffuse through the liquid-liquid interface between the two substrate streams. Despite the conceptual simplicity, numerous difficulties can be encountered such as the cross-diffusional mixing of substrates at the interface between the two streams. The fabrication of the microchannel and the lengths/diameters of the electrodes require particular care. One of the first use of a MCO-based biocathode in a microfluidic BFC has been reported by Palmore *et al.*[696] The anolyte consisted of 10 mM ABTS and the catholyte of 10 mM ABTS and 0.5 $mg.mL^{-1}$ of laccase.

Different strategies have been later proposed to immobilize the enzymes.[697] While PDMS has mainly been used to create microfluidic EBFCs, paper based microfluidic EBFCs are now emerging. For example, a compact and low volume carbon paper-based enzymatic microfluidic glucose/O_2 biofuel cell has been reported recently.[698] Over the 2.5-30 mM glucose concentration range, the power density was a linear function of the glucose concentration, and ranged from 20 to 90 µW.cm^{-2}.

5.4 Paper based EBFCs

Despite the low price of paper, its availability and ease of use, the first example of paper based EBFCs has only been reported in 2012 by Jenkins *et al.* with Whatman filter paper.[699] Its versatility allowed its use for various types of EBFCs. For example, Japanese paper has been used by Tsujimura *et al.*[369] to construct a flexible and high performance EBFC with an O_2 breathing cathode (Fig 50).

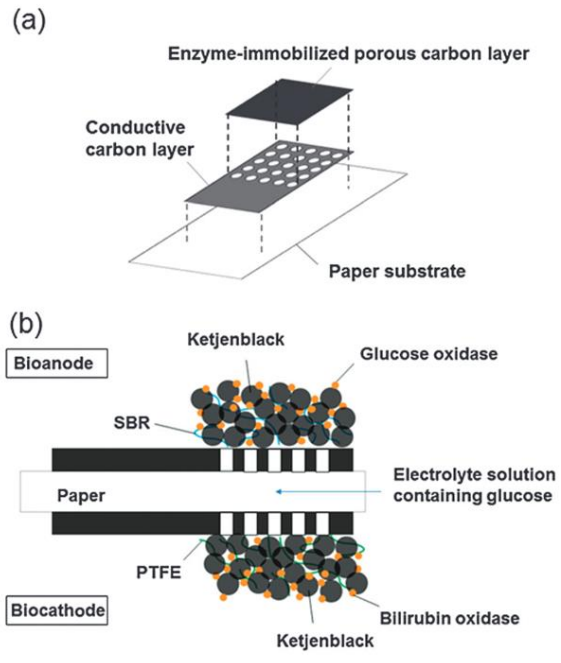

Figure 50. Illustratic us carbon electrode for bioanode or biocatho ed with permission from [369]. Copyright 2013 The Royal Society of Chemistry.

Japanese paper has been chosen because it has a high water absorbency. To be made conductive, it was first coated with a carbon ink. On the anodic side, the electrode was further

modified with a mixture of Ketjen black, glucose oxidase and tetrathiafulvalene. At the cathode, a mixture of KB and polytetrafluoroethylene was coated on the conductive paper before *Mv*-BOD addition. The power density of the fabricated EBFC reached 0.12 $mW.cm^{-2}$ at E_{cell} = 0.4 V in presence of 100 mM glucose in a 1 M phosphate buffer pH 7 at room temperature, which was the highest power reported in 2013. Paper based electrodes have also been used in microfludidic EBFCs,[700] in self-powered systems,[701] or to elaborate a self-powered hybrid micro-supercapacitor integrated system.[702] All used MCO-based cathodes. A recent and excellent review by Desmet *et al.*[76] summarizes the use of paper electrodes in biofuel cells.

5.5 MCOs with air-breathing electrodes

Most of the EBFCs are limited by the cathode because of the low diffusion coEfficient ($< 5.10^{-5}$ $cm^{-2}.s^{-1}$) and concentration of dissolved O_2 (~1.2 mM maximum at neutral pH) in aqueous solution. Increasing the low current densities and enhancing mass transport on the cathodic side are key challenges in EBFCs. These limitations could be circumvented by using an air-breathing cathode, where O_2 would diffuse directly from the air to the cathode. In 2005, Calabrese-Barton[703] reported a particularly interesting numerical simulation of a MCO-based cathode. The authors predicted that in an O_2 saturated pH 5 buffer at 37°C, a maximum current density of 9.2 $mA.cm^{-2}$ could be attained with dissolved oxygen. By introducing an air-breathing cathode, the model predicted that j_{max} = 60 $mA.cm^{-2}$ in air or j_{max} = 100 $mA.cm^{-2}$ in pure O_2 could be reached. However, designing a gas-diffusion cathode is not trivial. The gas-diffusion cathode usually consists of two layers: a gas-diffusion layer made of hydrophobized carbon black[704,705] or Ketjen black[690,706,707], which has to be permeable to gas; a hydrophilic catalytic layer made with carbon black[708], carbon cloth[709], CNTs[710-712] or carbon felt[713] and containing the MCO. These first two layers may also be added on top of a third

layer providing for mechanical stability. A delicate balance between hydrophobicity and hydrophilicity of the carbon/air and carbon/electrolyte interfaces has to be achieved (Fig 51).

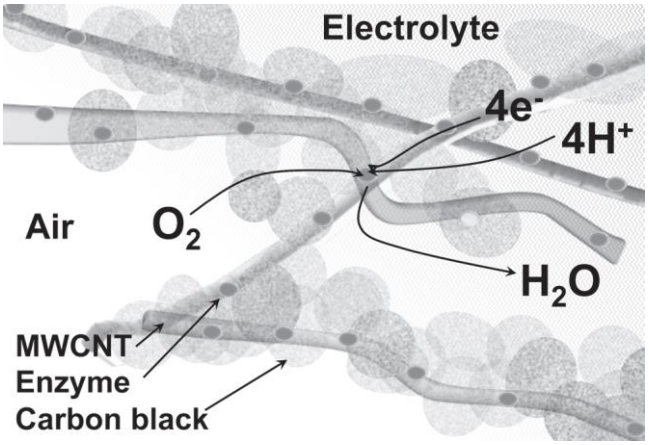

Figure 51. Schematic of the three-phase interphase of a gas-diffusion electrode. Reproduced with permission from [307] Copyright 2012 John Wiley and Sons.

It is challenging to obtain a tri-phase interface allowing simultaneously adequate immobilization of the MCO, and performant diffusion of gas and electrolytes. Design of experiments have been used to optimize such interface.[714] DET and MET based air-breathing electrodes have been reported with BODs,[368,466,712,715] laccases[708,709,716] and CueO.[706] For example, Atanassov *et al.* reported a DET-based laccase-modified gas-diffusion electrode with a current density ~0.5 $mA.cm^{-2}$.[307] 20 $mA.cm^{-2}$ have been reached for a DET-based CueO biocathode.[706] An interesting approach has been reported recently by Atanassov *et al.*[717] who combined BOD and non-platinum based catalysts. j_{max} = 1.2 $mA.cm^{-2}$ was reached in a 0.1 M phosphate buffer pH 7.5. MCO-based gas-diffusion electrode have been used in H_2/O_2,[466,467,690] methanol/O_2[718] or in fructose/O_2 biofuel cells.[305,368]

5.6 Biofuel cells for self-powered devices

Self-powered sensing devices do not need any external power source, and usually consist of only two electrodes. One electrode acts as the sensing part and both electrodes

combined together provide the power for the sensing device. The power output is usually proportional to the concentration of the analyzed substrate. The first self-powered system for the measurement of glucose using an EBFC, made with a glucose oxidase anode and an O_2-reducing cathode combining Cyt C and COx, has been reported by Willner and Katz in 2001.[632] Katz *et al.* have also pioneered the use of MCO-based cathodes to develop EBFCs with switchable power output and their use in enzymatic logic systems.[34,633,719-723] The principle of such systems has been described in their first report in 2009.[724] It is based on the dependence on pH of swelling/deswelling of the redox hydrogel used to immobilize the laccase (Fig 52).

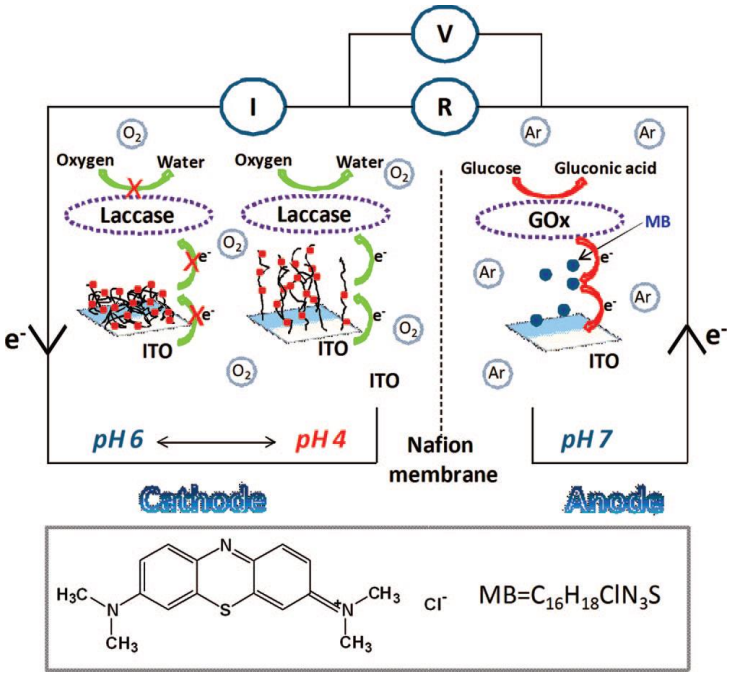

Figure 52. The Biofuel Cell Composed of the pH-Switchable Logically Controlled Biocatalytic Cathode and Glucose-Oxidizing Anode. Reprinted with permission from [724]. Copyright 2009 American Chemical Society.

The authors synthesized a polymer brush covalently functionalized with osmium redox centers. For pH > 5.5, mediated electron transfer was prohibited because of the shrinkage of the hydrogel; while for pH < 4.5, the fully swollen and hydrated hydrogel

allowed electron transfer. Two Boolean logic gates (AND/OR) were assembled using this concept. MCO-based biocathodes have also been used for example for self-powered immune sensors,[725] self-powered biosensors for arsenite and arsenate,[726] lactate biosensors,[336] antiobitic residue determination,[727,728]glucose measurement with amperometric[602] or optical readout,[729] neurochemical monitoring in rat brain,[730] self-powered fluorescence switch systems,[731] or for wireless signal transmission.[732] This field has been reviewed by Zhou *et al.*[43,47] and by Arechederra *et al.*[45]

5.7 Hybrid bio-devices

Hybrid biodevices exhibit dual function and are a combination of an enzymatic biofuel cell and an electrochemical capacitor. Once charged by the internal EBFC, the device can be discharged as a supercapacitor. The concept and denomination of "self-charging electrochemical biocapacitor" have been first published in 2014 by Pankratov *et al.*[733] Their 2-electrodes device is illustrated in Figure 53.

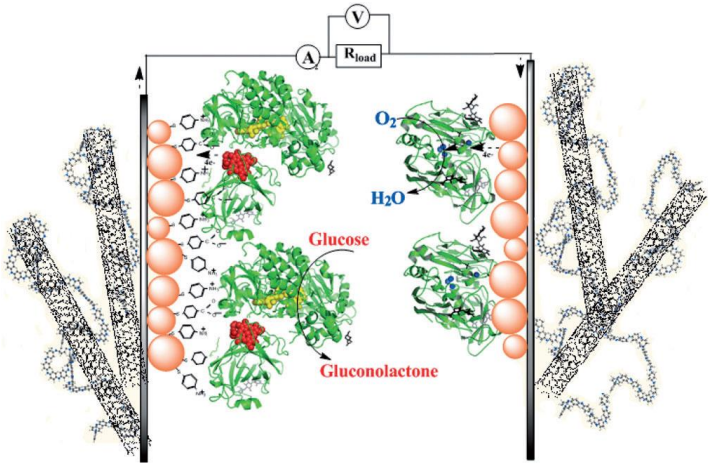

Figure 53. Schematic representation of a self-charging biological supercapacitor. The electrochemical capacitor is built using a graphite foil modified with a polyaniline/CNTs composite on one side (the capacitive side/face), and the enzymatic fuel cell is designed from three-dimensional gold NPs based nanobiostructures on the other (the charging side/face). Gold NPs: pink-orange spheres; thiol layer: black sticks. The structure of bilirubin oxidase was taken from the know crystal structure (PDB: 2XLL) and cellobiose dehydrogenase was

rendered using the cytochrome and the FAD domains of the enzyme from Phanerochaete chrysosporium (PDB: 1D7D and 1NAA, respectively). Protein globule: green ribbons; copper ions: blue spheres; heme: red spheres; FAD: yellow spheres; carbohydrates: black sticks. Reprinted with permission from [733] .Copyright 2014 Wiley-VCH Verlag GmbH & Co. KGaA.

One side of both electrodes was made of graphite modified with CNTs and polyaniline. The other face was modified with the enzyme (resp. cellobiose dehydrogenase or *Mv*-BOD) immobilized on gold nanoparticles. In an aerated PBS pH 7.4 buffer containing 50 mM glucose, the device displayed excellent reproducibility upon 4 cycles of charge/discharge, and provided a power density P_{max} = 1.2 mW.cm^{-2} at E_{cell} = 0.38 V, without being optimized. The authors reported also the same year a self-charging ascorbate/O_2 electrochemical capacitor.[734] In 2014 also, Cosnier *et al.*[735] published a similar concept using CNT matrixes modified with *Tv*-laccase. The authors demonstrated that their hybrid system was stable for at least 40 000 pulses of 2 mW. In 2016, the first self-charging Nernstian bio-supercapacitor operating with an identical redox mediator at the anode and cathode was reported.[736] In 2017, Xiao *et al.*[737] reported a hybrid device using *Mv*-BOD immobilized on de-alloyed nanoporous gold. Good operational stability was observed for 50 charge/discharge cycles at j = 0.2 mA cm^{-2}. A power density of 608.8 μW.cm^{-2} was obtained when discharged at 2 mA cm^{-2}, *i.e.* 468 higher than the power output of the BFC itself. The work of Bilewicz *et al.* using a laccase-based cathode deserves also attention in this field.[738-741] For example, they used a biocathode covered with laccase adsorbed on naphthylated multiwalled carbon nanotubes to elaborate an hybrid devices generating P_{max} = 1.6 mW.cm^{-2} at E_{cell} = 0.76 V. Hybrid devices may also rely on solar power, which allows simultaneous solar energy conversion and storage. Nanostructured indium tin oxide electrodes were therefore used.[742,743] This new promising

field, which may circumvent low power densities and substrates depletion arising in EBFCs, has been reviewed in 2014 by Pankratov *et al.*[67] and in 2016 by Sode *et al.*[79]

5.8. Wearable biofuel cells

Wearable electronics, and particularly wearable electrochemical sensors, have attracted recently a lot of attention.[744] Since they are likely to be in contact with the human skin or human tears[80,339], they should be flexible, light, and biocompatible. The detection of a wide variety of substrates, ranging from glucose to uric acid has been realized. Even more recently, the use of wearable biofuel cells has been envisioned as a power source for wearable applications. Bandodkar has written two reviews on this subject.[745,746] Surprisingly, Pt has been preferred so far to MCOs as the cathodic catalyst. For example, an epidermal EBFC able to harvest chemical energy from human perspiration and particularly from lactate,[747] or the fabrication of a wearable biofuel cell printed directly onto textile substrates have been reported.[748] In both cases, Pt was the catalyst of O_2-reduction. In 2014 however, *Mv*-BOD has been used by Ogawa *et al.*[749] The authors developed an organic transdermal iontophoresis patch with an integrated EBFC (Fig 54). The anodic electrode was made with fructose dehydrogenase coated on a CNT-modified carbon strip, and an O_2 diffusion cathode was based on *Mv*-BOD. Once immobilized on the skin, the OCP was 0.75 V and the maximal current density 300 $\mu A.cm^{-2}$.

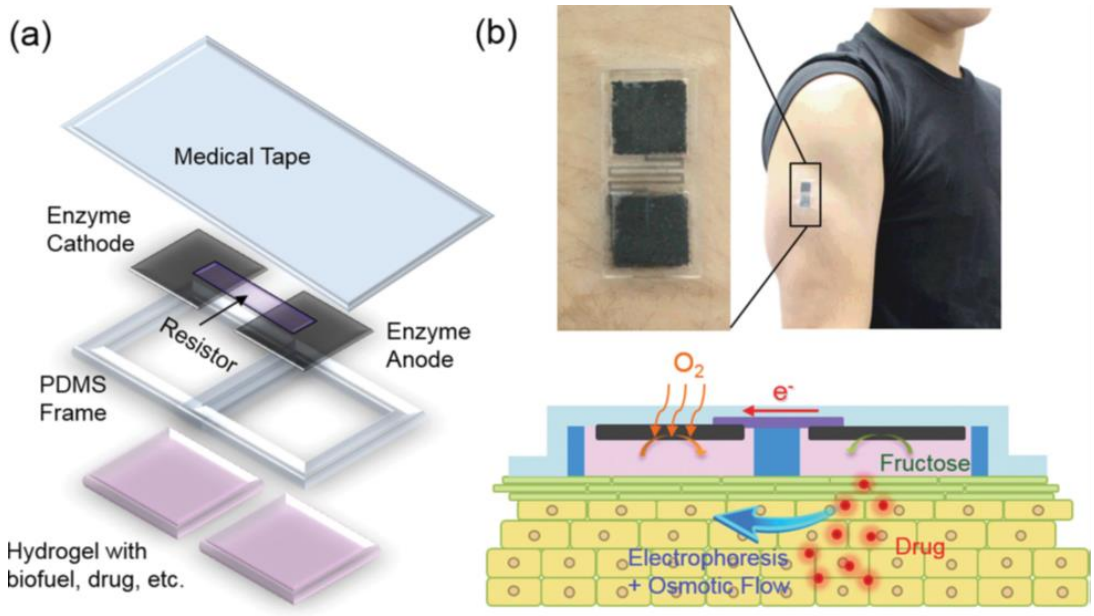

Figure 54. (A) Schematic of the transdermal iontophoresis patch that is an assembly of enzyme-modified CFs that serve as the electrodes, hydrogel films containing a biofuel and a chemical to be delivered, a conducting polymer-based stretchable resistor, a poly(dimethylsiloxane) (PDMS) frame, and O_2 permeable medical tape. (B) Photograph of the patch mounted on a human arm, and a schematic of the iontophoresis-assisted drug delivery mechanism. The fructose/O_2 biofuel cell generates a transdermal ionic current that is accompanied by an osmotic flow from the anode to the cathode, thereby assisting the electrophoretic movement of small molecules into the skin. Reprinted with permission from [749] Copyright 2015 Wiley-VCH Verlag GmbH & Co. KGaA

6. Conclusions and Outlook

The major cause of inefficiency in common EBFCs, envisioned as energy-converting devices for more than half a century, is the four-electron electroreduction of oxygen to water, particularly because of the low concentration and slow diffusion of O_2 in aqueous media. Studies in the recent decades aimed to overcome this limitation. We have witnessed an exponential growth in publications on optimizing MCO-based biocathodes. The different strategies that have been put forward are listed in Table 1. Two major research axes have

developed: 1) design of increasingly sophisticated nanostructured porous electrodes, allowing increased enzyme loadings without impeding the diffusion of O_2[91] and 2) improvement of the electrical connection between MCOs and the electrode surfaces, whether in MET or DET.[750] The continuous increase in OCP, current densities or power densities reflect particularly well the significant progress made along the two lines of research.

The studies have led to a fundamental milestone with the first implantation in a vertebrate and to a second milestone with the first operation in human blood. The latter now raises new questions and exciting challenges, such as immunogenicity, bioinertness and cytotoxicity issues. Solutions have to be found to minimize the reaction with the foreign body. It is likely that a protective/bioinert coating or membrane will be required to minimize the foreign body reaction. It must not be, however, detrimental to O_2 diffusion.

Because the enzymatic reduction of O_2 is becoming increasingly Efficient, new applications have emerged e.g. in wearable enzymatic biofuel cells and new promising field such has the development of hybrid supercapacitors, which may circumvent low power densities and substrates depletion arising in EBFCs.

In their 2004 pioneering review on EBFCs Calabrese-Barton and Atanassov[19] said that the development of successful biofuel cells is driven by demand arising from specific applications. The low current densities prevented the use of EBFCs in most of applications. However, high current densities are not a prerequisite in some, as a current of a few pA suffices, when the voltage is high enough, to power ACSICs.[751] For high power applications, EBCs/supercapacitor systems are of particular interest due to their ability to deliver high power densities within a very short burst.

Despite enormous advances and encouraging achievements, some limitations remain. One of the most underappreciated problem is the stability. Relatively few studies are dedicated to the study of stability of immobilized MCOs[231], and even fewer deal with their

thermostability. Stability studies are often only corollaries of other optimizations. If one envisions the use of EBFCs in medical or other long-term applications, this problem has to be tackled. As discussed in this review, the causes of the poor stability of MCOs immobilized on electrode surfaces are many and most are interrelated. Fundamental and mechanistic studies are needed to resolve these issues. Because electrochemistry by itself does not permit to link the catalytic stability with the structure/conformation of proteins, the electrochemical studies must be combined with others. Enzyme engineering can be a valuable tool to improve the stability/thermostability of MCOs in homogeneous solutions. However, solution phase stability does not predict the stability of immobilized enzymes. This is particularly well illustrated by their inhibition by halides. Inhibition by Cl^- varies between the MCOs, and differs for different MCOs immobilized on different electrodes, as well as for MET, depending on the redox mediator used. Again the combination of different analytical techniques in homogeneous and heterogeneous conditions is required to enhance our understanding of the MCOs and further improve cathodes for EBFCs applications.

In addition to catalyzing reactions in biofuel cells, enzymes also inspire the design of analogous inorganic and metal-organic catalysts.[752-754] "Bio-inspired" catalysts aim to reproduce the metal coordination observed in biological molecules to attain similar efficiency in a less complex structure. Further development is expected also along this axis.

7. Acknowledgments

The authors thank Prof Adam Heller (The university of Texas-Austin-USA) for critical reviewing/editing this MS. NM thanks his past PhD/Post Doctoral students and collaborators as indicated in the references cited for their outstanding contributions to this field. AP thanks her collaborators at the Laboratory of Bioenergetics and Protein Engineering, and especially Drs. V. Fourmond, M. Ilbert, E. Lojou, I. Mazurenko and M. Roger for fruitful

discussions. NM also acknowledges support from the Région Aquitaine, the Agence Nationale de la Recherche (12-BS08-0011-01 and 16-CE19-0001-02), the European project BIOENERGY (FP7-PEOPLE-2013-ITN607793) and the Labex AMADEus (ANR-10-LABX-0042-AMADEus) belonging to the program Initiative d'Excellence IdEx Bordeaux (ANR-10-IDEX-003-02).

Biographies:

Nicolas Mano is senior researcher at the CNRS. He received his Ph.D. from the University of Bordeaux (France) under the supervision of Prof Alexander Kuhn in 2001. He then carried out postdoctoral studies at the University of Texas at Austin (USA) with Prof Adam Heller, working towards the development of glucose sensors and miniature membrane-less glucose/O_2 biofuel cells. In 2006, he integrated the CNRS and created his team at the Centre de Recherche Paul Pascal located in Pessac (France) working on different fields of bioelectrochemistry with a special emphasis on biofuel cells. He also developed an activity in enzymes engineering on various oxidases including bilirubin oxidases. His contribution to the field of bioelectrochemistry has been recognized by numerous National and International Prizes

Anne de Poulpiquet got interested in electroenzymatic O_2 reduction during her PhD dedicated to the development of enzymatic H_2/O_2 biofuel cells. She obtained her degree under the direction of Dr. Elisabeth Lojou at Aix-Marseille University (France). After a postdoctoral stay at the Institute of Molecular Sciences in Bordeaux (France), she joined the Bioenergetic and Protein Engineering Laboratory (Marseille, France) as an assistant professor. Her research interests now focus on coupling electrochemistry to optical techniques to study the electro-enzymatic reactivity.

8. References

(1) Farquhar, J.; Bao, H. M.; Thiemens, M. Atmospheric Influence of Earth's Earliest Sulfur Cycle. *Science* **2000,** *289*, 756-758.

(2) Festa, R. A.; Thiele, D. J. Copper: an Essential Metal in biology. *Current Biology* **2011,** *21*, R877-R883.

(3) Ridge, P. G.; Zhang, Y.; Gladyshev, V. N. Comparative Genomic Analyses of Copper Transporters and Cuproproteomes Reveal Evolutionary Dynamics of Copper Utilization and Its Link to Oxygen. *Plos One* **2008,** *3*.

(4) Muttkowski, R. A. Copper: Its Occurrence and Role in Insects and Other Animals. *Trans Am. Microsc. Soc.* **1921,** *40*, 144-157.

(5) Solomon, E. I.; Heppner, D. E.; Johnston, E. M.; Ginsbach, J. W.; Cirera, J.; Qayyum, M.; Kieber-Emmons, M. T.; Kjaergaard, C. H.; Hadt, R. G.; Tian, L. Copper Active Sites in Biology. *Chem. Rev.* **2014,** *114*, 3659-3853.

(6) Liu, J.; Chakraborty, S.; Hosseinzadeh, P.; Yu, Y.; Tian, S. L.; Petrik, I.; Bhagi, A.; Lu, Y. Metalloproteins Containing Cytochrome, Iron-Sulfur, or Copper Redox Centers. *Chem. Rev.* **2014,** *114*, 4366-4469.

(7) Solomon, E. I.; Szilagyi, R. K.; George, S. D.; Basumallick, L. Electronic Structures of Metal Sites in Proteins and Models: Contributions to Function in Blue Copper Proteins. *Chem. Rev.* **2004,** *104*, 419-458.

(8) Yoshikawa, S.; Shimada, A. Reaction Mechanism of Cytochrome *c* Oxidase. *Chem. Rev.* **2015,** *115*, 1936-1989.

(9) Debe, M. K. Electrocatalyst Approaches and Challenges for Automotive Fuel Cells. *Nature* **2012,** *486*, 43-51.

(10) Tiwari, J. N.; Tiwari, R. N.; Singh, G.; Kim, K. S. Recent Progress in the Development of Anode and Cathode Catalysts for Direct Methanol Fuel Cells. *Nano Energy* **2013,** *2*, 553-578.

(11) Shleev, S.; Andoralov, V.; Pankratov, D.; Falk, M.; Aleksejeva, O.; Blum, Z. Oxygen Electroreduction versus Bioelectroreduction: Direct Electron Transfer Approach. *Electroanalysis* **2016,** *28*, 2270-2287.

(12) Kjaergaard, C. H.; Rossmeisl, J.; Norskov, J. K. Enzymatic versus Inorganic Oxygen Reduction Catalysts: Comparison of the Energy Levels in a Free-Energy Scheme. *Inorg. Chem.* **10,** *49*, 3567-3572.

(13) Zagal, J.; Bindra, P.; Yeager, E. A Mechanistic Study of O_2 Reduction of Water Soluble Phtalocyanines Adsorbed on Graphite Electrodes. *J. Electrochem. Soc.* **1980,** *127*, 1506-1517.

(14) Shi, C. N.; Anson, F. C. Catalytic Pathways for the Electroreduction of O_2 by Iron Tetrakis(4-N-methylpyridyl)porphyrin or Iron Tetraphenlyporphyrin Adsorbed on Edge Plane Pyrolytic Graphite Electrodes. *Inorg. Chem.* **1990,** *29*, 4298-4305.

(15) Heller, A. Integrated Medical Feedback Systems for Drug Delivery. *AIChE Journal* **2005,** *51*, 1054-1066.

(16) Mano, N.; Soukharev, V.; Heller, A. A Laccase-Wiring Redox Hydrogel for Efficient Catalysis of O_2 Electroreduction. *J. Phys. Chem. B* **2006,** *110*, 11180-11187.

(17) dos Santos, L.; Climent, V.; Blanford, C. F.; Armstrong, F. A. Mechanistic Studies of the 'Blue' Cu Enzyme, Bilirubin Oxidase, as a Highly Efficient Electrocatalyst for the Oxygen Reduction Reaction. *Phys. Chem. Chem. Phys.* **2010,** *12*, 13962-13974.

(18) Shleev, S.; Tkac, J.; Christenson, A.; Ruzgas, T.; Yaropolov, A. I.; Whittaker, J. W.; Gorton, L. Direct Electron Transfer between Copper-containing Proteins and Electrodes. *Biosens. Bioelectron.* **2005,** *20*, 2517-2554.

(19) Barton, S. C.; Gallaway, J.; Atanassov, P. Enzymatic Biofuel Cells for Implantable and Microscale Devices. *Chem. Rev.* **2004,** *104*, 4867-4886.

(20) Shukla, A. K.; Suresh, P.; Berchmans, S.; Rajendran, A. Biological Fuel Cells and Their Applications. *Curr. Sci.* **2004,** *87*, 455-468.

(21) Kim, J.; Jia, H.; Wang, P. Challenges in Biocatalysis for Enzyme-Based Biofuel Cells. *Biotech. Adv.* **2006,** *24*, 296-308.

(22) Bullen, R. A.; Arnot, T. C.; Lakeman, J. B.; Walsh, F. C. Biofuel Cells and Their Development. *Biosens. Bioelectron.* **2006,** *21*, 2015-2045.

(23) Heller, A. Potentially Implantable Miniature Batteries. *Anal. Bioanal. Chem.* **2006,** *385*, 469-473.

(24) Davis, F.; Higson, S. P. Biofuel Cells - Recent Advances and Applications. *Biosens. Bioelectron.* **2007,** *22*, 1224-1235.

(25) Minteer, S. D.; Liaw, B. Y.; Cooney, M. J. Enzyme-Based Biofuel Cells. *Curr. Opin. Biotechnol.* **2007,** *18*, 228-234.

(26) Kerzenmacher, S.; Ducrée, J.; Zengerle, R.; von Stetten, F. Energy Harvesting by Implantable Abiotically Catalyzed Glucose Fuel Cells. *J. Power Sources* **2008,** *182*, 1-17.

(27) Cracknell, J. A.; Vincent, K. A.; Armstrong, F. A. Enzymes as Working or Inspirational Electrocatalysts for Fuel Cells and Electrolysis. *Chem. Rev.* **2008,** *108*, 2439-2461.

(28) Cooney, M. J.; Svoboda, V.; Lau, C.; Martin, G.; Minteer, S. D. Enzyme Catalysed Biofuel Cells. *Energy Environ. Sci.* **2008,** *1*, 320-337.

(29) Moehlenbrock, M. J.; Minteer, S. D. Extended Lifetime Biofuel Cells. *Chem. Soc. Rev.* **2008,** *37*, 1188-1196.

(30) Willner, I.; Yan, Y.; Willner, B.; Tel-Vered, R. Integrated Enzyme-Based Biofuel Cells - A Review. *Fuel Cells* **2009,** *9*, 7-24.

(31) Ramanavicius, A.; Ramanaviciene, A. Hemoproteins in Design of Biofuel Cells. *Fuel Cells* **2009,** *9*, 25-36.

(32) Kjeang, E.; Djilali, N.; Sinton, D. Microfluidic Fuel Cells: A Review. *J. Power Sources* **2009,** *186*, 353-369.

(33) Aquino Neto, S.; de Andrade, A. R. An Overview of Enzymatic Biofuel Cells. *Electrocatalysis* **2010,** *1*, 87-94.

(34) Katz, E. Biofuel Cells with Switchable Power Output. *Electroanalysis* **2010,** *22*, 744-756.

(35) Güven, G.; Prodanovic, R.; Schwaneberg, U. Protein Engineering – an Option for Enzymatic Biofuel Cell Design. *Electroanalysis* **2010,** *22*, 765-775.

(36) Ivanov, I.; Vidaković-Koch, T.; Sundmacher, K. Recent Advances in Enzymatic Fuel Cells: Experiments and Modeling. *Energies* **2010,** *3*, 803-846.

(37) Gellet, W.; Kesmez, M.; Scumacher, J.; Akers, N. L.; Minteer, S. Biofuel Cells for Portable Power. *Electroanalysis* **2010,** *22*, 727-731.

(38) Hao Yu, E.; Scott, K. Enzymatic Biofuel Cells - Fabrication of Enzyme Electrodes. *Energies* **2010,** *3*, 23-42.

(39) Lee, J. w.; Kjeang, E. A Perspective on Microfluidic Biofuel Cells. *Biomicrofluidics* **2010,** *4*, 041301.

(40) Brito, P.; Turner, A. P. F. Mediated Biocatalytic Electrodes and Enzyme Stabilisation for Power Generation. *Electroanalysis* **2010,** *22*, 732-743.

(41) Caruana, D. J.; Howorka, S. Biosensors and Biofuel Cells with Engineered Proteins. *Mol. BioSyst.* **2010,** *6*, 1-9.

(42) Rubenwolf, S.; Kerzenmacher, S.; Zengerle, R.; von Stetten, F. Strategies to Extend the Lifetime of Bioelectrochemical Enzyme Electrodes for Biosensing and Biofuel Cell Applications. *Appl. Microbiol. Biotechnol.* **2011,** *89*, 1315-1322.

(43) Zhou, M.; Dong, S. Bioelectrochemical Interface Engineering: toward the Fabrication of Electrochemical Biosensors, Biofuel Cells and Self Powered Logic Biosensors. *Acc. Chem. Res.* **2011,** *44*, 1232-1243.

(44) Opallo, M.; Bilewicz, R. Recent Developments of Nanostructured Electrodes for Bioelectrocatalysis of Dioxygen Reduction. *Adv. Phys. Chem.* **2011,** *doi:10.1155/2011/947637*.

(45) Arechederra, R. L.; Minteer, S. D. Self-Powered Sensors. *Anal. Bioanal. Chem.* **2011,** *400*, 1605-1611.

(46) Osman, M. H.; Shah, A. A.; Walsh, F. C. Recent Progress and Continuing Challenges in Bio-Fuel Cells. Part I : Enzymatic Cells. *Biosens. Bioelectron.* **2011,** *26*, 3087-3102.

(47) Zhou, M.; Wang, J. Biofuel Cells for Self-Powered Electrochemical Biosensing and Logic Biosensing: a Review. *Electroanalysis* **2012,** *24*, 197-209.

(48) Freguia, S.; Virdis, B.; Harnisch, F.; Keller, J. Bioelectrochemical Systems: Microbial versus Enzymatic Catalysis. *Electrochim. Acta* **2012,** *82*, 165-174.

(49) Minteer, S. D.; Atanassov, P.; Luckarift, H. R.; Johnson, G. New Materials for Biological Fuel Cells *Materials Today* **2012,** *15*, 166-173.

(50) Yang, X.-Y.; Tian, G.; Jiang, N.; Su, B.-L. Immobilization Technology: a Sustainable Solution for Biofuel Cell Design. *Energy Environ. Sci.* **2012,** *5*, 5540-5563.

(51) Leech, D.; Kavanagh, P.; Schuhmann, W. Enzymatic Fuel Cells: Recent Progress *Electrochim. Acta.* **2012,** *84*, 223-234.

(52) Holzinger, M.; Le Goff, A.; Cosnier, S. Carbon Nanotube/Enzyme Biofuel Cells. *Electrochim. Acta.* **2012,** *82*, 179-190.

(53) Mano, N. Features and Applications of Bilirubin Oxidases. *Appl. Microbiol. Biotechnol.* **2012,** *96*, 301-307.

(54) Lapinsonnière, L.; Picot, M.; Barrière, F. Enzymatic versus Microbial Bio-Catalyzed Electrodes in Bio-Electrochemical Systems. *ChemSusChem* **2012,** *5*, 995-1005.

(55) Falk, M.; Blum, Z.; Shleev, S. Direct Electron Transfer Based Enzymatic Fuel Cells. *Electrochim. Acta* **2012,** *82*, 191-202.

(56) Falk, M.; Narváez Villarrubia, C. W.; Babanova, S.; Atanassov, P.; Shleev, S. Biofuel Cells for Biomedical Applications: Colonizing the Animal Kingdom. *ChemPhysChem* **2013,** *14*, 2045-2058.

(57) Liu, Y.; Du, Y.; Li, C. M. Direct Electrochemistry Based Biosensors and Biofuel Cells Enabled with Nanostructured Materials. *Electroanalysis* **2013,** *25*, 815-823.

(58) Mano, N.; Edembe, L. Bilirubin Oxidases in Bioelectrochemistry: Features and Recent Findings. *Biosens. Bioelectron.* **2013,** *50*, 478-485.

(59) Katz, E.; MacVittie, K. Implanted Biofuel Cells Operating *in vivo* – Methods, Applications and Perspectives *Energy Environ. Sci.* **2013,** *6*, 2791-2803.

(60) Aquino Neto, S.; De Andrade, A. R. New Energy Sources: the Enzymatic Biofuel Cell. *J. Braz. Chem. Soc.* **2013,** *24*, 1891-1912.

(61) Luz, R. A. S.; Pereira, A. R.; de Souza, J. C. P.; Sales, F. C. P. F.; Crespilho, F. N. Enzyme Biofuel Cells: Thermodynamics, Kinetics and Challenges in Applicability. *ChemElectroChem* **2014,** *1*, 1751-1777.

(62) Wen, D.; Eychmüller, A. Enzymatic Biofuel Cells on Porous Nanostructures. *Small* **2016,** *12*, 4649-4661.

(63) de Poulpiquet, A.; Ranava, D.; Monsalve, K.; Giudici-Orticoni, M.-T.; Lojou, E. Biohydrogen for a New Generation of H_2/O_2 Biofuel Cells: a Sustainable Energy Perspective. *ChemElectroChem.* **2014,** *1*, 1724-1750.

(64) de Poulpiquet, A.; Ciaccafava, A.; Lojou, E. New Trends in Enzyme Immobilization at Nanostructured Interfaces for Efficient Electrocatalysis in Biofuel Cells. *Electrochim. Acta* **2014,** *126*, 104-114.

(65) Nguyen, T. H.; Fraiwan, A.; Choi, S. Paper-Based Batteries: a Review. *Biosens. Bioelectron.* **2014,** *54*, 640-649.

(66) Cosnier, S.; Holzinger, M.; Le Goff, A. Recent Advances in Carbon Nanotubes-Based Enzymatic Fuel Cells. *Front. Bioeng. Biotechnol.* **2014,** *2*, 45.

(67) Pankratov, D.; Blum, Z.; Shleev, S. Hybrid Electric Power Biodevices. *ChemElectroChem* **2014,** *1*, 1798-1807.

(68) Ammam, M. Electrochemical and Electrophoretic Deposition of Enzymes: Principles, Differences and Application in Miniaturized Biosensor and Biofuel Cell Electrodes. *Biosens. Bioelectron.* **2014,** *58*, 121-131.

(69) Filip, J.; Tkac, J. Is Graphene Worth Using in Biofuel Cells? *Electrochim. Acta* **2014,** *136*, 340-354.

(70) Vazquez-Duhalt , R.; Aguila, S. A.; Arrocha, A. A.; Ayala, M. QM/MM Molecular Modeling and Marcus Theory in the Molecular Design of Electrodes for Enzymatic Fuel Cells. *ChemElectroChem* **2014,** *1*, 496-513.

(71) Cosnier, S.; Le Goff, A.; Holzinger, M. Towards Glucose Biofuel Cells Implanted in Human Body for Powering Artificial Organs: Review. *Electrochem. Commun.* **2014,** *38*, 19-23.

(72) Le Goff, A.; Holzinger, M.; Cosnier, S. Recent Progress in Oxygen-Reducing Laccase Biocathodes for Enzymatic Biofuel Cells. *Cel. Mol. Life Sci.* **2015,** *72*, 941-952.

(73) Catalano, P. N.; Wolosiuk, A.; Soler-Illia, G. J. A. A.; Bellino, M. G. Wired Enzymes in Mesoporous Materials: a Benchmark for Fabricating Biofuel Cells. *Bioelectrochem.* **2015,** *106, Part A*, 14-21.

(74) Karimi, A.; Othman, A.; Uzunoglu, A.; Stanciu, L.; Andreescu, S. Graphene Based Enzymatic Bioelectrodes and Biofuel Cells. *Nanoscale* **2015,** *7*, 6909-6923.

(75) Cosnier, S.; J. Gross, A.; Le Goff, A.; Holzinger, M. Recent Advances on Enzymatic Glucose/Oxygen and Hydrogen/Oxygen Biofuel Cells: Achievements and Limitations. *J. Power Sources* **2016,** *325*, 252-263.

(76) Desmet, C.; Marquette, C. A.; Blum, L. J.; Doumèche, B. Paper Electrodes for Bioelectrochemistry: Biosensors and Biofuel Cells. *Biosens. Bioelectron.* **2016,** *76*, 145-163.

(77) Babadi, A. A.; Bagheri, S.; Hamid, S. Bee A. Progress on Implantable Biofuel Cell: Nano-Carbon Functionalization for Enzyme Immobilization Enhancement. *Biosens. Bioelectron.* **2016,** *79*, 850-860.

(78) Bandodkar, A. J.; Wang, J. Wearable Biofuel Cells: a Review. *Electroanalysis* **2016,** *28*, 1188-1200.

(79) Sode, K.; Yamazaki, T.; Lee, I.; Hanashi, T.; Tsugawa, W. Biocapacitor: a Novel Principle for Biosensors. *Biosens. Bioelectron.* **2016,** *76*, 20-28.

(80) Pankratov, D.; Gonzalez-Arribas, E.; Blum, Z.; Shleev, S. Tear Based Bioelectronics. *Electroanalysis* **2016,** *28*, 1250-1266.

(81) Mate, D. M.; Alcalde, M. Laccase: A Multi-Purpose Biocatalyst At The Forefront Of Biotechnology. *Microbial Biotechnology* **2016**, DOI:10.1111/1751-7915.12422

(82) Safdar, M.; Janis, J.; Sanchez, S. Microfluidic Fuel Cells for Energy Generation. *Lab Chip* **2016,** *16*, 2754-2758.

(83) Qiu, H.-J.; Guan, Y.; Luo, P.; Wang, Y. Recent Advance in Fabricating Monolithic 3D Porous Graphene and Their Applications in Biosensing and Biofuel Cells. *Biosens. Bioelectron.* **2017,** *89, Part 1,* 85-95.

(84) Bandodkar, A. J. Review—Wearable Biofuel Cells: Past, Present and Future. *J. Electrochem. Soc.* **2017,** *164*, H3007-H3014.

(85) Xu, Q.; Zhang, F.; Xu, L.; Leung, P.; Yang, C.; Li, H. The Applications and Prospect of Fuel Cells in Medical Field: a Review. *Renew. Sust. Energy Rev.* **2017,** *67*, 574-580.

(86) Ghassemi, Z.; Slaughter, G. Biological Fuel Cells and Membranes. *Membranes* **2017,** *7*, 3-15

(87) Holade, Y.; Tingry, S.; Servat, K.; Napporn, T. W.; Cornu, D.; Kokoh, K. B. Nanostructured Inorganic Materials at Work in Electrochemical Sensing and Biofuel Cells. *Catalysts* **2017,** *7*. 31-73

(88) Kim, J.; Kumar, R.; BAndodkar, A. J.; Wang, J. Advanced Materials for Printed Wearable Electrochemical Devices: A Review. *Adv. Electron. Mat.* **2017,** *3*, 1600260

(89) Shleev, S. Quo Vadis, Implanted Fuel Cell? *ChemPlusChem* **2017,** *82*, 522-539.

(90) Rajendran, L.; Kirthiga, M.; Laborda, E. Mathematical Modeling of Nonlinear Reaction–Diffusion Processes in Enzymatic Biofuel Cells. *Cur. Opinion Electrochem.* **2017,** *1*, 121-132.

(91) Zhao, C.; Gai, P.; Song, R.; Chen, Y.; Zhang, J.; Zhu, J.-J. Nanostructured Material-Based Biofuel Cells: Recent Advances and Future Prospects. *Chem. Soc. Rev.* **2017,** *46*, 1545-1564.

(92) Jones, S. M.; Solomon, E. I. Electron Transfer and Reaction Mechanism of Laccases. *Cell. Mol. Life. Sci.* **2015,** *72*, 869-883.

(93) Solomon, E. I.; Augustine, A. J.; Yoon, J. O_2 Reduction to H_2O by the Multicopper Oxidases. *Dalton Trans.* **2008**, 3921-3932.

(94) Solomon, E. I.; Szilagyi, R. K.; DeBeer George, S.; Basumallick, L. Electronic Structures of Metal Sites in Proteins and Models: Contributions to Function in Blue Copper Proteins. *Chem. Rev.* **2004,** *104*, 419-458.

(95) Solomon, E. I.; Sundaram, U. M.; Machonkin, T. E. Multicopper Oxidases and Oxygenases. *Chem. Rev.* **1996,** *96*, 2563-2605.

(96) Solomon, E. I.; Baldwin, M. J.; Lowery, M. D. Electronic Structures of Active Sites in Copper Proteins: Contributions to Reactivity. *Chem. Rev.* **1992,** *92*, 521-542.

(97) Wherland, S.; Farver, O.; Pecht, I. Multicopper Oxidases: Intramolecular Electron Transfer and O_2 Reduction. *J. Biol. Inorg. Chem.* **2014,** *19*, 541-554.

(98) Komori, H.; Higuchi, Y. Structural Insights into the O_2 Reduction Mechanism of Multicopper Oxidase. *J. Biochem.* **2015,** *158*, 293-298.

(99) Quintanar, L.; Stoj, C.; Taylor, A. B.; Hart, P. J.; Kosman, D. J.; Solomon, E. I. Shall We Dance? How a Multicopper Oxidase Chooses Its Electron Transfer Partner. *Acc. Chem. Res.* **2007,** *40*, 445-452.

(100) Tanaka, N.; Murao, S. Difference Between Various Copper containing Enzymes (*Polyporus* Laccase, MushroomTyrosinase And Cucumber Ascorbate Oxidase) And Bilirubin Oxidase *Agric. Biol. Chem.* **1983,** *47*, 1627-1628.

(101) Durand, F.; Kjaergaard, C. H.; Suraniti, E.; Gounel, S.; Hadt, R. G.; Solomon, E. I.; Mano, N. Bilirubin Oxidase from *Bacillus pumilus*: a Promising Enzyme for the Elaboration of Efficient Cathodes in Biofuel Cells. *Biosens. Bioelectron.* **2012,** *35*, 140-146.

(102) Solomon, E. I.; Chen, P.; Metz, M.; Lee, S.-K.; Palmer, A. E. Oxygen Binding, Activation, and Reduction to Water by Copper Proteins. *Angew. Chem. Int. Ed.* **2001,** *40*, 4570-4590.

(103) Li, J.; Farrokhnia, M.; Rulíšek, L.; Ryde, U. Catalytic Cycle of Multicopper Oxidases Studied by Combined Quantum- and Molecular-Mechanical Free-Energy Perturbation Methods. *J. Phys. Chem. B* **2015,** *119*, 8268-8284.

(104) Ryde, U.; Hsiao, Y.-W.; Rulíšek, L.; Solomon, E. I. Identification of the Peroxy Adduct in Multi-Copper Oxidases by a Combination of Computational Chemistry and Extended X-Ray Absorption Fine-Structure Measurements. *J. Am. Chem. Soc.* **2007,** *129*, 726-727.

(105) Lee, S.-K.; DeBeer George, s.; Antholine, W. E.; Hedman, B.; Hodgson, K. O.; Solomon, E. I. Nature of the Intermediate Formed in the Reduction of O_2 to H_2O at the Trinuclear Copper Cluster Active Site in Native Laccase. *J. Am. Chem. Soc.* **2002,** *124*, 6180-6193.

(106) Cole, J. L.; Clark, P. A.; Solomon, E. I. Spectroscopic and Chemical Studies of the Laccase Trinuclear Copper Active Site: Geometric and Electronic Structure. *J. Am. Chem. Soc.* **1990,** *112*, 9534-9548.

(107) Guckert, J. A.; Lowery, M. D.; Solomon, E. I. Electronic Structure of the Reduced Blue Copper Active Site: Contributions to Reduction Potentials and Geometry. *J. Am. Chem. Soc.* **1995,** *117*, 2817-2844.

(108) Lowery, M. D.; Guckert, J. A.; Gebhard, M. S.; Solomon, E. I. Active-Site Electronic Structure Contributions to Electron-Transfer Pathways in Rubredoxin and Plastocyanin: Direct versus Superexchange. *J. Am. Chem. Soc.* **1993,** *115*, 3012-3013.

(109) Riva, S. Laccases: Blue Enzyme for Green Chemistry. *Trends Biotechnol.* **2006,** *24*, 219-226.

(110) Couto, S. R.; Herrea, J. L. Industrial and Biotechnological Applications of Laccase : a Review. *Biotechnol. Adv.* **2006,** *24*, 500-513.

(111) Mayer, A. M.; Staples, R. C. Laccase: New Functions for an Old Enzyme. *Phytochemistry* **2002,** *60*, 551-565.

(112) Mate, D. M.; Alcalde, M. Laccase Engineering: from Rational Design to Directed Evolution. *Biotechnol. Adv.* **2015,** *33*, 25-40.

(113) Claus, H. Laccases and their Occurrence in Prokaryotes. *Arch. Microbiol.* **2003,** *179*, 145-150.

(114) Baldrian, P. Fungal Laccases - Occurrence and Properties. *FEMS Microbiol. Rev.* **2006,** *30*, 215-242.

(115) Tarasevich, M. R.; Yaropolov, A. I.; Bogdanovskaya, V. A.; Varfolomeev, S. D. Electrocatalysis of a Cathodic Oxygen Reduction by Laccase. *Bioelectrochem. Bioenerg.* **1979,** *6*, 393-403.

(116) Palmer, A. E.; Randall, D. W.; Xu, F.; Solomon, E. I. Spectroscopic Studies and Electronic Structure Description of the High Potential Type 1 Copper Site in Fungal Laccase: Insight into the Effect of the Axial Ligand. *J. Am. Chem. Soc.* **1999,** *121*, 7138-7149.

(117) Marshall, N. M.; Garner, D. K.; Wilson, T. D.; Gao, Y. G.; Robinson, H.; Nilges, M. J.; Lu, Y. Rationally Tuning the Reduction Potential of a Single Cupredoxin beyond the Natural Range. *Nature* **2009,** *462*, 113-116.

(118) Shleev, S.; Christenson, A.; Serezhenkov, V.; Burbaev, D.; Yaropolov, A.; Gorton, L.; Ruzgas, T. Electrochemical Redox Transformations of T1 and T2 Copper Sites in Native *Trametes hirsuta* Laccase at Gold Electrode. *Biochem. J.* **2005,** *385*, 745-754.

(119) Murao, S.; Tanaka, N. A New Enzyme "Bilirubin Oxidase" Produced by *Myrothecium verrucaria MT-1*. *Agric. Biol. Chem.* **1981,** *45*, 2383-2384.

(120) Mano, N.; Kim, H.-H.; Heller, A. On the Relationship between the Characteristics of Bilirubin Oxidases and O_2 Cathodes Based on Their "Wiring". *J. Phys. Chem. B* **2002,** *106*, 8842-8848.

(121) Durand, F.; Gounel, S.; Kjaergaard, C. H.; Solomon, E. I.; Mano, N. Bilirubin Oxidase from *Magnaporthe oryzae*: an Attractive New Enzyme for Biotechnological Applications. *Appl. Microbiol. Biotechnol.* **2012,** *96*, 1489-1498.

(122) Tsujimura, S.; Tatsumi, H.; Ogawa, J.; Shimizu, S.; Kano, K.; Ikeda, T. Bioelectrocatalytic Reduction of Dioxygen to Water at Neutral pH Using Bilirubin Oxidase as an Enzyme and 2,2'-Azinobis(3-ethylbenzothiazolin-6-silfonate) as an Electron Transfer Mediator. *J. Electroanal. Chem.* **2001,** *496*, 69-75.

(123) Reiss, R.; Ihssen, J.; Thony-Meyer, L. *Bacillus pumilus* Laccase: a Heat Stable Enzyme with a Wide Substrate Spectrum. *BMC Biotechnol.* **2011,** *11*, 9.

(124) Sakasegawa, S.-i.; Ishikawa, H.; Imamura, S.; Sakuraba, H.; Goda, S.; Ohshima, T. Bilirubin Oxidase Activity of *Bacillus subtilis* CotA. *Appl. Environ. Microbiol.* **2006,** *72*, 972-975.

(125) Reiss, R.; Ihssen, J.; Thony-Meyer, L.; Richter, M.; Eichhorn, E.; Schilling, B. Laccase versus Laccase-Like Multi-Copper Oxidase: a Comparative Study of Similar Enzymes with Diverse Substrate Spectra. *PLOS One* **2013,** *8*, e65633.

(126) Durand, F.; Gounel, S.; Mano, N. Purification and Characterization of a New Laccase from the Filamentus Fungus *Podospora anserina*. *Prot. Exp. Purif.* **2013,** *88*, 61-66.

(127) Kjaergaard, C. H.; Durand, F.; Tasca, F.; Qayyum, M. F.; Kauffmann, B.; Gounel, S.; Suraniti, E.; Hodgson, K. O.; Hedman, B.; Mano, N.; E. I. Solomon, Spectroscopic and Crystallographic Characterization of "Alternative Resting" and "Resting Oxidized" Enzyme Forms of Bilirubin Oxidase: Implications for Activity and

Electrochemical Behavior of Multi Copper Oxidases. *J. Am. Chem. Soc.* **2012,** *134*, 5548-5551.

(128) Mizutani, K.; Toyoda, M.; Sagara, K.; Takahashi, N.; Sato, A.; Kamitaka, Y.; Tsujimura, S.; Nakanishi, Y.; Sugiura, T.; Yamaguchi, S.; Kano, K.; Mikami, B., X-Ray Analysis of Bilirubin Oxidase from *Myrothecium verrucaria* at 2.3 A Resolution Using a Twinned Crystal. *Acta Crystallogr. Sect. F Struct. Biol. Cryst. Commun.* **2010,** *66*, 765-770.

(129) Cracknell, J. A.; McNamara, T. P.; Lowe, E. D.; Blanford, C. F. Bilirubin Oxidase from *Myrothecium verrucaria*: X-Ray Determination of the Complete Crystal Structure and a Rational Surface Modification for Enhanced Electrocatalytic O_2 Reduction. *Dalton Trans.* **2011,** *40*, 6668-6675.

(130) Sakurai, T.; Kataoka, K. Basic and Applied Features of Multi-Copper Oxidases, CueO, Bilirubin Oxidase, and Laccase. *Chem. Rec.* **2007,** *7*, 220-229.

(131) Kataoka, K.; Komori, H.; Ueki, Y.; Konno, Y.; Kamitaka, Y.; Kurose, S.; Tsujimura, S.; Higuchi, Y.; Kano, K.; Seo, D.; Sakurai, T. Structure and Function of the Engineered Multi-Copper Oxidase CueO from *Escherichia coli*—Deletion of the Methionine-Rich Helical Region Covering the Substrate-Binding Site. *J. Mol. Biol.* **2007,** *373*, 141-152.

(132) Haberska, K.; Vaz-Domínguez, C.; De Lacey, A. L.; Dagys, M.; Reimann, C. T.; Shleev, S. Direct Electron Transfer Reactions between Human Ceruloplasmin and Electrodes. *Bioelectrochem.* **2009,** *76*, 34-41.

(133) Razumas, V. J.; Vidugiris, G. J. A.; Zapalskyté, A. A.; Gudavičius, A. V.; Kulys, J. J. 855 — Electrochemical Conversion of Lactoperoxidase, Ceruloplasmin and Alkaline Phosphatase on Mercury Electrodes. *Bioelectrochem. Bioenerg.* **1986,** *15*, 407-415.

(134) Yaropolov, A. I.; Kharybin, A. N.; Emnéus, J.; Marko-Varga, G.; Gorton, L. Electrochemical Properties of Some Copper-Containing Oxidases. *Bioelectrochem. Bioenerg.* **1996,** *40*, 49-57.

(135) Daigle, F.; Trudeau, F.; Robinson, G.; Smyth, M. R.; Leech, D. Mediated Reagentless Enzyme Inhibition Electrodes. *Biosens. Bioelectron.* **1998,** *13*, 417-425.

(136) Matysiak, E.; Botz, A. J. R.; Clausmeyer, J.; Wagner, B.; Schuhmann, W.; Stojek, Z.; Nowicka, A. M. Assembling Paramagnetic Ceruloplasmin at Electrode Surfaces Covered with Ferromagnetic Nanoparticles. Scanning Electrochemical Microscopy in the Presence of a Magnetic Field. *Langmuir* **2015,** *31*, 8176-8183.

(137) Ivnitski, D. M.; Khripin, C.; Luckarift, H. R.; Johnson, G. R.; Atanassov, P. Surface Characterization and Direct Bioelectrocatalysis of Multi-Copper Oxidases. *Electrochim. Acta* **2010,** *55*, 7385-7393.

(138) Urban, J.; Zloczewska, A.; Stryczniewicz, W.; Jonsson-Niedziolka, M. Enzymatic Oxygen Reduction under Quiescent Conditions — the Importance of Convection. *Electrochem. Commun.* **2013,** *34*, 94-97.

(139) Svoboda, V.; Cooney, M.; Liaw, B. Y.; Minteer, S.; Piles, E.; Lehnert, D.; Calabrese Barton, S.; Rincon, R.; Atanassov, P. Standardized Characterization of Electrocatalytic Electrodes. *Electroanalysis* **2008,** *20*, 1099-1109.

(140) Moehlenbrock, M. J.; Arechederra, R. L.; Sjöholm, K. H.; Minteer, S. D. Analytical Techniques for Characterizing Enzymatic Biofuel Cells. *Anal. Chem.* **2009,** *81*, 9538-9545.

(141) Flexer, V.; Brun, N.; Courjean, O.; Backov, R.; Mano, N. Porous Mediator-Free Enzyme Carbonaceous Electrodes Obtained through Integrative Chemistry for Biofuel Cells. *Energy Environ. Sci.* **2011,** *4*, 2097-2106.

(142) Ciaccafava, A.; de Poulpiquet, A.; Techer, V.; Giudici-Orticoni, M. T.; Tingry, S.; Innocent, C.; Lojou, E. An Innovative Powerful and Mediatorless H_2/O_2 Biofuel Cell Based on an Outstanding Bioanode. *Electrochem. Commun.* **2012,** *23*, 25-28.

(143) Xu, L.; Armstrong, F. A. Optimizing the Power of Enzyme-Based Membrane-Less Hydrogen Fuel Cells for Hydrogen-Rich H_2-Air Mixtures. *Energy Environ. Sci.* **2013,** *6*, 2166-2171.

(144) Marcus, R. A. On the Theory of Oxidation-Reduction Reactions Involving Electron Transfer. *J. Chem. Phys.* **1956,** *24*, 966-978.

(145) Marcus, R. A.; Sutin, N. Electron Transfers in Chemistry and Biology. *Biochim. Biophys. Acta* **1985,** *811*, 265-322.

(146) Page, C. C.; Moser, C. C.; Chen, X. X.; Dutton, P. L. Natural Engineering Principles of Electron Tunnelling in Biological Oxidation-Reduction. *Nature* **1999,** *402*, 47-52.

(147) Gray, H. B.; Winkler, J. R. Electron Tunneling through Proteins. *Q Rev Biophys* **2003,** *36*, 341-372.

(148) Leger, C.; Jones, A. K.; Albracht, S. P. J.; Armstrong, F. A. Effect of a Dispersion of Interfacial Electron Transfer Rates on Steady State Catalytic Electron Transport in NiFe -Hydrogenase and Other Enzymes. *J. Phys. Chem. B* **2002,** *106*, 13058-13063.

(149) Chi, Q. J.; Zhang, J. D.; Andersen, J. E. T.; Ulstrup, J. Ordered Assembly and Controlled Electron Transfer of the Blue Copper Protein Azurin at Gold (111) Single-Crystal Substrates. *J. Phys. Chem. B* **2001,** *105*, 4669-4679.

(150) Jeuken, L. J. C. Conformational Reorganisation in Interfacial Protein Electron Transfer. *Biochim. Biophys. Acta-Bioenergetics* **2003,** *1604*, 67-76.

(151) Tominaga, M.; Ohtani, M.; Taniguchi, I. Gold Single-Crystal Electrode Surface Modified with Self-Assembled Monolayers for Electron Tunneling with Bilirubin Oxidase. *Phys. Chem. Chem. Phys.* **2008,** *10*, 6928-6934.

(152) Gobel, G.; Lisdat, F. Organic Interlayers for Oxygen Reducing Electrodes Based on Bilirubin Oxidase and MWCNT Modified Gold. *Electrochem. Commun.* **2008,** *10*, 1691-1694.

(153) Ohara, T. J.; Rajagopalan, R.; Heller, A. Glucose Electrodes Based on Cross-Linked $Os(bpy)_2^{+/2+}$ Complexed Poly(L-vinyilimidazole) Films. *Anal. Chem.* **1993,** *65*, 3512-3517.

(154) Heller, A. Electron-Conducting Redox Hydrogels: Design, Characteristics and Synthesis. *Curr. Opin. Chem. Biol.* **2006,** *10*, 664-672.

(155) Stines-Chaumeil, C.; Roussarie, E.; Mano, N. The Nature of the Rate-Limiting Step of Blue Multi-Copper Oxidases: Homogeneous Studies versus Heterogeneous. *Biochimie Open* **2017,** *4*, 36-40.

(156) Xu, F.; Shin, W. S.; Brown, S. H.; Wahleithner, J. A.; Sundaram, U. M.; Solomon, E. I. A Study of a Series of Recombinant Fungal Laccases and Bilirubin Oxidase that Exhibit Significant Differences in Redox Potential, Substrate Specificity, and Stability. *Biochim. Biophys. Acta-Prot. Struct. Mol. Enzymol.* **1996,** *1292*, 303-311.

(157) Xu, F. Dioxygen Reactivity of Laccase: Dependence on Laccase Source, pH, and Anion Inhibition. *Appl. Biochem. Biotechnol.* **2001,** *95*, 125-133.

(158) Xu, F.; Berka, R. M.; Wahleithner, J. A.; Nelson, B. A.; Shuster, J. R.; Brown, S. H.; Palmer, A. E.; Solomon, E. I. Site-Directed Mutations in Fungal Laccase: Effect on Redox Potential, Activity and pH Profile. *Biochem. J.* **1998,** *334*, 63-70.

(159) Spira-Solomon, D. J.; Allendorf, M. D.; Solomon, E. I. Low-Temperature Magnetic Circular Dichroism Studies of Native Laccase: Confirmation of a Trinuclear Copper Active Site. *J. Am. Chem. Soc.* **1986,** *108*, 5318-5328.

(160) Cole, J. L.; Tan, G. O.; Yang, E. K.; Hodgson, K. O.; Solomon, E. I. Reactivity of the Laccase Trinuclear Copper Active Site with Dioxygen: an X-Ray Absorption Edge Study. *J. Am. Chem. Soc.* **1990,** *112,* 2243-2249.

(161) G. B. Koudelka; Ettinger, M. J. Fluoride Effects on the Activity of Rhus Laccase and the Catalytic Mechanism under Steady-State Conditions. *J. Biol. Chem* **1988,** *263,* 3698-3705.

(162) Xu, F. Effects of Redox Potential and Hydroxide Inhibition on the pH Activity Profile of Fungal Laccases. *J. Biol. Chem* **1997,** *272,* 924-928.

(163) Palmer, A. E.; Lee, S. K.; Solomon, E. I. Decay of the Peroxide Intermediate in Laccase: Reductive Cleavage of the O−O Bond. *J. Am. Chem. Soc.* **2001,** *123,* 6591-6599.

(164) Léger, C.; Bertrand, P. Direct Electrochemistry of Redox Enzymes as a Tool for Mechanistic Studies. *Chem. Rev.* **2008,** *108,* 2379-2438.

(165) Cracknell, J. A.; Blanford, C. F. Developing the Mechanism of Dioxygen Reduction Catalyzed by Multicopper Oxidases using Protein Film Electrochemistry. *Chem. Sci.* **2012,** *3,* 1567-1581.

(166) Gallaway, J.; Wheeldon, I.; Rincon, R.; Atanassov, P.; Banta, S.; Barton, S. C. Oxygen-Reducing Enzyme Cathodes Produced from SLAC, a Small Laccase from *Streptomyces coelicolor*. *Biosens. Bioelectron.* **2008,** *23,* 1229-1235.

(167) Guven, G.; Prodanovic, R.; Schwaneberg, U. Protein Engineering - An Option for Enzymatic Biofuel Cell Design. *Electroanalysis* **2010,** *22,* 765-775.

(168) Cusano, A. M.; Mekmouche, Y.; Meglecz, E.; Tron, T. Plasticity of Laccase Generated by Homeologous Recombination in Yeast. *FEBS Journal* **2009,** *276,* 5471-5480.

(169) Torres-Salas, P.; Mate, D. M.; Ghazi, I.; Plou, F. J.; A.O., B.; Alcalde, M. Widening the pH Activity Profile of a Fungal Laccase by Directed Evolution. *ChemBioChem* **2013,** *14*, 934-937.

(170) Mate, D. M.; Gonzalez-Perez, D.; Falk, M.; Kittl, R.; Pita, M.; De Lacey, A. L.; Ludwig, R.; Shleev, S.; Alcalde, M. Blood Tolerant Laccase by Directed Evolution. *Chem. Biol.* **2013,** *20*, 223-231.

(171) Clot, S.; Gutteriez-Sanchez, C.; Shleev, S.; De Lacey, A. L.; Pita, M. Laccase Cathode Approaches to Physiological Conditions by Local pH Acidification. *Electrochem. Commun.* **2012,** *18*, 37-40.

(172) Xu, F. Oxidation of Phenols, Anilines, and Benzenethiols by Fungal Laccases: Correlation between Activity and Redox Potentials as well as Halide Inhibition. *Biochemistry* **1996,** *35*, 7608-7614.

(173) Hirose, J.; Inoue, T.; Sakuragi, H.; Kikkawa, M.; Minakami, M.; Morikawa, T.; Iwamoto, H.; Hiromi, K. Anions Binding to Bilirubin Oxidase from *Trachyderma tsunodae K-2593*. *Inorg. Chim. Acta* **1998,** *273*, 204-212.

(174) Quintanar, L.; Yoon, J.; Aznar, C. P.; Palmer, A. E.; Andersson, K. K.; Britt, R. D.; Solomon, E. I. Spectroscopic and Electronic Structure Studies of the Trinuclear Cu Cluster Active Site of the Multicopper Oxidase Laccase: Nature of Its Coordination Unsaturation. *J. Am. Chem. Soc.* **2005,** *127*, 13832-13845.

(175) Mano, N.; Kim, H. H.; Zhang, Y.; Heller, A. An Oxygen Cathode Operating in a Physiological Solution. *J. Am. Chem. Soc.* **2002,** *124*, 6480-6486.

(176) Szamocki, R.; Flexer, V.; Levin, L.; Forchiasin, F.; Calvo, E. J. Oxygen Cathode Based on a Layer-by-Layer Self-Assembled Laccase and Osmium Redox Mediator. *Electrochim. Acta* **2009,** *54*, 1970-1977.

(177) Shin, H.; Cho, S.; Heller, A.; Kang, C. Stabilization of a Bilirubin Oxidase-Wiring Redox Polymer by Quaternization and Characteristics of the Resulting O_2 Cathode. *J. Electrochem. Soc.* **2009,** *156*, F87-F92.

(178) Barton, S. C.; Pickard, M.; Vazquez-Duhalt, R.; Heller, A. Electroreduction of O_2 to Water at 0.6 V (SHE) at pH 7 on the 'Wired' *Pleurotus ostreatus* Laccase Cathode. *Biosens. Bioelectron.* **2002,** *17*, 1071-1074.

(179) Enaud, E.; Trovaslet, M.; Naveau, F.; Decristoforo, A.; Bizet, S.; Vanhulle, S.; Jolivalt, C. Laccase Chloride Inhibition Reduction by an Anthraquinone Susbtrate. *Enzyme Microb. Technol.* **2011,** *49*, 517-525.

(180) Beyl, Y.; Guschin, D. A.; Shleev, S.; Schuhmann, W. A Chloride Resistant High Potential Oxygen Reducing Biocathode Based on a Fungal Laccase Incorporated into an Optimized Os-Complex Modified Redox Hydrogel. *Electrochem. Commun.* **2011,** *13*, 474-476.

(181) Beneyton, T.; Beyl, Y.; Guschin, D. A.; Griffiths, A. D.; Taly, V.; Schuhmann, W. The Thermophilic CotA Laccase from *Bacillus subtilis*: Bioelectrocatalytic Evaluation of O_2 Reduction in the Direct and Mediated Electron Transfer Regime. *Electroanalysis* **2011,** *23*, 1781-1789.

(182) Kiiskinen, L.-L.; Viikari, L.; Kruus, K. Purification and Characterisation of a Novel Laccase from the Ascomycete *Melanocarpus albomyces*. *Appl. Microbiol. Biotechnol.* **2002,** *59*, 198-204.

(183) Kavanagh, P.; Jenkins, P.; Leech, D. Electroreduction of O_2 at a Mediated *Melanocarpus albomyces* Laccase Cathode in a Physiological Buffer. *Electrochem. Commun.* **2008,** *10*, 970-972.

(184) Kavanagh, P.; Boland, S.; Jenkins, P.; Leech, D. Performance of a Glucose/O_2 Enzymatic Biofuel Cell Containing a Mediated *Melanocarpus albomyces* Laccase Cathode in a Physiological Buffer. *Fuel Cells* **2009,** *9*, 79-84.

(185) Jensen, U. B.; Vagin, M.; Koroleva, O.; Sutherland, D. S.; Besenbacher, F.; Ferapontova, E. E. Activation of Laccase Bioelectrocatalysis of O_2 Reduction to H_2O by Carbon Nanoparticles. *J. Electroanal. Chem.* **2012,** *667*, 11-18.

(186) Salaj-Kosla, U.; Poller, S.; Schuhmann, W.; Shleev, S.; Magner, E. Direct Electron Transfer of *Trametes hirsuta* Laccase Adsorbed at Unmodified Nanoporous Gold Electrodes. *Bioelectrochem.* **2013,** *91*, 15-20.

(187) Vaz-Dominguez, C.; Campuzano, S.; Rüdiger, O.; Pita, M.; Gorbacheva, M.; Shleev, S.; FernAndez, V. M.; De Lacey, A. L. Laccase Electrode for Direct Electrocatalytic Reduction of O_2 to H_2O with High Operational Stability and Resistance to Chloride Inhibition. *Biosens. Bioelectron.* **2008,** *24*, 531-537.

(188) Bartlett, P. N.; Pratt, K. F. E. Theoretical Treatment of Diffusion and Kinetics in Amperometric Immobilized Enzyme Electrodes. 1 Redox Mediator Entrapped within the Film. *J. Electroanal. Chem.* **1995,** *397*, 61-78.

(189) Tamaki, T.; Ito, T.; Yamaguchi, T. Modelling of Reaction and Diffusion Processes in a High-Surface-Area Biofuel Cell Electrode Made of Redox Polymer-Grafted Carbon. *Fuel Cells* **2009,** *9*, 37-43.

(190) Gallaway, J. W.; Barton, S. A. C. Kinetics of Redox Polymer-Mediated Enzyme Electrodes. *J. Am. Chem. Soc.* **2008,** *130*, 8527-8536.

(191) Flexer, V.; Pratt, K. F. E.; Garay, F.; Bartlett, P. N.; Calvo, E. J. Relaxation and Simplex Mathematical Algorithms Applied to the Study of Steady-State Electrochemical Responses of Immobilized Enzyme Biosensors: Comparison with Experiments. *J. Electroanal. Chem.* **2008,** *616*, 87-98.

(192) Rasi, M.; Rajendran, L.; Sangaranarayanan, M. V. Enzyme-Catalyzed Oxygen Reduction Reaction in Biofuel Cells: Analytical Expressions for Chronoamperometric Current Densities. *J. Electrochem. Soc.* **2015,** *162*, H671-H680.

(193) Barton, S. C. Oxygen Transport in Composite Mediated Biocathodes. *Electrochim. Acta.* **2005,** *50*, 2145-2153.

(194) Osman, M. H.; Shah, A. A.; Wills, R. G. A. Detailed Mathematical Model of an Enzymatic Fuel Cell. *J. Electrochem. Soc.* **2013,** *160*, F806-F814.

(195) Saravanakumar, K.; Ganesan, S. P.; Rajendran, L. Theoretical Analysis of Reaction and Diffusion Processes in a Biofuel Cell Electrode. *Fuel Cells* **2015,** *15*, 523-536.

(196) Saravanakumar, K.; Rajendran, L.; Sangaranarayanan, M. V. Current-Potential Response and Concentration Profiles of Redox Polymer-Mediated Enzyme Catalysis in Biofuel Cells - Estimation of Michaelis-Menten Constants. *Chem. Phys. Lett.* **2015,** *621*, 117-123.

(197) Sakai, H.; Nakagawa, T.; Tokita, Y.; Hatazawa, T.; Ikeda, T.; Tsujimura, S.; Kano, K. A High-Power Glucose/Oxygen Biofuel Cell Operating under Quiescent Conditions. *Energy Environ. Sci.* **2009,** *2*, 133-138.

(198) Christenson, A.; Dimcheva, N.; Ferapontova, E. E.; Gorton, L.; Ruzgas, T.; Stoica, L.; Shleev, S.; Yaropolov, A. L.; Haltrich, D.; Thorneley, R. N. F.; Aust, S. D. Direct Electron Transfer Between Ligninolytic Redox Enzymes and Electrodes. *Electroanalysis* **2004,** *16*, 1074-1092.

(199) Reinhammar, B. R.; Vanngard, T. I. Electron Accepting Sites in *Rhus vernicifera* Laccase as Studied by Anaerobic Oxidation-Reduction Titrations. *Eur. J. Biochem.* **1971,** *18*, 463-468.

(200) Reinhammar, B. R. Oxidation-Reduction Potentials of Electron Acceptors in Laccases and Stellacyanin. *Biochim. Biophys. Acta* **1972,** *275*, 245-259.

(201) Tsujimura, S.; Kuriyama, A.; Fujieda, N.; Kano, K.; Ikeda, T. Mediated Spectroelectrochemical Titration of Proteins for Redox Potential Measurements by a Separator-Less One-Compartment Bulk Electrolysis Method. *Anal. Biochem.* **2005,** *337*, 325-331.

(202) Christenson, A.; Shleev, S.; Mano, N.; Heller, A.; Gorton, L. Redox Potentials of the Blue Copper Sites of Bilirubin Oxidases. *Biochim. Biophys. Acta-Bioenergetics* **2006,** *1757*, 1634-1641.

(203) Ramirez, P.; Mano, N.; Andreu, R.; RuzGas, T.; Heller, A.; Gorton, L.; Shleev, S. Direct Electron Transfer from Graphite and Functionalized Gold Electrodes to T1 and T2/T3 Copper Centers of Bilirubin Oxidase. *Biochim. Biophys. Acta-Bioenergetics* **2008,** *1777*, 1364-1369.

(204) Shleev, S.; Andoralov, V.; Falk, M.; Reimann, C. T.; RuzGas, T.; Srnec, M.; Ryde, U.; Rulisek, L. On the Possibility of Uphill Intramolecular Electron Transfer in Multicopper Oxidases: Electrochemical and Quantum Chemical Study of Bilirubin Oxidase. *Electroanalysis* **2012,** *24*, 1524-1540.

(205) Pita, M.; Shleev, S.; RuzGas, T.; FernAndez, V. M.; Yaropolov, A. I.; Gorton, L. Direct Heterogeneous Electron Transfer Reactions of Fungal Laccases at Bare and Thiol-Modified Gold Electrodes. *Electrochem. Commun.* **2006,** *8*, 747-753.

(206) Gelo-Pujic, M.; Kim, H. H.; Butlin, N. G.; Palmore, G. T. R. Electrochemical Studies of a Truncated Laccase Produced in *Pichia pastoris*. *Appl. Environ. Microbiol.* **1999,** *65*, 5515-5521.

(207) Cabrita, J. F.; Abrantes, L. M.; Viana, A. S. N-Hydroxysuccinimide-Terminated Self-Assembled Monolayers on Gold for Biomolecules Immobilisation. *Electrochim. Acta.* **2005,** *50*, 2117-2124.

(208) Frasconi, M.; Boer, H.; Koivula, A.; Mazzei, F. Electrochemical Evaluation of Electron Transfer Kinetics of High and Low Redox Potential Laccases on Gold Electrode Surface. *Electrochim. Acta.* **2010,** *56*, 817-827.

(209) Li, Y.; Zhang, J. W.; Huang, X. R.; Wang, T. H. Construction and Direct Electrochemistry of Orientation-Controlled Laccase Electrode. *Biochem. Biophys. Research Commun.* **2014,** *446*, 201-205.

(210) Shleev, S.; Jarosz-Wilkolazka, A.; Khalunina, A.; Morozova, O.; Yaropolov, A.; Ruzgas, T.; Gorton, L. Direct Electron Transfer Reactions of Laccases from Different Origins on Carbon Electrodes. *Bioelectrochem.* **2005,** *67*, 115-124.

(211) Lee, C. W.; Gray, H. B.; Anson, F. C.; Malmstrom, B. G. Catalysis of the Reduction of Dioxygen at Graphite Electrodes Coated with Fungal Laccase. *J. Electroanal. Chem.* **1984,** *172*, 289-300.

(212) Thuesen, M. H.; Farver, O.; Reinhammar, B.; Ulstrup, J. Cyclic Voltammetry and Electrocatalysis of the Blue Copper Oxidase *Polyporus versicolor* Laccase. *Acta Chem. Scand.* **1998,** *52*, 555-562.

(213) Santucci, R.; Ferri, T.; Morpurgo, L.; Savini, I.; Avigliano, L. Unmediated Heterogeneous Electron Transfer Reaction of Ascorbate Oxidase and Laccase at a Gold Electrode. *Biochem. J.* **1998,** *332*, 611-615.

(214) Johnson, D. L.; Thompson, J. L.; Brinkmann, S. M.; Schuller, K. A.; Martin, L. L. Electrochemical Characterization of Purified *Rhus vernicifera* Laccase: Voltammetric Evidence for a Sequential Four-Electron Transfer. *Biochemistry* **2003,** *42*, 10229-10237.

(215) Shleev, S.; El Kasmi, A.; RuzGas, T.; Gorton, L. Direct Heterogeneous Electron Transfer Reactions of Bilirubin Oxidase at a Spectrographic Graphite Electrode. *Electrochem. Commun.* **2004,** *6*, 934-939.

(216) Lalaoui, N.; Holzinger, M.; Le Goff, A.; Cosnier, S. Diazonium Functionalisation of Carbon Nanotubes for Specific Orientation of Multicopper Oxidases: Controlling Electron Entry Points and Oxygen Diffusion to the Enzyme. *Chem. Eur. J.* **2016,** *22,* 10494-10500.

(217) Filip, J.; Tkac, J. The pH dependence of the cathodic peak potential of the Active Sites in Bilirubin Oxidase. *Bioelectrochem.* **2014,** *96,* 14-20.

(218) Schubert, K.; Goebel, G.; Lisdat, F. Bilirubin Oxidase Bound to Multi-Walled Carbon Nanotube-Modified Gold. *Electrochim. Acta.* **2009,** *54,* 3033-3038.

(219) Filip, J.; Sefcovicova, J.; Gemeiner, P.; Tkac, J. Electrochemistry of Bilirubin Oxidase and Its Use in Preparation of a Low Cost Enzymatic Biofuel Cell Based on a Renewable Composite Binder Chitosan. *Electrochim. Acta.* **2013,** *87,* 366-374.

(220) Gutierrez-Sanchez, C.; Ciaccafava, A.; Blanchard, P. Y.; Monsalve, K.; Giudici-Orticoni, M. T.; Lecomte, S.; Lojou, E. Efficiency of Enzymatic O_2 Reduction by *Myrothecium verrucaria* Bilirubin Oxidase Probed by Surface Plasmon Resonance, PMIRRAS, and Electrochemistry. *ACS Catal.* **2016,** *6,* 5482-5492.

(221) Yaropolov, A. I.; Kharybin, A. N.; Emneus, J.; MarkoVarga, G.; Gorton, L. Electrochemical Properties of some Copper-Containing Oxidases. *Bioelectrochem. Bioenerg.* **1996,** *40,* 49-57.

(222) Gupta, G.; Rajendran, V.; Atanassov, P. Bioelectrocatalysis of Oxygen Reduction Reaction by Laccase on Gold Electrodes. *Electroanalysis* **2004,** *16,* 1182-1185.

(223) Dronov, R.; Kurth, D. G.; Scheller, F. W.; Lisdat, F. Direct and Cytochrome *c* Mediated Electrochemistry of Bilirubin Oxidase on Gold. *Electroanalysis* **2007,** *19,* 1642-1646.

(224) Brocato, S.; Lau, C.; Atanassov, P. Mechanistic Study of Direct Electron Transfer in Bilirubin Oxidase. *Electrochim. Acta.* **2012,** *61,* 44-49.

(225) Pankratov, D.; Sotres, J.; Barrantes, A.; Arnebrant, T.; Shleev, S. Interfacial Behavior and Activity of Laccase and Bilirubin Oxidase on Bare Gold Surfaces. *Langmuir* **2014,** *30*, 2943-2951.

(226) Arzola, K. G.; Gimeno, Y.; Arevalo, M. C.; Falcon, M. A.; Creus, A. H. Electrochemical and AFM characterization on Gold and Carbon Electrodes of a High Redox Potential Laccase from *Fusarium proliferatum*. *Bioelectrochem.* **2010,** *79*, 17-24.

(227) Arzola, K. G.; Orive, A. G.; Arevalo, M. C.; Vazquez, L.; Creus, A. H.; Falcon, M. A. Adsorption of a Laccase from *Fusarium proliferatum* on Au(111) and HOPG Electrodes: a Scanning Probe Microscopy and Electrochemical Approach. *Int. J. Electrochem. Sci*. **2012,** *7*, 1011-1026.

(228) Kamitaka, Y.; Tsujimura, S.; Ikeda, T.; Kano, K. Electrochemical Quartz Crystal Microbalance Study of Direct Bioelectrocatalytic Reduction of Bilirubin Oxidase. *Electrochemistry* **2006,** *74*, 642-644.

(229) Singh, K.; McArdle, T.; Sullivan, P. R.; Blanford, C. F. Sources of Activity Loss in the Fuel Cell Enzyme Bilirubin Oxidase. *Energy Environ. Sci.* **2013,** *6*, 2460-2464.

(230) Singh, K.; Blanford, C. F. Electrochemical Quartz Crystal Microbalance with Dissipation Monitoring: a Technique to Optimize Enzyme Use in Bioelectrocatalysis. *ChemCatChem* **2014,** *6*, 921-929.

(231) McArdle, T.; McNamara, T. P.; Fei, F.; Singh, K.; Blanford, C. F. Optimizing the Mass-Specific Activity of Bilirubin Oxidase Adlayers through Combined Electrochemical Quartz Crystal Microbalance and Dual Polarization Interferometry Analyses. *ACS Appl. Mater. Interfaces* **2015,** *7*, 25270-25280.

(232) Shleev, S.; Pita, M.; Yaropolov, A. I.; RuzGas, T.; Gorton, L. Direct Heterogeneous Electron Transfer Reactions of *Trametes hirsuta* Laccase at Bare and Thiol-Modified Gold Electrodes. *Electroanalysis* **2006,** *18*, 1901-1908.

(233) Climent, V.; Zhang, J. D.; Friis, E. P.; Ostergaard, L. H.; Ulstrup, J. Voltammetry and Single-Molecule *in situ* Scanning Tunneling Microscopy of Laccases and Bilirubin Oxidase in Electrocatalytic Dioxygen Reduction on Au(111) Single-Crystal Electrodes. *J. Phys. Chem. C* **2012,** *116*, 1232-1243.

(234) Dagys, M.; Laurynenas, A.; Ratautas, D.; Kulys, J.; Vidziunaite, R.; Talaikis, M.; Niaura, G.; Marcinkeviciene, L.; Meskys, R.; Shleev, S. Oxygen Electroreduction Catalysed by Laccase Wired to Gold Nanoparticles via the Trinuclear Copper Cluster. *Energy Environ. Sci.* **2017,** *10*, 498-502.

(235) Tsujimura, S.; Nakagawa, T.; Kano, K.; Ikeda, T. Kinetic Study of Direct Bioelectrocatalysis of Dioxygen Reduction with Bilirubin Oxidase at Carbon Electrodes. *Electrochemistry* **2004,** *72*, 437-439.

(236) Salaj-Kosla, U.; Poller, S.; Beyl, Y.; Scanlon, M. D.; Beloshapkin, S.; Shleev, S.; Schuhmann, W.; Magner, E. Direct Electron Transfer of Bilirubin Oxidase (*Myrothecium verrucaria*) at an Unmodified Nanoporous Gold Biocathode. *Electrochem. Commun.* **2012,** *16*, 92-95.

(237) Di Bari, C.; Goni-Urtiaga, A.; Pita, M.; Shleev, S.; Toscano, M. D.; Sainz, R.; De Lacey, A. L. Fabrication of High Surface Area Graphene Electrodes with High Performance towards Enzymatic Oxygen Reduction. *Electrochim. Acta.* **2016,** *191*, 500-509.

(238) Hexter, S. V.; Grey, F.; Happe, T.; Climent, V.; Armstrong, F. A. Electrocatalytic Mechanism of Reversible Hydrogen Cycling by Enzymes and Distinctions between

the Major Classes of Hydrogenases. *Proc. Natl. Acad. Sci. USA* **2012,** *109*, 11516-11521.

(239) Hexter, S. V.; Esterle, T. F.; Armstrong, F. A. A Unified Model for Surface Electrocatalysis Based on Observations with Enzymes. *Phys. Chem. Chem. Phys.* **2014,** *16*, 11822-11833.

(240) Leger, C.; Bertrand, P. Direct Electrochemistry of Redox Enzymes as a Tool for Mechanistic Studies. *Chem. Rev.* **2008,** *108*, 2379-2438.

(241) Coman, V.; Ludwig, R.; Harreither, W.; Haltrich, D.; Gorton, L.; Ruzgas, T.; Shleev, S. A Direct Electron Transfer-Based Glucose/Oxygen Biofuel Cell Operating in Human Serum. *Fuel Cells* **2010,** *10*, 9-16.

(242) Kuznetsov, A. M.; Bogdanovskaya, V. A.; Tarasevich, M. R.; Gavrilova, E. F. The Mechanism of Cathode Reduction of Oxygen in a Carbon Carrier Laccase System. *FEBS Letters* **1987,** *215*, 219-222.

(243) Tarasevich, M. R.; Yaropolov, A. I.; Bogdanovskaya, V. A.; Varfolomeev, S. D. Electrocatalysis of a Cathodic Oxygen Reduction by Laccase. *Bioelectrochem. Bioenerg.* **1979,** *6*, 393-403.

(244) Weigel, M. C.; Tritscher, E.; Lisdat, F. Direct Electrochemical Conversion of Bilirubin Oxidase at Carbon Nanotube-Modified Glassy Carbon Electrodes. *Electrochem. Commun.* **2007,** *9*, 689-693.

(245) Otsuka, K.; Sugihara, T.; Tsujino, Y.; Osakai, T.; Tamiya, E. Electrochemical Consideration on the Optimum pH of Bilirubin Oxidase. *Anal. Biochem.* **2007,** *370*, 98-106.

(246) Fourmond, V.; Baffert, C.; Sybirna, K.; Lautier, T.; Abou Hamdan, A.; Dementin, S.; Soucaille, P.; Meynial-Salles, I.; Bottin, H.; Léger, C. Steady-State Catalytic Wave-

Shapes for 2-Electron Reversible Electrocatalysts and Enzymes. *J. Am. Chem. Soc.* **2013,** *135*, 3926-3938.

(247) Kamitaka, Y.; Tsujimura, S.; Kataoka, K.; Sakurai, T.; Ikeda, T.; Kano, K. Effects of Axial Ligand Mutation of the Type I Copper Site in Bilirubin Oxidase on Direct Electron Transfer-Type Bioelectrocatalytic Reduction of Dioxygen. *J. Electroanal. Chem.* **2007,** *601*, 119-124.

(248) Shimizu, A.; Sasaki, T.; Kwon, J. H.; Odaka, A.; Satoh, T.; Sakurai, N.; Sakurai, T.; Yamaguchi, S.; Samejima, T. Site-Directed Mutagenesis of a Possible Type 1 Copper Ligand of Bilirubin Oxidase; a Met467Gln Mutant Shows Stellacyanin-Like Properties. *J. Biochem.* **1999,** *125*, 662-668.

(249) Pita, M.; Gutierrez-Sanchez, C.; Olea, D.; Velez, M.; Garcia-Diego, C.; Shleev, S.; Fernandez, V. M.; De Lacey, A. L. High Redox Potential Cathode Based On Laccase Covalently Attached to Gold Electrode. *J. Phys. Chem. C* **2011,** *115*, 13420-13428.

(250) Shin, W.; Sundaram, U. M.; Cole, J. L.; Zhang, H. H.; Hedman, B.; Hodgson, K. O.; Solomon, E. I. Chemical and Spectroscopic Definition of the Peroxide-Level Intermediate in the Multicopper Oxidases: Relevance to the Catalytic Mechanism of Dioxygen Reduction to Water. *J. Am. Chem. Soc.* **1996,** *118*, 3202-3215.

(251) Jones, M. L.; Kurnikov, I. V.; Beratan, D. N. The Nature of Tunneling Pathway and Average Packing Density Models for Protein-Mediated Electron Transfer. *J. Phys. Chem. A* **2002,** *106*, 2002-2006.

(252) Tsujimura, S.; Kano, K.; Ikeda, T. Bilirubin Oxidase in Multiple Layers Catalyzes Four-Electron Reduction of Dioxygen to Water Without Redox Mediators. *J. Electroanal. Chem.* **2005,** *576*, 113-120.

(253) Adam, C.; Scodeller, P.; Grattieri, M.; Villalba, M.; Calvo, E. J. Revisiting Direct Electron Transfer in Nanostructured Carbon Laccase Oxygen Cathodes. *Bioelectrochem.* **2016,** *109*, 101-107.

(254) Agbo, P.; Heath, J. R.; Gray, H. B. Modeling Dioxygen Reduction at Multicopper Oxidase Cathodes. *J. Am. Chem. Soc.* **2014,** *136*, 13882-13887.

(255) Kjaergaard, C. H.; Jones, S. M.; Gounel, S.; Mano, N.; Solomon, E. I. Two-Electron Reduction versus One-Electron Oxidation of the Type 3 Pair in the Multicopper Oxidases. *J. Am. Chem. Soc.* **2015,** *137*, 8783-8794.

(256) de Poulpiquet, A.; Kjaergaard, C.; Rouhana, J.; Mazurenko, I.; Infossi, P.; Gounel, S.; Gadiou, R.; Giudici-Orticoni, M.-T.; Solomon, E.; Mano, N.; Lojou, E. Mechanism of Chloride Inhibition of Bilirubin Oxidase from *Bacillus pumilus* and Its Dependence on Potential and pH. *ACS Cat.* **2017,** *7*, 3916-3923.

(257) Tominaga, M.; Sasaki, A.; Togami, M. Bioelectrocatalytic Oxygen Reaction and Chloride Inhibition Resistance of Laccase Immobilized on Single-Walled Carbon Nanotube and Carbon Paper Electrodes. *Electrochemistry* **2016,** *84*, 315-318.

(258) Jensen, U. B.; Vagin, M.; Koroleva, O.; Sutherland, D. S.; Besenbacher, F.; Ferapontova, E. E. Activation of Laccase Bioelectrocatalysis of O_2 Reduction to H_2O by Carbon Nanoparticles. *J. Electroanal. Chem.* **2012,** *667*, 11-18.

(259) Vaz-Dominguez, C.; Campuzano, S.; Rudiger, O.; Pita, M.; Gorbacheva, M.; Shleev, S.; Fernandez, V. M.; De Lacey, A. L. Laccase Electrode for Direct Electrocatalytic Reduction of O_2 to H_2O with High-Operational Stability and Resistance to Chloride Inhibition. *Biosens. Bioelectron.* **2008,** *24*, 531-537.

(260) Scodeller, P.; Carballo, R.; Szamocki, R.; Levin, L.; Forchiassin, F.; Calvo, E. J. Layer-by-Layer Self-Assembled Osmium Polymer-Mediated Laccase Oxygen

Cathodes for Biofuel Cells: the Role of Hydrogen Peroxide. *J. Am. Chem. Soc.* **2010,** *132*, 11132-11140.

(261) Grattieri, M.; Scodeller, P.; Adam, C.; Calvo, E. J. Non-Competitive Reversible Inhibition of Laccase by H_2O_2 in Osmium Mediated Layer-by-Layer Multilayer O_2 Biocathodes. *J. Electrochem. Soc.* **2015,** *162*, G82-G86.

(262) Kau, L. S.; Spira-Solomon, D. J.; Penner-Hahn, J. E.; Hodgson, K. O.; Solomon, E. I. X-Ray Absorption Edge Determination of the Oxidation State and Coordination Number of Copper. Application to the Type 3 Site in *Rhus vernicifera* Laccase and Its Reaction with Oxygen. *J. Am. Chem. Soc.* **1987,** *109*, 6433-6442.

(263) Lubien, C. D.; Winkler, M. E.; Thamann, T. J.; Scott, R. A.; Co, M. S.; Hodgson, K. O.; Solomon, E. I. Chemical and Spectroscopic Properties of the Binuclear Copper Active Site in Rhus Laccase: Direct Confirmation of a Reduced Binuclear Type 3 Copper Site in Type 2 Depleted Laccase and Intramolecular Coupling of the Type 3 to the Type 1 and Type 2 Copper Sites. *J. Am. Chem. Soc.* **1981,** *103*, 7014-7016.

(264) Milton, R. D.; Minteer, S. D. Investigating the Reversible Inhibition Model of Laccase by Hydrogen Peroxide for Bioelectrocatalytic Aplications. *J. Electrochem. Soc.* **2014,** *161*, H3011-H3014.

(265) Milton, R. D.; Giroud, F.; Thumser, A. E.; Minteer, S. D.; Slade, R. C. T. Hydrogen Peroxide Produced by Glucose Oxidase Affects the Performance of Laccase Cathodes in Glucose/Oxygen Fuel Cells: FAD-Dependent Glucose Dehydrogenase as a Replacement. *Phys. Chem. Chem. Phys.* **2013,** *15*, 19371-19379.

(266) Milton, R. D.; Giroud, F.; Thumser, A. E.; Minteer, S. D.; Slade, R. C. T. Bilirubin Oxidase Bioelectrocatalytic Cathodes: the Impact of Hydrogen Peroxide. *Chem. Commun. (Camb)* **2014,** *50*, 94-96.

(267) Milton, R. D.; Giroud, F.; Thumser, A. E.; Minteer, S. D.; Slade, R. C. T. Glucose Oxidase Progressively Lowers Bilirubin Oxidase Bioelectrocatalytic Cathode Performance in Single-Compartment Glucose/Oxygen Biological Fuel Cells. *Electrochim. Acta* **2014,** *140*, 59-64.

(268) Tremey, E.; Suraniti, E.; Courjean, O.; Gounel, S.; Stines-Chaumeil, C.; Louerat, F.; Mano, N. Switching an O_2 sensitive Glucose Oxidase Bioelectrode into an almost Insensitive by Cofactor Redesign. *Chem. Commun.* **2014,** *50*, 5912-5914.

(269) Li, X.; Faghri, A. Review and advances of Direct Methanol Fuel Cells (DMFCs) Part I: Design, Fabrication, and Testing with High Concentration Methanol Solutions. *J. Power Sources* **2013,** *226*, 223-240.

(270) Fei, J.; Song, H.-K.; Palmore, G. T. R. A Biopolymer Composite that Catalyzes the Reduction of Oxygen to Water. *Chem. Mater.* **2007,** *19*, 1565-1570.

(271) Bogdanovskaya, V. A.; Tarasevich, M. R.; Kuznetsova, L. N.; Reznik, M. F.; Kasatkin, E. V. Peculiarities of Direct Bioelectrocatalysis by Laccase in Aqueous–Nonaqueous Mixtures. *Biosens. Bioelectron.* **2002,** *17*, 945-951.

(272) Hudak, N. S.; Barton, S. C. Mediated Biocatalytic Cathode for Direct Methanol Membrane-Electrode Assemblies. *J. Electrochem. Soc.* **2005,** *152*, A876-A881.

(273) Sun, Y.; Barton, S. C. Methanol Tolerance of a Mediated, Biocatalytic Oxygen Cathode. *J. Electroanal. Chem.* **2006,** *590*, 57-65.

(274) Chakraborty, D.; Barton, S. C. Influence of Mediator Redox Potential on Fuel Sensitivity of Mediated Laccase Oxygen Reduction Electrodes. *J. Electrochem. Soc.* **2011,** *158*, B440-B447.

(275) Blanford, C. F.; Foster, C. E.; Heath, R. S.; Armstrong, F. A. Efficient Electrocatalytic Oxygen Reduction by the 'Blue' Copper Oxidase, Laccase, Directly Attached to Chemically Modified Carbons. *Farad. Disc.* **2009,** *140*, 319-335.

(276) Xiao, X.; Magner, E. A Biofuel Cell in Non-Aqueous Solution. *Chem. Commun. (Camb)* **2015,** *51*, 13478-13480.

(277) Aquino Neto, S.; Zimbardi, A. L. R. L.; Cardoso, F. P.; Crepaldi, L. B.; Minteer, S. D.; Jorge, J. A.; Furriel, R. P. M.; De Andrade, A. R. Potential Application of Laccase from *Pycnoporus sanguineus* in Methanol/O_2 Biofuel Cells. *J. Electroanal. Chem.* **2016,** *765*, 2-7.

(278) Cardoso, F. P.; Aquino Neto, S.; Fenga, P. G.; Ciancaglini, P.; De Andrade, A. R. Electrochemical Characterization of Methanol/O_2 Biofuel Cell: Use of Laccase Biocathode Immobilized with Polypyrrole Film and PAMAM Dendrimers. *Electrochim. Acta* **2013,** *90*, 90-94.

(279) Ivnitski, D. M.; Khripin, C.; Luckarift, H. R.; Johnson, G. R.; Atanassov, P. Surface Characterization and Direct Bioelectrocatalysis of Multicopper Oxidases. *Electrochim. Acta.* **2010,** *55*, 7385-7393.

(280) Shleev, S.; Wang, Y.; Gorbacheva, M.; Christenson, A.; Haltrich, D.; Ludwig, R.; Ruzgas, T.; Gorton, L. Direct Heterogeneous Electron Transfer Reactions of *Bacillus halodurans* Bacterial Blue Multicopper Oxidase. *Electroanalysis* **2008,** *20*, 963-969.

(281) Saito, K.; Kurose, S.; Tsujino, Y.; Osakai, T.; Kataoka, K.; Sakurai, T.; Tamiya, E. Electrochemical Characterization of a Unique, "Neutral" Laccase from *Flammulina velutipes*. *J. Biosci. Bioeng.* **2013,** *115*, 159-167.

(282) Vincent, K. A.; Cracknell, J. A.; Clark, J. R.; Ludwig, M.; Lenz, O.; Friedrich, B.; Armstrong, F. A. Electricity from Low-Level H_2 in Still Air - an Ultimate Test for an Oxygen Tolerant Hydrogenase. *Chem. Commun.* **2006**, *28*, 5033-5035.

(283) Vincent, K. A.; Cracknell, J. A.; Lenz, O.; Zebger, I.; Friedrich, B.; Armstrong, F. A. Electrocatalytic Hydrogen Oxidation by an Enzyme at High Carbon Monoxide or Oxygen Levels. *Proc. Natl. Acad. Sci. USA* **2005,** *102*, 16951-16954.

(284) Shao, M. L.; Zafar, M. N.; Falk, M.; Ludwig, R.; Sygmund, C.; Peterbauer, C. K.; Guschin, D. A.; MacAodha, D.; Conghaile, P. O.; Leech, D.; Toscano, M.D.; Shleev, S.; Schuhmann, W.; Gorton, L. Optimization of a Membraneless Glucose/Oxygen Enzymatic Fuel Cell Based on a Bioanode with High Coulombic Efficiency and Current Density. *ChemPhysChem* **2013,** *14*, 2260-2269.

(285) Stolarczyk, K.; Nazaruk, E.; Rogalski, J.; Bilewicz, R. Mediatorless Catalytic Oxygen Reduction at Boron-Doped Diamond Electrodes. *Electrochem. Commun.* **2007,** *9*, 115-118.

(286) Skorupska, K.; Lewerenz, H. J.; Berzal, P. U.; Rutkowska, I. A.; Kulesza, P. J. A Semiconductor-Enzyme Photoelectrode for Oxygen Reduction by Direct Transfer of Photogenerated Electrons to Laccase. *J. Mat. Chem.* **2012,** *22*, 15267-15274.

(287) Jensen, U. B.; Lorcher, S.; Vagin, M.; Chevallier, J.; Shipovskov, S.; Koroleva, O.; Besenbacher, F.; Ferapontova, E. E. A 1.76 V Hybrid Zn-O_2 Biofuel Cell with a Fungal Laccase-Carbon Cloth Biocathode. *Electrochim. Acta.* **2012,** *62*, 218-226.

(288) Ueda, A.; Kato, D.; Kurita, R.; Kamata, T.; Inokuchi, H.; Umemura, S.; Hirono, S.; Niwa, O. Efficient Direct Electron Transfer with Enzyme on a Nanostructured Carbon Film Fabricated with a Maskless Top-Down UV/Ozone Process. *J. Am. Chem. Soc.* **2011,** *133*, 4840-4846.

(289) Atanassov, P.; Rojas-Carbonell, S.; Babanova, S.; Serov, A.; Artyushkova, K.; Workman, M.; Santoro, C.; Mirabal, A.; Calabrese Barton, S. Integration of Platinum Group Metal-Free Catalysts with Bilirubin Oxidase into a Hybrid Material for Oxygen Reduction Reaction: Interplay of Chemistry and Morphology. *ChemSusChem* **2017**, DOI:10.1002/cssc.201601822 10.1002/cssc.201601822, n/a-n/a.

(290) Iijima, S. Helical Microtubules of Graphitic Carbon. *Nature* **1991,** *354*, 56-58.

(291) Yu, M. F.; Lourie, O.; Dyer, M. J.; Moloni, K.; Kelly, T. F.; Ruoff, R. S. Strength and Breaking Mechanism of Multiwalled Carbon Nanotubes under Tensile Load. *Science* **2000,** *287*, 637-640.

(292) Britto, P. J.; Santhanam, K. S. V.; Ajayan, P. M. Carbon Nanotube Electrode for Oxidation of Dopamine. *Bioelectrochem. Bioenerg.* **1996,** *41*, 121-125.

(293) Musameh, M.; Lawrence, N. S.; Wang, J. Electrochemical Activation of Carbon Nanotubes. *Electrochem. Commun.* **2005,** *7*, 14-18.

(294) Guell, A. G.; Ebejer, N.; Snowden, M. E.; McKelvey, K.; Macpherson, J. V.; Unwin, P. R. Quantitative Nanoscale Visualization of Heterogeneous Electron Transfer Rates in 2D Carbon Nanotube Networks. *Proc. Natl. Acad. Sci. USA* **2012,** *109*, 11487-11492.

(295) Zheng, W.; Li, Q. F.; Su, L.; Yan, Y. M.; Zhang, J.; Mao, L. Q. Direct Electrochemistry of Multi-Copper Oxidases at Carbon Nanotubes Noncovalently Functionalized with Cellulose Derivatives. *Electroanalysis* **2006,** *18*, 587-594.

(296) Yan, Y. M.; Yehezkeli, O.; Willner, I. Integrated, Electrically Contacted NAD(P)(+)-Dependent Enzyme - Carbon Nanotube Electrodes for Biosensors and Biofuel Cell Applications. *Chem. Eur. J.* **2007,** *13*, 10168-10175.

(297) Ivnitski, D.; Artyushkova, K.; Atanassov, P. Surface Characterization and Direct Electrochemistry of Redox Copper Centers of Bilirubin Oxidase from Fungi *Myrothecium verrucaria*. *Bioelectrochem.* **2008,** *74*, 101-110.

(298) Korani, A.; Salimi, A. Fabrication of High Performance Bioanode Based on Fruitful Association of Dendrimer and Carbon Nanotube Used for Design O_2/Glucose Membrane-Less Biofuel Cell with Improved Bilirubine Oxidase Biocathode. *Biosens. Bioelectron.* **2013,** *50*, 186-193.

(299) Yan, Y. M.; Zheng, W.; Su, L.; Mao, L. Q. Carbon-Nanotube-Based Glucose/O_2 Biofuel Cells. *Adv. Mater.* **2006,** *18*, 2639-2643.

(300) Gao, F.; Yan, Y. M.; Su, L.; Wang, L.; Mao, L. Q. An Enzymatic Glucose/O_2 Biofuel Cell: Preparation, Characterization and Performance in Serum. *Electrochem. Commun.* **2007,** *9*, 989-996.

(301) Nazaruk, E.; Sadowska, K.; Madrak, K.; Biernat, J. F.; Rogalski, J.; Bilewicz, R. Composite Bioelectrodes Based on Lipidic Cubic Phase with Carbon Nanotube Network. *Electroanalysis* **2009,** *21*, 507-511.

(302) Li, X.; Zhang, L.; Su, L.; Ohsaka, T.; Mao, L. A Miniature Glucose/O_2 Biofuel Cell with a High Tolerance against Ascorbic Acid. *Fuel Cells* **2009,** *9*, 85-91.

(303) Ogawa, Y.; Takai, Y.; Kato, Y.; Kai, H.; Miyake, T.; Nishizawa, M. Stretchable Biofuel Cell With Enzyme-Modified Conductive Textiles. *Biosens. Bioelectron.* **2015,** *74*, 947-952.

(304) Garcia, K. E.; Babanova, S.; Scheffler, W.; Hans, M.; Baker, D.; Atanassov, P.; Banta, S. Designed Protein Aggregates Entrapping Carbon Nanotubes for Bioelectrochemical Oxygen Reduction. *Biotechnol. Bioeng.* **2016,** *113*, 2321-2327.

(305) Miyake, T.; Haneda, K.; Yoshino, S.; Nishizawa, M. Flexible, Layered Biofuel Cells. *Biosens. Bioelectron.* **2013,** *40*, 45-49.

(306) Calkins, J. O.; Umasankar, Y.; O'Neill, H.; Ramasamy, R. P. High Photo-Electrochemical Activity of Thylakoid-Carbon Nanotube Composites for Photosynthetic Energy Conversion. *Energy Environ. Sci.* **2013,** *6*, 1891-1900.

(307) Lau, C.; Adkins, E. R.; Ramasamy, R. P.; Luckarift, H. R.; Johnson, G. R.; Atanassov, P. Design of Carbon Nanotube-Based Gas-Diffusion Cathode for O_2 Reduction by Multicopper Oxidases. *Adv. Energy Mat.* **2012,** *2*, 162-168.

(308) Krishnan, S.; Armstrong, F. A. Order-of-Magnitude Enhancement of an Enzymatic Hydrogen-Air Fuel Cell Based on Pyrenyl Carbon Nanostructures. *Chem. Sci.* **2012,** *3*, 1015-1023.

(309) Zheng, W.; Zhao, H. Y.; Zhou, H. M.; Xu, X. X.; Ding, M. H.; Zheng, Y. F. Electrochemistry of Bilirubin Oxidase at Carbon Nanotubes. *J. Solid State Electrochem.* **2010,** *14*, 249-254.

(310) Mateo-Mateo, C.; Michardière, A.-S.; Gounel, S.; Ly, I.; Rouhana, J.; Poulin, P.; Mano, N. Wet-Spun Bioelectronic Fibers of Imbricated Enzymes and Carbon Nanotubes for Efficient Microelectrodes. *ChemElectroChem* **2015,** *2*, 1908-1912.

(311) Wu, X.; Zhao, F.; Varcoe, J. R.; Thumser, A. E.; Avignone-Rossa, C.; Slade, R. C. T. A One-Compartment Fructose/Air Biological Fuel Cell Based on Direct Electron Transfer. *Biosens. Bioelectron.* **2009,** *25*, 326-331.

(312) Reid, R. C.; Jones, S. R.; Hickey, D. P.; Minteer, S. D.; Gale, B. K. Modeling Carbon Nanotube Connectivity and Surface Activity in a Contact Lens Biofuel Cell. *Electrochim. Acta.* **2016,** *203*, 30-40.

(313) Wang, S. C.; Yang, F.; Silva, M.; Zarow, A.; Wang, Y. B.; Iqbal, Z. Membrane-Less and Mediator-Free Enzymatic Biofuel Cell Using Carbon Nanotube/Porous Silicon Electrodes. *Electrochem. Commun.* **2009,** *11*, 34-37.

(314) Vivekananthan, J.; Rincon, R. A.; Kuznetsov, V.; Poller, S.; Schuhmann, W. Biofuel-Cell Cathodes Based on Bilirubin Oxidase Immobilized through Organic Linkers on 3D Hierarchically Structured Carbon Electrodes. *ChemElectroChem* **2014,** *1*, 1901-1908.

(315) Hussein, L.; Rubenwolf, S.; von Stetten, F.; Urban, G.; Zengerle, R.; Krueger, M.; Kerzenmacher, S. A Highly Efficient Buckypaper-Based Electrode Material for

Mediatorless Laccase-Catalyzed Dioxygen Reduction. *Biosens. Bioelectron.* **2011,** *26*, 4133-4138.

(316) Zebda, A.; Gondran, C.; Le Goff, A.; Holzinger, M.; Cinquin, P.; Cosnier, S. Mediatorless High-Power Glucose Biofuel Cells Based on Compressed Carbon Nanotube-Enzyme Electrodes. *Nature Commun.* **2011,** *2*.

(317) Reuillard, B.; Le Goff, A.; Agnes, C.; Zebda, A.; Holzinger, M.; Cosnier, S. Direct Electron Transfer between Tyrosinase and Multi-Walled Carbon Nanotubes for Bioelectrocatalytic Oxygen Reduction. *Electrochem. Commun.* **2012,** *20*, 19-22.

(318) Reuillard, B.; Abreu, C.; Lalaoui, N.; Le Goff, A.; Holzinger, M.; Ondel, O.; Buret, F.; Cosnier, S. One-Year Stability for a Glucose/Oxygen Biofuel Cell Combined with pH Reactivation of the Laccase/Carbon Nanotube Biocathode. *Bioelectrochem.* **2015,** *106*, 73-76.

(319) Scherbahn, V.; Putze, M. T.; Dietzel, B.; Heinlein, T.; Schneider, J. J.; Lisdat, F. Biofuel Cells Based on Direct Enzyme-Electrode Contacts Using PQQ-Dependent Glucose Dehydrogenase/Bilirubin Oxidase and Modified Carbon Nanotube Materials. *Biosens. Bioelectron.* **2014,** *61*, 631-638.

(320) Pankratov, D. V.; Zeifman, Y. S.; Morozova, O. V.; Shumakovich, G. P.; Vasileva, I. S.; Shleev, S.; Popov, V. O.; Yaropolov, A. I. A Comparative Study of Biocathodes Based on Multiwall Carbon Nanotube Buckypapers Modified with Three Different Multicopper Oxidases. *Electroanalysis* **2013,** *25*, 1143-1149.

(321) Halamkova, L.; Halamek, J.; Bocharova, V.; Szczupak, A.; Alfonta, L.; Katz, E. Implanted Biofuel Cell Operating in a Living Snail. *J. Am. Chem. Soc.* **2012,** *134*, 5040-5043.

(322) Stolarczyk, K.; Nazaruk, E.; Rogalski, J.; Bilewicz, R. Nanostructured Carbon Electrodes for Laccase-Catalyzed Oxygen Reduction without Added Mediators. *Electrochim. Acta.* **2008,** *53*, 3983-3990.

(323) Zhao, H. Y.; Zhou, H. M.; Zhang, J. X.; Zheng, W.; Zheng, Y. F. Carbon Nanotube-Hydroxyapatite Nanocomposite: a Novel Platform for Glucose/O_2 Biofuel Cell. *Biosens. Bioelectron.* **2009,** *25*, 463-468.

(324) Katz, E. Applications of Bifunctionnal Reagents for Immobilization of Proteins on a Carbon Electrode Surface - Oriented Immobilization of Photosynthetic Reaction Centers. *J. Electroanal. Chem.* **1994,** *365*, 157-164.

(325) Chen, R. J.; Zhang, Y. G.; Wang, D. W.; Dai, H. J. Noncovalent Sidewall Functionalization of Single-Walled Carbon Nanotubes for Protein Immobilization. *J. Am. Chem. Soc.* **2001,** *123*, 3838-3839.

(326) Strack, G.; Luckarift, H. R.; Nichols, R.; Cozart, K.; Katz, E.; Johnson, G. R. Bioelectrocatalytic Generation of Directly Readable Code: Harnessing Cathodic Current for Long-Term Information Relay. *Chem. Commun.* **2011,** *47*, 7662-7664.

(327) Szczupak, A.; Halamek, J.; Halamkova, L.; Bocharova, V.; Alfonta, L.; Katz, E. Living Battery - Biofuel Cells Operating *in vivo* in Clams. *Energy Environ. Sci.* **2012,** *5*, 8891-8895.

(328) Li, Y.; Huang, X. R.; Qu, Y. B. A Strategy for Efficient Immobilization of Laccase and Horseradish Peroxidase on Single-Walled Carbon Nanotubes. *J. Chem. Technol. Biotechnol.* **2013,** *88*, 2227-2232.

(329) Zheng, W.; Zho, H. M.; Zheng, Y. F.; Wang, N. A Comparative Study on Electrochemistry of Laccase at Two Kinds of Carbon Nanotubes and Its Application for Biofuel Cell. *Chem. Phys. Lett.* **2008,** *457*, 381-385.

(330) So, K.; Onizuka, M.; Komukai, T.; Kitazumi, Y.; Shirai, O.; Kano, K. Significance of the Length of Carbon Nanotubes on the Bioelectrocatalytic Activity of Bilirubin Oxidase for Dioxygen Reduction. *Electrochim. Acta.* **2016,** *192*, 133-138.

(331) Tominaga, M.; Togami, M.; Tsushida, M.; Kawai, D. Effect of N-Doping of Single-Walled Carbon Nanotubes on Bioelectrocatalysis of Laccase. *Anal. Chem.* **2014,** *86*, 5053-5060.

(332) Nogala, W.; Szot, K.; Burchardt, M.; Jonsson-Niedziolka, M.; Rogalski, J.; Wittstock, G.; Opallo, M. Scanning Electrochemical Microscopy Activity Mapping of Electrodes Modified with Laccase Encapsulated in Sol-Gel Processed Matrix. *Bioelectrochem.* **2010,** *79*, 101-107.

(333) Gutierrez-Sanchez, C.; Jia, W. Z.; Beyl, Y.; Pita, M.; Schuhmann, W.; De Lacey, A. L.; Stoica, L. Enhanced Direct Electron Transfer Between Laccase and Hierarchical Carbon Microfibers/Carbon Nanotubes Composite Electrodes. Comparison of Three Enzyme Immobilization Methods. *Electrochim. Acta.* **2012,** *82*, 218-223.

(334) Sosna, M.; Stoica, L.; Wright, E.; Kilburn, J. D.; Schuhmann, W.; Bartlett, P. N. Mass Transport Controlled Oxygen Reduction at Anthraquinone Modified 3D-CNT Electrodes with Immobilized *Trametes hirsuta* Laccase. *Phys. Chem. Chem. Phys.* **2012,** *14*, 11882-11885.

(335) Monsalve, K.; Mazurenko, I.; Lalaoui, N.; Le Goff, A.; Holzinger, M.; Infossi, P.; Nitsche, S.; Lojou, J. Y.; Giudici-Orticoni, M. T.; Cosnier, S.; Lojou, E. A H_2/O_2 Enzymatic Fuel Cell as a Sustainable Power for a Wireless Device. *Electrochem. Commun.* **2015,** *60*, 216-220.

(336) Hickey, D. P.; Reid, R. C.; Milton, R. D.; Minteer, S. D. A Self-Powered Amperometric Lactate Biosensor Based on Lactate Oxidase Immobilized in Dimethylferrocene-modified LPEI. *Biosens. Bioelectron.* **2016,** *77*, 26-31.

(337) Bourourou, M.; Holzinger, M.; Elouarzaki, K.; Le Goff, A.; Bossard, F.; Rossignol, C.; Djurado, E.; Martin, V.; Curtil, D.; Chaussy, D.; Maaref, A.; Cosnier, S. Laccase Wiring on Free-Standing Electrospun Carbon Nanofibres Using a Mediator Plug. *Chem. Commun.* **2015,** *51*, 14574-14577.

(338) Gobel, G.; Beltran, M. L.; Mundhenk, J.; Heinlein, T.; Schneider, J.; Lisdat, F. Operation of a Carbon Nanotube-Based Glucose/Oxygen Biofuel Cell in Human Body Liquids-Performance Factors and Characteristics. *Electrochim. Acta.* **2016,** *218*, 278-284.

(339) Reid, R. C.; Minteer, S. D.; Gale, B. K. Contact Lens Biofuel Cell Tested in a Synthetic Tear Solution. *Biosens. Bioelectron.* **2015,** *68*, 142-148.

(340) Bellucci, S.; Chiaretti, M.; Cucina, A.; Carru, G. A.; Chiaretti, A. I. Multiwalled Carbon Nanotube Buckypaper: Toxicology and Biological Effects *in vitro* and *in vivo*. *Nanomedicine* **2009,** *4*, 531-540.

(341) Miyake, T.; Yoshino, S.; Yamada, T.; Hata, K.; Nishizawa, M. Self-Regulating Enzyme-Nanotube Ensemble Films and Their Application as Flexible Electrodes for Biofuel Cells. *J. Am. Chem. Soc.* **2011,** *133*, 5129-5134.

(342) Reuillard, B.; Le Goff, A.; Agnes, C.; Holzinger, M.; Zebda, A.; Gondran, C.; Elouarzaki, K.; Cosnier, S. High Power Enzymatic Biofuel Cell Based On Naphthoquinone-Mediated Oxidation of Glucose by Glucose Oxidase in a Carbon Nanotube 3D Matrix. *Phys. Chem. Chem. Phys.* **2013,** *15*, 4892-4896.

(343) Katsnelson, M. I.; Novoselov, K. S.; Geim, A. K. Chiral Tunnelling and the Klein Paradox in Graphene. *Nature Phys.* **2006,** *2*, 620-625.

(344) Zhou, X. H.; Huang, X. R.; Liu, L. H.; Bai, X.; Shi, H. C. Direct Electron Transfer Reaction of Laccase on a Glassy Carbon Electrode Modified with 1-Aminopyrene Functionalized Reduced Graphene Oxide. *RSC Adv.* **2013,** *3*, 18036-18043.

(345) Swietlikowska, A.; Gniadek, M.; Palys, B. Electrodeposited Graphene Nano-Stacks for Biosensor Applications. Surface Groups as Redox Mediators for Laccase. *Electrochim. Acta.* **2013,** *98*, 75-81.

(346) Filip, J.; Sefcovicova, J.; Gemeiner, P.; Tkac, J. In *Materials And Applications for Sensors And Transducers Ii*; Hristoforou, E.;Vlachos, D. S., Eds., 2013; Vol. 543.

(347) Filip, J.; Tkac, J. Is Graphene Worth Using in Biofuel Cells? *Electrochim. Acta.* **2014,** *136*, 340-354.

(348) Lalaoui, N.; Le Goff, A.; Holzinger, M.; Mermoux, M.; Cosnier, S. Wiring Laccase on Covalently Modified Graphene: Carbon Nanotube Assemblies for the Direct Bio-electrocatalytic Reduction of Oxygen. *Chem. Eur. J.* **2015,** *21*, 3198-3201.

(349) Campbell, A. S.; Jeong, Y. J.; Geier, S. M.; Koepsel, R. R.; Russell, A. J.; Islam, M. F. Membrane/Mediator-Free Rechargeable Enzymatic Biofuel Cell Utilizing Graphene/Single-Wall Carbon Nanotube Cogel Electrodes. *ACS Appl. Mater. Interfaces* **2015,** *7*, 4056-4065.

(350) Campbell, A. S.; Jose, M. V.; Marx, S.; Cornelius, S.; Koepsel, R. R.; Islam, M. F.; Russell, A. J. Improved Power Density of an Enzymatic Biofuel Cell with Fibrous Supports of High Curvature. *RSC Adv.* **2016,** *6*, 10150-10158.

(351) Chen, J. Y.; Zhou, C.; Liu, H. Y.; Li, P.; Song, Y. H.; Xu, F. G. Signal Amplification of Self-Potential Biosensor for Glucose Monitoring. *Int. J. Electrochem. Sci.* **2015,** *10*, 9142-9153.

(352) Lee, H. U.; Yoo, H. Y.; Lkhagvasuren, T.; Song, Y. S.; Park, C.; Kim, J.; Kim, S. W. Enzymatic Fuel Cells Based on Electrodeposited Graphite Oxide/Cobalt Hydroxide/Chitosan Composite-Enzyme Electrode. *Biosens. Bioelectron.* **2013,** *42*, 342-348.

(353) Shiba, S.; Inoue, J.; Kato, D.; Yoshioka, K.; Niwa, O. Graphene Modified Electrode for the Direct Electron Transfer of Bilirubin Oxidase. *Electrochemistry* **2015,** *83*, 332-334.

(354) Korkut, S.; Kilic, M. S.; Uzuncar, S.; Hazer, B. Novel Graphene-Modified Poly(styrene-b-isoprene-b-styrene) Enzymatic Fuel Cell with Operation in Plant Leaves. *Anal. Lett.* **2016,** *49*, 2322-2336.

(355) Filip, J.; Tkac, J. Effective Bioelectrocatalysis of Bilirubin Oxidase on Electrochemically Reduced Graphene Oxide. *Electrochem. Commun.* **2014,** *49*, 70-74.

(356) Tominaga, M.; Noda, N.; Hashiguchi, T.; Mizuta, H.; Kawai, D.; Togami, M. Improvement of Laccase Bioelectrocatalyst at a Phosphate Templating Graphene Nanoplatelet Plate Electrode. *Electrochem. Commun.* **2015,** *59*, 32-35.

(357) Hoshi, K.; Muramatsu, K.; Sumi, H.; Nishioka, Y. Graphene-Coated Carbon Fiber Cloth for Flexible Electrodes of Glucose Fuel Cells. *Jpn. J. Appl. Phys.* **2016,** *55*.

(358) Filip, J.; Andicsova-Eckstein, A.; Vikartovska, A.; Tkac, J. Immobilization of Bilirubin Oxidase on Graphene Oxide Flakes with Different Negative Charge Density for Oxygen Reduction. The Effect of GO Charge Density on Enzyme Coverage, Electron Transfer Rate and Current Density. *Biosens. Bioelectron.* **2017,** *89*, 384-389.

(359) Song, Y.; Chen, C. H.; Wang, C. L. Graphene/Enzyme-Encrusted Three-Dimensional Carbon Micropillar Arrays for Mediatorless Micro-Biofuel Cells. *Nanoscale* **2015,** *7*, 7084-7090.

(360) Koushanpour, A.; Guz, N.; Gamella, M.; Katz, E. Biofuel Cell Based on Carbon Fiber Electrodes Functionalized with Graphene Nanosheets. *ECS J Solid State Sci. Technol.* **2016,** *5*, M3037-M3040.

(361) Zhao, M.; Gao, Y.; Sun, J. Y.; Gao, F. Mediatorless Glucose Biosensor and Direct Electron Transfer Type Glucose/Air Biofuel Cell Enabled with Carbon Nanodots. *Anal. Chem.* **2015,** *87,* 2615-2622.

(362) Gao, F.; Guo, X. Y.; Yin, J.; Zhao, D.; Li, M. G.; Wang, L. Electrocatalytic Activity of Carbon Spheres towards NADH Oxidation at Low Overpotential and Its Applications in Biosensors and Biofuel Cells. *RSC Adv.* **2011,** *1,* 1301-1309.

(363) Habrioux, A.; Napporn, T.; Servat, K.; Tingry, S.; Kokoh, K. B. Electrochemical Characterization of Adsorbed Bilirubin Oxidase on Vulcan XC 72R for the Biocathode Preparation in a Glucose/O_2 Biofuel Cell. *Electrochim. Acta.* **2010,** *55,* 7701-7705.

(364) Szot, K.; Nogala, W.; Niedziolka-Jonsson, J.; Jonsson-Niedziolka, M.; Marken, F.; Rogalski, J.; Kirchner, C. N.; Wittstock, G.; Opallo, M. Hydrophilic Carbon Nanoparticle-Laccase Thin Film Electrode for Mediatorless Dioxygen Reduction SECM Activity Mapping and Application in Zinc-Dioxygen Battery. *Electrochim. Acta.* **2009,** *54,* 4620-4625.

(365) Wang, K. Q.; Tang, J.; Zhang, Z. M.; Gao, Y.; Chen, G. Laccase on Black Pearl 2000 Modified Glassy Carbon Electrode: Characterization of Direct Electron Transfer and Biological Sensing Properties for Pyrocatechol. *Electrochim. Acta.* **2012,** *70,* 112-117.

(366) Shleev, S.; Shumakovich, G.; Morozova, O.; Yaropolov, A. Stable 'Floating' Air Diffusion Biocathode Based on Direct Electron Transfer Reactions Between Carbon Particles and High Redox Potential Laccase. *Fuel Cells* **2010,** *10,* 726-733.

(367) Santoro, C.; Babanova, S.; Erable, B.; Schuler, A.; Atanassov, P. Bilirubin Oxidase Based Enzymatic Air-Breathing Cathode: Operation under Pristine and Contaminated Conditions. *Bioelectrochem.* **2016,** *108,* 1-7.

(368) Haneda, K.; Yoshino, S.; Ofuji, T.; Miyake, T.; Nishizawa, M. Sheet-Shaped Biofuel Cell Constructed from Enzyme-Modified Nanoengineered Carbon Fabric. *Electrochim. Acta* **2012,** *82*, 175-178.

(369) ShitAnda, I.; Kato, S.; Hoshi, Y.; Itagaki, M.; Tsujimura, S. Flexible and High-Performance Paper-Based Biofuel Cells Using Printed Porous Carbon Electrodes. *Chem. Commun. (Camb)* **2013,** *49*, 11110-11112.

(370) Filip, J.; Tkac, J. Direct Electron Transfer of Bilirubin Oxidase on Graphene and Carbon Black. *J. Biotech.* **2014,** *185*, S21-S22.

(371) Sugimoto, Y.; Kitazumi, Y.; Shirai, O.; Kano, K. Effects of Mesoporous Structures on Direct Electron Transfer-Type Bioelectrocatalysis: Facts and Simulation on a Three-Dimensional Model of Random Orientation of Enzymes. *Electrochemistry* **2017,** *85*, 82-87.

(372) de Poulpiquet, A.; Ciaccafava, A.; Gadiou, R.; Gounel, S.; Giudici-Orticoni, M. T.; Mano, N.; Lojou, E. Design of a H_2/O_2 Biofuel Cell Based on Thermostable Enzymes. *Electrochem. Commun.* **2014,** *42*, 72-74.

(373) Trifonov, A.; Herkendell, K.; Tel-Vered, R.; Yehezkeli, O.; Woerner, M.; Willner, I. Enzyme-Capped Relay-Functionalized Mesoporous Carbon Nanoparticles: Effective Bioelectrocatalytic Matrices for Sensing and Biofuel Cell Applications. *ACS Nano* **2013,** *7*, 11358-11368.

(374) Kamitaka, Y.; Tsujimura, S.; Setoyama, N.; Kajino, T.; Kano, K. Fructose/Dioxygen Biofuel Based on Direct Electron Transfer-Type Bioelectrocatalysis. *Phys. Chem. Chem. Phys.* **2007,** *9*, 1793-1801.

(375) Tsujimura, S.; Kamitaka, Y.; Kano, K. Diffusion-Controlled Oxygen Reduction on Multicopper Oxidase-Adsorbed Carbon Aerogel Electrodes without Mediator. *Fuel Cells* **2007,** *7*, 463-469.

(376) Tsujimura, S.; Suraniti, E.; Durand, F.; Mano, N. Oxygen Reduction Reactions of the Thermostable Bilirubin Oxidase from *Bacillus Pumilus* on Mesoporous Carbon-Cryogel Electrodes. *Electrochim. Acta* **2014,** *117*, 263-267.

(377) Filip, J.; Monosik, R.; Tkac, J. Poly(lactic acid)-Based Nanocomposite for Construction of Efficient Bilirubin Oxidase-Based Biocathodes and Stable Biofuel Cells. *Int. J. Electrochem. Sci.* **2014,** *9*, 2491-2506.

(378) Laviron, E. Voltammetric Methods for the Study of Adsorbed Species. *Electroanal. Chem.* **1982,** *12*, 53-157.

(379) Sugimoto, Y.; Takeuchi, R.; Kitazumi, Y.; Shirai, O.; Kano, K. Significance of Mesoporous Electrodes for Non Catalytic Faradaic Process of Randomly Oriented Redox Proteins. *J. Phys. Chem. C* **2016,** *120*, 26270-26277.

(380) Funabashi, H.; Takeuchi, S.; Tsujimura, S. Hierarchical Meso/Macro-porous Carbon Fabricated from Dual MgO Templates for Direct Electron Transfer Enzymatic Electrodes. *Sci. Rep.* **2017,** *7*, 45147.

(381) Xu, L.; Armstrong, F. A. Pushing the Limits for Enzyme-based Membrane-Less Hydrogen Fuel Cells - Achieving Useful Power and Stability. *RSC Adv.* **2015,** *5*, 3649-3656.

(382) Rubenwolf, S.; Strohmeier, O.; Kloke, A.; Kerzenmacher, S.; Zengerle, R.; von Stetten, F. Carbon Electrodes for Direct Electron Transfer Type Laccase Cathodes Investigated by Current Density-Cathode Potential Behavior. *Biosens. Bioelectron.* **2010,** *26*, 841-845.

(383) Lyskawa, J.; Belanger, D. Direct Modification of a Gold Electrode with Aminophenyl Groups by Electrochemical Reduction of *in situ* Generated Aminophenyl Monodiazonium Cations. *Chem. Mater.* **2006,** *18*, 4755-4763.

(384) Bernard, M. C.; Chausse, A.; Cabet-Deliry, E.; Chehimi, M. M.; Pinson, J.; Podvorica, F.; Vautrin-Ul, C. Organic Layers Bonded to Industrial, Coinage, and Noble Metals through Electrochemical Reduction of Aryldiazonium Salts. *Chem. Mater.* **2003,** *15*, 3450-3462.

(385) Wang, X. J.; Falk, M.; Ortiz, R.; Matsumura, H.; Bobacka, J.; Ludwig, R.; Bergelin, M.; Gorton, L.; Shleev, S. Mediatorless Sugar/Oxygen Enzymatic Fuel Cells Based on Gold Nanoparticle-Modified Electrodes. *Biosens. Bioelectron.* **2012,** *31*, 219-225.

(386) Pankratov, D.; Sundberg, R.; Suyatin, D. B.; Sotres, J.; Barrantes, A.; Ruzgas, T.; Maximov, I.; Montelius, L.; Shleev, S. The Influence of Nanoparticles on Enzymatic Bioelectrocatalysis. *RSC Adv.* **2014,** *4*, 38164-38168.

(387) Pankratov, D. V.; Zeifman, Y. S.; Dudareva, A. V.; Pankratova, G. K.; Khlupova, M. E.; Parunova, Y. M.; Zajtsev, D. N.; Bashirova, N. F.; Popov, V. O.; Shleev, S. V. Impact of Surface Modification with Gold Nanoparticles on the Bioelectrocatalytic Parameters of Immobilized Bilirubin Oxidase. *Acta Naturae* **2014,** *6*, 102-106.

(388) Krikstolaityte, V.; Lamberg, P.; Toscano, M. D.; Silow, M.; Eicher-Lorka, O.; Ramanavicius, A.; Niaura, G.; Abariute, L.; Ruzgas, T.; Shleev, S. Mediatorless Carbohydrate/Oxygen Biofuel Cells with Improved Cellobiose Dehydrogenase Based Bioanode. *Fuel Cells* **2014,** *14*, 792-800.

(389) Lamberg, P.; Shleev, S.; Ludwig, R.; Arnebrant, T.; Ruzgas, T. Performance of Enzymatic Fuel Cell in Cell Culture. *Biosens. Bioelectron.* **2014,** *55*, 168-173.

(390) Murata, K.; Kajiya, K.; Nakamura, N.; Ohno, H. Direct Electrochemistry of Bilirubin Oxidase on Three-Dimensional Gold Nanoparticle Electrodes and Its Application in a Biofuel Cell. *Energy Environ. Sci.* **2009,** *2*, 1280-1285.

(391) Falk, M.; Andoralov, V.; Silow, M.; Toscano, M. D.; Shleev, S. Miniature Biofuel Cell as a Potential Power Source for Glucose-Sensing Contact Lenses. *Anal. Chem.* **2013,** *85*, 6342-6348.

(392) Monsalve, K.; Roger, M.; Gutierrez-Sanchez, C.; Ilbert, M.; Nitsche, S.; Byrne-Kodjabachian, D.; Marchi, V.; Lojou, E. Hydrogen Bioelectrooxidation on Gold Nanoparticle-Based Electrodes Modified by *Aquifex aeolicus* Hydrogenase: Application to Hydrogen/Oxygen Enzymatic Biofuel Cells. *Bioelectrochem.* **2015,** *106*, 47-55.

(393) Gutierrez-Sanchez, C.; Pita, M.; Vaz-Dominguez, C.; Shleev, S.; De Lacey, A. L. Gold Nanoparticles as Electronic Bridges for Laccase-Based Biocathodes. *J. Am. Chem. Soc.* **2012,** *134*, 17212-17220.

(394) Di Bari, C.; Shleev, S.; De Lacey, A. L.; Pita, M. Laccase-Modified Gold Nanorods for Electrocatalytic Reduction of Oxygen. *Bioelectrochem.* **2016,** *107*, 30-36.

(395) Le, T. X. H.; Bechelany, M.; Engel, A. B.; Cretin, M.; Tingry, S. Gold Particles Growth on Carbon Felt for Efficient Micropower Generation in a Hybrid Biofuel Cell. *Electrochim. Acta.* **2016,** *219*, 121-129.

(396) Diaconu, M.; Chira, A.; Radu, L. Modulating Indium Doped Tin Oxide Electrode Properties for Laccase Electron Transfer Enhancement. *Thin Solid Films* **2014,** *565*, 84-88.

(397) Gao, C. M.; Zhang, L. N.; Wang, Y. H.; Yu, J. H.; Song, X. R. Visible-Light Driven Biofuel Cell Based on Hierarchically Branched Titanium Dioxide Nanorods Photoanode for Tumor Marker Detection. *Biosens. Bioelectron.* **2016,** *83*, 327-333.

(398) Siepenkoetter, T.; Salaj-Kosla, U.; Xiao, X. X.; Belochapkine, S.; Magner, E. Nanoporous Gold Electrodes with Tuneable Pore Sizes for Bioelectrochemical Applications. *Electroanalysis* **2016,** *28*, 2415-2423.

(399) Ressine, A.; Vaz-Dominguez, C.; Fernandez, V. M.; De Lacey, A. L.; Laurell, T.; Ruzgas, T.; Shleev, S. Bioelectrochemical Studies of Azurin and Laccase Confined in Three-Dimensional Chips Based on Gold-modified Nano-/Microstructured Silicon. *Biosens. Bioelectron.* **2010,** *25*, 1001-1007.

(400) du Toit, H.; Di Lorenzo, M. Glucose Oxidase Directly Immobilized onto Highly Porous Gold Electrodes for Sensing and Fuel Cell Applications. *Electrochim. Acta.* **2014,** *138*, 86-92.

(401) Hou, C. T.; Yang, D. P.; Liang, B.; Liu, A. H. Enhanced Performance of a Glucose/O_2 Biofuel Cell Assembled with Laccase-Covalently Immobilized Three-Dimensional Macroporous Gold Film-Based Biocathode and Bacterial Surface Displayed Glucose Dehydrogenase-Based Bioanode. *Anal. Chem.* **2014,** *86*, 6057-6063.

(402) Karajic, A.; Reculusa, S.; Heim, M.; Garrigue, P.; Ravaine, S.; Mano, N.; Kuhn, A. Bottom-up Generation of Miniaturized Coaxial Double Electrodes with Tunable Porosity. *Adv. Mat. Int.* **2015,** *2*, 1500192

(403) Karajic, A.; Reculusa, S.; Ravaine, S.; Mano, N.; Kuhn, A. Miniaturized Electrochemical Device from Assembled Cylindrical Macroporous Gold Electrodes. *ChemElectroChem* **2016,** *3*, 2031-2035.

(404) Xiao, X.; Si, P.; Magner, E. An Overview of Dealloyed Nanoporous Gold in Bioelectrochemistry. *Bioelectrochem.* **2016,** *109*, 117-126.

(405) Trasatti, S.; Petrii, O. A. Real Surface-Area Measurements in Electrochemistry. *Pure Appl. Chem.* **1991,** *63*, 711-734.

(406) Yan, Y.-M.; Baravik, I.; Tel-Vered, R.; Willner, I. An Ethanol/O_2 Biofuel Cell Based on an Electropolymerized Bilirubin Oxidase/Pt Nanoparticle Bioelectrocatalytic O_2-Reduction Cathode. *Adv. Mater.* **2009,** *21*, 4275-4279.

(407) Nakamura, R.; Kamiya, K.; Hashimoto, K. Direct Electron Transfer Conduits Constructed at the Interface between Multicopper Oxidase and Nanocrystalline Semiconductive Fe Oxides. *Chem. Phys. Lett.* **2010,** *498*, 307-311.

(408) Wen, D.; Liu, W.; Herrmann, A. K.; Eychmuller, A. A Membraneless Glucose/O_2 Biofuel Cell Based on Pd Aerogels. *Chem. Eur. J.* **2014,** *20*, 4380-4385.

(409) Zhou, Y.; Umasankar, Y.; Ramasamy, R. P. Laccase-TiO_2 Nanoconjugates as Catalysts for Oxygen Reduction Reaction in Biocathodes. *J. Electrochem. Soc.* **2015,** *162*, H911-H917.

(410) Kashyap, D.; Yadav, R. S.; Gohil, S.; Venkateswaran, P. S.; Pandey, J. K.; Kim, G. M.; Kim, Y. H.; Dwivedi, P. K.; Sharma, A.; Ayyub, P.; Goel, S. Fabrication of Vertically Aligned Copper Nanotubes as a Novel Electrode for Enzymatic Biofuel Cells. *Electrochim. Acta.* **2015,** *167*, 213-218.

(411) Almeida, I.; Henriques, F.; Carvalho, M. D.; Viana, A. S. Carbon Disulfide Mediated Self-Assembly of Laccase and Iron Oxide Nanoparticles on Gold Surfaces for Biosensing Applications. *J. Colloid Interface Sci.* **2017,** *485*, 242-250.

(412) Li, Y.; Chen, S. M.; Chen, W. C.; Li, Y. S.; Ali, M. A.; AlHemaid, F. M. A. Platinum Nanoparticles (PtNPs) - Laccase Assisted Biocathode Reduction of Oxygen for Biofuel Cells. *Int. J. Electrochem. Sci.* **2011,** *6*, 6398-6409.

(413) Dagys, M.; Haberska, K.; Shleev, S.; Arnebrant, T.; Kulys, J.; Ruzgas, T. Laccase-Gold Nanoparticle Assisted Bioelectrocatalytic Reduction of Oxygen. *Electrochem. Commun.* **2010,** *12*, 933-935.

(414) Krikstolaityte, V.; Barrantes, A.; Ramanavicius, A.; Arnebrant, T.; Shleev, S.; Ruzgas, T. Bioelectrocatalytic Reduction of Oxygen at Gold Nanoparticles Modified with Laccase. *Bioelectrochem.* **2014,** *95*, 1-6.

(415) Gutierrez-Sanchez, C.; Pita, M.; Toscano, M. D.; De Lacey, A. L. Bilirubin Oxidase-Based Nanobiocathode Working in Serum-Mimic Buffer for Implantable Biofuel Cell. *Electroanalysis* **2013,** *25*, 1359-1362.

(416) Suzuki, M.; Murata, K.; Nakamura, N.; Ohno, H. The Effect of Particle Size on the Direct Electron Transfer Reactions of Metalloproteins Using Au Nanoparticle-Modified Electrodes. *Electrochemistry* **2012,** *80*, 337-339.

(417) Rahman, M. A.; Noh, H. B.; Shim, Y. B. Direct Electrochemistry of Laccase Immobilized on Au Nanoparticles Encapsulated-Dendrimer Bonded Conducting Polymer: Application for a Catechin Sensor. *Anal. Chem.* **2008,** *80*, 8020-8027.

(418) Ilcikova, M.; Filip, J.; Mrlik, M.; Plachy, T.; Tkac, J.; Kasak, P. Polypyrrole Nanotubes Decorated with Gold Particles Applied for Construction of Enzymatic Bioanodes and Biocathodes. *Int. J. Electrochem. Sci.* **2015,** *10*, 6558-6571.

(419) Dagys, M.; Lamberg, P.; Shleev, S.; Niaura, G.; Bachmatova, I.; Marcinkeviciene, L.; Meskys, R.; Kulys, J.; Arnebrant, T.; Ruzgas, T. Comparison of Bioelectrocatalysis at *Trichaptum abietinum* and *Trametes hirsuta* Laccase Modified Electrodes. *Electrochim. Acta.* **2014,** *130*, 141-147.

(420) Kizling, M.; Dzwonek, M.; Olszewski, B.; Bącal, P.; Tymecki, Ł.; Więckowska, A.; Stolarczyk, K.; Bilewicz, R. Reticulated Vitreous Carbon as a Scaffold for Enzymatic Fuel Cell Designing. *Biosens. Bioelectron.* **2017,** *95*, 1-7.

(421) Falk, M.; Andoralov, V.; Blum, Z.; Sotres, J.; Suyatin, D. B.; Ruzgas, T.; Arnebrant, T.; Shleev, S. Biofuel Cell as a Power Source for Electronic Contact Lenses. *Biosens. Bioelectron.* **2012,** *37*, 38-45.

(422) Falk, M.; Pankratov, D.; Lindh, L.; Arnebrant, T.; Shleev, S. Miniature Direct Electron Transfer Based Enzymatic Fuel Cell Operating in Human Sweat and Saliva. *Fuel Cells* **2014,** *14*, 1050-1056.

(423) Zeng, T.; Pankratov, D.; Falk, M.; Leimkuhler, S.; Shleev, S.; Wollenberger, U. Miniature Direct Electron Transfer Based Sulphite/Oxygen Enzymatic Fuel Cells. *Biosens. Bioelectron.* **2015,** *66*, 39-42.

(424) Grippo, V.; Pawłowska, J.; Biernat, J. F.; Bilewicz, R. Synergic Effect of Naphthylated Carbon Nanotubes and Gold Nanoparticles on Catalytic Performance of Hybrid Films Containing Bilirubin Oxidase for the Dioxygen Reduction. *Electroanalysis* **2017,** *29*, 103-109.

(425) Pankratov, D.; Sundberg, R.; Sotres, J.; Suyatin, D. B.; Maximov, I.; Shleev, S.; Montelius, L. Scalable, High Performance, Enzymatic Cathodes Based on Nanoimprint Lithography. *Beilstein J. Nanotech.* **2015,** *6*, 1377-1384.

(426) Siepenkoetter, T.; Salaj-Kosla, U.; Xiao, X.; Conghaile, P. Ó.; Pita, M.; Ludwig, R.; Magner, E. Immobilization of Redox Enzymes on Nanoporous Gold Electrodes: Applications in Biofuel Cells. *ChemPlusChem* **2016**, 82, 553-560

(427) Coman, V.; Vaz-Dominguez, C.; Ludwig, R.; Herreither, W.; Haltrich, D.; De Lacey, A. L.; RuzGas, T.; Gorton, L.; Shleev, S. A Membrane-, Mediator-, Cofactor-Less Glucose/Oxygen Biofuel Cell. *Phys. Chem. Chem. Phys.* **2008,** *10*, 6093-6096.

(428) Olejnik, P.; Palys, B.; Kowalczyk, A.; Nowicka, A. M. Orientation of Laccase on Charged Surfaces. Mediatorless Oxygen Reduction on Amino- and Carboxyl-Ended Ethylphenyl Groups. *J. Phys. Chem. C* **2012,** *116*, 25911-25918.

(429) Doppelt, P.; Hallais, G.; Pinson, J.; Podvorica, F.; Verneyre, S. Surface Modification of Conducting Substrates. Existence of Azo Bonds in the Structure of Organic Layers Obtained from Diazonium Salts. *Chem. Mater.* **2007,** *19*, 4570-4575.

(430) Ardhaoui, M.; Zheng, M. H.; Pulpytel, J.; Dowling, D.; Jolivalt, C.; Khonsari, F. A. Plasma Functionalized Carbon Electrode for Laccase-Catalyzed Oxygen Reduction by Direct Electron Transfer. *Bioelectrochem.* **2013,** *91*, 52-61.

(431) Xue, Q.; Kato, D.; Kamata, T.; Guo, Q.; You, T.; Niwa, O. Improved Direct Electrochemistry for Proteins Adsorbed on a UV/Ozone-Treated Carbon Nanofiber Electrode. *Anal. Sci.* **2013,** *29*, 611-618.

(432) Lalaoui, N.; Le Goff, A.; Holzinger, M.; Cosnier, S. Fully Oriented Bilirubin Oxidase on Porphyrin-Functionalized Carbon Nanotube Electrodes for Electrocatalytic Oxygen Reduction. *Chem. Eur. J.* **2015,** *21*, 16868-16873.

(433) Lalaoui, N.; David, R.; Jamet, H.; Holzinger, M.; Le Goff, A.; Cosnier, S. Hosting Adamantane in the Substrate Pocket of Laccase: Direct Bioelectrocatalytic Reduction of O_2 on Functionalized Carbon Nanotubes. *ACS Catal.* **2016,** *6*, 4259-4264.

(434) Mazurenko, I.; Monsalve, K.; Rouhana, J.; Parent, P.; Laffon, C.; Le Goff, A.; Szunerits, S.; Boukherroub, R.; Giudici-Orticoni, M. T.; Mano, N.; Lojou E. How The Intricate Interactions between Carbon Nanotubes and two Bilirubin Oxidases Control Direct and Mediated O_2 Reduction. *ACS Appl. Mater. Interfaces* **2016,** *8*, 23074-23085.

(435) Giroud, F.; Sawada, K.; Taya, M.; Cosnier, S. 5,5-Dithiobis(2-nitrobenzoic acid) Pyrene Derivative-Carbon Nanotube Electrodes for NADH Electrooxidation and Oriented Immobilization of Multicopper Oxidases for the Development of Glucose/O_2 Biofuel Cells. *Biosens. Bioelectron.* **2017,** *87*, 957-963.

(436) Giroud, F.; Milton, R. D.; Tan, B. X.; Minteer, S. D. Simplifying Enzymatic Biofuel Cells: Immobilized Naphthoquinone as a Biocathodic Orientational Moiety and Bioanodic Electron Mediator. *ACS Catal.* **2015,** *5*, 1240-1244.

(437) Korani, A.; Salimi, A. High Performance Glucose/O_2 Compartment-Less Biofuel Cell Using DNA/CNTs as Platform for Immobilizing Bilirubin Oxidase as Novel Biocathode and Integrated NH_2-CNTs/Dendrimer/Glucose Dehydrogenase/Nile Blue as Bioanode. *Electrochim. Acta.* **2015,** *185*, 90-100.

(438) Blanford, C. F.; Heath, R. S.; Armstrong, F. A. A Stable Electrode for High-Potential, Electrocatalytic O_2 Reduction Based on Rational Attachment of a Blue Copper Oxidase to a Graphite Surface. *Chem. Commun.* **2007**, 17, 1710-1712.

(439) Meredith, M. T.; Minson, M.; Hickey, D.; Artyushkova, K.; Glatzhofer, D. T.; Minteer, S. D. Anthracene-modified Multi-Walled Carbon Nanotubes as Direct Electron Transfer Scaffolds for Enzymatic Oxygen Reduction. *ACS Catal.* **2011,** *1*, 1683-1690.

(440) Giroud, F.; Minteer, S. D. Anthracene-Modified Pyrenes Immobilized on Carbon Nanotubes for Direct Electroreduction of O_2 by Laccase. *Electrochem. Commun.* **2013,** *34*, 157-160.

(441) Stolarczyk, K.; Lyp, D.; Zelechowska, K.; Biernat, J. F.; Rogalski, J.; Bilewicz, R. Arylated Carbon Nanotubes for Biobatteries and Biofuel Cells. *Electrochim. Acta.* **2012,** *79*, 74-81.

(442) Stolarczyk, K.; Sepelowska, M.; Lyp, D.; Zelechowska, K.; Biernat, J. F.; Rogalski, J.; Farmer, K. D.; Roberts, K. N.; Bilewicz, R. Hybrid Biobattery Based on Arylated Carbon Nanotubes and Laccase. *Bioelectrochem.* **2012,** *87*, 154-163.

(443) Lorcher, S.; Lopes, P.; Kartashov, A.; Ferapontova, E. E. Direct Bio-electrocatalysis of O_2 Reduction by *Streptomyces coelicolor* Laccase Orientated at Promoter-Modified Graphite Electrodes. *ChemPhysChem* **2013,** *14*, 2112-2124.

(444) Sosna, M.; Chretien, J. M.; Kilburn, J. D.; Bartlett, P. N. Monolayer Anthracene and Anthraquinone Modified Electrodes as Platforms for *Trametes hirsuta* Laccase Immobilisation. *Phys. Chem. Chem. Phys.* **2010,** *12*, 10018-10026.

(445) Thorum, M. S.; Anderson, C. A.; Hatch, J. J.; Campbell, A. S.; Marshall, N. M.; Zimmerman, S. C.; Lu, Y.; Gewirth, A. A. Direct, Electrocatalytic Oxygen Reduction

by Laccase on Anthracene-2-Methanethiol-Modified Gold. *J. Phys. Chem. Lett.* **2010,** *1*, 2251-2254.

(446) Traunsteiner, C.; Sek, S.; Huber, V.; Valero-Vidal, C.; Kunze-Liebhauser, J. Laccase Immobilized on a Mixed Thiol Monolayer on Au(111) - Structure-Dependent Activity towards Oxygen Reduction. *Electrochim. Acta.* **2016,** *213*, 761-770.

(447) Karaskiewicz, M.; Nazaruk, E.; Zelechowska, K.; Biernat, J. F.; Rogalski, J.; Bilewicz, R. Fully Enzymatic Mediatorless Fuel Cell with Efficient Naphthylated Carbon Nanotube-Laccase Composite Cathodes. *Electrochem. Commun.* **2012,** *20*, 124-127.

(448) Nazaruk, E.; Karaskiewicz, M.; Zelechowska, K.; Biernat, J. F.; Rogalski, J.; Bilewicz, R. Powerful Connection of Laccase and Carbon Nanotubes Material for Mediator-Free Electron Transport on the Enzymatic Cathode of the Biobattery. *Electrochem. Commun.* **2012,** *14*, 67-70.

(449) Neto, S. A.; Zimbardi, A.; Cardoso, F. P.; Crepaldi, L. B.; Minteer, S. D.; Jorge, J. A.; Furriel, R. P. M.; De Andrade, A. R. Potential Application of Laccase from *Pycnoporus sanguineus* in Methanol/O_2 Biofuel Cells. *J. Electroanal. Chem.* **2016,** *765*, 2-7.

(450) Kizling, M.; Stolarczyk, K.; Kiat, J. S. S.; Tammela, P.; Wang, Z. H.; Nyholm, L.; Bilewicz, R. Pseudocapacitive Polypyrrole-Nanocellulose Composite for Sugar-Air Enzymatic Fuel Cells. *Electrochem. Commun.* **2015,** *50*, 55-59.

(451) Stolarczyk, K.; Kizling, M.; Majdecka, D.; Zelechowska, K.; Biernat, J. F.; Rogalski, J.; Bilewicz, R. Biobatteries and Biofuel Cells with Biphenylated Carbon Nanotubes. *J. Power Sources* **2014,** *249*, 263-269.

(452) Bourourou, M.; Elouarzaki, K.; Lalaoui, N.; Agnes, C.; Le Goff, A.; Holzinger, M.; Maaref, A.; Cosnier, S. Supramolecular Immobilization of Laccase on Carbon

Nanotube Electrodes Functionalized with (Methylpyrenylaminomethyl)anthraquinone for Direct Electron Reduction of Oxygen. *Chem. Eur. J.* **2013,** *19*, 9371-9375.

(453) Tominaga, M.; Sasaki, A.; Togami, M. Laccase Bioelectrocatalyst at a Steroid-Type Biosurfactant-Modified Carbon Nanotube Interface. *Anal. Chem.* **2015,** *87*, 5417-5421.

(454) Tominaga, M.; Sasaki, A.; Tsushida, M.; Togami, M. Biosurfactant Functionalized Single-Walled Carbon Nanotubes to Promote Laccase Bioelectrocatalysis. *New J. Chem.* **2017,** *41*, 231-236.

(455) Wang, X.; Latonen, R. M.; Sjooberg-Eerola, P.; Eriksson, J. E.; Bobacka, J.; Boer, H.; Bergelin, M. Direct Electron Transfer of *Trametes hirsuta* Laccase in a Dual-Layer Architecture of Poly(3,4-ethylenedioxythiophene) Films. *J. Phys. Chem. C* **2011,** *115*, 5919-5929.

(456) Kuwahara, T.; Asano, T.; Kondo, M.; Shimomura, M. Bioelectrocatalytic O_2 Reduction with a Laccase-bearing Poly(3-methylthiophene) Film Based on Direct Electron Transfer from the Polymer to Laccase. *Bioelectrochem.* **2013,** *91*, 28-31.

(457) Trohalaki, S.; Pachter, R.; Luckarift, H. R.; Johnson, G. R. Immobilization of the Laccases from *Trametes versicolor* and *Streptomyces coelicolo*r on Single-Wall Carbon Nanotube Electrodes: a Molecular Dynamics Study. *Fuel Cells* **2012,** *12*, 656-664.

(458) Jonsson-Niedziolka, M.; Szot, K.; Rogalski, J.; Opallo, M. Pyrene Sulfonate Functionalised Single-Walled Carbon Nanotubes for Mediatorless Dioxygen Bioelectrocatalysis. *Electrochem. Commun.* **2009,** *11*, 1042-1044.

(459) Tsujimura, S.; Asahi, M.; Goda-Tsutsumi, M.; Shirai, O.; Kano, K.; Miyazaki, K. Direct Electron Transfer to a Metagenome-Derived Laccase Fused to Affinity Tags Near the Electroactive Copper Site. *Phys. Chem. Chem. Phys.* **2013,** *15*, 20585-20589.

(460) Blanford, C. F.; Armstrong, F. A. The Pyrolytic Graphite Surface as an Enzyme Substrate: Microscopic and Spectroscopic Studies. *J. Solid State Electrochem.* **2006,** *10*, 826-832.

(461) Xia, H. Q.; Kitazumi, Y.; Shirai, O.; Kano, K. Enhanced Direct Electron Transfer-Type Bioelectrocatalysis of Bilirubin Oxidase on Negatively Charged Aromatic Compound-Modified Carbon Electrode. *J. Electroanal. Chem.* **2016,** *763*, 104-109.

(462) Navaee, A.; Salimi, A.; Jafari, F. Electrochemical Pretreatment of Amino-Carbon Nanotubes on Graphene Support as a Novel Platform for Bilirubin Oxidase with Improved Bioelectrocatalytic Activity towards Oxygen Reduction. *Chem. Eur. J.* **2015,** *21*, 4949-4953.

(463) Jonsson-Niedziolka, M.; Kaminska, A.; Opallo, M. Pyrene-Functionalised Single-Walled Carbon Nanotubes for Mediatorless Dioxygen Bioelectrocatalysis. *Electrochim. Acta.* **2010,** *55*, 8744-8750.

(464) Milton, R. D.; Lim, K.; Hickey, D. P.; Minteer, S. D. Employing FAD-Dependent Glucose Dehydrogenase within a Glucose/Oxygen Enzymatic Fuel Cell Operating in Human Serum. *Bioelectrochem.* **2015,** *106, Part A*, 56-63.

(465) Holade, Y.; Yuan, M.; Milton, R. D.; Hickey, D. P.; Sugawara, A.; Peterbauer, C. K.; Haltrich, D.; Minteer, S. D. Rational Combination of Promiscuous Enzymes Yields a Versatile Enzymatic Fuel Cell with Improved Coulombic Efficiency. *J. Electrochem. Soc.* **2017,** *164*, H3073-H3082.

(466) Lalaoui, N.; de Poulpiquet, A.; Haddad, R.; Le Goff, A.; Holzinger, M.; Gounel, S.; Mermoux, M.; Infossi, P.; Mano, N.; Lojou, E.; Cosnier S. A Membraneless Air-Breathing Hydrogen Biofuel Cell Based on Direct Wiring of Thermostable Enzymes on Carbon Nanotube Electrodes. *Chem. Commun.* **2015,** *51*, 7447-7450.

(467) So, K.; Kitazumi, Y.; Shirai, O.; Nishikawa, K.; Higuchi, Y.; Kano, K. Direct Electron Transfer-Type Dual Gas Diffusion H_2/O_2 Biofuel Cells. *J. Mater. Chem. A* **2016,** *4*, 8742-8749.

(468) Lopez, R. J.; Babanova, S.; Ulyanova, Y.; Singhal, S.; Atanassov, P. Improved Interfacial Electron Transfer in Modified Bilirubin Oxidase Biocathodes. *ChemElectroChem* **2014,** *1*, 241-248.

(469) So, K.; Kitazumi, Y.; Shirai, O.; Kano, K. Analysis of Factors Governing Direct Electron Transfer-Type Bioelectrocatalysis of Bilirubin Oxidase at Modified Electrodes. *J. Electroanal. Chem.* **2016,** *783*, 316-323.

(470) So, K.; Kawai, S.; Hamano, Y.; Kitazumi, Y.; Shirai, O.; Hibi, M.; Ogawa, J.; Kano, K. Improvement of a Direct Electron Transfer-Type Fructose/Dioxygen Biofuel Cell with a Substrate-Modified Biocathode. *Phys. Chem. Chem. Phys.* **2014,** *16*, 4823-4829.

(471) Matanovic, I.; Babanova, S.; Chavez, M. S.; Atanassov, P. Protein-Support Interactions for Rationally Designed Bilirubin Oxidase Based Cathode: a Computational Study. *J. Phys. Chem. B* **2016,** *120*, 3634-3641.

(472) Ulyanova, Y.; Babanova, S.; Pinchon, E.; Matanovic, I.; Singhal, S.; Atanassov, P. Effect of Enzymatic Orientation through the Use of Syringaldazine Molecules on Multiple Multicopper Oxidase Enzymes. *Phys. Chem. Chem. Phys.* **2014,** *16*, 13367-13375.

(473) Zheng, M. H.; Griveau, S.; Dupont-Gillain, C.; Genet, M. J.; Jolivalt, C. Oxidation of Laccase for Improved Cathode Biofuel Cell Performances. *Bioelectrochem.* **2015,** *106*, 77-87.

(474) Polyakov, K. M.; Fedorova, T. V.; Stepanova, E. V.; Cherkashin, E. A.; Kurzeev, S. A.; Strokopytov, B. V.; Lamzin, V. S.; Koroleva, O. V. Structure of Native Laccase

from *Trametes hirsuta* at 1.8 Angstrom Resolution. *Acta Crystallogr. Sect. D-Biol. Crystallogr.* **2009,** *65*, 611-617.

(475) Piontek, K.; Antorini, M.; Choinowski, T. Crystal Structure of a Laccase from the Fungus *Trametes versicolor* at 1.90-Angstrom Resolution Containing a Full Complement of Coppers. *J. Biol. Chem.* **2002,** *277*, 37663-37669.

(476) Martinez-Ortiz, J.; Flores, R.; Vazquez-Duhalt, R. Molecular Design of Laccase Cathode for Direct Electron Transfer in a Biofuel Cell. *Biosens. Bioelectron.* **2011,** *26*, 2626-2631.

(477) Hochuli, E.; Dobeli, H.; Schacher, A. New Metal Chelate Adsorbent Selective for Proteins and Peptides Containing Neighboring Histidine-Residues. *J. Chrom.* **1987,** *411*, 177-184.

(478) Balland, V.; Hureau, C.; Cusano, A. M.; Liu, Y.; Tron, T.; Limoges, B. Oriented Immobilization of a Fully Active Monolayer of Histidine-Tagged Recombinant Laccase on Modified Gold Electrodes. *Chem. Eur. J.* **2008,** *14*, 7186-7192.

(479) Sosna, M.; Boer, H.; Bartlett, P. N. A His-Tagged *Melanocarpus albomyces* Laccase and Its Electrochemistry Upon Immobilisation on NTA-Modified Electrodes and in Conducting Polymer Films. *ChemPhysChem* **2013,** *14*, 2225-2231.

(480) Guan, D. L.; Kurra, Y.; Liu, W. S.; Chen, Z. L. A Click Chemistry Approach to Site-Specific Immobilization of a Small Laccase Enables Efficient Direct Electron Transfer in a Biocathode. *Chem. Commun.* **2015,** *51*, 2522-2525.

(481) Lalaoui, N.; Rousselot-Pailley, P.; Robert, V.; Mekmouche, Y.; Villalonga, R.; Holzinger, M.; Cosnier, S.; Tron, T.; Le Goff, A. Direct Electron Transfer between a Site-Specific Pyrene-Modified Laccase and Carbon Nanotube/Gold Nanoparticle Supramolecular Assemblies for Bioelectrocatalytic Dioxygen Reduction. *ACS Catal.* **2016,** *6*, 1894-1900.

(482) Nowicka, A. M.; Kowalczyk, A.; Donten, M. L.; Donten, M.; Bystrzejewski, M.; Stojek, Z. Carbon-Encapsulated Iron Nanoparticles as Ferromagnetic Matrix for Oxygen Reduction in Absence and Presence of Immobilized Laccase. *Electrochim. Acta.* **2014,** *126*, 115-121.

(483) Matysiak, E.; Nowicka, A. M.; Wagner, B.; Donten, M. Space-Oriented Immobilization of Fully Active Laccase on PPy-Ferromagnetic Nanoparticles Composite Layer. *Electrochim. Acta.* **2016,** *191*, 586-593.

(484) Wu, F.; Su, L.; Yu, P.; Mao, L. Q. Role of Organic Solvents in Immobilizing Fungus Laccase on Single Walled Carbon Nanotubes or Improved Current Response in Direct Bioelectrocatalysis. *J. Am. Chem. Soc.* **2017,** *139*, 1565-1574.

(485) Yang, H.; Liu, L.; Li, J.; Chen, J.; Du, G. Rational Design to Improve Protein Thermostability: Recent Advances and Prospects. *Chem. Bio. Eng. Rev.* **2015,** *2*, 87-94.

(486) Shrier, A.; Giroud, F.; Rasmussen, M.; Minteer, S. D. Operational Stability Assays for Bioelectrodes for Biofuel Cells: Effect of Immobilization Matrix on Laccase Biocathode Stability. *J. Electrochem. Soc.* **2014,** *161*, H244-H248.

(487) Lim, J.; Cirigliano, N.; Wang, J.; Dunn, B. Direct Electron Transfer in Nanostructured Sol-Gel Electrodes Containing Bilirubin Oxidase. *Phys. Chem. Chem. Phys.* **2007,** *9*, 1809-1814.

(488) Katano, H.; Tatsumi, H.; Hibi, T.; Ikeda, T.; Tsukatani, T. Application of Polyammonium Cations to Enzyme-Immobilized Electrode: Application as Enzyme Stabilizer for Bilirubin Oxidase. *Anal. Sci.* **2008,** *24*, 1421-1424.

(489) Qian, Q.; Su, L.; Yu, P.; Cheng, H.; Lin, Y.; Jin, X.; Mao, L. Ionic Liquid-Assisted Preparation of Laccase-Based BioCathodes with Improved Biocompatibility. *J. Phys. Chem. B* **2012,** *116*, 5185-5191.

(490) Kuwahara, J.; Ikari, R.; Murata, K.; Nakamura, N.; Ohno, H. Electrocatalytic Reduction of Oxygen by Bilirubin Oxidase in Hydrophobic Ionic Liquids Containing a Small Quantity of Water. *Catal. Today* **2013,** *200*, 49-53.

(491) Moore, C. M.; Akers, N. L.; Minteer, S. Improving the Environment for Immobilized Dehydrogenase Enzymes by Modifying Nafion with Tetraalkylammonium Bromides. *Biomacromol.* **2004,** *5*, 1241.

(492) Rubenwolf, S.; Sane, S.; Hussein, L.; Kestel, J.; von Stetten, F.; Urban, G.; Krueger, M.; Zengerle, R.; Kerzenmacher, S. Prolongation of Electrode Lifetime in Biofuel Cells by Periodic Enzyme Renewal. *App. Microbiol. Biotech.* **2012,** *96*, 841-849.

(493) Sane, S.; Jolivalt, C.; Mittler, G.; Nielsen, P. J.; Rubenwolf, S.; Zengerle, R.; Kerzenmacher, S. Overcoming Bottlenecks of Enzymatic Biofuel Cell Cathodes: Crude Fungal Culture Supernatant Can Help to Extend Lifetime and Reduce Cost. *Chemsuschem* **2013,** *6*, 1209-1215.

(494) Xu, F.; Shin, W.; Brown, S. H.; Walhleithner, J. A.; Sundaram, U. M.; Solomon, E. I. A Study of a Series of Recombinant Fungal Laccases and Bilirubin Oxidase that Exhibit Significant Differences in Redox Potential, Substrate Specificity and Stability. *Biochim. Biophys. Acta* **1996,** *1292*, 303-311.

(495) Ikeda, T.; Uematsu, K.; Ma, H.; Katano, H.; Hibi, T. Measurements of Reversible and Irreversible Inactivation Processes of a Redox Enzyme, Bilirubin Oxidase, by Electrochemical Methods Based on Bioelectrocatalysis. *Anal. Sci.* **2009,** *25*, 1283-1288.

(496) Tsujimura, S.; Fujita, M.; Tatsumi, H.; kano, K.; Ikeda, T. Bioelectrocatalysis-based Dihydrogen/Dioxygen Fuel Cell Operating at PhysioLogical pH. *Phys. Chem. Chem. Phys.* **2001,** *3*, 1331-1335.

(497) Nakagawa, T.; Tsujimura, S.; kano, K.; Ikeda, T. Bilirubin Oxidase and $[Fe(CN_6)]^{3-/4-}$ Modified Electrodes Allowing Diffusion Controlled Reduction of O_2 to Water at pH 7. *Chem. Lett.* **2003,** *32*, 54-55.

(498) Li, D.-A.; Okajima, T.; Mao, L.; Ohsaka, T. Bioelectrocatalytic Oxygen Reduction Reaction By Bilirubin Oxidase Adsorbed on Glassy Carbon And Edge-Plane Pyrolytic Graphite Electrodes: Effect Of Redox Mediators *Int. J. Electrochem. Sci.*, **2014,** *9*, 1390-1398.

(499) Fokina, O.; Eipper, J.; Kerzenmacher, S.; Fischer, R. Selective Natural Induction of Laccases in *Pleurotus sajor-caju*, Suitable for Application at a Biofuel Cell Cathode at Neutral pH. *Biores.Tech.* **2016,** *218*, 455-462.

(500) Guttierez-Sanchez, C.; Pita, M.; Toscano, M. D.; De Lacey, A. L. Bilirubin Oxidase-Based Nano-Bio-Cathode Working in Serum-Mimic Buffer for Implantable Biofuel Cell. *Electroanalysis* **2013,** *25*, 1359-1362.

(501) Chen, Y.; Gai, P.; Zhang, J.; Zhu, J.-J. Design of an Enzymatic Biofuel Cell with Large Power Output. *J. Mater. Chem. A* **2015,** *3*, 11511-11516.

(502) Beneyton , T.; El Harrah, A.; Griffiths, A. D.; Hellwig, P.; Taly, V. Immobilization of CotA, an Extremophilic Laccase from *Bacillus subtilis*, on Glassy Carbon Electrodes for Biofuel Cell Applications. *Electrochem. Commun.* **2011,** *13*, 24-27.

(503) Mazurenko, I.; Monsalve, K.; Rouhana, J.; Parent, P.; Laffon, C.; Goff, A. L.; Szunerits, S.; Boukherroub, R.; Giudici-Orticoni, M.-T.; Mano, N.; Lojou E. How the Intricate Interactions between Carbon Nanotubes and Two Bilirubin Oxidases Control Direct and Mediated O_2 Reduction. *ACS Appl. Mat. Interfaces* **2016,** *8*, 23074-23085.

(504) Zloczewska, A.; Jonsson-Niedziolka, M.; Rogalski, J.; Opallo, M. Vertically Aligned Carbon Nanotube Film Electrodes for Bioelectrocatalytic Dioxygen Reduction. *Electrochim. Acta.* **2011,** *56*, 3947-3953.

(505) Szot, K.; Lynch, R. P.; Lesniewski, A.; Majewska, E.; Sirieix-Plenet, J.; Gaillon, L.; Opallo, M. The Effect of Linker of Electrodes Prepared from Sol–Gel Ionic Liquid Precursor and Carbon Nanoparticles on Dioxygen Electroreduction Bioelectrocatalysis. *Electrochim. Acta* **2011,** *56*, 10306-10312.

(506) Engel, A. B.; Holade, Y.; Cornu, D.; Servat, K.; Napporn, T. W.; Kokoh, K. B.; Tingry, S. Optimization of Chitosan Film-Templated Biocathode for Enzymatic Oxygen Reduction in Glucose Hybrid Biofuel Cell. *J. Electrochem. Soc.* **2017,** *164*, G29-G35.

(507) Quan, D.; Kim, Y.; Shin, W. Characterization of an Amperometric Laccase Electrode Covalently Immobilized on Platinum Surface. *J. Electroanal. Chem.* **2004,** *561*, 181-189.

(508) Tsujimura, S.; Murata, K. Electrochemical Oxygen Reduction Catalyzed by Bilirubin Oxidase with the Aid of 2,2′-Azinobis(3-ethylbenzothiazolin-6-sulfonate) on a MgO-Template Carbon Electrode. *Electrochim. Acta* **2015,** *180*, 555-559.

(509) Fernández-Sánchez, C.; Tzanov, T.; Gübitz, G. M.; Cavaco-Paulo, A. Voltammetric Monitoring of Laccase-catalysed Mediated Reactions. *Bioelectrochem.* **2002,** *58*, 149-156.

(510) Topcagic, S.; Minteer, S. Development of a Membraneless Ethanol/Oxygen Biofuel Cell. *Electrochim. Acta.* **2005,** *52*, 2168-2172.

(511) Tsujimura, S.; Kawaharada, M.; Nakagawa, T.; Kano, K.; Ikeda, T. Mediated Bioelectrocatalytic O_2 Reduction to Water at Highly Positive Electrode Potentials near Neutral pH. *Electrochem. Commun.* **2003,** *5*, 138-141.

(512) Liu, Y.; Wang, M.; Zhao, F.; LIu, B.; Dong, S. A Low-Cost Biofuel Cell with pH-Dependent Power Output Based on Porous Carbon as Matrix. *Chem. Eur. J.* **2005,** *11*, 4970-4974.

(513) Palmore, G. T. R.; Kim, H.-H. Electro-Enzymatic Reduction of Dioxygen to Water in the Cathode Compartment of a Biofuel Cell. *J. Electroanal. Chem.* **1999,** *464*, 110-117.

(514) Heller, A. Electrical Wiring of Redox Enzymes. *Acc. Chem. Res.* **1990,** *23*, 128-134.

(515) Degani, Y.; Heller, A. Direct Electrochemical Communication between Chemically Modified Enzymes and Metal Electrodes. 2. Methods for Bonding Electron-Transfer Relays to Glucose Oxidase and D-Amino-Acid Oxidase. *J. Am. Chem. Soc.* **1988,** *110*, 2615-2620.

(516) Degani, Y.; Heller, A. Electrical Communication between Redox Centers of Glucose Oxidase and Electrodes via Electrostatically and Covantly Bound Redox Polymers. *J. Am. Chem. Soc.* **1989,** *111*, 2357-2358.

(517) Gregg, B. A.; Heller, A. Redox Polymer Films Containing Enzymes. 2. Glucose Oxidase Containing Enzymes Electrodes. *J. Phys. Chem.* **1991,** *95*, 5976-5980.

(518) Gregg, B. A.; Heller, A. Redox Polymer Films Containing Enzymes. 1. A Redox-Conducting Epoxy Cement : Synthesis, Characterisation, and Electrocatalytic Oxidation of Hydroquinone. *J. Phys. Chem.* **1991,** *95*, 5970-5975.

(519) Heller, A. Electrical Connection of Enzyme Redox Centers to Electrodes. *J. Phys. Chem. B* **1992,** *96*, 3579-3587.

(520) Heller, A.; Feldman, B. Electrochemistry in Diabetes Management. *Acc. Chem. Res.* **2009,** *43*, 963-973.

(521) Schmidtke, D. W.; Freeland, A. C.; Heller, A.; Bonnecaze, R. T. Measurement and Modeling of the Transient Difference between Blood and Subcutaneous Glucose Concentrations in the Rat after Injection of Insulin. *Proc. Natl. Acad. Sci. USA* **1998,** *95*, 294-299.

(522) Kenausis, G.; Chen, Q.; Heller, A. Electrochemical Glucose and Lactate Sensors Based on "Wired' Thermostable Soyeban Peroxidase Operating Continuously and Stability at 37°C. *Anal. Chem.* **1997,** *69*, 1054-1060.

(523) Csoregi, E.; Schmidtke, D. W.; Heller, A. Design and Optimization of a Selective Subcutaneously Implantable Glucose Electrode Based on "Wired' Glucose Oxidase. *Anal. Chem.* **1995,** *34*, 1240-1244.

(524) Katakis, I.; Heller, A. L-alpha-Glycerophosphate and L-Lactate Electrodes Based on the Electrochemical "Wiring" of Oxidases. *Anal. Chem.* **1992,** *64*, 1008-1013.

(525) Schumann, W.; Ohara, T. J.; H-L., S.; Heller, A. Electron Transfer between Glucose Oxidase and Electrodes via Redox Mediators Bound with Flexible Chains to the Enzyme Surface. *J. Am. Chem. Soc.* **1991,** *113*, 1394-1397.

(526) Heller, A. Miniature Biofuel Cells. *Phys. Chem. Chem. Phys.* **2004,** *6*, 209-216.

(527) Mao, F.; Mano, N.; Heller, A. Long Tethers Binding Redox Centers to Polymer Backbones Enhance Electron Transport in Enzyme "Wiring" Hydrogels. *J. Am. Chem. Soc.* **2003,** *125*, 4951-4957.

(528) Mano, N.; Mao, F.; Heller, A. On the Parameters Affecting the Characteristics of the "Wired" Glucose Oxidase. *J. Electroanal. Chem.* **2005,** *574*, 347-357.

(529) Forster, R. J.; Walsh, D. A.; Mano, N.; Mao, F.; Heller, A. Modulating the Redox Properties of an Osmium-Containing Metallopolymer through the Supporting Electrolyte and Cross-Linking. *Langmuir* **2004,** *20*, 862-868.

(530) Gallaway, J. W.; Calabrese Barton, S. A. Effect of Redox Polymer Synthesis on the Performance of a Mediated Laccase Oxygen Cathode. *J. Electroanal. Chem.* **2009,** *626*, 149-155.

(531) Cadet, M.; Brilland, S.; Gounel, S.; Louerat, F.; Mano, N. Designing a Highly Efficient O_2 Cathode Based on Bilirubin Oxidase from *Magnaporthe oryzae*. *ChemPhysChem* **2013,** *14*, 2097-2100.

(532) Ackermann, Y.; Guschin, D. A.; Eckhard, K.; Shleev, S.; Schuhmann, W. Design of a Bioelectrocatalytic Electrode Interface for Oxygen Reduction in Biofuel Cells Based on a Specifically Adapted Os-Complex Containing Redox Polymer with Entrapped *Trametes hirsuta* Laccase. *Electrochem. Commun.* **2010,** *12*, 640-643.

(533) Soukharev, V.; Mano, N.; Heller, A. A Four-Electron O_2 Electroreduction Biocatalyst Superior to Platinum and a Biofuel Cell Operating at 0.88 V. *J. Am. Chem. Soc.* **2004,** *126*, 8368-8369.

(534) Shin, H.; Chi, S.; Heller, A.; Kang, C. Stabilization of a Bilirubin Oxidase-Wiring Redox Polymer by Quaternization and Characteristics of the Resulting O_2 Cathode Physical and Analytical Electrochemistry *J. Electrochem. Soc.* **2009,** *156*, F87-F92.

(535) Rajagopalan, R.; Aoki, A.; Heller, A. Effect of Quaternization of the Glucose Oxidase "Wiring" Redox Polymer on the Maximum Densities of Glucose Electrode. *J. Phys. Chem.* **1996,** *100*, 3719-3727.

(536) Fernandez, J. L.; Mano, N.; Heller, A.; Bard, A. J. Optimization of "Wired" Enzyme O_2-Electroreduction Catalyst Compositions by Scanning Electrochemichal Microscopy. *Angew. Chem. Int. Ed* . **2004,** *43*, 6355-6357.

(537) Chakraborty, D.; McClellan, E.; Hasselbeck, R.; Barton, S. C. Characterization of Enzyme-Redox Hydrogel Thin-Film Electrodes for Improved Utilization. *J. Electrochem. Soc.* **2014,** *161*, H3076-H3082.

(538) Suraniti, E.; AbIntou, M.; Durand, F.; Mano, N. Heat and Drying Time Modulate the O_2 Reduction Current of Modified Glassy Carbon Electrodes with Bilirubin Oxidases. *Bioelectrochem.* **2012,** *88*, 65-69.

(539) Barrière, F.; Ferry, Y.; RocheFort, D.; Leech, D. Targetting Redox Polymers as Mediators for Laccase Oxygen Reduction in a Membraneless Biofuel Cell. *Electrochem. Commun.* **2004,** *6,* 237-241.

(540) Forster, R. J.; Vos, J. G. Synthesis, Characterization, and Properties of a Series of Osmium- and Ruthenium-Containing Metallopolymers. *Macromolecules* **1990,** *23,* 4372.

(541) Barrière, F.; Kavanagh, P.; Leech, D. A Laccase-Glucose Oxidase Biofuel Cell Prototype Operating in a Physiological Buffer. *Electrochim. Acta* **2006,** *51*, 5187-5192.

(542) Jenkins, P. A.; Boland, S.; Kavanagh, P.; Leech, D. Evaluation of Performance and Stability of Biocatalytic Redox Films Constructed with Different Copper Oxygenases and Osmium-Based Redox Polymers. *Bioelectrochem.* **2009,** *76*, 162-168.

(543) Boland, S.; Jenkins, P.; Kavanagh, P.; Leech, D. Biocatalytic Fuel Cells: a Comparison of Surface Pre-Treatments for Anchoring Biocatalytic Redox Films on Electrode Surfaces. *J. Electroanal. Chem.* **2009,** *626*, 111-115.

(544) Rengaraj, S.; Kavanagh, P.; Leech, D. A Comparison of Redox Polymer and Enzyme Co-Immobilization on Carbon Electrodes to Provide Membraneless Glucose/O_2 Enzymatic Fuel Cells with Improved Power Output and Stability. *Biosens. Bioelectron.* **2011,** *30*, 294-299.

(545) Mano, N.; Fernandez, J. L.; Kim, Y.; Shin, W.; Bard, A. J.; Heller, A. Oxygen Is Electroreduced to Water on a "Wired" Enzyme Electrode at a Lesser Overpotential than on Platinum. *J. Am. Chem. Soc.* **2003,** *125,* 15290-15291.

(546) Edembe, L.; Gounel, S.; Cadet, M.; Durand, F.; Mano, N. A Highly Efficient O_2 Cathode Based on Bilirubin Oxidase from *Bacillus pumilus* Operating in Serum *Electrochem. Commun.* **2012,** *23*, 80-82.

(547) Suraniti, E.; Tsujimura, S.; Durand, F.; Mano, N. Thermophilic Biocathode with Bilirubin Oxidase from *Bacillus pumilus*. *Electrochem. Commun.* **2013,** *26*, 41-44.

(548) Rasmussen, M.; Ritzmann, R. E.; Lee, I.; Pollack, A. J.; Scherson, D. An Implantable Biofuel Cell for a Live Insect. *J. Am. Chem. Soc.* **2012,** *134*, 1458-1460.

(549) Schwefel, J.; Ritzmann, R. E.; Lee, I. N.; Pollack, A.; Weeman, W.; Garverick, S.; Willis, M.; Rasmussen, M.; Scherson, D. Wireless Communication By an Autonomous Self-Powered Cyborg Insect. *J. Electrochem. Soc.* **2015,** *161*, H3113-H3116.

(550) Gao, Z.; Binyamin, G.; Kim, H.-H.; Barton, S. C.; Zhang, Z.; Heller, A. Electrodeposition of Redox Polymers and Co-Electrodeposition of Enzymes by Coordinative Crosslinking. *Angew. Chem. Int. Ed.* **2002,** *41*, 810-813.

(551) Song, J.; Shin, H.; Kang, C. A Carbon Nanotube Layered Electrode for the Construction of the Wired Bilirubin Oxidase Oxygen Cathode *Electroanalysis* **2011,** *23*, 2941-2948.

(552) Shin, H.; Kang, C. Co-Electrodeposition of Bilirubin Oxidase with Redox Polymer through Ligand Substitution for Use as an Oxygen Reduction Cathode. *Bull. Korean Chem. Soc.* **2010,** *31*, 3118-3122.

(553) Hudak, N. S.; Gallaway, J. W.; Barton, S. C. Formation of Mediated Biocatalytic Cathodes by Electrodeposition of a Redox Polymer and Laccase. *J. Electroanal. Chem.* **2009,** *629*, 57-62.

(554) Shen, W.; Deng, H.; Teo, A. K. L.; Gao, Z. An Electrodeposited Redox Polymer-Laccase Composite Film for Highly Efficient Four-Electron Oxygen Reduction. *J. Power Sources* **2013,** *226*, 27-32.

(555) Suraniti, E.; Studer, V.; Sojic, N.; Mano, N. Fast and Easy Enzyme Immobilization by Photoinitiated Polymerization for Efficient Bioelectrochemichal Devices. *Anal. Chem.* **2011,** *83,* 2824-2828.

(556) Rengaraj, S.; Mani, V.; Kavanagh, P.; Rusling, J.; Leech, D. A Membrane-Less Enzymatic Fuel Cell with Layer-by-Layer Assembly of Redox Polymer and Enzyme Over Graphite Electrodes. *Chem Commun (Camb)* **2011,** *47,* 11861-11863.

(557) Pöller, S.; Beyl, Y.; VivekananThan, J.; Guschin, D. A.; Schuhmann, W. A New Synthesis Route for Os-Complex Modified Redox Polymers for Potential Biofuel Cell Applications. *Bioelectrochem.* **2012,** *87,* 178-184.

(558) Wheeldon, I. R.; Gallaway, J. W.; Barton, S. C.; Banta, S. Bioelectrocatalytic Hydrogels from Electron-Conducting Metallopolypeptides Coassembled with Bifunctional Enzymatic Building Blocks. *Proc. Natl. Acad. Sci. USA* **2008,** *105,* 15275-15280.

(559) Lalaoui, N.; Reuillard, B.; Philouze, C.; Holzinger, M.; Cosnier, S.; Le Goff, A. Osmium(II) Complexes Bearing Chelating N-heterocyclic Carbene and Pyrene-Modified Ligands: Surface Electrochemistry and Electron Transfer Mediation of Oxygen Reduction by Multicopper Enzymes. *Organometallics* **2016,** *35,* 2987-2992.

(560) Garrett, D. J.; Jenkins, P.; Polson, M. I. J.; Leech, D.; Baronian, K. H. R.; Downard, A. J. Diazonium Salt Derivatives of Osmium Bipyridine Complexes: Electrochemical Grafting and Characterisation of Modified Surfaces. *Electrochim. Acta* **2011,** *56,* 2213-2220.

(561) Cosnier, S. Biomolecule Immobilization on Electrode Surfaces by Entrapment or Attachment to Electrochemichally Polymerized Films. A Review. *Biosens. Bioelectron.* **1999,** *14,* 443-456.

(562) Kim, J.; Yoo, K.-H. Glucose Oxidase Nanotube-Based Enzymatic Biofuel Cells with Improved Laccase Biocathodes. *Phys. Chem. Chem. Phys.* **2013,** *15*, 3510-3517.

(563) Zebda, A.; Tingry, S.; Innocent, C.; Cosnier, S.; Forano, C.; Mousty, C. Hybrid Layered Double Hydroxides-Polypyrrole Composites for Construction of Glucose/O_2 Biofuel Cell. *Electrochim. Acta* **2011,** *56*, 10378-10384.

(564) Ammam, M.; Fransaer, J. Micro-Biofuel Cell Powered by Glucose/O_2 Based on Electro-Deposition of Enzyme, Conducting Polymer and Redox Mediators: Preparation, Characterization and Performance in Human Serum. *Biosens. Bioelectron.* **2010,** *25*, 1474-1480.

(565) Ammam, M.; Fransaer, J. Glucose/O_2 Biofuel Cell Based On Enzymes, Redox Mediators And Multiple Walled Carbon Nanotubes Deposited By AC-electrophoresis then Stabilized By Electropolymerized Polypyrrole. *Biotechnol. Bioeng.* **2012**, *109*, 1601-1609.

(566) Ammam, M.; Fransaer, J. Combination of Laccase and Catalase in Construction of H_2O_2–O_2 Based Biocathode for Applications in Glucose Biofuel Cells. *Biosens. Bioelectron.* **2013,** *39*, 274-281.

(567) Servat, K.; Tingry, S.; Brunel, L.; Querelle, S.; Crétin, M.; Innocent, C.; Jolivalt, C.; Rolland, M. Modification of Porous Carbon Tubes with Enzymes: Application for Biofuel Cells *J. Appl. Electrochem.* **2007,** *37*, 121-127.

(568) Merle, G.; Brunel, L.; Tingry, S.; Cretin, M.; Rolland, M.; Servat, K.; Jolivalt, C.; Innocent, C.; Seta, P. Electrode Biomaterials Based on Immobilized Laccase. Application for Enzymatic Reduction of Dioxygen. *Mater. Sci. Eng. C* **2008,** *28*, 932-938.

(569) Brunel, L.; Denele, J.; Servat, K.; Kokoh, K. B.; Jolivalt, C.; Innocent, C.; Cretin, M.; Rolland, M.; Tingry, S. Oxygen Transport through Laccase Biocathodes for a Membraneless Glucose/O_2 Biofuel Cell. *Electrochem. Commun.* **2007,** *9*, 331-336.

(570) Habrioux, A.; Merle, G.; Servat, K.; Kokoh, K. B.; Innocent, C.; Cretin, M.; Tingry, S. Concentric Glucose/O_2 Biofuel Cell. *J. Electroanal. Chem.* **2008,** *622*, 97-102.

(571) Merle, G.; Habrioux, A.; Servat, K.; Rolland, M.; Innocent, C.; Kokoh, K. B.; Tingry, S. Long-Term Activity of Covalent Grafted Biocatalysts during Intermittent Use of a Glucose/O_2 Biofuel Cell. *Electrochim. Acta.* **2009,** *54*, 2998-3003.

(572) Cardoso, F. P.; Aquino Neto, S.; Crepaldi, L. B.; Nikolaou, S.; Barros, V. P.; De Andrade, A. R. Biocathodes for Enzymatic Biofuel Cells Using Laccase and Different Redox Mediators Entrapped in Polypyrrole Matrix. *J. Electrochem. Soc.* **2014,** *161*, F445-F450.

(573) Kuwahara, T.; Homma, H.; Kondo, M.; Shimomura, M. Fabrication of Enzyme Electrodes with a Polythiophene Derivative and Application of Them to a Glucose Fuel Cell. *Synt. Met.* **2009,** *159*, 1859-1864.

(574) Yu, M.; Parunova, S.; Bushnev, O.; Gonzalez-Arriba, E.; Falkman, P.; Lipkin, A. V.; Popov, V. O.; Shleev, S. V.; Pankratov, D. V. Potentially Implantable Biocathode with the Function of Charge Accumulation Based on Nanocomposite of Polyaniline/Carbon Nanotubes. *Russ. J. Electrochem.* **2016,** *52*, 1166-1171.

(575) Sakurai, T. Kinetics of Electron Transfer between Cytochrome *c* and Laccase. *Biochemistry* **1992,** *31*, 9844-9847.

(576) Silveira, C. M.; Gabriela Almeida, M. Small Electron-Transfer Proteins as Mediators in Enzymatic Electrochemichal Biosensors. *Anal. Bioanal. Chem.* **2013,** *405*, 3619-3635.

(577) Feifel, S. C.; Kapp, A.; Ludwig, R.; Lisdat, F. Nanobiomolecular Multiprotein Clusters on Electrodes for the Formation of a Switchable Cascadic Reaction Scheme. *Angew. Chem. Int. Ed.* **2014,** *53*, 5676-5679.

(578) Dronov, R.; Kurth, D. G.; Mohwald, H.; Scheller, F. W.; Lisdat, F. Communication in a Protein Stack: Electron Transfer between Cytochrome *c* and Bilirubin Oxidase within a Polyelectrolyte Multilayer. *Angew. Chem. Int. Ed.* **2008,** *47*, 3000-3003.

(579) Lisdat, F.; Dronov, R.; Mohwald, H.; Scheller, F. W.; Kurth, D. G. Self-Assembly Of Electro-Active Protein Architectures On Electrodes For The Construction Of Biomimetic Signal Chains. *Chem. Commun. (Camb)* **2009**, *0*, 274-283.

(580) Balkenhohl, T.; Adelt, S.; Dronov, R.; Lisdat, F. Oxygen-Reducing Electrodes Based on Layer-by-Layer Assemblies of Cytochrome *c* and Laccase. *Electrochem. Commun.* **2008,** *10*, 914-917.

(581) Wegerich, F.; Turano, P.; Allegrozzi, M.; Mohwald, H.; Lisdat, F. Electroactive Multilayer Assemblies of Bilirubin Oxidase and Human Cytochrome *c* Mutants: Insight in Formation and Kinetic Behavior. *Langmuir* **2011,** *27*, 4202-4211.

(582) Altamura, L.; Horvath, C.; Rengaraj, S.; Rongier, A.; Elouarzaki, K.; Gondran, C.; Maçon, A. L. B.; Vendrely, C.; Bouchiat, V.; Fontecave, M.et al. A Synthetic Redox Biofilm Made From Metalloprotein–Prion Domain Chimera Nanowires. *Nat. Chem.* **2016,** *9*, 157-163

(583) Yamamoto, K.; Matsumoto, T.; Shimada, S.; Tanaka, T.; Kondo, A. Starchy Biomass-Powered Enzymatic Biofuel Cell Based on Amylases and Glucose Oxidase Multi-Immobilized Bioanode. *N. Biotechnol.* **2013,** *30*, 531-535.

(584) Habrioux, A.; Servat, K.; Tingry, S.; Kokoh, K. B. Enhancement of the Performances of a Single Concentric Glucose/O_2 Biofuel Cell by Combination of Bilirubin

Oxidase/Nafion Cathode and Au–Pt Anode. *Electrochem. Commun.* **2009,** *11*, 111-113.

(585) Cosnier, S.; Shan, D.; Ding, S.-H. An Easy Compartmentless Biofuel Cell Construction Based on the Physical Co-Inclusion of Enzyme and Mediator Redox within Pressed Graphite Discs. *Electrochem. Commun.* **2010,** *12*, 266-269.

(586) Liu, C.; Alwarappan, S.; Chen, Z.; Kong, X.; Li, C.-Z. Membraneless Enzymatic Biofuel Cells Based on Graphene Nanosheets. *Biosens. Bioelectron.* **2010,** *25*, 1829-1833.

(587) Nazaruk, E.; Smoliński, S.; Swatko-Ossor, M.; Ginalska, G.; Fiedurek, J.; Rogalski, J.; Bilewicz, R. Enzymatic Biofuel Cell Based on Electrodes Modified with Lipid Liquid-Crystalline Cubic Phases. *J. Power Sources* **2008,** *183*, 533-538.

(588) Smolander, M.; Boer, H.; Valkiainen, M.; Roozeman, R.; Bergelin, M.; Eriksson, J.-E.; Zhang, X.-C.; Koivula, A.; Viikari, L. Development of a Printable Laccase-based Biocathode for Fuel Cell Applications. *Enz. Microbial. Tech.* **2008,** *43*, 93-102.

(589) Jenkins, P.; Tuurala, S.; Vaari, A.; Valkiainen, M.; Smolander, M.; Leech, D. A Comparison of Glucose Oxidase and Aldose Dehydrogenase as Mediated Anodes in Printed Glucose/Oxygen Enzymatic Fuel Cells Using ABTS/Laccase Cathodes. *Bioelectrochem.* **2012,** *87*, 172-177.

(590) MacAodha, D.; Conghaile, P. Ó.; Egan, B.; Kavanagh, P.; Leech, D. Membraneless Glucose/Oxygen Enzymatic Fuel Cells Using Redox Hydrogel Films Containing Carbon Nanotubes. *ChemPhysChem* **2013,** *14*, 2302-2307.

(591) Ó Conghaile, P.; MacAodha, D.; Egan, B.; Kavanagh, P.; Leech, D. Tethering Osmium Complexes within Enzyme Films on Electrodes to Provide a Fully Enzymatic Membraneless Glucose/Oxygen Fuel Cell. *J. Electrochem. Soc.* **2013,** *160*, G3165-G3170.

(592) Osadebe, I.; Conghaile, P. Ó.; Kavanagh, P.; Leech, D. Glucose Oxidation by Osmium Redox Polymer Mediated Enzyme Electrodes Operating at Low Potential and in Oxygen, for Application to Enzymatic Fuel Cells. *Electrochim. Acta* **2015,** *182*, 320-326.

(593) Sadowska, K.; Stolarczyk, K.; Biernat, J. F.; Roberts, K. P.; Rogalski, J.; Bilewicz, R. Derivatization of Single-Walled Carbon Nanotubes with Redox Mediator for Biocatalytic Oxygen Electrodes. *Bioelectrochem.* **2010,** *80*, 73-80.

(594) Prasad, K. P.; Chen, Y.; Chen, P. Three-Dimensional Graphene-Carbon Nanotube Hybrid for High-Performance Enzymatic Biofuel Cells. *ACS Appl. Mat. Interfaces* **2014,** *6*, 3387-3393.

(595) Bard, A. J.; Faulkner, L. R. *Electrochemichal Methods. Fundamentals and Applications*; 2nd Ed.; John Wiley and Sons: New-York, 2001.

(596) Mano, N.; Mao, F.; Heller, A. A Miniature Membraneless Biofuel Cell Operating at +0.60 V under Physiological Conditions. *ChemBioChem* **2004,** *5*, 1703-1705.

(597) Mano, N.; Mao, F.; Shin, W.; Chen, T.; Heller, A. A Miniature Biofuel Cell Operating at 0.78 V. *Chem Commun (Camb)* **2003**, 518-519.

(598) Mano, N.; Mao, F.; Heller, A. Characteristics of a Miniature Compartmentless Glucose-O_2 Biofuel Cell and Its Operation in a Living Plant. *J. Am. Chem. Soc.* **2003,** *125*, 6588-6594.

(599) Mano, N.; Heller, A. A Miniature Membraneless Biofuel Cell Operating at 0.36 V under Physiological Conditions. *J. Electrochem. Soc.* **2003,** *150*, A1136-A1138.

(600) Kim, H.-H.; Mano, N.; Zhang, Y.; Heller, A. A Miniature Membraneless Biofuel Cell Operating under Physiological Conditions at 0.5 V. *J. Electrochem. Soc.* **2003,** *150*, A209-A213.

(601) Mano, N.; Mao, F.; Heller, A. A Miniature Biofuel Cell Operating in a Physiological Buffer. *J. Am. Chem. Soc.* **2002,** *124*, 12962-12963.

(602) Cadet, M.; Gounel, S.; Stines-Chaumeil, C.; Brilland, X.; Rouhana, J.; Louerat, F.; Mano, N. An Enzymatic Glucose/O_2 Biofuel Cell Operating in Human Blood. *Biosens. Bioelectron.* **2016,** *83*, 60-67.

(603) Che, A.-F.; Germain, V.; Cretin, M.; Cornu, D.; Innocent, C.; Tingry, S. Fabrication of Free-Standing Electrospun Carbon Nanofibers as Efficient Electrode Materials for Bioelectrocatalysis. *New J. Chem.* **2011,** *35*, 2848-2853.

(604) Barton, S. C.; Sun, Y. C., B.; White, S.; Hone, J. Mediated Enzyme Electrodes with Combined Micro- and Nanoscale Supports. *Electrochem. Sol. State Lett.* **2007,** *10*, B96-B100.

(605) Barton, S. C.; Kim, H.-H.; Binyamin, G.; Zhang, Y.; Heller, A. Electroreduction of O_2 to Water on the "Wired" Laccase Cathode. *J. Phys. Chem. B* **2001,** *105*, 11917-11921.

(606) Barton, S. C.; Kim, H.-H.; Binyamin, G.; Zhang, Y.; Heller, A. The "Wired' Laccase Cathode : High Current Density Electroreduction of O_2 to Water at + 0.7V (NHE) at pH 5. *J. Am. Chem. Soc.* **2001,** *123*, 5802-5803.

(607) Mano, N.; Soukharev, V.; Heller, A. A Laccase-Wiring Redox Hydrogel for Efficient Catalysis of O_2 Electroreduction. *J. Phys. Chem. B* **2006,** *110*, 11180-11187.

(608) Rowinski, P.; Kang, C.; Shin, C.; Heller, A. Mechanical and Chemical Protection of a Wired Enzyme Oxygen Cathode by a Cubic Phase Lyotropic Liquid Crystal. *Anal. Chem.* **2007,** *79*, 1173-1180.

(609) Jain, D.; Karajic, A.; Murawska, M.; Goudeau, B.; Bichon, S.; Gounel, S.; Mano, N.; Kuhn, A.; Barthélémy, P. Low-Molecular-Weight Hydrogels as New Supramolecular Materials for Bioelectrochemichal Interfaces. *ACS Appl. Mat. Interfaces* **2017,** *9*, 1093-1098.

(610) Haddad, R.; Xia, W.; Guschin, D. A.; Pöller, S.; Shao, M.; VivekananThan, J.; Muhler, M.; Schuhmann, W. Carbon Cloth/Carbon Nanotube Electrodes for Biofuel Cells Development. *Electroanalysis* **2013,** *25*, 59-67.

(611) Bourourou, M.; Elouarzaki, K.; Holzinger, M.; Agnes, C.; Le Goff, A.; Reverdy-Bruas, N.; Chaussy, D.; Party, M.; Maaref, A.; Cosnier, S. Freestanding Redox Buckypaper Electrodes from Multi-Wall Carbon Nanotubes for Bioelectrocatalytic Oxygen Reduction via Mediated Electron Transfer. *Chem. Sci.* **2014,** *5*, 2885-2888.

(612) Hussein, L.; Feng, Y. J.; Alonso-Vante, N.; Urban, G.; Krüger, M. Functionalized Carbon Nanotube Supported Electrocatalysts and Buckypaper-Based Biocathodes for Glucose Fuel Cell Applications. *Electrochim. Acta* **2011,** *56*, 7659-7665.

(613) Hussein, L.; Urban, G.; Kruger, M. Fabrication and Characterization of Buckypaper-Based Nanostructured Electrodes as a Novel Material for Biofuel Cell Applications. *Phys. Chem. Chem. Phys.* **2011,** *13*, 5831-5839.

(614) Bunte, C.; Hussein, L.; Urban, G. A. Performance of Non-Compartmentalized Enzymatic Biofuel Cell Based on Buckypaper Cathode and Ferrocene-Containing Redox Polymer Anode. *J. Power Sources* **2014,** *247*, 579-586.

(615) Gao, F.; Viry, L.; Maugey, M.; Poulin, P.; Mano, N. Engineering Hybrid Nanotube Wires for High-Power Biofuel Cells. *Nat. Commun.* **2010,** *1*, 10.1038/ncomms1000.

(616) Shin, H.; Kang, C. Enhanced Performance of the Wired Bilirubin Oxidase Oxygen Cathode with Incorporation of Carboxylated Single-Walled Carbon Nanotubes. *Electrochim. Acta* **2014,** *115*, 599-606.

(617) Kwon, C. H.; Lee, S.-H.; Choi, Y.-B.; Lee, J. A.; Kim, S. H.; Kim, H.-H.; Spinks, G. M.; Wallace, G. G.; Lima, M. D.; Kozlov, M. E.; Baughmann R.H.; Kim S.J. High-Power Biofuel Cell Textiles from Woven Biscrolled Carbon Nanotube Yarns. *Nat. Commun.* **2014,** *5*, 3928.

(618) Tsujimura, S.; Murata, K.; Akatsuka, W. Exceptionally High Glucose Current on a Hierarchically Structured Porous Carbon Electrode with "Wired" Flavin Adenine Dinucleotide-Dependent Glucose Dehydrogenase. *J. Am. Chem. Soc.* **2014,** *136*, 14432-14437.

(619) Little, S. J.; Ralph, S. F.; Mano, N.; Chen, J.; Wallace, G. G. A Novel Enzymatic Bioelectrode System Combining a Redox Hydrogel with a Carbon NanoWeb. *Chem Commun (Camb)* **2011,** *47*, 8886-8888.

(620) Scanlon, M. D.; Salaj-Kosla, U.; Belochapkine, S.; MacAodha, D.; Leech, D.; Ding, Y.; Magner, E. Characterization of Nanoporous Gold Electrodes for Bioelectrochemical Applications. *Langmuir* **2012,** *28*, 2251-2261.

(621) Boland, S.; Leech, D. A Glucose/Oxygen Enzymatic Fuel Cell Based on Redox Polymer and Enzyme Immobilisation at Highly-Ordered Macroporous Gold Electrodes. *Analyst* **2012,** *137*, 113-117.

(622) Gomez, C.; Shipovskov, S.; Ferapontova, E. E. Peroxidase Biocathodes for a Biofuel Cell Development *J. Renew. Sust. Energy.* **2010,** *2*, 013103.

(623) Jia, W.; Jin, C.; Xia, W.; Muhler, M.; Schuhmann, W.; Stoica, L. Glucose Oxidase/Horseradish Peroxidase Coimmobilized at a CNT-Modified Graphite Electrode: towards Potentially Implantable Biocathodes. *Chem. Eur. J.* **2012,** *18*, 2783-2786.

(624) Elouarzaki, K.; Bourourou, M.; Holzinger, M.; Le Goff, A.; Marks, R. S.; Cosnier, S. Freestanding HRP-GOx Redox Buckypaper as an Oxygen-Reducing Biocathode for Biofuel Cell Applications. *Energy Environ. Sci.* **2015,** *8*, 2069-2074.

(625) Agnès, C.; Reuillard, B.; Le Goff, A.; Holzinger, M.; Cosnier, S. A Double-Walled Carbon Nanotube-Based Glucose/H_2O_2 Biofuel Cell Operating under Physiological Conditions. *Electrochem. Commun.* **2013,** *34*, 105-108.

(626) Krikstolaityte, V.; Oztekin, Y.; Kuliesius, J.; Ramanaviciene, A.; Yazicigil, Z.; Ersoz, M.; Okumus, A.; Kausaite-Minkstimiene, A.; Kilic, Z.; Solak, A. O.; Makaraviciute A.; Ramanavicius A. Biofuel Cell Based on Anode and Cathode Modified by Glucose Oxidase. *Electroanalysis* **2013,** *25*, 2677-2683.

(627) Katz, E.; Willner, I.; Kotlyar, A. B. A Non-Compartmentalized Glucose O_2 Biofuel Cell by Bioengineered Electrode Surfaces. *J. Electroanal. Chem.* **1999,** *479*, 64-68.

(628) Hill, H. A. O.; Walton, N. J. Investigation of Some Intermolecular Electron Transfer Reactions of Cytochrome *c* by Electrochemichal Methods. *J. Am. Chem. Soc.* **1982,** *104*, 6515-6519.

(629) Pardo-Yissar, V.; Katz, E.; Willner, I.; Kotlyar, A. B.; Sanders, C.; Lill, H. Biomaterial Engineered Electrodes for Bioelectronics. *Farad. Disc.* **2000,** *116*, 119-134.

(630) Zayats, M.; Willner, B.; Willner, I. Design of Amperometric Biosensors and Biofuel Cells by the Reconstitution of Electrically Contacted Enzyme Electrodes. *Electroanalysis* **2008,** *20*, 583-601.

(631) Willner, I.; Katz, E. Integration of Layered Redox Proteins and Conductive Supports for Bioelectronic Applications. *Angew. Chem. Int. Ed.* **2000,** *39*, 1180-1218.

(632) Katz, E.; Buckmann, A. F.; Willner, I. Self-Powered Enzyme-Based Biosensors. *J. Am. Chem. Soc.* **2001,** *123*, 10752-10753.

(633) Katz, E.; Willner, I. A Biofuel Cell with Electrochemichally Switchable and Tunable Power Output. *J. Am. Chem. Soc.* **2003,** *125*, 6803-6813.

(634) Katz, E.; Lioubashevski, O.; Willner, I. Magnetic Field Effects on Bioelectrocatalytic Reactions of Surface-Confined Enzyme Systems: Enhanced Performance of Biofuel Cells. *J. Am. Chem. Soc.* **2005,** *127*, 3979-3988.

(635) Miura, Y.; Tsujimura, S.; Kamitaka, Y.; Kurose, S.; Kataoka, K.; Sakurai, T.; Kano, K. Bioelectrocatalytic Reduction of O_2 Catalyzed by CueO from *Escherichia coli* Adsorbed on a Highly Oriented Pyrolytic Graphite Electrode. *Chem. Lett.* **2007,** *36*, 132-133.

(636) Miura, Y.; Tsujimura, S.; Kurose, S.; Kamitaka, Y.; Kataoka, K.; Sakurai, T.; Kano, K. Direct Electrochemistry of CueO and Its Mutants at Residues to and Near Type I Cu for Oxygen-Reducing Biocathode. *Fuel Cells* **2009,** *9*, 70-78.

(637) Tsujimura, S.; Miura, Y.; Kano, K. CueO-Immobilized Porous Carbon Electrode Exhibiting Improved Performance of Electrochemichal Reduction of Dioxygen to Water. *Electrochim. Acta* **2008,** *53*, 5716-5720.

(638) Roberts, S. A.; Weichsel, A.; Grass, G.; Thakali, K.; Hazzard, J. T.; Tollin, G.; Rensing, C.; MontFort, W. R. Crystal Structure and Electron Transfer Kinetics of CueO, a Multicopper Oxidase Required for Copper Homeostasis in *Escherichia coli*. *Proc. Natl. Acad. Sci. USA* **2002,** *99*, 2766-2771.

(639) Sané, S.; Richter, K.; Rubenwolf, S.; Matschke, N. J.; Jolivalt, C.; Madzak, C.; Zengerle, R.; Gescher, J.; Kerzenmacher, S. Using Planktonic Microorganisms to Supply the Unpurified Multi-Copper Oxidases Laccase and Copper Efflux Oxidases at a Biofuel Cell Cathode. *Biores.Tech.* **2014,** *158*, 231-238.

(640) Kang, C.; Shin, H.; Heller, A. On the Stability of the "Wired" Bilirubin Oxidase Oxygen Cathode in Serum. *Bioelectrochem.* **2006,** *68*, 22-26.

(641) Kang, C.; Cho, S.; Shin, H.; Heller, A. An Oxidizable Anion Excluding Polymer Overlayer for Oxygen Electrodes. *Electroanalysis* **2009,** *24*, 2709-2712.

(642) Cinquin, P.; Gondran, C.; Giroud, F.; Mazabrard, S.; Pellissier, A.; Boucher, F.; Alcaraz, J. P.; Gorgy, K.; Lenouvel, F.; Mathe, S.; Porcu, P.; Cosnier, S. A Glucose Biofuel Cell Implanted in Rats. *PLOS One* **2010,** *5*, e10476.

(643) Giroud, F.; Gondran, C.; Gorgy, K.; Vivier, V.; Cosnier, S. An Enzymatic Biofuel Cell Based on Electrically Wired Polyphenol Oxidase and Glucose Oxidase Operating under Physiological Conditions. *Electrochim. Acta* **2012,** *85*, 278-282.

(644) Gu, Y.; Sattayasamitsathit, S.; Jia, W.; Kaufmann, K.; Wang, C.; Wang, J. High-Power Low-Cost Tissue-Based Biofuel Cell. *Electroanalysis* **2013,** *25*, 838-844.

(645) Zhou, H.; Liu, L.; Yin, K.; Liu, S.; Li, G. Electrochemical Investigation on the Catalytic Ability of Tyrosinase with the Effect of Nano Titanium Dioxide. *Electrochem. Commun.* **2006,** *8*, 1168-1172.

(646) Ye, B.; Zhou, X. Direct Electrochemichal Redox of Tyrosinase at Silver Electrodes. *Talanta* **1997,** *44*, 831-836.

(647) Mohammadi, A.; Moghaddam, A.; Dinarvand, R.; Rezaei-Zarchi, S. Direct Electron Transfer of Polyphenol Oxidase on Carbon Nanotube Surfaces: Application in Biosensing *Int. J. Electrochem. Sci.* **2009,** *4*, 895-905.

(648) Faridnouri, H.; Ghourchian, H.; Hashemnia, S. Direct Electron Transfer Enhancement of Covalently Bound Tyrosinase to Glassy Carbon via Woodward's Reagent K. *Bioelectrochem.* **2011,** *8*, 1-9.

(649) Reuillard, B.; Le Goff, A.; Agnès, C.; Zebda, A.; Holzinger, M.; Cosnier, S. Direct Electron Transfer between Tyrosinase and Multi-Walled Carbon Nanotubes for Bioelectrocatalytic Oxygen Reduction. *Electrochem. Commun.* **2012,** *20*, 19-22.

(650) Halfen, J. A.; Mahapatra, S.; Wilkinson, E. C.; Kaderli, S.; Young, V. G.; Que, L.; Zuberbühler, A. D.; Tolman, W. B. Reversible Cleavage and Formation of the Dioxygen O-O Bond within a Dicopper Complex. *Science* **1996,** *271*, 1397-1400.

(651) Rasmussen, M.; Abdellaoui, S.; Minteer, S. D. Enzymatic Biofuel Cells: 30 Years of Critical Advancements. *Biosens. Bioelectron.* **2016,** *76*, 91-102.

(652) Chen, T.; Barton, S. C.; Binyamin, G.; Gao, Z.; Zhang, Y.; Kim, H.-H.; Heller, A. A Miniature Biofuel Cell. *J. Am. Chem. Soc.* **2001,** *123*, 8630-8631.

(653) Mano, N. A 280 microW cm^{-2} Biofuel Cell Operating At Low Glucose Concentration. *Chem Commun (Camb)* **2008**, *0*, 2221-2223

(654) Gao, F.; Courjean, O.; Mano, N. An Improved Glucose/O_2 Membrane-Less Biofuel Cell through Glucose Oxidase Purification. *Biosens. Bioelectron.* **2009,** *25*, 356-361.

(655) Zafar, M. N.; Tasca, F.; Boland, S.; Kujawa, M.; Patel, I.; Peterbauer, C. K.; Leech, D.; Gorton, L. Wiring of Pyranose Dehydrogenase with Osmium Polymers of Different Redox Potentials. *Bioelectrochem.* **2010,** *80*, 38-42.

(656) Pinyou, P.; Ruff, A.; Pöller, S.; Ma, S.; Ludwig, R.; Schuhmann, W. Design of an Os Complex-Modified Hydrogel with Optimized Redox Potential for Biosensors and Biofuel Cells. *Chem. Eur. J.* **2016,** *22*, 5319-5326.

(657) Saleh, F. S.; Mao, L.; Ohsaka, T. A Promising Dehydrogenase-Based Bioanode for a Glucose Biosensor and Glucose/O_2 Biofuel Cell. *Analyst* **2012,** *137*, 2233-2238.

(658) Scherbahn, V.; Putze, M. T.; Dietzel, B.; Heinlein, T.; Schneider, J. J.; Lisdat, F. Biofuel Cells Based on Direct Enzyme/Electrode Contacts Using PQQ-dependent Glucose Dehydrogenase/Bilirubin Oxidase and Modified Carbon Nanotube Materials. *Biosens. Bioelectron.* **2014,** *61*, 631-638.

(659) Fapyane, D.; Lee, Y.; Lim, C. Y.; Ahn, J.-H.; Kim, S.-W.; Chang, I. S. Immobilisation of Flavin-Adenine-Dinucleotide-Dependent Glucose Dehydrogenase α Subunit in Free-Standing Graphitised Carbon Nanofiber Paper Using a Bifunctional Cross-Linker for an Enzymatic Biofuel Cell. *ChemElectroChem.* **2014,** *1*, 1844-1848.

(660) Ludwig, R.; Harreither, W.; Tasca, F.; Gorton, L. Cellobiose Dehydrogenase: a Versatile Catalyst for Electrochemichal Applications. *ChemPhysChem.* **2010,** *11*, 2674-2697.

(661) Tasca, F.; Gorton, L.; Harreither, W.; Haltrich, D.; Ludwig, R.; Noll, G. Highly Efficient and Versatile Anodes for Biofuel Cells Based on Cellobiose Dehydrogenase from *Myriococcum thermophilum*. *J. Phys. Chem. C* **2008,** *112*, 13668-13673.

(662) Stoica, L.; Dimcheva, N.; Ackermann, Y.; Karnicka, K.; Guschin, D. A.; Kulesza, P. J.; Rogalski, J.; Haltrich, D.; Ludwig, R.; Gorton, L.; Schuhmann, W. Membrane-Less Biofuel Cell Based on Cellobiose Dehydrogenase (Anode)/Laccase (Cathode) Wired via Specific Os-Redox Polymers. *Fuel Cells* **2009,** *9*, 53-62.

(663) Wang, X.; Falk, M.; Ortiz, R.; Matsumura, H.; Bobacka, J.; Ludwig, R.; Bergelin, M.; Gorton, L.; Shleev, S. Mediatorless Sugar/Oxygen Enzymatic Fuel Cells Based on Gold Nanoparticle-Modified Electrodes. *Biosens. Bioelectron.* **2012,** *31*, 219-225.

(664) Tasca, F.; Gorton, L.; Kujawa, M.; Patel, I.; Harreither, W.; Peterbauer, C. K.; Ludwig, R.; Noll, G. Increasing the Coulombic Efficiency of Glucose Biofuel Cell Anodes by Combination of Redox Enzymes. *Biosens. Bioelectron.* **2010,** *25*, 1710-1716.

(665) Moehlenbrock, M. J.; Toby, T. K.; Waheed, A.; Minteer, S. D. Metabolon Catalyzed Pyruvate/Air Biofuel Cell. *J. Am. Chem. Soc.* **2010,** *132*, 6288-6289.

(666) Sokic-Lazic, D.; Arechederra, R. L.; Treu, B. L.; Minteer, S. D. Oxidation of Biofuels: Fuel Diversity and Effectiveness of Fuel Oxidation through Multiple Enzyme Cascades. *Electroanalysis* **2010,** *22*, 757-764.

(667) Liu, Y.; Dong, S. A Biofuel Cell Harvesting Energy from Glucose-Air and Fruit Juice-Air. *Biosens. Bioelectron.* **2007,** *23*, 593-597.

(668) MacVittie, K.; Conlon, T.; Katz, E. A Wireless Transmission System Powered by an Enzyme Biofuel Cell Implanted in an Orange. *Bioelectrochem.* **2015,** *106, Part A*, 28-33.

(669) Wen, D.; Xu, X.; Dong, S. A Single-Walled Carbon Nanohorn-Based Miniature Glucose/Air Biofuel Cell for Harvesting Energy from Soft Drinks. *Energy Environ. Sci.* **2011,** *4*, 1358-1363.

(670) Miyake, T.; Haneda, K.; Nagai, N.; Yatagawa, Y.; Onami, H.; Yoshino, S.; Abe, T.; Nishizawa, M. Enzymatic Biofuel Cells Designed for Direct Power Generation from Biofluids in Living Organisms. *Energy Environ. Sci.* **2011,** *4*, 5008-5012.

(671) Flexer, V.; Mano, N. From Dynamic Measurements of Photosynthesis in a Living Plant to Sunlight Transformation into Electricity. *Anal. Chem.* **2010,** *82*, 1444-1449.

(672) Drake, R. F. A Tissue Implantable Fuel Cell Power Supply. *Trans - ASAIO* **1970,** *16*, 199-205.

(673) Giner, J.; Holleck, G.; Malachesky, P. A. Eine implantierbare Brennstoffzelle zum Betrieb eines mechanischen Herzens. *Berichte der Bunsengesellschaft für Physikalische Chemie* **1973,** *77*, 782.

(674) Zebda, A.; Cosnier, S.; Alcaraz, J.-P.; Holzinger, M.; Le Goff, A.; Gondran, C.; Boucher, F.; Giroud, F.; Gorgy, K.; Lamraoui, H.; Cinquin P. Single Glucose Biofuel Cells Implanted in Rats Power Electronic Devices. *Sci. Rep.* **2013,** *3*, 1-5.

(675) Castorena-Gonzalez, J. A.; Foote, C.; MacVittie, K.; Halamek, J.; Halamkova, L.; Martinez-Lemus, L. A.; Katz, E. Biofuel Cell Operating *in vivo* in Rat. *Electroanalysis* **2013,** *25*, 1579-1584.

(676) Halámková, L.; Halámek, J.; Bocharova, V.; Szczupak, A.; Alfonta, L.; Katz, E. Implanted Biofuel Cell Operating in a Living Snail. *J. Am. Chem. Soc.* **2012,** *134*, 5040-5043.

(677) MacVittie, K.; Halamek, J.; Halamkova, L.; Southcott, M.; Jemison, W. D.; Lobel, R.; Katz, E. From "Cyborg" Lobsters to a Pacemaker Powered by Implantable Biofuel Cells. *Energy Environ. Sci.* **2013,** *6*, 81-86.

(678) Cadet, M. *Vers la conception d'une biopile enzymatique Glucose/oxygène efficace en milieu biologique*; The University of Bordeaux, 2015.

(679) Southcott, M.; MacVittie, K.; Halamek, J.; Halamkova, L.; Jemison, W. D.; Lobel, R.; Katz, E. A Pacemaker Powered by an Implantable Biofuel Cell Operating under Conditions Mimicking the Human Blood Circulatory System - Battery Not Included. *Phys. Chem. Chem. Phys.* **2013,** *15*, 6278-6283.

(680) Gao, F.; Yan, Y.; Su, L.; Wang, L.; Mao, L. An Enzymatic Glucose/O_2 Biofuel Cell: Preparation, Characterization and Performance in Serum. *Electrochem. Commun.* **2007,** *9*, 989-996.

(681) Ammam, M.; Fransaer, J. Glucose/O_2 Biofuel Cell Based on Enzymes, Redox Mediators, and Multiple-Walled Carbon Nanotubes Deposited by AC-Electrophoresis then Stabilized by Electropolymerized Polypyrrole. *Biotech. Bioeng.* **2012,** *109*, 1601-1609.

(682) MacAodha, D.; O Conghaile, P.; Egan, B.; Kavanagh, P.; Leech, D. Membraneless Glucose/Oxygen Enzymatic Fuel Cells Using Redox Hydrogel Films Containing Carbon Nanotubes. *ChemPhysChem* **2013,** *14*, 2302-2307.

(683) Kwon, C. H.; Lee, J. A.; Choi, Y.-B.; Kim, H.-H.; Spinks, G. M.; Lima, M. D.; Baughman, R. H.; Kim, S. J. Stability of Carbon Nanotube Yarn Biofuel Cell in Human Body Fluid. *J. Power Sources* **2015,** *286*, 103-108.

(684) Pan, C.; Fang, Y.; Wu, H.; Ahmad, M.; Luo, Z.; Li, Q.; Xie, J.; Yan, X.; Wu, L.; Wang, Z. L.et al. Generating Electricity from Biofluid with a Nanowire-Based Biofuel Cell for Self-Powered Nanodevices. *Adv. Mater.* **2010,** *22*, 5388-5392.

(685) Ó Conghaile, P.; Falk, M.; MacAodha, D.; Yakovleva, M. E.; Gonaus, C.; Peterbauer, C. K.; Gorton, L.; Shleev, S.; Leech, D. Fully Enzymatic Membraneless Glucose|Oxygen Fuel Cell that Provides 0.275 mA cm^{-2} in 5 mM Glucose, Operates in

Human Physiological Solutions, and Powers Transmission of Sensing Data. *Anal. Chem.* **2016,** *88*, 2156-2163.

(686) Pankratov, D.; Ohlsson, L.; Gudmundsson, P.; Halak, S.; Ljunggren, L.; Blum, Z.; Shleev, S. *Ex vivo* Electric Power Generation in Human Blood Using an Enzymatic Fuel Cell in a Vein Replica. *RSC Adv.* **2016,** *6*, 70215-70220.

(687) Göbel, G.; Beltran, M. L.; Mundhenk, J.; Heinlein, T.; Schneider, J.; Lisdat, F. Operation of a Carbon Nanotube-Based Glucose/Oxygen Biofuel Cell in Human Body Liquids — Performance Factors and Characteristics. *Electrochim. Acta* **2016,** *218*, 278-284.

(688) Plumeré, N.; Rüdiger, O.; Oughli, A. A.; Williams, R.; VivekananThan, J.; Pöller, S.; Schuhmann, W.; Lubitz, W. A Redox Hydrogel Protects Hydrogenase from High-Potential Deactivation and Oxygen Damage. *Nat. Chem.* **2014,** *6*, 822-827.

(689) Fourmond, V.; Stapf, S.; Li, H.; Buesen, D.; Birrell, J.; Rüdiger, O.; Lubitz, W.; Schuhmann, W.; Plumeré, N.; Léger, C. Mechanism of Protection of Catalysts Supported in Redox Hydrogel Films. *J. Am. Chem. Soc.* **2015,** *137*, 5494-5505.

(690) Xia, H.-q.; So, K.; Kitazumi, Y.; Shirai, O.; Nishikawa, K.; Higuchi, Y.; Kano, K. Dual Gas-Diffusion Membrane- and Mediatorless Dihydrogen/Air-Breathing Biofuel Cell Operating at Room Temperature. *J. Power Sources* **2016,** *335*, 105-112.

(691) Palmore, G. T.; Bertschy, H.; Bergens, S. H.; Whitesides, G. M. A Methanol/Dioxygen Biofuel Cell that Uses NAD^+-dependent Dehydrogenases as Catalysts : Application of an Electro-Enzymatic Method to Regenerate Nicotinamide Adenine Dinucleotide at Low Overpotentials. *J. Electroanal. Chem.* **1998,** *443*, 155-161.

(692) Aquino Neto, S.; Milton, R. D.; Hickey, D. P.; De Andrade, A. R.; Minteer, S. D. Membraneless Enzymatic Ethanol/O_2 Fuel Cell: Transitioning from an Air-Breathing

Pt-Based Cathode to a Bilirubin Oxidase-Based Biocathode. *J. Power Sources* **2016,** *324*, 208-214.

(693) Ramanavicius, A.; Kausaite, A.; Ramanaviciene, A. Enzymatic Biofuel Cell Based on Anode and Cathode Powered by Ethanol. *Biosens. Bioelectron.* **2008,** *24*, 767-772.

(694) Moore, C. M.; Minteer, S. D.; Martin, R. S. Microchip-Based Ethanol/Oxygen Biofuel Cell. *Lab Chip* **2005,** *5*, 218-225.

(695) Giroud, F.; Hickey, D. P.; Schmidtke, D. W.; Glatzhofer, D. T.; Minteer, S. D. A Monosaccharide-Based Coin-Cell Biobattery. *ChemElectroChem.* **2014,** *1*, 1880-1885.

(696) Lim, K. G.; Palmore, G. T. R. Microfluidic Biofuel Cells: the Influence of Electrode Diffusion Layer on Performance. *Biosens. Bioelectron.* **2007,** *22*, 941-947.

(697) Kjeang, E.; Sinton, D.; Harrington, D. A. Strategic Enzyme Patterning for Microfluidic Biofuel Cells. *J. Power Sources* **2006,** *158*, 1-12.

(698) González-Guerrero, M. J.; del Campo, F. J.; Esquivel, J. P.; Leech, D.; Sabaté, N. Paper-Based Microfluidic Biofuel Cell Operating under Glucose Concentrations within Physiological Range. *Biosens. Bioelectron.* **2017,** *90*, 475-480.

(699) Jenkins, P.; Tuurala, S.; Vaari, A.; Valkiainen, M.; Smolander, M.; Leech, D. A Mediated Glucose/Oxygen Enzymatic Fuel Cell Based on Printed Carbon Inks Containing Aldose Dehydrogenase and Laccase as Anode and Cathode. *Enz. Microbial Tech.* **2012,** *50*, 181-187.

(700) González-Guerrero, M. J.; del Campo, F. J.; Esquivel, J. P.; Giroud, F.; Minteer, S. D.; Sabaté, N. Paper-Based Enzymatic Microfluidic Fuel Cell: from a Two-Stream Flow Device to a Single-Stream Lateral Flow Strip. *J. Power Sources* **2016,** *326*, 410-416.

(701) Fischer, C.; Fraiwan, A.; Choi, S. A 3D Paper-Based Enzymatic Fuel Cell for Self-Powered, Low-Cost Glucose Monitoring. *Biosens. Bioelectron.* **2016,** *79*, 193-197.

(702) Narvaez Villarrubia, C. W.; Soavi, F.; Santoro, C.; Arbizzani, C.; Serov, A.; Rojas-Carbonell, S.; Gupta, G.; Atanassov, P. Self-Feeding Paper-Based Biofuel Cell/Self-Powered Hybrid μ-Supercapacitor Integrated System. *Biosens. Bioelectron.* **2016,** *86*, 459-465.

(703) Calabrese Barton, S. Oxygen Transport in Composite Mediated Biocathodes. *Electrochim. Acta* **2005,** *50*, 2145-2153.

(704) Gupta, G.; Lau, C.; Rajendran, V.; Colon, F.; Branch, B.; Ivnitski, D.; Atanassov, P. Direct Electron Transfer Catalyzed by Bilirubin Oxidase for Air Breathing Gas-Diffusion Electrodes. *Electrochem. Commun.* **2011,** *13*, 247-249.

(705) Gupta, A.; Lau, C.; Branch, B.; Rajendran, A.; Ivnitski, D.; Atanassov, P. Direct Bio-Electrocatalysis by Multicopper Oxidases: Gas-Diffusion Laccase-Catalyzed Cathodes for Biofuel Cells. *Electrochim. Acta* **2011,** *56*, 10767-10771.

(706) Kontani, R.; Tsujimura, S.; Kano, K. Air Diffusion Biocathode with CueO as Electrocatalyst Adsorbed on Carbon Particle-Modified Electrodes. *Bioelectrochem.* **2009,** *76*, 10-13.

(707) Yamagiwa, K.; Ikeda, Y.; Yasueda, K.; Handa, Y.; Yabuuchi, N.; Komaba, S. Improvement of Electrochemichal Performance of Bilirubin Oxidase Modified Gas Diffusion Biocathode by Hydrophilic Binder. *J. Electrochem. Soc.* **2015,** *162*, F1425-F1430.

(708) Gellett, W.; Schumacher, J.; Kesmez, M.; Le, D.; Minteer, S. D. High Current Density Air-Breathing Laccase Biocathode. *J. Electrochem. Soc.* **2010,** *157*, B557-B562.

(709) Hudak, N. S.; Gallaway, J. W.; Calabrese Barton, S. Mediated Biocatalytic Cathodes Operating on Gas-Phase Air and Oxygen in Fuel Cells. *J. Electrochem. Soc.* **2009,** *156*, B9-B15.

(710) Zloczewska, A.; Jonsson-Niedziolka, M. Efficient Air-Breathing Biocathodes for Zinc/Oxygen Batteries. *J. Power Sources* **2013,** *228*, 104-111.

(711) So, K.; Onizuka, M.; Komukai, T.; Kitazumi, Y.; Shirai, O.; Kano, K. Binder/Surfactant-Free Biocathode with Bilirubin Oxidase for Gas-Diffusion-Type System. *Electrochem. Commun.* **2016,** *66*, 58-61.

(712) Omar Garcia, S.; Narvaez Villarrubia, C.; Falase, A.; Atanassov, P. Gas-Diffusion Cathodes Integrating Carbon Nanotube-Modified Toray Paper and Bilirubin Oxidase. *J. Electrochem. Soc.* **2014,** *161*, H523-H528.

(713) Borole, A. P.; LaBarge, S.; Spott, B. A. Three-Dimensional, Gas Phase Fuel Cell with a Laccase Biocathode. *J. Power Sources* **2009,** *188*, 421-426.

(714) Babanova, S.; Artyushkova, K.; Ulyanova, Y.; Singhal, S.; Atanassov, P. Design of Experiments and Principal Component Analysis as Approaches for Enhancing Performance of Gas-Diffusional Air-Breathing Bilirubin Oxidase Cathode. *J. Power Sources* **2014,** *247*, 1055.

(715) Ciniciato, G. P. M. K.; Lau, C.; Cochrane, A.; Sibbett, S. S.; Gonzalez, E. R.; Atanassov, P. Development of Paper-Based Electrodes: from Air-Breathing to Paintable Enzymatic Cathodes. *Electrochim. Acta* **2012,** *82*, 208-213.

(716) Rincon, R. A.; Lau, C.; Luckarift, H. R.; Garcia, K. E.; Adkins, E.; Johnson, G. R.; Atanassov, P. Enzymatic Fuel Cells: Integrating Flow-through Anode and Air-Breathing Cathode into a Membrane-Less Biofuel Cell Design. *Biosens. Bioelectron.* **2011,** *27*, 132-136.

(717) Rojas-Carbonell, S.; Babanova, S.; Serov, A.; Ulyanova, Y.; Singhal, S.; Atanassov, P. Hybrid Electrocatalysts for Oxygen Reduction Reaction: Integrating Enzymatic and Non-Platinum Group Metal Catalysis. *Electrochim. Acta* **2016,** *190*, 504-510.

(718) Das, M.; Barbora, L.; Das, P.; Goswami, P. Biofuel Cell for Generating Power from Methanol Substrate using Alcohol Oxidase Coanode and Air-Breathed Laccase Biocathode. *Biosens. Bioelectron.* **2014,** *59*, 184-191.

(719) Tam, T. K.; Pita, M.; Ornatska, M.; Katz, E. Biofuel Cell Controlled by Enzyme Logic Network - Approaching Physiologically Regulated Devices. *Bioelectrochem.* **2009,** *76*, 4-9.

(720) Katz, E.; Pita, M. Biofuel Cells Controlled by Logically Processed Biochemical Signals: towards Physiologically Regulated Bioelectronic Devices. *Chem. Eur. J.* **2009,** *15*, 12554-12564.

(721) Tam, T. K.; Strack, G.; Pita, M.; Katz, E. Biofuel Cell Logically Controlled by Antigen-Antibody Recognition: towards Immune-Regulated Bioelectronic Devices. *J. Am. Chem. Soc.* **2009,** *131*, 11670-11671.

(722) Halamek, J.; Tam, T. K.; Strack, G.; Bocharova, V.; Pita, M.; Katz, E. Self-Powered Biomolecular Keypad Lock Security System Based on a Biofuel Cell. *Chem Commun (Camb)* **2010,** *46*, 2405-2407.

(723) Katz, E.; Fernández, V. M.; Pita, M. Switchable Bioelectrocatalysis Controlled by pH Changes. *Electroanalysis* **2015,** *27*, 2063-2073.

(724) Amir, L.; Tam, T. K.; Pita, M.; Meijler, M. M.; Alfonta, L.; Katz, E. Biofuel Cell Controlled by Enzyme Logic Systems. *J. Am. Chem. Soc.* **2009,** *131*, 826-832.

(725) Cheng, J.; Han, Y.; Deng, L.; Guo, S. Carbon Nanotube–Bilirubin Oxidase Bioconjugate as a New Biofuel Cell Label for Self-Powered Immunosensor. *Anal. Chem.* **2014,** *86*, 11782-11788.

(726) Wang, T.; Milton, R. D.; Abdellaoui, S.; Hickey, D. P.; Minteer, S. D. Laccase Inhibition by Arsenite/Arsenate: Determination of Inhibition Mechanism and

Preliminary Application to a Self-Powered Biosensor. *Anal. Chem.* **2016,** *88*, 3243-3248.

(727) Conzuelo, F.; VivekananThan, J.; Pöller, S.; Pingarrón, J. M.; Schuhmann, W. Immunologically Controlled Biofuel Cell as a Self-Powered Biosensor for Antibiotic Residue Determination. *ChemElectroChem.* **2014,** *1*, 1854-1858.

(728) Panpan, G.; Chengcheng, G.; Ting, H.; Feng, L. Ultrasensitive Self-Powered Aptasensor Based on Enzyme Biofuel Cell and DNA Bioconjugate: a Facile and Powerful Tool for Antibiotic Residue Detection. *Anal. Chem.* **2017,** *89*, 2163-2169.

(729) Pinyou, P.; Conzuelo, F.; Sliozberg, K.; VivekananThan, J.; Contin, A.; Pöller, S.; Plumeré, N.; Schuhmann, W. Coupling of an Enzymatic Biofuel Cell to an Electrochemichal Cell for Self-Powered Glucose Sensing with Optical Readout. *Bioelectrochem.* **2015,** *106, Part A*, 22-27.

(730) Cheng, H.; Yu, P.; Lu, X.; Lin, Y.; Ohsaka, T.; Mao, L. Biofuel Cell-Based Self-Powered Biogenerators for Online Continuous Monitoring of Neurochemicals in Rat Brain. *Analyst* **2013,** *138*, 179-185.

(731) Bai, L.; Jin, L.; Han, L.; Dong, S. Self-Powered Fluorescence Controlled Switch Systems Based on Biofuel Cells. *Energy Environ. Sci.* **2013,** *6*, 3015-3021.

(732) Falk, M.; Alcalde, M.; Bartlett, P. N.; De Lacey, A. L.; Gorton, L.; Gutierrez-Sanchez, C.; Haddad, R.; Kilburn, J.; Leech, D.; Ludwig, R.et al. Self-Powered Wireless Carbohydrate/Oxygen Sensitive Biodevice Based on Radio Signal Transmission. *PLOS ONE* **2014,** *9*, e109104.

(733) Pankratov, D.; Blum, Z.; Suyatin, D. B.; Popov, V. O.; Shleev, S. Self-Charging Electrochemichal Biocapacitor. *ChemElectroChem* **2014,** *1*, 343-346.

(734) Pankratov, D.; Falkman, P.; Blum, Z.; Shleev, S. A Hybrid Electric Power Device for Simultaneous Generation and Storage of Electric Energy. *Energy Environ. Sci.* **2014,** *7*, 989-993.

(735) Agnes, C.; Holzinger, M.; Le Goff, A.; Reuillard, B.; Elouarzaki, K.; Tingry, S.; Cosnier, S. Supercapacitor/Biofuel Cell Hybrids Based on Wired Enzymes on Carbon Nanotube Matrices: Autonomous Reloading after High Power Pulses in Neutral Buffered Glucose Solutions. *Energy Environ. Sci.* **2014,** *7*, 1884-1888.

(736) Pankratov, D.; Conzuelo, F.; Pinyou, P.; Alsaoub, S.; Schuhmann, W.; Shleev, S. A Nernstian Biosupercapacitor. *Angew. Chem. Int. Ed.* **2016,** *55*, 15434-15438.

(737) Xiao, X.; Conghaile, P. Ó.; Leech, D.; Ludwig, R.; Magner, E. A Symmetric Supercapacitor/Biofuel Cell Hybrid Device Based on Enzyme-modified Nanoporous Gold: an Autonomous Pulse Generator. *Biosens. Bioelectron.* **2017,** *90*, 96-102.

(738) Kizling, M.; Stolarczyk, K.; Tammela, P.; Wang, Z.; Nyholm, L.; Golimowski, J.; Bilewicz, R. Bioelectrodes Based on Pseudocapacitive Cellulose/Polypyrrole Composite Improve Performance of Biofuel Cell. *Bioelectrochem.* **2016,** *112*, 184-190.

(739) Kizling, M.; Stolarczyk, K.; Kiat, J. S. S.; Tammela, P.; Wang, Z.; Nyholm, L.; Bilewicz, R. Pseudocapacitive Polypyrrole–Nanocellulose Composite for Sugar-Air Enzymatic Fuel Cells. *Electrochem. Commun.* **2015,** *50*, 55-59.

(740) Kizling, M.; Draminska, S.; Stolarczyk, K.; Tammela, P.; Wang, Z.; Nyholm, L.; Bilewicz, R. Biosupercapacitors for Powering Oxygen Sensing Devices. *Bioelectrochem.* **2015,** *106, Part A*, 34-40.

(741) Stolarczyk, K.; Kizling, M.; Majdecka, D.; Żelechowska, K.; Biernat, J. F.; Rogalski, J.; Bilewicz, R. Biobatteries and Biofuel Cells with Biphenylated Carbon Nanotubes. *J. Power Sources* **2014,** *249*, 263-269.

(742) González-ArribAs, E.; Aleksejeva, O.; Bobrowski, T.; Toscano, M. D.; Gorton, L.; Schuhmann, W.; Shleev, S. Solar Biosupercapacitor. *Electrochem. Commun.* **2017,** *74*, 9-13.

(743) Pankratova, G.; Pankratov, D.; HAsan, K.; Åkerlund, H.-E.; Albertsson, P.-Å.; Leech, D.; Shleev, S.; Gorton, L. Supercapacitive Photo-Bioanodes and Biosolar Cells: a Novel Approach for Solar Energy Harnessing. *Adv. Energy Mat.* **2017**, DOI:10.1002/aenm.201602285 10.1002/aenm.201602285, 1602285-n/a.

(744) Steinberg, M. D.; Kassal, P.; Steinberg, I. M. System Architectures in Wearable Electrochemichal Sensors. *Electroanalysis* **2016,** *28*, 1149-1169.

(745) Bandodkar, A. J.; Wang, J. Non-Invasive Wearable Electrochemichal Sensors: a Review. *Trends Biotech.* **2014,** *32*, 363-371.

(746) Bandodkar, A. J.; Molinnus, D.; Mirza, O.; Guinovart, T.; Windmiller, J. R.; Valdès-Ramirez, G.; Andrade, F. J.; Schöning, M. J.; Wang, J. Epidermal Tattoo Potentiometric Sodium Sensors with Wireless Signal Transduction for Continuous Non-Invasive Sweat Monitoring. *Biosens. Bioelectron.* **2014,** *54*, 603-609.

(747) Jia, W.; Valdès-Ramirez, G.; Bandodkar, A. J.; Windmiller, J. R.; Wang, J. Epidermal Biofuel Cells: Energy Harvesting from Human Perspiration. *Angew. Chem. Int. Ed.* **2013,** *52*, 7233-7236.

(748) Jia, W. Z.; Wang, X.; Imani, S.; Bandodkar, A. J.; Ramirez, J.; Mercier, P. P.; Wang, J. Wearable Textile Biofuel Cells for Powering Electronics. *J. Mater. Chem. A* **2014,** *2*, 18184-18189.

(749) Ogawa, Y.; Kato, K.; Miyake, T.; Nagamine, K.; Ofuji, T.; Yoshino, S.; Nishizawa, M. Organic Transdermal Iontophoresis Patch with Built-In Biofuel Cell. *Adv. Health. Mat.* **2015,** *4*, 506-510.

(750) Laftsoglou, T.; Jeuken, L. J. C. Supramolecular Electrode Assemblies for Bioelectrochemistry. *Chem. Commun. (Camb)* **2017,** *53*, 3801-3809.

(751) Suraniti, E.; Mark, A.; Roche, J.; Richter, H.; Kuhn, A.; Mano, N.; Fischer, P. An Integrated Enzymatic Micro Biofuel Cell for Powering Logic Operations in Application Specific Integrated Circuits. *Lab Chip* **2017,** *17*, 1761–1768.

(752) Gentil, S.; Lalaoui, N.; Dutta, A.; Nedellec, Y.; Cosnier, S.; Shaw, W. J.; Artero, V.; Le Goff, A. Carbon Nanotube-Supported Bio-Inspired Nickel Catalyst and Its Integration in Hybrid Hydrogen/Air Fuel Cells. *Angew. Chem. Int. Ed.* **2017,** *56*, 1845-1849.

(753) Collman, J. P.; Devaraj, N. K.; Decréau, R. A.; Yang, Y.; Yan, Y.-L.; Ebina, W.; Eberspacher, T. A.; Chidsey, C. E. D. A Cytochrome *c* Oxidase Model Catalyzes Oxygen to Water Reduction under Rate-Limiting Electron Flux. *Science* **2007,** *315*, 1565-1568.

(754) Chenevier, P.; Mugherli, L.; Darbe, S.; Darchy, L.; DiManno, S.; Tran, P. D.; Valentino, F.; Iannello, M.; Volbeda, A.; Cavazza, C.; Artero, V. Hydrogenase Enzymes: Application in Biofuel Cells and Inspiration for the Design of Noble-Metal Free Catalysts for H_2 Oxidation. C. R. *Chim.* **2013,** *16*, 491-505.